Investigating the Molecular Mechanism of Replication Restart in Fission Yeast



DEPARTMENT OF BIOCHEMISTRY
UNIVERSITY OF OXFORD

A thesis presented to the Faculty of Medical Sciences Division,
University of Oxford for the degree of Doctor of Philosophy in Biochemistry

MICHAEL ONG NGUYEN

Merton College,
University of Oxford
Department of Biochemistry
Trinity Term, 2014

DECLARATION

I hereby declare that this report entitled “Investigating the Molecular Mechanism of Replication Restart in Fission Yeast” has been originally carried out by me under the supervision of Professor Matthew Whitby, Faculty Scientist, Department of Biochemistry, University of Oxford. This work has not formed the basis for award of any degree or diploma previously. The particulars given in the report are true to the best of my knowledge.

_____ Date: _____

Michael Ong Nguyen
Merton College,
University of Oxford
Department of Biochemistry

ACKNOWLEDGEMENTS

I would sincerely like to thank Professor Matthew Whitby for all of the endless support and guidance that he has provided me with over the past few years. His contributions to my personal and intellectual growth have been innumerable and extend far beyond shaping this dissertation. It has been both a pleasure and a privilege learning from him, and I am forever indebted to him for all of the opportunities that he has given me and opened up for me in the future.

I would also like to express my heartfelt appreciation for the fellow members of the Whitby Lab, specifically Dr. Alexander Lorenz, Dr. Fikret Osman, Claire Bryer, Jacqueline Neo, Manisha Jalan, Sonali Bhattacharjee, Dr. Carl Morrow, Dr. Io-Nam Wong, and Dr. Roland Steinacher, for all their assistance, encouragement, and much needed antics along the way. Special thanks to Camille Lemey, Brittany Ulloa, and Yi Fei Lee for being my wonderful students that went beyond helping me push my research forward. It has been a pleasure working alongside each and every one of them every day, and I know that the friendships we formed will last for years to come.

I would also like to extend my deepest gratitude to the US-UK Fulbright Commission and the Clarendon Fund, which awarded me with the scholarships that allowed me to pursue my doctoral degree.

Words could never express how thankful I am to my family and friends for their constant inspiration, support, and love.

Lastly, I would like to thank colleagues from my past and people whose names that I do not even know, who have given me their time and provided me with the strength and means to be where I am today.



Investigating the Molecular Mechanism of Replication Restart in Fission Yeast

A thesis submitted for the degree of Doctor of Philosophy in Biochemistry

by

Michael Ong Nguyen
Merton College,
University of Oxford
Department of Biochemistry
Trinity Term, 2014

ABSTRACT

Successful replication of the genome during each cell cycle requires that every replication fork merge with its opposing fork. However, lesions in the template DNA or protein-DNA barriers often impede replication forks and threaten the timely completion of genome duplication. If a fork encounters a replication fork barrier (RFB), it can be subject to a variety of fates. In some cases the replisome is maintained in a manner such that it can resume DNA synthesis when the barrier is removed. Alternatively the stalled fork is simply held in a competent state to merge with the opposing fork when it arrives. However, fork stalling can also precipitate dissociation of the replisome (fork collapse) or even fork breakage. If this happens the recombination machinery can intervene to restore DNA integrity and restart replication, albeit with a risk of causing deleterious genetic change if ectopic homologous sequences are recombined. I have exploited a site-specific RFB in fission yeast termed *RTS1* to investigate the consequences of perturbing a single replication fork. *RTS1* is a polar RFB (i.e. it blocks fork progression in a unidirectional fashion), enabling replication to be completed by the opposing fork. Despite this, fork blockage at *RTS1* triggers a strong recombinational response that is able to restart DNA synthesis, which at least initially is highly error prone. Here, I present my work in establishing a live cell imaging approach to visualizing the recombinational response at the *RTS1* RFB, demonstrating that the majority of cells initiate recombination-dependent replication (RDR). RDR begins within a few minutes of fork blockage and is only curtailed by the arrival of the opposing fork. It depends on the Rad52 protein, which remains associated with the restarted fork and whose presence correlates with its infidelity. I also illustrate the significance of various genetic factors, including Rad51, the Rad51 mediators, Fml1 helicase, Rad54 translocase, Pfh1 sweepase, and Cds1 checkpoint kinase, in modulating Rad52 localization and block-induced recombination at the *RTS1* RFB.

ABBREVIATIONS

AO	*RTS1* active orientation
ATP	adenosine triphosphate
ATPase	adenosine triphosphatase
BIR	break-induced replication
BLM	Bloom's syndrome helicase
bp	base pair
BSA	bovine serum albumin
CFP	cyan fluorescent protein
CPT	camptothecin
D-loop	displacement loop
dHJ	double Holliday junction
DMSO	dimethylsulfoxide
DNA	deoxyribonucleic acid
dNTP	deoxynucleotide triphosphate
DSB	double-strand break
DSBR	double-strand break repair
DTT	dithiothreitol
ECL	enhanced chemiluminescence
EDTA	ethylenediaminetetraacetic acid
EMMG	Edinburgh minimal media glutamate
GFP	green fluorescent protein
HJ	Holliday junction
HR	homologous recombination
HRP	horseradish peroxidase
HU	hydroxyurea
ICL	interstrand crosslink
IO	*RTS1* inactive orientation
IR	ionizing radiation
kb	kilobases
LA	low adenine

LB	Luria-Bertani
LOH	loss of heterozygosity
MCM	minichromosome maintenance
MEA	malt extract agar
MMR	mismatch repair
MMS	methyl methanesulfonate
MRN	Mre11-Rad50-Nbs1 complex
MRX	Mre11-Rad50-Xrs2 complex
NER	nucleotide excision repair
NHEJ	non-homologous end-joining
NLS	nuclear localization signal
nmt	no message in thiamine
ORC	origin recognition complex
ORF	open reading frame
PBS	phosphate-buffered saline
PCNA	proliferating cell nuclear antigen
PCR	polymerase chain reaction
PMSF	phenylmethylsulphonylfluoride
PRR	post-replication repair
rDNA	ribosomal DNA
RDR	recombination-dependent replication
RFB	replication fork barrier
RFC	replication factor C
RPA	replication protein A
RTS1	replication termination sequence 1
Sc	*Saccharomyces cerevisiae*
SDS-PAGE	sodium dodecyl sulfate polyacrylamide gel electrophoresis
SDSA	synthesis-dependent strand annealing
Sp	*Schizosaccharomyces pombe*
SSA	single-strand annealing
SSC	saline sodium citrate

ssDNA	single-stranded DNA
TBS	tris-buffered saline
TBZ	thiabendazole
TLS	translesion synthesis
UV	ultraviolet light
WRN	Werner syndrome helicase
YE	yeast extract
YES	yeast extract with supplements
YFP	yellow fluorescent protein

TABLE OF CONTENTS

Acknowledgements iii

Abstract iv

Abbreviations v

1 Introduction 1

1.1 Overview of homologous recombination in double-strand break repair 3

1.1.1 Importance of error-free repair by homologous recombination 4

1.1.2 Models for homologous recombination in double-strand break repair 6

1.1.2.1 Synthesis-dependent strand annealing 8

1.1.2.2 Classical double-strand break repair and double Holliday junction dissolution 10

1.1.2.3 Single-strand annealing 11

1.1.2.4 Break-induced replication 13

1.1.3 Resection 16

1.1.3.1 Mre11-Rad50-Nbs1/Xrs2 16

1.1.3.2 Ctp1/Sae2/CtIP 18

1.1.3.3 Exo1 19

1.1.3.4 Rqh1/Sgs1-Dna2 20

1.1.4 Rad51 nucleoprotein filament formation and strand invasion 20

1.1.4.1 RPA 20

1.1.4.2 Rad52 22

1.1.4.3 Rad55-Rad57 24

1.1.4.4 Swi5-Sfr1 26

1.1.4.5 Rdl1-Rlp1-Sws1/Shu1-Shu2-Psy3-Csm2 28

1.1.4.6 Rad54 29

1.1.4.7 Rad51 30

1.1.5 Postsynapsis and resolution of recombination intermediates 31

1.1.5.1 D-loop disruption 31

1.1.5.2 Double Holliday junction resolution 33

1.1.5.3 Double Holliday junction dissolution 34

1.2 DNA replication and the strategies cells employ to overcome DNA impediments **35**

1.2.1 Fundamentals of DNA replication 36

1.2.2 Impediments to DNA replication 39

1.2.3 Programmed DNA replication perturbations 42

1.2.3.1 Mating-type switching in yeast 42
1.2.4 Protein-DNA barriers 45
1.2.4.1 Tus-*ter* barrier in *Escherichia coli* 45
1.2.4.2 *Fob1* barrier in *Saccharomyces cerevisiae* 46
1.2.4.3 *RTS1* barrier in *Schizosaccharomyces pombe* 47
1.2.5 Responses to replication fork perturbation 48
1.2.5.1 Post-replicative repair 48
1.2.5.2 Translesion synthesis 50
1.2.5.3 Template-switch mediated lesion bypass 50
1.2.5.4 Role of checkpoint proteins in fork protection 55
1.2.5.5 Pushing past barriers using accessory helicases 59
1.2.5.6 Overcoming interstrand crosslinks 60
1.2.5.7 PriA-directed replication fork restart in *Escherichia coli* and recombination-dependent replication in Bacteriophage T4 62
1.2.5.8 Recombination-dependent replication restart in eukaryotes 63
1.3 Aim of study 67

2 Materials and Methods 70
2.1 Molecular biology techniques 71
2.1.1 *Escherichia coli* media 71
2.1.2 *Escherichia coli* transformation 71
2.1.3 Cloning and subcloning DNA fragments 72
2.1.4 One-dimensional gel electrophoresis for detection of DNA breaks 72
2.1.5 Southern blotting 73
2.1.6 SDS-polyacrylamide gel electrophoresis 74
2.1.7 Western blotting 74
2.2 Protocols for the handling and genetics of *Schizosaccharomyces pombe* 75
2.2.1 Media 75
2.2.2 Integration of DNA constructs into the *Schizosaccharomyces pombe* genome 76
2.2.3 Genetic crosses 77
2.2.4 Genomic DNA extraction embedded in agarose plugs 78
2.2.5 Alkaline lysis for protein extraction 78
2.2.6 Genotoxin sensitivity spot assays 79
2.2.7 Direct repeat recombination assays 80

2.2.8 Microscopy 80
2.3 Analysis 81
2.3.1 Image processing and analysis 81
2.3.2 Statistics 82

3 Establishing a System for Visualizing Replication Restart at a Site-Specific Replication Fork Barrier 103
3.1 Introduction 104
3.2 Results 105
3.2.1 Effect of adding *lac* operator sequences between direct repeats on direct repeat recombination 105
3.2.2 Expressing fluorescently tagged LacI at levels that produce a detectable *lacO*-LacI focus and do not induce recombination 111
3.2.3 Rad52-YFP is biologically functional 118
3.2.4 The *lacO*-LacI array does not induce Rad52-YFP foci in strains with either *RTS1-IO* or *RTS1-AO* 124
3.3 Discussion 126

4 Spatio-Temporal Dynamics of Recombination and Replication Foci During the Cell Cycle in Cells Containing *RTS1-IO* and *RTS1-AO* 131
4.1 Introduction 132
4.2 Results 132
4.2.1 Tracking the timing of replication foci during the cell cycle 132
4.2.2 The *RTS1* replication fork barrier stimulates the recruitment of Rad52-YFP to the *ade6* locus 135
4.2.3 Temporal dynamics of the Rad52-YFP focus at *RTS1* during the cell cycle 139
4.2.4 Rad52 focus assembly at *RTS1* has a random distribution in daughter cells 141
4.2.5 Comparison between the temporal dynamics of spontaneous and *RTS1*-induced Rad52 foci during the cell cycle 144
4.2.6 Rad51-CFP does not form detectable foci at *RTS1* 145
4.2.7 Rad54-GFP does not form detectable foci at *RTS1* 149

4.2.8 Rad11-GFP is recruited to the *RTS1* replication fork barrier 153
4.2.9 Timing of Rad11-GFP focus formation at *RTS1-AO* during the cell cycle 156
4.3 Discussion 159
4.3.1 Dynamics of Rad52 foci at replication forks blocked at *RTS1* 159
4.3.2 Involvement of recombinases at replication forks blocked at *RTS1* 160
4.3.3 Comparison of recombination responses to forks blocked at *RTS1* and spontaneous lesions 163
4.3.4 Failure to detect Rad51 and Rad54 foci at blocked forks 163
4.3.5 Dynamics of Rad11 foci at the *RTS1* replication fork barrier 166

5 The Effect of Delaying Fork Merging at *RTS1* on Direct Repeat Recombination and Rad52-YFP Foci 167
5.1 Introduction 168
5.2 Results 170
5.2.1 Deleting *ori-1253* increases direct repeat recombination at the *RTS1* replication fork barrier 170
5.2.2 Deleting *ori-1253* increases the recruitment of Rad52-YFP to the *RTS1* replication fork barrier 173
5.2.3 Deleting *ori-1253* increases the duration of Rad52 localization at the *RTS1* replication fork barrier 176
5.2.4 Slightly more cells with *ori-1253* deleted exhibit early Rad52 recruitment to *RTS1-AO* than wild-type cells 178
5.3 Discussion 180
5.3.1 Delaying fork merging increases the percentage of *RTS1-AO* cells performing recombination-dependent replication restart 180
5.3.2 Local and global effects of deleting an individual origin of replication 181
5.3.3 Restarted replication forks remain associated with Rad52 and prone to template switching 183
5.3.4 Examining the effect of inserting a pausing site to delay fork merging at *RTS1* 184

6 Role of Rad51 and Rad51 Mediators in Replication Restart at *RTS1* 186
6.1 Introduction 187

6.2 Results 188
6.2.1 Rad55 and Rad57 are required for replication fork block-induced gene conversion and the majority of deletion events 188
6.2.2 Rdl1, Rlp1, and Sws1 have critical roles in promoting replication fork block-induced gene conversions and deletions 190
6.2.3 Sfr1 and Swi5 have minor roles in promoting replication fork block-induced recombination 192
6.2.4 Epistasis analysis reveals that the Rad51 mediators function in the same pathway for promoting replication fork block-induced recombination 192
6.2.5 Rad51 and its mediators have a role in preventing replication fork block-induced deletions 197
6.2.6 Recruitment of Rad52-YFP to *RTS1-AO* is not affected by the loss of Rad51 or its mediators 201
6.2.7 Timing of Rad52 recruitment to forks blocked at *RTS1* is not affected by the loss of downstream recombination proteins 203
6.3 Discussion 206

7 Consequences of Pathological Fork Merging at *RTS1* 210
7.1 Introduction 211
7.2 Results 212
7.2.1 Fml1 has a dual role in modulating replication fork block-induced recombination 212
7.2.2 Rad52-YFP foci persist longer at *RTS1-AO* in the absence of *fml1* 215
7.2.3 Rad52's recruitment to forks blocked at *RTS1* is not significantly delayed in the absence of *fml1* 215
7.2.4 Rad54 has a role in promoting gene conversions and preventing deletions during replication fork block-induced recombination 218
7.2.5 Rad54's ATPase activity is essential in promoting gene conversions and some deletions during replication fork block-induced recombination 220
7.2.6 Fml1 and Rad54 have an additive effect in suppressing deletions during replication fork block-induced recombination 222
7.2.7 Investigating the consequence of fork merging during replication restart in Pfh1 mutants 223

7.2.8 The hyperrecombination at forks blocked at *RTS1* in the absence of Pfh1 is partly dependent on Rad54 225
7.3 Discussion 229
7.3.1 Fml1 and Rad54's role in modulating recombination at blocked replication forks 229
7.3.2 Fork convergence at *RTS1* in *pfh1* mutants 233

8 Importance of the Cds1 Checkpoint Kinase in Processing the Fork at *RTS1* 234
8.1 Introduction 235
8.2 Results 235
8.2.1 Cds1 has a role in suppressing recombination at *RTS1* 235
8.2.2 Mus81-dependent replication fork block-induced recombination is prevented by Cds1 238
8.2.3 Cds1 limits deletions independently of Fml1 at *RTS1-AO* 238
8.2.4 Rad52-YFP foci persists longer at *RTS1-AO* in *cds1Δ* and *mus81Δ* mutants 240
8.2.5 Timing of Rad52-YFP focus formation at *RTS1-AO* is not significantly changed in the absence of Cds1 or Mus81 242
8.2.6 Detecting breaks at *RTS1-AO* in a *cds1Δ* mutant 242
8.2.7 Mus81 resolves toxic intermediates in cells treated with hydroxyurea in the absence of Cds1 244
8.3 Discussion 246

9 Concluding Remarks 250

Appendix 258
Bibliography 281

Chapter 1

Introduction

The road to completing genome duplication is scattered with obstacles that challenge the progression of replication forks (Rothstein et al. 2000; McGlynn and Lloyd 2002b; Lambert and Carr 2013). These replication fork barriers (RFBs) can cause the replisome to skip or stall at various accidental and programmed blockades. When a replication fork stalls, it can be protected such that either DNA synthesis can resume when the barrier is removed or it can merge with the opposing fork when it arrives to complete DNA replication. However, fork stalling can also elicit fork collapse (i.e. the dissociation of the replisome) or even fork breakage. If this occurs, the homologous recombination (HR) machinery can intervene to restore DNA integrity and restart replication, albeit with a risk of restarting at the wrong, non-contiguous sequence and causing changes to the genome if ectopic homologous sequences are recombined. These consequential gross chromosomal rearrangements, which include deletions, duplications, inversions, and translocations, can lead to the development of diseases such as cancer in humans (Lambert et al. 2005; Chen et al. 2010; Heyer et al. 2010; Lambert et al. 2010; Carr and Lambert 2013). Therefore, the use of recombination at perturbed replication forks must be carefully governed.

My research uses the fission yeast *Schizosaccharomyces pombe* (*S. pombe*) as a model system to study recombination that is induced by replication fork blockage. In this chapter, I will highlight what we know about HR in this system. However, because HR has also been studied in an array of other organisms and is best understood in the budding yeast *Saccharomyces*

cerevisiae (*S. cerevisiae*) and the bacterium *Escherichia coli* (*E. coli*), I will also discuss key insights that have been obtained using these and other organisms. Furthermore, as much of our current understanding of the molecular mechanism of HR has been largely characterized in the context of double-strand break (DSB) repair, I will first explain its role in the repair of DNA DSBs. Building on this foundation, I will subsequently discuss its involvement in processing arrested replication forks while also reviewing the array of strategies cells employ to overcome impediments during DNA replication.

1.1 Overview of homologous recombination in double-strand break repair

HR is required in both mitotic and meiotic cells. Beyond mending DSBs and recovering stalled and broken replication forks (Horiuchi and Fujimura 1995; Michel et al. 2001; McGlynn and Lloyd 2002a), HR also has critical roles in eliminating interstrand crosslinks (ICLs) (Hinz 2010) and maintaining telomeres (Tarsounas and West 2005). Furthermore, programmed genome rearrangements exploit HR to repair DSBs that are intentionally induced in various biological processes. These include: i) meiosis to produce chiasmata, which provides the physical linkage between homologous chromosomes to ensure their proper segregation (Whitby 2005; Neale and Keeney 2006), ii) mating-type switching in yeast to facilitate self-fertilization (Haber 1998; Egel 2005), and iii) antigenic variation in pathogens to evade the host cell's immune system (Palmer et al. 2009).

1.1.1 Importance of error-free repair by homologous recombination

Although HR is generally presumed to be error-free, mistakes can be introduced when recombination is carried out with a non-allelic, ectopic, yet homologous sequence, which for example can occur when recombination occurs out of register in repeated sequences (Figure 1.1). These instances of recombination can lead to loss of heterozygosity (LOH), gene duplication, gene deletion, and gross chromosomal rearrangements (van Gent et al. 2001; Stankiewicz and Lupski 2002). These errors can propagate into serious health implications in humans. For instance, LOH is the most frequent type of tumor-associated mutation in breast cancer that can cause the inactivation of tumor-suppressor genes, such as *BRCA2* and the retinoblastoma tumor-suppressor gene (Bieche and Lidereau 1995; Hamann et al. 1996; Tsukamoto et al. 1996). Intriguingly, downregulation of HR can also place the cell at a heightened risk of chromosomal rearrangements from repair by non-homologous end-joining (NHEJ) (Yu et al. 2000). In NHEJ, the two DNA ends from a DSB are simply joined after little to no end processing without any requirements for a homologous template. NHEJ tends to be error-prone, particularly when DSBs occur with base pair (bp) loss since repair results in deletions. Therefore, despite HR's crucial role in genomic maintenance, it is stringently regulated to prevent its inappropriate and untimely use. In fact, many of the protein-protein interactions are regulated by reversible posttranslational modifications (Heyer et al. 2010; Krejci et al. 2012). Furthermore, key intermediate steps in HR can often be reversed. For example, formation of the Rad51 nucleoprotein filament, initial D-loop

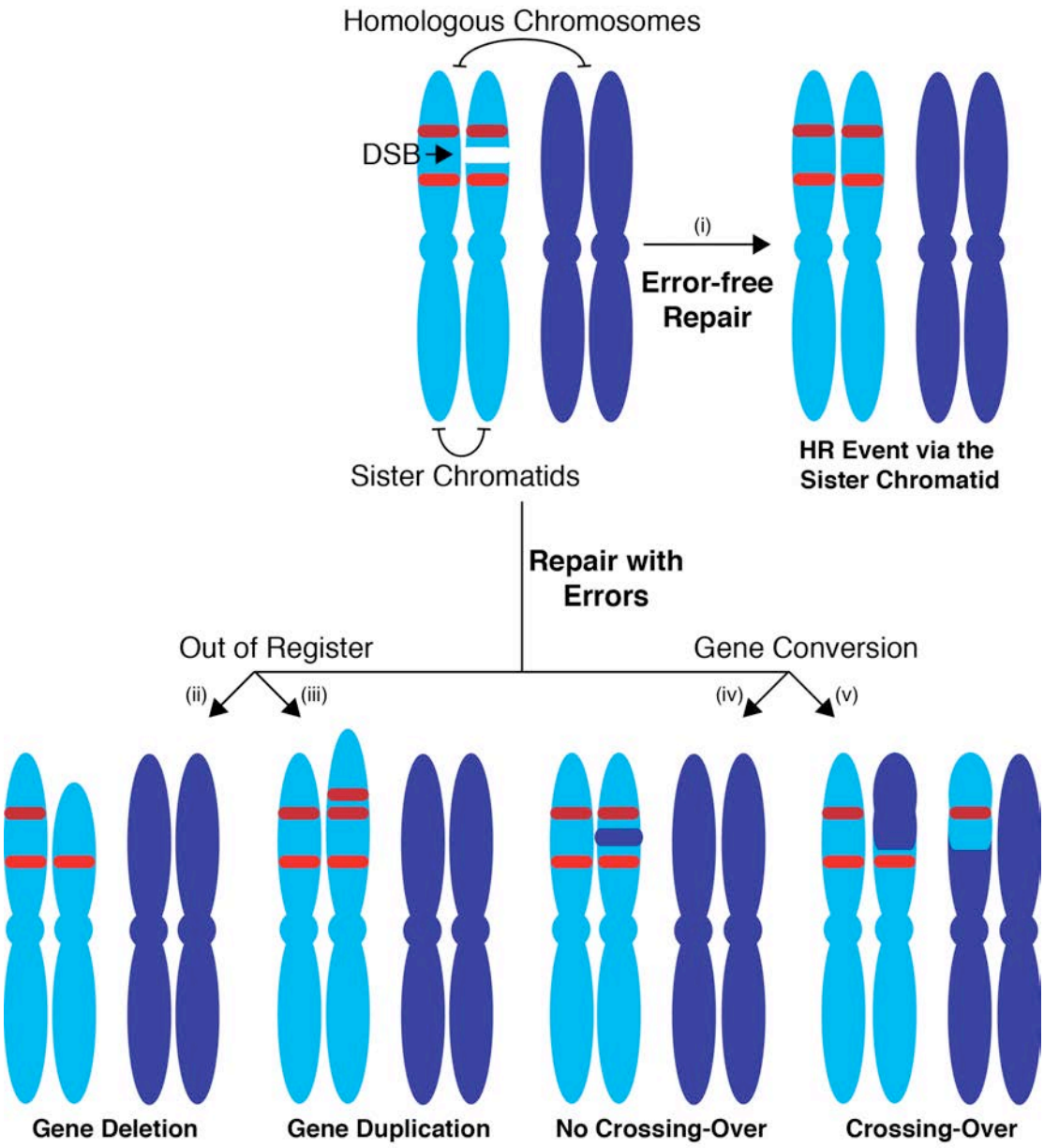


Figure 1.1 I Repair of DNA double-strand breaks by homologous recombination can lead to gross chromosomal rearrangements. DSBs repaired by HR can proceed without introducing any errors if recombination occurs in register through the use of the sister chromatid as the repair template (i). However, if repair occurs in repetitive regions, recombination may occur out of register and lead to gene deletions (ii) or duplications (iii). Furthermore, the sequence at the DSB may be altered through a gene conversion if it is replaced with a similar sequence from the homologous chromosome (iv, v). Additional rearrangements of the genome can occur when flanking regions of the DSB are reciprocally exchanged during crossing-over events (v).

following strand invasion, polymerase extended D-loop, and double Holliday junction (dHJ) can all be displaced and disrupted. This feature of reversibility is critically exemplified in cells with particular double-mutant combinations of recombination proteins, which perish from toxic HR intermediates that require processing by specific nucleases and motor proteins (Doe et al. 2002).

1.1.2 Models for homologous recombination in double-strand break repair

Although the basic principle of HR involves the invasion of a homologous, intact DNA strand from the sister chromatid or homologous chromosome as the template to retrieve genetic information for the repair of the DSB, there are different models for the HR repair of DSBs. These include the classical double-strand break repair (DSBR) (Szostak et al. 1983), dHJ dissolution (Wu and Hickson 2003), synthesis-dependent strand annealing (SDSA) (Resnick 1976; Allers and Lichten 2001), break-induced replication (BIR) (Morrow et al. 1997; Bosco and Haber 1998), and single-strand annealing (SSA) models (Lin et al. 1984). These pathways differ in how they form and resolve the intermediate HR structures. Regardless, these carefully choreographed processes feature some common players that perform the same acts (refer to Table 1.1 for a list of key HR proteins in fission and budding yeasts and their functional homologs in bacteria and mammals).

In eukaryotes, the initial steps of HR in DSB repair involve processing of broken DNA by exonucleases to generate 3’ ssDNA tails during the pre-

Table 1.1 Homologous Recombination Proteins

	E. coli	*S. cerevisiae*	*S. pombe*	Mammals
Presynapsis Processing of broken DNA ends	RecBCD	Mre11-Rad50-Xrs2	Mre11 (Rad32)-Rad50-Nbs1	MRE11-RAD50-NBS1
		Sae2	Ctp1	CtIP
	RecQ	Sgs1	Rqh1	BLM
		Dna2	Dna2	DNA2
	RecE, RecJ	Exo1	Exo1	EXO1
			Fbh1	FBH1
	UvrD	Srs2	Srs2	PARI
Synapsis Homologous pairing and DNA strand exchange	SSB	RPA	RPA	RPA
	RecA	Rad51	Rad51 (Rhp51)	RAD51
	RecO	Rad52	Rad52 (Rad22)	RAD52
		Rad59		
	RecF-RecR	Rad55-Rad57	Rad55 (Rhp55)-Rad57 (Rhp57)	RAD51B-RAD51C XRCC3
		Sae3-Mei5	Swi5-Sfr1	SWI5-SFR1
		Shu1-Shu2-Psy3-Csm2	Rlp1-Sws1-Rdl1	XRCC2-SWS1-RAD51D-SWSAP1
		Rad54	Rad54 (Rhp54)	RAD54
Postsynapsis Resolution of recombination intermediates	RecQ	Sgs1	Rqh1	BLM, RECQ1, RECQ4, RECQ5, WRN
	TopoIII	Top3	Top3	TopoIIIα
		Mph1	Fml1	FANCM
	RecG			
	RuvABC			
	RusA			
		Mus81-Mms4	Mus81-Eme1	MUS81-EME1
		Yen1		GEN1
		Slx1-Slx4	Slx1-Slx4	SLX1-SLX4

synapsis stage, loading of Rad51 onto these tails to form the Rad51 nucleoprotein filament, and searching by this filament for the homologous DNA template through strand invasion during the synapsis stage. DNA polymerases subsequently extend the invaded tail to restore the lost information. Lastly, this intermediate structure is resolved during post-synapsis. DNA helicases and translocases play critical roles in the latter stages because they are likely involved in removing recombination proteins from the invaded 3' end, facilitating the recruitment of DNA polymerase to the end, and unwinding of the duplex for continued DNA synthesis. Note that the recombination proteins that will be discussed can be deployed in various pathways and sometimes catalyze different reactions. These processes will be discussed in detail below.

1.1.2.1 Synthesis-dependent strand annealing

In SDSA, the 3' end of the invaded strand is displaced from the template to allow it to anneal to its complementary strand on the other side of the DSB (Nassif et al. 1994) (see Figure 1.2). This can occur by helicases that actively dismantle the structure or by bubble migration that simultaneously occurs with the extension of the invaded strand such that the newly synthesized strand is constantly unwound from its template (Formosa and Alberts 1986). The strand annealing ability of Rad52 may mediate the reengagement of the extended end with the second end. The gaps in the DNA that remain from when the two ends of the DSBs anneal are then filled in though DNA synthesis, which is followed by DNA ligation to complete the reaction. This model is supported by

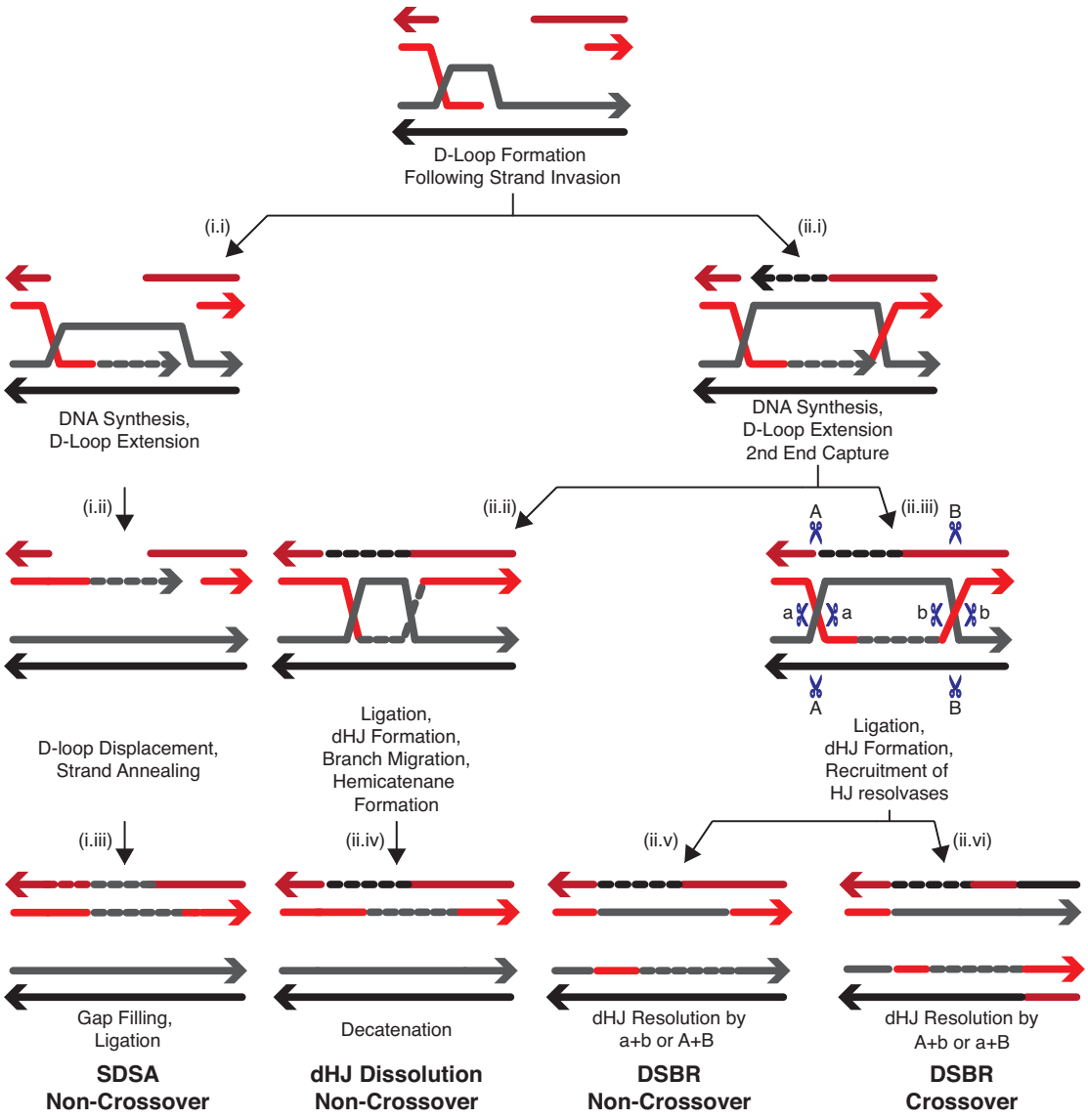


Figure 1.2 I The heteroduplex structure can be resolved by various subpathways. Depending on the cell type, the intermediate structure may be preferentially resolved by one pathway over another, as DSBs in mitotic and meiotic cells are preferentially repaired by non-crossover and crossover events, respectively. In SDSA, the extended DNA strand is simply displaced to allow it to anneal to its complementary strand on the other side of the DSB (i.i, i.ii) and gaps are filled in though DNA synthesis (i.iii). Alternatively, the extended DNA strand anneals to its complementary strand on the other side of the DSB forming a double Holliday junction (dHJ) (Szostak et al. 1983) (ii.i). This intermediate is resolved by either endonucleolytic cleavage (ii.iii, ii.v, ii.vi) or the concerted action of a RecQ helicase with topoisomerase III (ii.ii, ii.iv), referred to as DSBR dHJ resolution and dHJ dissolution, respectively.

all newly synthesized DNA being found in opposite strands of the same heteroduplex (i.e. conservative DNA synthesis), as opposed to the semi-conservative DNA synthesis that is predicted from the DSBR model (Gilbertson and Stahl 1996). The importance of SDSA is that it disrupts the D-loop before it forms a more complex recombinogenic structure that has the potential to be resolved as a crossover. Crossovers occur when there is a reciprocal exchange between the recombining molecules of the DNA region flanking the site of recombination. SDSA exclusively leads to noncrossovers, and it was proposed as a model to explain the low number of crossovers in mitotic cells.

1.1.2.2 Classical double-strand break repair and double Holliday junction dissolution

In an alternative pathway suggested by Szostak, the 3' invaded DNA strand is extended such that the ssDNA on the displaced strand eventually compliments the other end of the break. This allows the invaded strand to anneal to its complementary strand on the other side of the DSB without the D-loop being disrupted (Szostak et al. 1983) (see Figure 1.2). This process involves second end capture, which is promoted by the strand annealing activity of Rad52 (Lao et al. 2008; McIlwraith and West 2008). The displaced strand serves as a template to prime DNA synthesis to fill in the gap. This leads to a dHJ, which is a HR intermediate that consists of two separate Holliday junctions (HJs) between the four strands of DNA (Bzymek et al. 2010). HJs are four-way junctions between two dsDNA molecules of

homologous sequence, which are mobile and can be branch migrated by DNA helicases. This intermediate can be resolved by either endonucleolytic cleavage or through the concerted action of a RecQ-type helicase with topoisomerase III, referred to as dHJ resolution and dHJ dissolution, respectively.

1.1.2.3 Single-strand annealing

HR can also proceed in a Rad51-independent pathway through SSA (Figure 1.3). SSA repairs DSBs that occur between a direct repeat of homologous sequences (Lin et al. 1984). Similar to NHEJ, SSA is distinct from other HR pathways because it occurs within the context of one DNA molecule and does not require the sister chromatid or homologous chromosome. In the human genome, there are many repeat sequences, as illustrated by the excess of 500,000 copies of the short-interspersed repetitive element *Alu* sequence. Similar to SDSA and DSBR, it involves strand resection to generate the 3' overhangs, but because of the direct DNA repeat, the resected ends will reveal complementary sequences. Thus, instead of Rad51 loading, the complementary ssDNA ends coated with RPA (see Section 1.1.4.1) can anneal through the aid of Rad52's strand annealing capabilities. In budding yeast, this reaction is promoted by Rad52's interaction with Rad59, which also has strand annealing properties *in vitro* that depend on Rad52 as it is unable to compete with RPA (Petukhova et al. 1999a; Davis and Symington 2001). The nonhomologous DNA that is within the direct repeats is subsequently flipped out to form 3' flaps that are cleaved by nucleotide excision repair

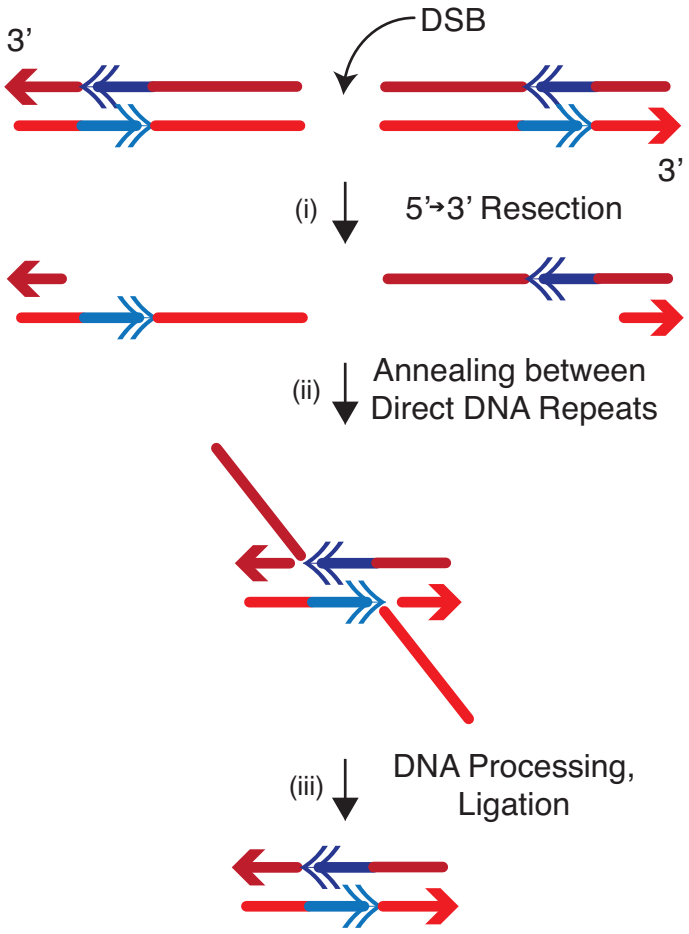


Figure 1.3 I Single-strand annealing is an error-prone subpathway of homologous recombination. When DSBs occur within direct DNA repeats (shown in blue), 5'→3' resection can reveal complementary sequences in the single-strand overhangs that can be annealed by Rad52 in a Rad51-independent process. The 3' flaps between the direct repeats can then be processed by DNA endonucleases, and the resulting DNA nicks can be ligated following any additional DNA processing steps required, such as gap filling. The end results leads to a deletion of the intervening sequence and of one of the repeats.

(NER) proteins Rad1 and Rad10 in *S. cerevisiae* (Rad16 and Swi10 in *S. pombe*) (Fishmanlobell and Haber 1992; Mcanulty and Lippard 1995). Mismatch repair (MMR) proteins Msh2 and Msh3 are also involved as they stabilize the ds/ssDNA junction and recruit Rad1 and Rad10 to these sites (Sugawara et al. 1997; Bertrand et al. 1998). The final steps involve DNA processing, such as gap filling and ligation of the nicks. The end result of SSA is considered mutagenic as it is a deletion of one of the two repeats and of the nonhomologous sequence flanked by the direct repeats.

1.1.2.4 Break-induced replication

The last HR pathway is BIR, and it involves the repair of a one-ended DSB (Figure 1.4), which can arise from replication forks collapsing and the two free DSB ends finding homology in different areas of the genome, or a telomere becoming uncapped and degraded. In fact, BIR is suppressed when the second end is in close proximity, which potentially could be communicated through the physical bridging of the ends by the Mre11-Rad50-Xrs2 (MRX) complex (Jain et al. 2009). In BIR, following resection, the 3' tail invades a homologous DNA duplex, and establishes a replication fork that can: i) duplicate large chromosomal regions by proceeding for potentially hundreds of kilobases (kb) to the end of the chromosome (Mosig 1987; Malkova et al. 1996; Kogoma 1997) and ii) lead to conservative inheritance of newly synthesized DNA (Donnianni and Symington 2013; Saini et al. 2013; Wilson et al. 2013). Consequently, if the invaded duplex is the homolog rather than the sister chromatid, extensive LOH may result. Unlike SDSA and DSBR, which

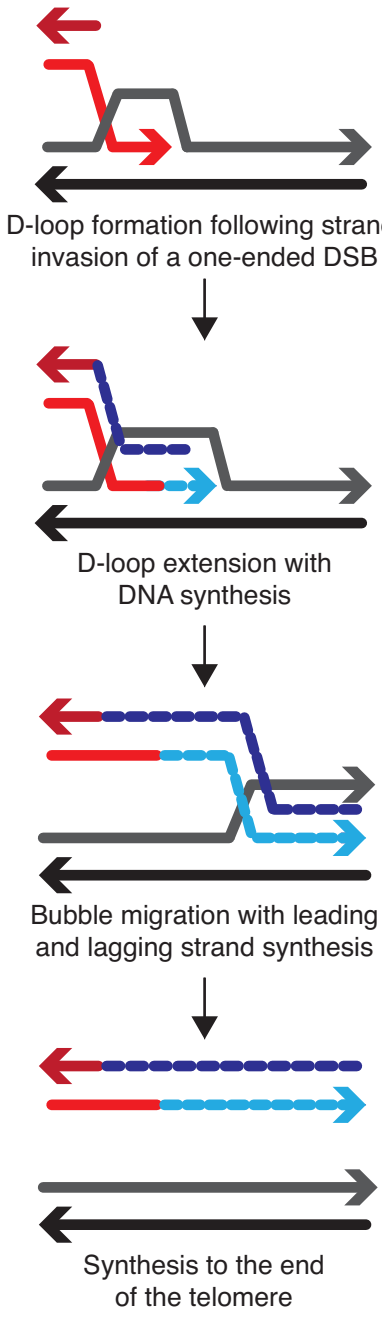


Figure 1.4 | Break-induced replication involves a one-ended double-strand break and proceeds to the end of the chromosome. BIR ensues when a one-ended DSB invades into a homologous DNA sequence. This leads to a migrating bubble that persists for potentially hundreds of kilobases down the length of the chromosome and to the end of the telomere. It results in conservative inheritance of the newly synthesized DNA.

only use leading strand synthesis machinery to extend the first end and subsequently, the second end, BIR uses both leading and lagging strand synthesis machinery; however, it is currently unclear whether leading and lagging strand synthesis proceeds synchronously or asynchronously.

Although BIR is proposed as a model to explain recombination-dependent restart of collapsed replication forks, BIR may not accurately model collapsed forks *in vivo* because collapsed forks probably lead to one broken end with a gapped sister chromatid while studies of BIR proceed outside of the context of replication through the analysis of a broken DNA fragment performing a strand invasion into intact duplex DNA. One key difference between DNA synthesis initiated from BIR and from replication forks emanating from an origin of replication is that BIR is highly mutagenic (Deem et al. 2011) despite the fact that it requires nearly all the essential proteins needed for initiation of normal replication (Lydeard et al. 2010). However, in budding yeast, BIR also requires Pol32, a subunit of polymerase δ, which is not required in S-phase DNA replication (Lydeard et al. 2007), and its long-range synthesis is dependent on the Pif1 helicase (Saini et al. 2013; Wilson et al. 2013). Kinetically, the rate of DNA synthesis during BIR is comparable to normal S-phase DNA replication, but the initiation of BIR is much slower than SDSA (Malkova et al. 2005). Therefore, BIR is outcompeted by SDSA in mitotic DSB repair. In fact, BIR occurs through several rounds of strand invasion, DNA synthesis, and dissociation, which is a feature that is argued to prevent BIR from occurring at two-ended DSBs (Smith et al. 2007). Interestingly, although

more than 95% of BIR events are dependent on Rad51 in budding yeast, 100% of BIR events are dependent on Rad52, which indicates that a minority of BIR events occur at specific chromosomal sites where Rad52 may be able to promote “strand invasion” independent of Rad51 via its single-strand annealing activity (Bosco and Haber 1998; Davis and Symington 2004).

1.1.3 Resection

DSBs processed by HR require nucleolytic resection of the DNA ends to form the 3’ single-stranded overhangs employed for strand invasion. In fact, initiation of resection is a critical determinant of pathway choice as efficient resection represses NHEJ (Zhang et al. 2009) and is regulated during the cell cycle to occur primarily in S and G2 (Aylon et al. 2004; Ira et al. 2004). There are three main models that have been mechanistically proposed to explain extensive resection that can proceed to a few kb away from the ends of DSBs (Figure 1.5). The key proteins are discussed below.

1.1.3.1 Mre11-Rad50-Nbs1/Xrs2

Resection is believed to begin when the Mre11-Rad50-Nbs1 (MRN) complex is recruited to the DSB site. The MRN complex provides three critical roles: DSB recognition, initiation of DSB and cell-cycle checkpoint signaling, and regulation of chromatin remodeling in the vicinity of the DSB (Williams et al. 2007). Mre11 is widely conserved, and has a structure-specific endonuclease activity and 3’→5’ exonuclease activity (Furuse et al. 1998; Trujillo and Sung 2001). Note that this exonuclease activity has the opposite polarity needed to

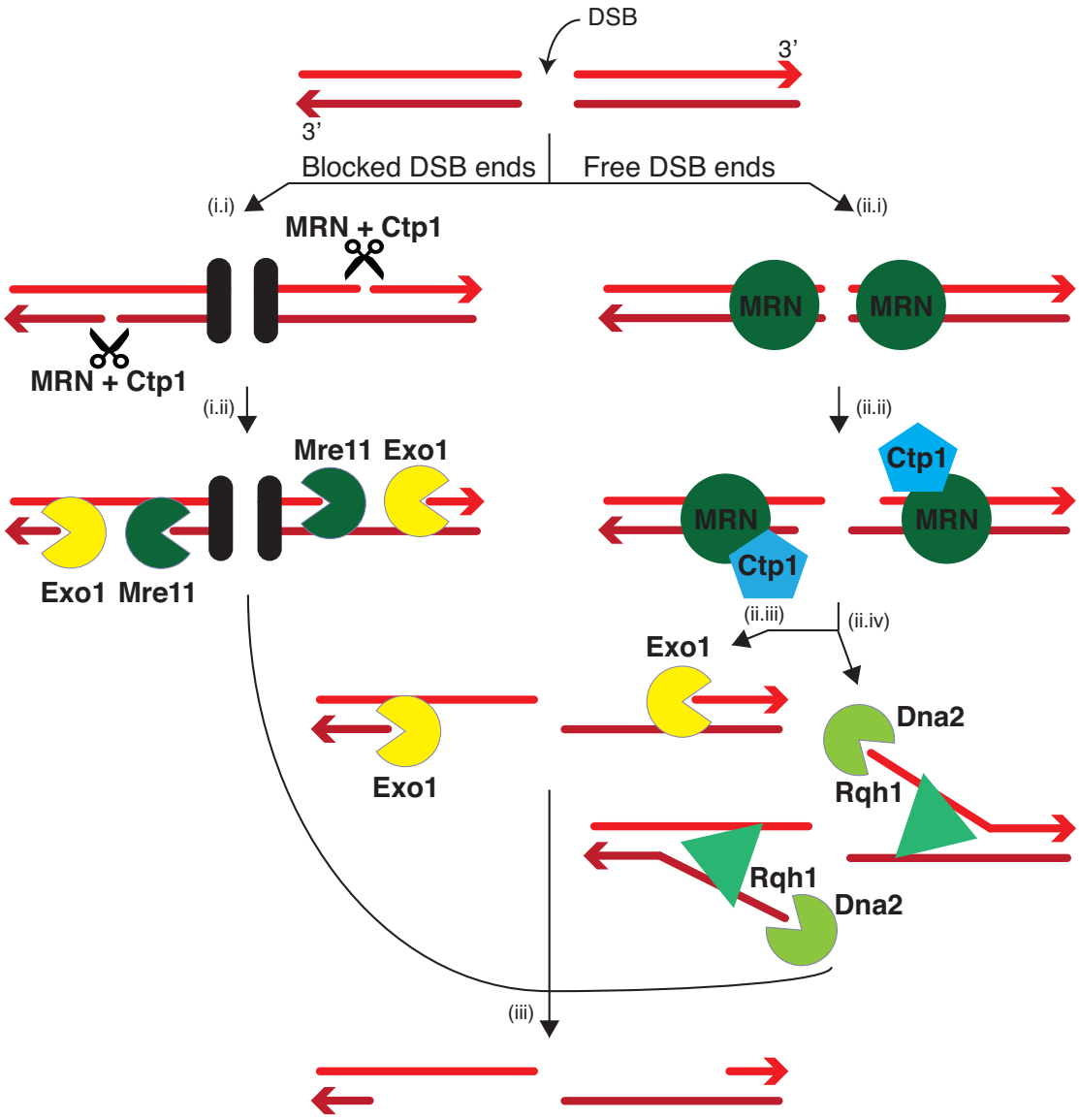


Figure 1.5 I Hypothetical models for DNA end 5'→3' resection in fission yeast based on related findings in budding yeast. Resection begins when the Mre11-Rad50-Nbs1 (MRN) complex and Ctp1 is recruited to the DSB site (i.i, ii.i, ii.ii). Mre11 has an endonuclease and 3'→5' exonuclease activity (Furuse et al. 1998; Trujillo and Sung 2001). In the case of DSBs with blocked termini, Mre11 nicks the strand to be resected, and this nick enables bidirectional resection with Exo1 and Mre11 performing 5'→3' and 3'→5' exonuclease activity, respectively (Hartsuiker et al. 2009; Garcia et al. 2011) (i.ii). In the case of DSBs with free ends, Exo1, through its 5'→3' exonuclease activity, can work together with the MRN complex and Ctp1 to produce the 3' overhang (Szankasi and Smith 1992) (ii.iii). Alternatively, resection can be performed by the concerted action of the RecQ-type helicase Rqh1 with the exonuclease Dna2 (Langerak et al. 2011) (ii.iv). In all cases, both ends of the break are resected to give an extended 3' overhang that is used as the substrate for strand invasion (iii).

produce the 3' tails, and thus, Mre11 needs to work in conjunction with other factors to produce the overhang. The N-terminus of Mre11 maintains its interaction with Rad50, whereas the C-terminus maintains its interaction with Nbs1 (Ueno et al. 2003; Krogh et al. 2005). Rad50 enhances the endonuclease activity of Mre11 and provides a means to hold the broken ends together (Trujillo and Sung 2001; Lobachev et al. 2004). The Nbs1 ortholog in budding yeast is Xrs2, which has DNA binding activity that helps target the complex to DNA ends (Trujillo et al. 2003). Interestingly, the MRN/X complex can also displace Ku, a protein required for the initiation of NHEJ, suggesting MRN/X has a role in preventing NHEJ if HR is the preferred response (Wu et al. 2008a; Shim et al. 2010).

1.1.3.2 Ctp1/Sae2/CtIP

Another key component involved in resection is the endonuclease Ctp1. Unlike MRN, which is abundant throughout the cell cycle, Ctp1 expression is cell-cycle regulated so that there is no Ctp1 during G1 but high levels during S and G2 phase (Limbo et al. 2007). This switch in expression may transition the preferred response to DSBs from NHEJ to HR. Furthermore, Ctp1 can also displace Ku from DSB ends (Langerak et al. 2011). Upon DNA damage, Ctp1 becomes phosphorylated, and this modified form is recruited by Nbs1 to work with the MRN complex to promote resection and generate single-stranded DNA (ssDNA) by catalyzing the initial elimination of a few hundred bases at the break (Sartori et al. 2007; Chen et al. 2008a; Williams et al. 2009). Phosphorylation of Ctp1 orthologs in budding yeast Sae2 and human

CtIP has also been observed, suggesting it may be a conserved point of regulation that initiates resection and repair by HR (Huertas et al. 2008; Huertas and Jackson 2009).

1.1.3.3 Exo1

Extensive resection can be promoted by Exo1, which has 5'→3' exonuclease activity that preferentially acts on duplex ends or nicks (Szankasi and Smith 1992). This exonuclease activity has the correct polarity needed to produce the 3' tail, and thus, together with the MRN complex and Ctp1, Exo1 can produce the 3' overhang. This mechanism has been reconstituted with the budding yeast enzymes MRX, Sae2, and Exo1 (Nicolette et al. 2010). Note that Ku inhibits Exo1 from initiating resection (Shim et al. 2010; Langerak et al. 2011). Exo1 may also be inhibited through phosphorylation as suggested through studies at uncapped telomeres in budding yeast (Morin et al. 2008) and hydroxyurea (HU)-induced stalled replication forks in human cells (El-Shemerly et al. 2008).

In the case of DSBs with termini blocked by Spo11 in meiotic recombination, failed topoisomerase reactions, or ends competitively bound by NHEJ machinery, the ssDNA overhang may be established through a bidirectional resection. In this model (Figure 1.5), Mre11 nicks the strand to be resected up to 300 nucleotides from the 5' end of the DSB, and this nicks enables Exo1 and Mre11 to perform 5'→3' and 3'→5' exonuclease activity, respectively, as Exo1 moves away from the DSB end and Mre11 moves towards it (Garcia et

al. 2011).

1.1.3.4 Rqh1/Sgs1-Dna2

Extensive resection can also be performed by the concerted action of the RecQ-type helicase Rqh1/Sgs1 unwinding the DNA for the digestion of the intermediate by the exonuclease Dna2; however, this may play a more minor role in fission yeast (Langerak et al. 2011). This mechanism has been reconstituted *in vitro* with the budding yeast enzymes Sgs1 (the ortholog of Rqh1), Top3-Rmi1, MRX, Dna2 and RPA (Cejka et al. 2010; Niu et al. 2010). These models for extensive resection are further supported by *in vivo* data showing an accumulation of unprocessed meiotic DSBs in Mre11-nuclease defective cells (Furuse et al. 1998), and partly resected DSBs that are poor substrates for HR in *exo1*Δ*sgs1*Δ double mutants (Mimitou and Symington 2008; Zhu et al. 2008).

1.1.4 Rad51 nucleoprotein filament formation and strand invasion

Following resection, the next phase of HR involves synapsis of the broken DNA end with an intact DNA molecule that has a homologous sequence for the repair of the damaged site (Figure 1.6). The central proteins facilitating this process are described below.

1.1.4.1 RPA

The ssDNA tail generated by resection is initially coated with RPA. RPA is a highly conserved heterotrimeric, ssDNA binding protein that is involved in

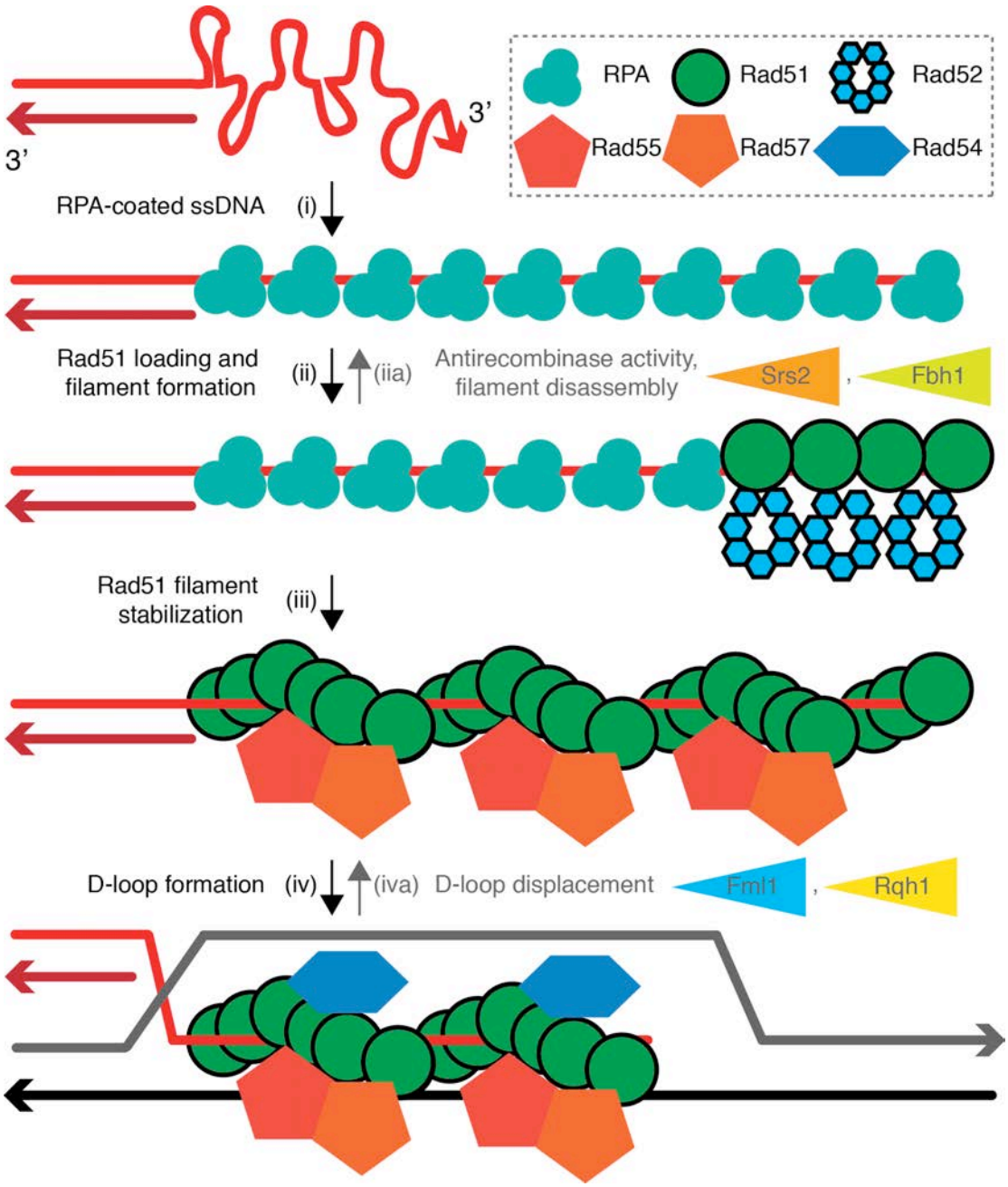


Figure 1.6 | The central reaction of homologous recombination proceeds through Rad51 nucleoprotein filament formation and strand invasion. Following resection, the ssDNA tail is initially coated with RPA (i), which removes secondary structures and protects the DNA from nucleolytic attack. Heptameric Rad52 then facilitates the exchange of RPA for Rad51 (ii). The heterodimeric Rad51 paralogs, Rad55-Rad57, stabilize the Rad51 nucleoprotein filament (iii). Alternatively, the Swi5-Sfr1 complex can stabilize the Rad51 nucleoprotein filament (not depicted). Rad54 clears histones from recombinogenic lesions and remodels the homologous duplex for Rad51-invasion (iv). Finally, Rad51 catalyzes the base pair exchange that leads to a heteroduplex structure. The helicases, Fbh1, Fml1, Rqh1, and Srs2, can act as antirecombinases by disrupting this process at different steps (iia, iva).

replication, repair, and recombination. Its activity in replication is switched to recombination through its phosphorylation by the checkpoint machinery in response to DNA damage, which likely changes its protein interactions (Binz et al. 2004). RPA has a high affinity for ssDNA, and its critical role in recombination is believed to be the removal of secondary structures before the loading of Rad51 while also protecting the DNA from nucleolytic attack (Sung et al. 2003). Furthermore, following strand invasion, it aids Rad51 by binding to the displaced strand during D-loop formation (Eggler et al. 2002). However, RPA can paradoxically inhibit Rad51 loading because it outcompetes Rad51 for ssDNA as *in vitro* experiments suggest that strand exchange proceeds efficiently when RPA is added after Rad51 but not vice versa (Sung 1997b). Yet RPA is very abundant *in vivo* and is likely to bind ssDNA before Rad51.

1.1.4.2 Rad52

The strand invasion mediated by Rad51 is dependent on mediator proteins that can facilitate the exchange of RPA for Rad51. In yeast, Rad52 (formerly known as Rad22 in *S. pombe*) completes this critical function (Kurokawa et al. 2008). Physically, Rad52 has been shown to interact with both Rad51 and RPA (Shinohara et al. 1992; Hays et al. 1998). Structurally, the N-terminus of Rad52 contains a self-association domain and a DNA binding domain, the C-terminus contains a Rad51 binding domain and another DNA binding domain, while the central portion contains a RPA interaction domain (Kagawa et al. 2002). In Rad51-dependent recombination events, such as SDSA, it works by

catalyzing the exchange of RPA for Rad51 on ssDNA as suggested by the recovery of efficient strand exchange when Rad52 is included with Rad51 in the presence of RPA in the aforementioned *in vitro* experiment (Sung 1997a) and by Rad52-stimulation of Rad51 mediated displacement of RPA from ssDNA (Sugiyama and Kowalczykowski 2002). Rad51's reliance on Rad52 is additionally highlighted by *in vivo* experiments that reveal Rad51 is dependent on Rad52 for localization to foci (Lisby et al. 2004) and for recruitment to DSBs as shown by chromatin immunoprecipitation (Wolner et al. 2003).

Rad52 is a required factor for all recombination events whether they are Rad51-dependent or -independent (Doe et al. 2004). In fact, budding yeast *rad52* mutants are extremely sensitive to DNA damaging agents such as ionizing radiation (IR), which induces DSBs (Malkova et al. 1996; Symington 2002). Yet despite it being widely conserved in eukaryotes, Rad52 appears to be functionally redundant in mammals (Rijkers et al. 1998), which may underlie the importance of the role it performs. To illustrate this fact, in mammals, BRCA2 appears to perform the key Rad52 role (Thorslund and West 2007), and heterozygous mutations in BRCA2 increase susceptibility to breast, ovarian, and prostate cancer while homozygous mutations cause the cancer predisposition syndrome Fanconi anaemia (Howlett et al. 2002; Narod and Foulkes 2004). Knockout of the *BRCA2* gene in mice is embryonic lethal (Sharan et al. 1997). Although RAD52 cannot fully substitute for BRCA2, loss of RAD52 function in BRCA2-deficient cells is synthetically lethal (Feng et al. 2011).

In vivo, Rad52 has been shown to bind to DNA ends at DSBs by chromatin immunoprecipitation (Kim et al. 2000) and form discrete foci following IR treatment and during S-phase in mitotic cells (Lisby et al. 2001; Meister et al. 2003). The ability of Rad52 to form detectable foci is partly due to its association into a multimeric, ring-structured protein, which also increases the efficiency of its nuclear localization since each subunit contains a nuclear localization signal (NLS) (Plate et al. 2008). Furthermore, budding yeast Rad52 becomes SUMOylated following the induction of DSBs as a means to protect it from proteasomal degradation during recombinational repair (Sacher et al. 2006).

With regards to its Rad51-independent roles, biochemically, Rad52 can bind ssDNA and promote DNA strand annealing between complementary sequences (Mortensen et al. 1996) through an activity stimulated by RPA (Sugiyama et al. 1998). In fact, human RAD52 may be more critical for promoting efficient strand annealing during processes such as second end capture, particularly as other mediators like BRCA2 lack this ability (Grimme et al. 2010; Jensen et al. 2010; Thorslund et al. 2010). In the subset of HR pathways that are Rad51-independent, such as SSA, Rad52 anneals the complementary ssDNA regions that have been exposed by resection and in the case of SSA, interacts with Rad59 (Davis and Symington 2001).

1.1.4.3 Rad55-Rad57

Formation of the Rad51 nucleoprotein filament is further mediated by the so-

called Rad51 paralogs. In fission and budding yeast, they include Rad55 and Rad57. In mammals, the Rad51 paralogs that facilitate Rad51 loading are RAD51B, RAD51C, RAD51D, XRCC2, and XRCC3. They are classified as Rad51 paralogs because they share sequence similarity to Rad51 (Kans and Mortimer 1991; Lovett 1994; Khasanov et al. 1999; Tsutsui et al. 2000). In response to DNA damage and to replication blocks, Rad55 is phosphorylated on multiple residues, which has been suggested to positively regulate HR (Bashkirov et al. 2000; Herzberg et al. 2006; Janke et al. 2010). Rad55 and Rad57 form a stable heterodimer, and, similar to Rad52 *in vitro*, are also able to overcome RPA inhibition of Rad51-mediated strand exchange (Sung 1997b). The mechanism of action is different from Rad52, however, in that Rad55 has been shown to interact with Rad51, but unlike Rad52, neither Rad55 nor Rad57 interact with RPA (Hays et al. 1995; Johnson and Symington 1995; Hays et al. 1998).

The role of Rad55-Rad57 is believed to be the stabilization of the Rad51 nucleoprotein filament as suggested by a Rad51 mutant with a higher ssDNA binding affinity bypassing the need for Rad55 and Rad57 in strand exchange but not RPA, Rad52, or Rad54 (Fortin and Symington 2002). Furthermore, *rad55Δ* mutants exhibit cold sensitivity to ionizing radiation, which is indicative of a role for Rad55 as a protein complex stabilizer since the formation of protein assemblies is more difficult in lower temperatures (Lovett and Mortimer 1987). This is also supported by the DNA damage sensitivity of *rad55Δ* and *rad57Δ* mutants being suppressed by overexpression of Rad51

(Hays et al. 1995; Johnson and Symington 1995) and by *rad55Δ* mutants exhibiting a defect in Rad51 foci assembly in response to γ-irradiation (Gasior et al. 2001). Furthermore, Rad55-Rad57 stabilized Rad51 nucleofilaments protect Rad51 from being displaced by the anti-recombinase activity of the Srs2 helicase (Liu et al. 2011b). Srs2 triggers ATP hydrolysis within the Rad51 filament, which causes Rad51 to dissociate from DNA (Antony et al. 2009), and once a Rad51 molecule is displaced from DNA, Srs2 can translocate in the 3'→5' direction along the ssDNA to displace the next Rad51 subunit in the filament (Krejci et al. 2003; Veaute et al. 2003; Qiu et al. 2013). Interestingly, in budding yeast, Srs2 is recruited by a NHEJ factor, Nej1, at DSBs to repress Rad51-dependent HR and favor NHEJ or SSA as a way to prevent the assembly of nonproductive recombination intermediates (Carter et al. 2009). Therefore, the stabilization of the Rad51 nucleofilament is a critical moment for the progression of HR.

1.1.4.4 Swi5-Sfr1

In addition to the aforementioned Rad51 paralogs, fission yeast and mammalian cells additionally have a Swi5-Sfr1 complex, which also mediates Rad51 nucleation and stimulates Rad51-mediated strand exchange by snugly binding within the helical groove of the Rad51 filament (Akamatsu et al. 2003; Haruta et al. 2006; Kuwabara et al. 2012). The N-terminal domain of Sfr1 interacts with Rad51 and recruits the complex to Rad51 filaments (Kuwabara et al. 2012). When either Swi5 or Sfr1 is mutated, mitotic and meiotic cells experience reduced HR (Schmidt et al. 1989; Ellermeier et al. 2004; Haruta et

al. 2006). However, the Swi5-Sfr1 complex differentially regulates Rad51-dependent recombination outcomes in mitotic cells because, unlike Rad55-Rad57, it is not essential for crossover production (Akamatsu et al. 2007). The Rad55-Rad57 and Swi5-Sfr1 complexes are proposed to work in parallel pathways promoting Rad51. This is partly supported by the observations that: i) Rad51 foci induced by ultraviolet light (UV) are partially reduced in *swi5Δ* and *rad57Δ* single mutants, while they are completely abolished in *swi5Δrad57Δ* double mutants (Akamatsu et al. 2007); ii) *swi5Δrad55Δ* double mutants are as sensitive to DNA damaging agents as *rad51Δ* mutants and are more sensitive than either a *swi5Δ* or *rad55Δ* single mutant; and iii) overexpression of Sfr1 partly suppresses the defects in DNA repair in *rad55Δ* mutants (Salakhova et al. 2005).

Besides Sfr1, Swi5 also physically interacts with Swi2, a Sfr1-related protein, in a separate complex. The Swi5-Swi2 complex is important for promoting HR during mating-type switching. Note though that Swi2 and Sfr1 do not have redundant functions despite sharing domains that possess an interaction site with Swi5 since overexpression of Swi2 does not suppress DSB repair defects in *sfr1Δ* mutants and overexpression of Sfr1 does not suppress mating-type switching defects in *swi2Δ* mutants (Akamatsu et al. 2003). In budding yeast, the homologs of Swi5-Sfr1 are Sae3-Mei5, and they are meiosis-specific genes that stimulate the meiosis-specific RecA homolog Dmc1 (McKee and Kleckner 1997; Hayase et al. 2004).

1.1.4.5 Rdl1-Rlp1-Sws1/Shu1-Shu2-Psy3-Csm2

Rdl1-Rlp1-Sws1, the functionally equivalent budding yeast Shu complex, consisting of Shu1-Shu2-Psy3-Csm2, and the human enzymes XRCC2-SWS1-RAD51D-SWSAP1 are the most recently identified partner proteins that promote HR. In contrast to Rad55-Rad57 and Swi5-Sfr1, single mutants of the Rdl1-Rlp1-Sws1 complex are only mildly sensitive to HU, camptothecin (CPT), methyl methanesulphonate (MMS), UV, and γ-irradiation (Khasanov et al. 2004; Martin et al. 2006). However, the Rdl1-Rlp1-Sws1 complex is proposed to work with Rad55-Rad57 as yeast two-hybrid analysis indicates that Rlp1 and Rad57 interact and epistasis analysis reveals that *rlp1Δrad55Δ* double mutants are epistatic to *rad55Δ* for MMS and IR sensitivity (Khasanov et al. 2004). Accordingly, in budding yeast, Csm2 has been shown to interact with Rad55 independently of Rad51 in yeast two-hybrid assays (Godin et al. 2013; Xu et al. 2013) and promote both Rad55 foci induced by IR and Rad51-dependent recombination events in direct repeat recombination assays (Godin et al. 2013). Intriguingly, the Rdl1-Rlp1-Sws1 complex is distinct from Rad55-Rad57 because the *rdl1Δ* and *sws1Δ* single mutants do not exhibit a cell elongation phenotype, which would be indicative of having a role in spontaneous DNA damage, or have a hyperrecombinant phenotype in spontaneous intrachromosomal recombination assays, which both characterize *rad55Δ* mutants (Khasanov et al. 2004; Martin et al. 2006). Interestingly, Sws1 has been shown to interact with Srs2 in yeast two-hybrid screens (Martin et al. 2006), and deletion of the budding yeast Shu1 leads to increased Srs2 recruitment to both induced and spontaneous foci and a

corresponding decrease in Rad51 foci (Bernstein et al. 2011). This suggests that the Shu complex may have a conserved and direct role in antagonizing Srs2's antirecombinase activity in disassembling Rad51 filaments.

1.1.4.6 Rad54

Rad54 is another critical protein that facilitates Rad51 nucleation. Like the other mediators, it stabilizes Rad51 filaments on ssDNA, but it also has many other distinct functions in HR. It is part of the Swi2/Snf2 family of chromatin remodeling DNA-dependent ATPases. As such, Rad54 can translocate along duplex DNA and clear histones from recombinogenic lesions or remodel the chromatin in the intact homologous duplex to promote Rad51-mediated strand invasion (Alexeev et al. 2003). Rad54 physically interacts with Rad51, and because both proteins are conserved from yeast to humans, their interaction may be functionally important for efficient HR repair (Clever et al. 1997). Paradoxically, Rad54 has also been shown to dissociate Rad51 from dsDNA filaments after strand invasion, and this has been proposed as a means to allow access of the invading 3' strand to a DNA polymerase for extension (Solinger et al. 2002; Chi et al. 2006; Heyer et al. 2006; Li and Heyer 2009). This is a critical step in regulating recombination because it is potentially the last antirecombination step since disruption of a D-loop prior to extension by DNA polymerase prevents new DNA synthesis. In fission yeast, Rad54 levels are regulated in G1 by ubiquitylation by the anaphase-promoting complex/cyclosome (APC/C), which leads to Rad54 proteolysis and a means to suppress HR during G1 (Trickey et al. 2008).

1.1.4.7 Rad51

Once Rad51 is loaded onto the 3' ssDNA tail, it performs the central reaction of HR. Rad51-dependent recombination is the most efficient HR pathway for gene conversion, and Rad51 is the key protein that catalyzes homologous DNA pairing during strand exchange (Sung 1994). Rad51 is the RecA homolog in eukaryotes and is evolutionarily conserved. Although null mutants of Rad51 in yeast are viable, they are embryonic lethal in higher eukaryotes, which may be a consequence of the demands in having to preserve larger genomes (Vainio and Imhof 1995; Lim and Hasty 1996; Tsuzuki et al. 1996). Biochemically, Rad51 binds DNA (Shinohara et al. 1992) and can catalyze an ATP-dependent strand exchange between a circular ssDNA molecule and homologous linear dsDNA molecule (Sung 1994; Baumann et al. 1996; Namsaraev and Berg 1997). It works by first polymerizing onto DNA in a right-handed helical filament and then stretching the DNA to 18.6 bps per turn from 12.5 bps per turn (Ogawa et al. 1993). This extension is thought to facilitate the accessibility of the bps within the filament for fast and efficient strand exchange (Nishinaka et al. 1998; Klapstein et al. 2004; Chen et al. 2008b). Importantly, it is responsible for searching within the cell for homology with the 3' overhang in a timely manner. Single-molecule analyses of RecA filaments have suggested that Rad51 may accomplish this feat through both an 'intersegmental contact sampling model' that consists of the filament sampling multiple disconnected dsDNA segments simultaneously (Forget and Kowalczykowski 2012) and a 'sliding model' that recognizes that the filament can diffuse along dsDNA at a rate of 7700 bp^2/second, which allows the

filament to sample several hundred bps before dissociating (Ragunathan et al. 2012). Once a homologous sequence is found, the Rad51 nucleoprotein filament performs a strand invasion into the DNA duplex (McIlwraith et al. 2000) and catalyzes the bp exchange that leads to a heteroduplex structure that forms a displacement loop (D-loop). In mitotic cells, the invaded strand will usually be the sister chromatid, which will have an identical sequence to the damaged site. Conversely, in meiotic cells, the invaded strand will typically be from the homologous chromosome, which may have a similar sequence but will not necessarily be identical. Importantly, the formation of a Rad51 filament also strongly inhibits Rad51-independent Rad52-mediated strand annealing (Wu et al. 2008b).

1.1.5 Postsynapsis and resolution of recombination intermediates

Following strand invasion, a DNA polymerase will use the invaded duplex as a template to extend the end of the invading 3' overhang to synthesize new DNA and copy the genetic information that was lost due to the DSB. The subsequent steps to resolve the heteroduplex structure will then vary depending on the particular HR pathway used. The differences are outlined below.

1.1.5.1 D-loop disruption

D-loop disruption may be catalyzed by DNA helicases. In yeasts and mammals, Fml1/Mph1/FANCM, Srs2, and the RecQ-type helicases Rqh1/Sgs1/BLM-WRN-RECQ1-RECQ4-RECQ5 have all been shown to

promote D-loop unwinding (Sharma et al. 2005; Bachrati et al. 2006; Dupaigne et al. 2008; Sun et al. 2008; Lorenz et al. 2009; Prakash et al. 2009; Bernstein et al. 2010; Lorenz et al. 2012), and thus, may all play a role in promoting SDSA. Interestingly, Rad54 has also been shown to disrupt D-loops *in vitro* despite the fact that it lacks classical helicase activity (Bugreev et al. 2007). Srs2, a 3' to 5' helicase (Rong and Klein 1993), can additionally promote SDSA by disrupting the Rad51 nucleofilament to prevent engagement or invasion of the second end with the invaded strand (Dupaigne et al. 2008). The idea that these helicases have a role in SDSA is further supported by genetic data that shows an increase in crossover events in yeast cells with the genes encoding Fbh1, Fml1/Mph1, Rqh1/Sgs1 or Srs2 deleted (Ira et al. 2003; Morishita et al. 2005; Robert et al. 2006; Sun et al. 2008; Prakash et al. 2009; Bzymek et al. 2010; Lorenz et al. 2012). Interestingly, unlike fission yeast, budding yeast lack an FBH1 ortholog (Chiolo et al. 2007), which may suggest that these helicases are partially redundant in this process. The fundamental importance of these helicases, however, is underlined in humans as the FANCM and RecQ-type helicases, BLM, WRN, and RECQ4 have been genetically linked to the autosomal recessive diseases, Fanconi anemia and Bloom's, Werner's, and Rothmund-Thomson Syndrome, respectively, which are associated with chromosomal instability, congenital defects, mental retardation, premature aging, and increased susceptibility to cancer (Ellis et al. 1995; Yu et al. 1996; Gray et al. 1997; Kitao et al. 1999; Kennedy and D'Andrea 2005).

1.1.5.2 Double Holliday junction resolution

dHJ resolution can lead to both crossovers and noncrossovers depending on how the two HJs are cleaved. HJs can be cleaved by a resolvase that cuts the two non-crossed strands or the two crossed strands. If these cuts are done in the same manner for both HJs, they lead to noncrossovers; however, if these cuts are performed in the opposite manner, they lead to crossovers. In *E. coli*, the classical HJ resolvase is RuvC, which has been found to resolve HJs through a nick and counter nick mechanism in which incisions are made in symmetrically related strands of like polarity at or close to the junction point (Iwasaki et al. 1991; Bennett and West 1995). RuvC works in a complex with RuvA and RuvB, which are responsible for targeting the complex to HJs and driving branch migration to allow RuvC to scan potential cleavage sites (van Gool et al. 1999). The final cleavage of a HJ by RuvC occurs preferentially at consensus sites in a mechanism similar to restriction enzymes (Shah et al. 1997).

It took many years before HJ resolvases were identified in eukaryotes; however, in the last 15 years, a series of structure-specific nucleases have been shown to cleave HJs *in vitro*. In budding yeast and human cells, Yen1 and GEN1, respectively, have been shown to be functionally similar to RuvC (Ip et al. 2008). GEN1 is a monomeric 5'-flap endonuclease that dimerizes on HJs to make symmetrical nicks on noncrossing strands thereby resolving them (Rass et al. 2010). Curiously, there is no GEN1 ortholog in fission yeast, but the endonuclease Mus81-Eme1 (Mus81-Mms4 in budding yeast and

MUS81-EME1 in mammals) may fill this functional niche. In meiotic cells, Mus81-Eme1 plays a central role in fission yeast in cleaving recombination intermediates to form crossovers (Osman et al. 2003; Smith et al. 2003). Mus81-Eme1, however, does not preferentially cleave four-way HJs, but prefers nicked HJs and D-loops (Osman and Whitby 2007). Another structure-specific endonuclease complex that has been identified in yeast and humans is Slx1-Slx4 (Fricke and Brill 2003; Coulon et al. 2004; Andersen et al. 2009; Fekairi et al. 2009; Munoz et al. 2009; Saito et al. 2009; Svendsen et al. 2009). Biochemically, Slx1-Slx4 interact and have Y junction, 5' flap, and HJ endonuclease activity that resides within Slx1 (Fricke and Brill 2003). Interestingly, there is evidence that shows that HJ resolvases, such as Mus81-Mms4 and Yen1, are not activated until G2/M phase, which suggests that dHJs may primarily be dissolved and potentially only cleaved as a backup mechanism if the dHJ persists towards the end of mitosis (Matos et al. 2011).

1.1.5.3 Double Holliday junction dissolution

Unlike dHJ resolution, dHJ dissolution exclusively leads to noncrossovers. This noncrossover pathway is initiated through the convergent branch migration of the two HJs, which can be performed by Rqh1 in fission yeast and its counterparts, Sgs1 in budding yeast and BLM in mammals (Wu and Hickson 2003). This leads to a hemicatenane intermediate, which topoisomerase III can decatenate (Hiasa et al. 1994). The evidence supporting this pathway includes: crossover events increasing when the RecQ-type helicase is deleted in yeast (Ira et al. 2003; Hope et al. 2007), the

inviability of *top3* deletion in yeast being suppressed by concurrent loss of *rqh1* helicase activity (Maftahi et al. 1999; Laursen et al. 2003), and the physical interaction between the two proteins (Bennett et al. 2000; Wu et al. 2000; Ahmad and Stewart 2005). The latter of which importantly, has been shown to work together to dissolve dHJ intermediates (Wu and Hickson 2003) in a complex that also includes Rmi1 (Mankouri and Hickson 2007). The importance of dHJ dissolution is exemplified through the elevated levels of inter-sister chromatid exchange that manifest in BLM deficient patients (Wu and Hickson 2003).

1.2 DNA replication and the strategies cells employ to overcome DNA impediments

The faithful transmission of the genetic information encoded in chromosomes to successive cellular generations depends on accurate replication. To maintain genome integrity, the cell must ensure that it duplicates its entire DNA exactly once; however, this is not without complications. In fact, the ten DSBs that human cells experience during each cellular division mainly arise from problems during replication (Haber 1999). Furthermore, activated oncogenes have been found to induce stalling and collapse of replication forks in precancerous lesions and cancers, which give rise to DSBs and genomic instability (Halazonetis et al. 2008). Although there are error-prone mechanisms, such as translesion synthesis (TLS), which can rescue stalled replication forks at the expense of replication fidelity, there are also error-free mechanisms for replication to bypass lesions or to remove the blockage and

then resume/restart DNA synthesis. Following a discussion of the basic molecular mechanism of DNA replication, I will give examples of the different impediments DNA replication forks may encounter and then outline the various molecular strategies cells have at their disposal to deal with them.

1.2.1 Fundamentals of DNA replication

DNA replication is initiated at specific loci called replication origins, whereby sister replication forks emanate and move bidirectionally away from the origin (Figure 1.7). Replication begins when the Origin Recognition Complex (ORC), which recruits the pre-replication complex (pre-RC), binds to a replication origin and licenses it for firing. Not all origins of replication that are licensed end up firing. If the origin does fire though, then the double helix is unwound to form a replication bubble at which the replicon, consisting of two sister replication forks, will be assembled. Each replication fork proceeds with a large complex, known as the replisome, which includes DNA helicases, polymerases, and accessory proteins, such as proliferating cell nuclear antigen (PCNA) and replication factor C (RFC) (Waga and Stillman 1998). The replicative helicase unwinds the dsDNA into single strands to establish the replication fork, so that each strand can be copied by polymerases. Due to the antiparallel structure of DNA and the fact that DNA polymerases synthesize DNA only in the 5' to 3' direction, one strand is replicated continuously in the same direction of the replication fork, while the other strand is replicated discontinuously in the opposite direction of the replication fork. These strands are known as the leading and lagging strands,

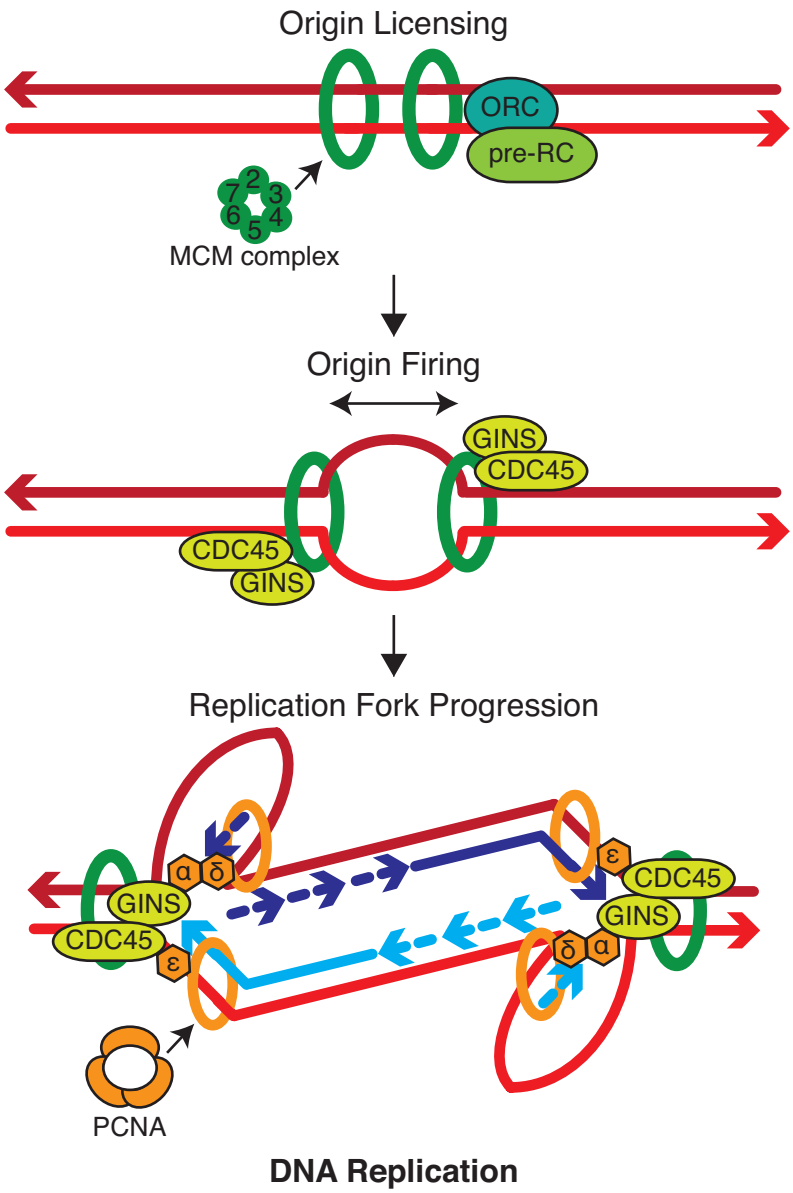


Figure 1.7 | DNA replication proceeds bidirectionally from origins of replication. DNA Replication begins when origins of replication are licensed by the MCM2-7, ORC, and pre-RC complexes. Upon activation, a proportion of licensed origins will fire following the recruitment of CDC45 and GINS. This leads to DNA unwinding and replisome loading to initiate DNA replication. The GINS complex maintains interactions within the replisome, which contains the MCM2-7 and CDC45 replicative helicase, the sliding clamp PCNA, and DNA polymerases Polα, Polδ and Polε – the latter two polymerases replicate the lagging (dashed blue lines) and leading strands (continuous blue lines) respectively.

respectively. The discontinuously synthesized fragments on the lagging strand are known as Okazaki fragments, and the nicks between them are ligated to complete lagging strand replication. In contrast to most prokaryotes, which only have one replication origin, eukaryotes have many origins of replication distributed along linear chromosomes. Replication forks that arise from these origins of replication then must converge in a process called termination to complete replication. Thus if a single fork becomes blocked, the unreplicated portion could be duplicated by the fork emanating from the adjacent origin to complete replication.

In budding yeast, the MCM complex, composed of Mcm2 – Mcm7 subunits, serves as the replicative helicase with the help of accessory factors Cdc45 and GINS, which maintain the protein-protein interactions within the replisome (Maiorano et al. 2006). Together, Cdc45, MCM, and GINS constitute the CMG complex, which, further to its role in replication fork progression, also has a role in initiating replication at origins. RFC, composed of Rfc1 – Rfc5 subunits, is a clamp-loading complex that recognizes ss/dsDNA junctions and loads the replicative helicase and PCNA (Majka and Burgers 2004). PCNA forms a homotrimeric complex and acts as the DNA polymerase clamp that maintains the speed and processivity of DNA polymerases during replication. DNA synthesis is initiated through the primase activity of Polα, which synthesizes a short (~ 10 bp) RNA primer. Polα is substituted by Polδ and Polε on the lagging and leading strand, respectively, in a manner that is regulated by RFC and PCNA (Miyabe et al. 2011). On the lagging strand, the RNA primers are

displaced by Polδ and processed by the flap endonuclease activity of FEN1 (flap endonuclease 1) and Dna2, which act on uncoated and RPA-coated flaps, respectively (Kang et al. 2000; Stewart et al. 2008; Stewart et al. 2009).

In eukaryotes, replication termination involves the convergence of two forks, which generates catenated sister chromatids that require resolution by DNA topoisomerase II (DiNardo et al. 1984). A failure to decatenate sister chromatids results in the formation of DNA anaphase bridges between daughter nuclei during anaphase and may result in DNA breakage (Chan et al. 2007; Rouzeau et al. 2012). In humans, anaphase bridges are resolved by either TOPII or the concerted actions of the dHJ dissolution complex, BLM-TOPIIIα-RMI1 (Chan et al. 2007). Importantly, chromosome fragments resulting from breakage of anaphase bridges can give rise to micronuclei, which can persist through several cell cycles. The DNA within micronuclei appears to experience high rates of damage and rearrangement resulting from elevated levels of replication stress. Upon reassimilation into the main nucleus such derivative chromosomes could drive tumorigenesis. Indeed the phenomenon of chromothripsis, which is associated with some cancers, is thought to occur by such a mechanism of micronuclei formation and re-assimilation (Hoffelder et al. 2004; Crasta et al. 2012).

1.2.2 Impediments to DNA replication

Although replication complexes are highly processive, they rarely complete genome replication without encountering a lesion that has potential to cause

its stalling or collapse (Sandler and Marians 2000; Lambert and Carr 2013). Fork stalling is defined as an arrested replication fork that remains associated with the DNA and maintained in a configuration that may resume progression following removal of the replication barrier, whereas fork collapse entails replisome components not stably being maintained at an arrested fork, such that resumption is impaired and other factors must act to aid in reloading the replisome components to restart replication. Note that a collapsed fork can become a broken fork, where there is a one-ended DSB, but not all collapsed forks are broken. Alternatively, if replication is not restarted at a stalled or collapsed fork, the fork structure needs to be maintained in a configuration that will be capable of merging with the opposing fork.

Examples of accidental blockades include various types of damage to the DNA template, such as strand breaks, UV photodimers, and ICLs. Additionally, replication fork progression can be impeded by unusual or repetitive DNA sequences/structures, such as G-quartets and palindromic sequences that form hairpins and triplet repeats (Voineagu et al. 2008; Paeschke et al. 2011). DNA at stalled replication forks is susceptible to breakage by torsional stress or cleavage by enzymes. Interestingly, the same barriers that block replication forks can also interfere with transcription complexes that concurrently occupy the DNA template. If this occurs, RNA polymerases will stall, reverse translocate, which leads to the displacement of the 3’ end of the growing transcript from the active site, and become a more stable, inactivated complex that inadvertently becomes a barrier to the

replisome (Park et al. 2002). Thus, there is also an inevitable conflict between genome duplication and gene expression, particularly as DNA replication complexes move faster than transcription complexes, ~ 1000 bp/second (Hirose et al. 1983) vs. 50 nucleotides/second (Gotta et al. 1991) in *E. coli*, leading to co-directional and head-on collisions (Pomerantz and O'Donnell 2010; Merrikh et al. 2011; McGlynn et al. 2012).

Due to the discontinuous nature of lagging strand synthesis, lesions on the lagging strand may stop extension of a single Okazaki fragment, but should not stop replication as new Okazaki fragments can continue to be synthesized. In contrast, lesions on the leading strand are believed to stop leading strand synthesis since leading strand synthesis is naturally continuous; however, it was recently shown that leading strand synthesis could also tolerate some lesions, such as pyrimidine dimers, through discontinuous synthesis without the replisome dissociating in an event that is independent of any known replication-restart proteins (Lopes et al. 2006; Yeeles and Marians 2011). Nicks on either strand of the DNA template, however, can cause DSBs as the leading strand polymerase or the replicative helicase, which encircles the lagging strand template (Yuzhakov et al. 1996), could run off the template and result in a collapsed replication fork (Cox 2001; Cortes-Ledesma and Aguilera 2006).

Lesions that interfere with strand separation, which inhibit the progression of the replicative helicase, include ICLs, protein-DNA complexes, and a subset

of DNA secondary structures. Replication fork blockage at both accidental and programmed DNA–protein barriers can induce recombination events to restart replication, which in turn can cause genomic rearrangements that can be deleterious (Ahn et al. 2005; Lambert et al. 2005; Mizuno et al. 2009; Lambert et al. 2010; Jacome and Fernandez-Capetillo 2011; Sofueva et al. 2011; Steinacher et al. 2012). However, not all replication fork stalling induces recombination (Calzada et al. 2005), and even when it does, the outcome can differ. For example, UV-induced lesions strongly promote gene conversion between direct repeats, whereas CPT induces deletions (Ahn et al. 2005).

1.2.3 Programmed DNA replication perturbations

Surprisingly, cells have exploited the mutagenic potential of recovering from DNA replication perturbations to drive certain biological processes, which particularly rely on changes to specific genes for survival. One such process is discussed below.

1.2.3.1 Mating-type switching in yeast

S. pombe cells exist as one of two mating types, plus (P) or minus (M), and during mitotic growth, they can efficiently switch between mating types during a programmed DNA rearrangement induced by a stalled replication fork (Miyata and Miyata 1981; Egel et al. 1984; Arcangioli 1998; Dalgaard and Klar 1999). In fission yeast, the expressed mating type at the *mat1* locus can be replaced through gene conversion with information of the opposite mating type, which will be at one of the two transcriptionally silenced donor loci,

mat2P and *mat3M* (Figure 1.8A). This switch depends on an imprint formed when two ribonucleotides are incorporated into the DNA during lagging strand synthesis of the *mat1* cassette at the junction adjacent to the *H1* homology domain, which in the next round of replication, leads to a break in the one daughter that inherits the imprint when the leading strand replication complex encounters it (Arcangioli 1998; Dalgaard and Klar 2000; Holmes et al. 2005; Vengrova and Dalgaard 2006). This break initiates recombination between *mat1* and the opposite silent donor locus that leads to switching of the mating type (Klar 1990; Yamada-Inagawa et al. 2007). This programmed recombination event proceeds through SDSA as the 3' end of the *H1* homology domain of the *mat1* locus invades the *H1* domains of one of the two donor cassettes, where it is then extended across the donor locus until it reaches the *H2* domain and then displaced for annealing to the homologous *H2* domain in the *mat1* locus (Arcangioli and de Lahondes 2000; Yamada-Inagawa et al. 2007). Interestingly, the directionality of switching is controlled by the location, rather than the content, of the silent cassettes in the chromosome as swapping of the content in the *mat2* and *mat3* locus lead to inefficient mating-type switching (Thon and Klar 1993). This directionality is mediated by the Swi5-Swi2 complex, which exhibits mating type-specific localization patterns whereby in P cells, it exclusively localizes adjacent to the *mat3M* locus, but in M cells, it is distributed across the entire silent mating type interval, including the mat2P locus (Jia et al. 2004). The Swi5-Swi2 localized on the donor loci stabilizes the Rad51-filament during mating-type switching (Akamatsu et al. 2003).

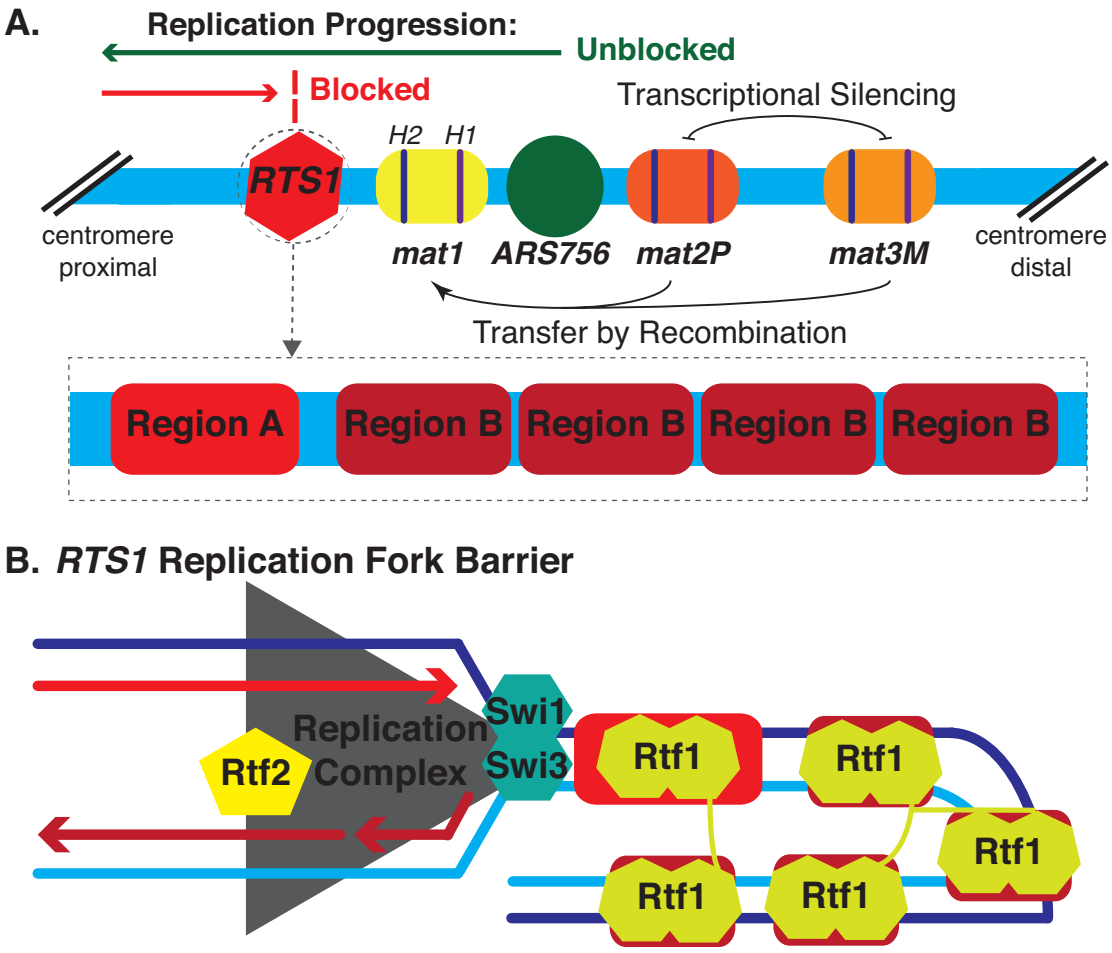


Figure 1.8 | The *RTS1* replication fork barrier facilitates mating-type switching at its natural locus in fission yeast. (A) Cartoon depicting the endogenous mating type locus on chromosome II. The expressed mating type is encoded at the *mat1* locus. During mating-type switching, it can be replaced through gene conversion with information of the opposite mating type from one of the two transcriptionally silenced donor loci, *mat2P* and *mat3M*. The strand invasion reaction is facilitated through homology box regions named *H1* and *H2*, which are represented in light and dark purple lines, respectively. They are found in all three mating type cassettes. As a polar RFB, *RTS1* optimizes the switch by enforcing replication across the region in the centromere-proximal direction by blocking replication in the centromere-distal direction. The *cis*-acting sequences of the *RTS1* element include an enhancer region and four repeated motifs named Region A and Region B, respectively, that cooperate together for efficient barrier activity. (B) Cartoon depicting the termination of replication forks at the *RTS1* barrier, which is also dependent on the four *trans*-acting factors: Rtf1, Rtf2, Swi1, and Swi3.

1.2.4 Protein-DNA barriers

Interestingly, cells have also evolved programmed protein-DNA barriers to act as polar DNA RFBs to ensure that replication occurs in a unidirectional direction across certain loci for specific purposes. In some instances, these programmed RFBs are employed to prevent potentially more catastrophic problems from arising, such as DNA re-replication of chromosomes and clashes between the transcription and replication machineries. Three of the most extensively studied protein-DNA barriers are discussed below.

1.2.4.1 Tus-*ter* barrier in *Escherichia coli*

Because prokaryotic DNA replication is initiated at only a single origin of replication with two replication forks moving bidirectionally around the circular genome, a blocked replication fork is arguably more dangerous in *E. coli* than in eukaryotes. Despite this, more than halfway in each direction there are specific termination sites, *terA* – *terF*, bound by the Tus protein that unidirectionally block replication forks by preventing the unwinding of DNA by the replicative helicase DnaB (Khatri et al. 1989; Hill and Marians 1990). The Tus-*ter* barrier ensures that the bidirectional forks originating from the origin converge at one point to primarily prevent instances of over-replication (Hiasa and Marians 1994). Interestingly, at forks blocked at the Tus-*ter* barrier, the leading strand is 50 – 70 nucleotides longer than the lagging strand (Hill and Marians 1990). In prokaryotes, when there is persistent ssDNA in the cell, usually arising as a consequence of unreplicated regions resulting from stalled forks, the SOS response is induced (Janion 2008). This response

regulates transcription of proteins required for reinitiation of stalled replication forks, which are also involved in NER, HR, and TLS. The kinetics of the SOS response ensures that NER removes the majority of lesions, recombination is used when NER is insufficient, and error-prone TLS is avoided as long as possible (Berdichevsky et al. 2002; Crowley and Courcelle 2002; McGlynn 2004). At the Tus-*ter* barrier, replication forks remain stable, and the programmed barrier only elicits recombination if the fork from the subsequent round of replication runs into it and generates a DSB (Bidnenko et al. 2002). Surprisingly, the Tus-*ter* barrier has also recently been found to induce polar replication fork pausing when it is introduced into budding yeast in a manner in which neither the Rrm3 sweepase or HR proteins are needed to counteract it (Larsen et al. 2014).

1.2.4.2 *Fob1* barrier in *Saccharomyces cerevisiae*

Remarkably, yeasts also exploit RFBs for key biological functions. To avoid head-on collisions between replication and transcription complexes, *S. cerevisiae* employs a specific Fob1 protein-DNA RFB downstream of the highly transcribed and highly repetitive ribosomal DNA (rDNA) regions, which also contain a potential origin of replication, to limit replication in the direction opposite to transcription by arresting replication forks that it encounters (Brewer and Fangman 1988). As a result, replication forks move only in the same direction as transcription. The Fob1 protein-DNA barrier is insufficient for promoting inter/intra-repeat recombination. A key requirement for this is a non-coding bidirectional promoter called E-Pro (Labib and Hodgson 2007).

Interestingly, barriers that maintain rDNA repeat copy number, such as Fob1, are evolutionarily conserved from yeast to humans (Gerber et al. 1997).

1.2.4.3 *RTS1* barrier in *Schizosaccharomyces pombe*

In *S. pombe*, the *RTS1* (Replication Termination Sequence 1) barrier is employed for efficient mating-type switching that occurs through a replication-coupled recombination event (Dalgaard and Klar 2001). *RTS1* promotes this process as a polar replication terminator that enforces unidirectional replication of the *mat1* locus in the centromere-proximal direction by blocking forks moving in the centromere-distal direction, which optimizes the occurrence of the imprint (Figure 1.8). *RTS1* consists of four repeated 55 bp motifs named region B and an ~ 60 bp enhancer region called region A that cooperate together for efficient replication termination (Codlin and Dalgaard 2003). The function of *RTS1* is also dependent on proteins, which include Rtf1 (Replication Termination Factor 1), Rtf2, Swi1, and Swi3. Rtf1 binds to the four repeated motifs as well as the enhancer region A, and self-interacts through its C-terminal tail to stabilize the interactions and, additionally, provide constraints to the unwinding of the DNA template by the approaching replicative helicase (Eydmann et al. 2008). Rtf2 stabilizes the stalled fork at *RTS1* by preventing replication fork collapse and Srs2-dependent replication restart so that DNA replication is completed by a converging replication fork that is initiated at a flanking origin arriving at the site (Inagawa et al. 2009). The remaining two factors, Swi1 and Swi3, move with the replication fork as part of the Replication Progression Complex and serve critical roles at *RTS1*

by protecting the replication fork and stabilizing stalled forks (Dalgaard and Klar 2000; Noguchi et al. 2004).

1.2.5 Responses to replication fork perturbation

The various obstacles on the DNA template raise different issues for the replication complex, such as blocked progression of the helicase or replicative polymerase and/or decoupling of leading and lagging strand synthesis. In any case, resumption of replication will depend on the lesion being removed or bypassed. Therefore, the nature of the lesions will lead to a preferential means to resolve it. These responses are discussed below.

1.2.5.1 Post-replicative repair

In certain situations, the replication fork does not collapse when encountering a lesion and instead can skip the lesion. Consequently, this generates a gap while the fork continues to replicate past the lesion (Rupp and Howard-Flanders 1968). This scenario could arise from a lesion in the lagging strand template, which would only block the extension of one Okazaki fragment, but have no effect on the progression of the replisome as a whole (Langston and O'Donnell 2006). In this case, HR can mediate the repair post-replicatively so that the gap opposite the lesion can be filled through the use of the replicated sister chromatid as the template (Lopes et al. 2006) (Figure 1.9). Instead of a resection step to generate the 3' tail, this process proceeds through the 3' end of the gapped strand invading the sister chromatid. Following D-loop formation, the 3' end is extended by a polymerase. The D-loop can then be

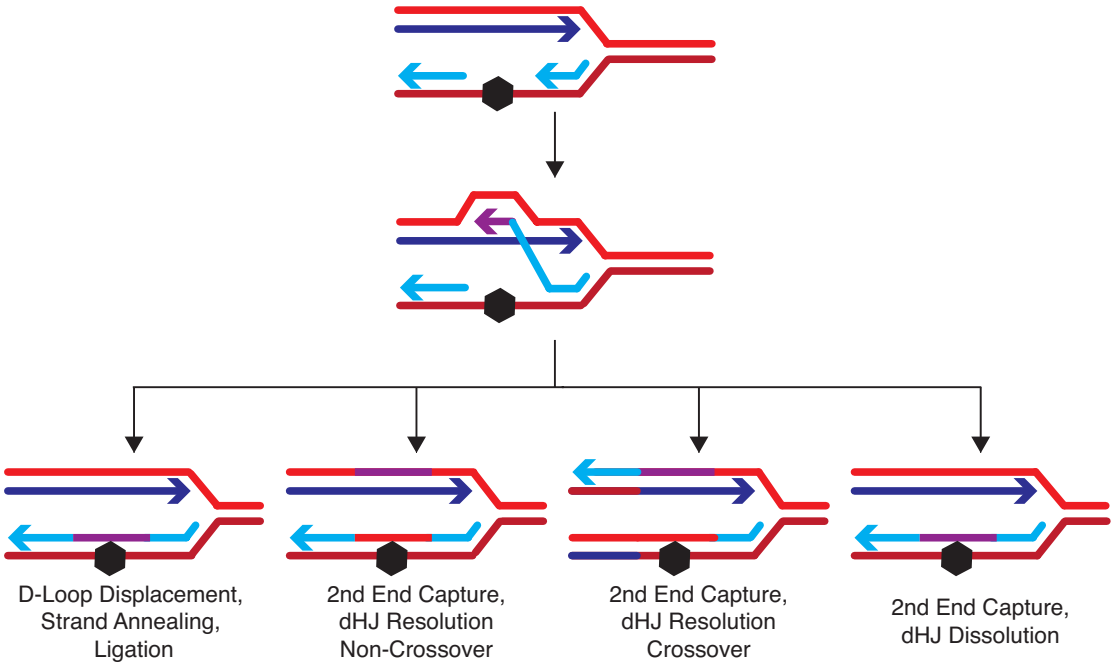


Figure 1.9 I Single-strand DNA gaps remaining following DNA replication can be repaired post-replicatively. Lesions that are skipped during DNA replication, particularly in the lagging strand, can lead to ssDNA gaps in the chromosome. These gaps can be filled through a post-replicative repair process that is dependent on recombination factors. Using the 3' end of the gapped strand, the 3' tail can invade the sister chromatid, which is used to copy information to fill in the gap. The recombination intermediate is then resolved in a variety of ways resulting in different outcomes. Refer to the text for more details.

displaced. Alternatively, if second-end capture occurs, dHJ resolution or dissolution can resolve the intermediate structure.

1.2.5.2 Translesion synthesis

If the homology directed pathway is not employed to skip the lesion, then alternatively, TLS may occur through the use of a specialized DNA polymerase that inserts a nucleotide opposite the lesion (Reuven et al. 1998; Tang et al. 1999) (see Figure 1.10). In eukaryotes, PCNA provides the scaffold to give one of the five different polymerases that have been implicated in TLS, which include Polη, Polι, Polκ, Polζ, and Rev1, access to the replication site at the lesion (Prakash et al. 2005). However, in contrast to HR-mediated post-replicative repair, TLS is prone to generate mutations because TLS polymerases have relatively large active sites, which accommodate DNA mismatched bps, and lack proofreading exonuclease activity (Yang and Woodgate 2007).

1.2.5.3 Template-switch mediated lesion bypass

In certain cases, the lesion cannot be directly skipped but can be bypassed when the polymerase switches template strands through the remodeling and regression of the stalled fork into a chicken foot structure (see Figure 1.10). This occurs when the two nascent DNA strands anneal to each other to form a HJ between the newly formed sister chromatids (Higgins et al. 1976; Postow et al. 2001; Sogo et al. 2002). These chicken foot structures are considered pathological as they are very rarely observed in wild-type cells but they are

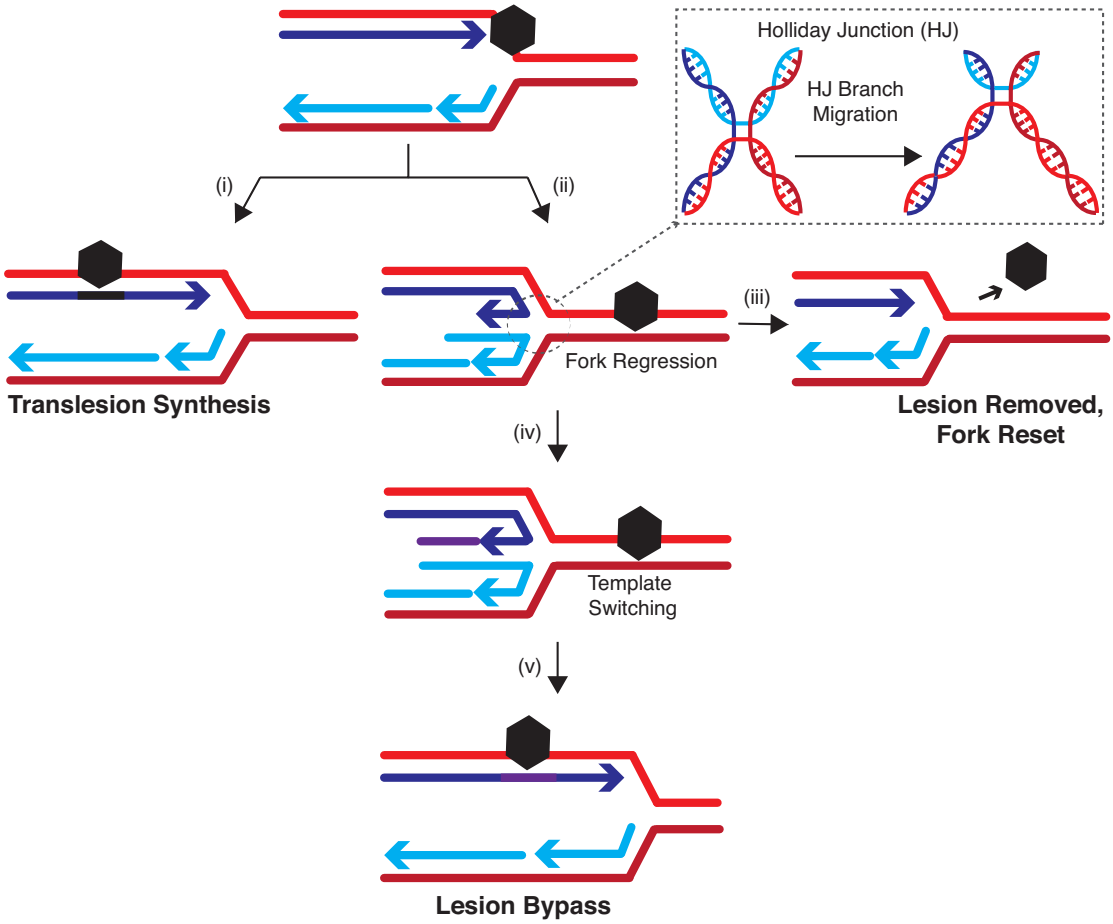


Figure 1.10 I Stalled replication forks can be rescued by various pathways. Lesions on the leading strand can block progression of the helicase or replicative polymerase and/or decouple leading and lagging strand synthesis. If a translesion polymerase is not used to prime opposite the lesion (i), recombination proteins can intervene and catalyze fork regression (ii) and form a Holliday junction (HJ), also known as a chicken foot structure (Higgins et al. 1976; Postow et al. 2001; Sogo et al. 2002). This may provide room for factors to remove the lesion and the fork can simply be reset (iii). Alternatively, if the lagging strand synthesized beyond the respective position of the lesion on the leading strand, the leading strand can switch templates and copy information from the lagging strand (iv) and through branch migration, bypass the lesion (v).

more readily detected in *rad53Δ/cds1Δ* checkpoint deficient cells (Lopes et al. 2001; Hu et al. 2012). However, the process of fork regression at a stalled fork has been reproduced *in vitro* with T4 bacteriophage enzymes, supporting the notion for fork regression as a lesion bypass strategy (Manosas et al. 2012). This branch migration into a HJ can be catalyzed by DNA helicases and translocases, and the HJ can also be reset by them.

Although deemed as pathological structures, there is growing evidence that the chicken foot can serve as a productive role in the processing of perturbed replication forks. Firstly, fork reversal may provide room for lesion repair to occur, following which the reversed fork may be reset to enable the resumption of DNA synthesis (Courcelle et al. 2003). If the lesion cannot be removed, however, then fork reversal can offer the opportunity for lesion bypass if the lagging strand polymerase has proceeded beyond the position in which the leading strand polymerase has been blocked through a template switching mechanism. In this scenario, the 3' tail from the leading strand copies information from the overhanging 5' ssDNA tail from the lagging strand. Note that no mutations are introduced during template switching as the lagging strand contains precisely the same information as the "original" template strand of the leading strand. This allows the leading strand to bypass the lesion following reversal of the chicken foot structure. If the template switching mechanism is not used following fork reversal, the chicken foot structure can alternatively be used to prime a recombination-dependent restart process (see Section 1.2.5.8).

In budding yeast, the choice between error-prone translesion DNA synthesis and error-free lesion bypass by some type of template switching mechanism is partly governed by the posttranslational modification of PCNA. PCNA is a homotrimeric sliding clamp for various DNA replication polymerases and serves as a scaffold for many DNA repair and recombination proteins. In budding yeast, its monoubiquitylation, polyubiquitylation, or SUMOylation has different signaling effects. Protein ubiquitination involves an E1 activating enzyme, which passes the ubiquitin protein to an E2 conjugating enzyme. E2 forms a complex with an E3 ubiquitin ligase, which catalyzes the transfer of ubiquitin onto the targeted protein. When PCNA is monoubiquitylated on lysine 164 in response to DNA damage by the Rad6-Rad18 E2-E3 complex, the TLS polymerase, Polη, has increased affinity for PCNA and TLS becomes favored (Haracska et al. 2001; Prakash et al. 2005). This increased affinity is attributed to Polη containing a specialized ubiquitin-binding domain, the UBZ domain, which allows it to bind the ubiquitin on PCNA (Bienko et al. 2005). Following TLS, PCNA is deubiquitinated by USP1-UAF1, which is a critical step to prevent error-prone TLS polymerase mutagenesis during normal cell division (Huang et al. 2006). If the monoubiquitylated form of PCNA, however, then becomes polyubiquitylated though lysine 63 ubiquitin linkages by the Rad5/Mms2-Ubc13 heterotrimer, error-free post-replicative repair is signaled by an unknown mechanism (Hofmann and Pickart 1999). Polyubiquitylated PCNA can serve as a docking site for proteins with ubiquitin-binding domains and thereby can recruit proteins that promote lesion bypass. Alternatively, PCNA can also be SUMOylated at lysine 164 and/or lysine 127 by the Ubc9-

Siz1 E2-E3 complex, which leads to the recruitment of the antirecombinase Srs2 (Papouli et al. 2005; Pfander et al. 2005). The fact that Rad51 becomes enriched at replication forks in a *srs2Δ* mutant indicates that Srs2 disrupts Rad51 filament formation *in vivo* (Papouli et al. 2005). Thus, this SUMOylation of PCNA can restrict recombination at stalled replication forks, and may in conjunction with its ubiquitination ensure that Rad5-mediated lesion bypass operates without the interference of an extensive Rad51 nucleofilament (Hoege et al. 2002).

Interestingly, in contrast to budding yeast, the fission yeast Srs2 does not contain the C-terminal region that is known to interact with SUMOylated PCNA, which may suggest that recombination is inhibited by another mechanism (Watts 2006). In fission yeast, Fbh1 has also been reported to be a Rad51 disruptase at blocked replication forks (Lorenz et al. 2009). This is supported by the fact that in an *fbh1Δ* mutant, there is an increase in spontaneous Rad51 foci and Rad51-dependent recombination intermediates induced by UV irradiation (Morishita et al. 2005). Through its translocase activity, Fbh1 can similarly strip Rad51 from nucleofilaments (Simandlova et al. 2013) and potentially work in direct opposition to Rad52 during pre-synapsis (Lorenz et al. 2009). Support for Fbh1's role in opposing mediating Rad51 nucleofilament formation is exemplified in the reduced viability of *fbh1Δ* mutants being suppressed by deletion of any one of the mediator proteins, including Rad52, Rad55, and Swi5 (Osman et al. 2005). Note that in budding yeast, the Shu complex (see Section 1.1.4.5) links error free post replicative

repair to HR by recruiting HR factors to facilitate template switching and lead to recombination intermediates that are ultimately processed by the concerted actions of Sgs1-Top3-Rmi1 as suggested by the severe phenotypes of *sgs1Δ* and *top3Δ* mutants being abrogated by inactivation of any of the Shu complex genes (Ball et al. 2009). Furthermore, the Shu complex physically interacts with the antirecombinase Srs2 and inhibits its Rad51 disassembly role, providing a mechanism for shifting the balance to HR and Rad51 nucleofilament stabilization (Bernstein et al. 2011).

1.2.5.4 Role of checkpoint proteins in fork protection

In response to DNA damage or perturbed replication, eukaryotes activate checkpoint responses to coordinate repair with cell cycle progression or stabilize stalled forks (Lopes et al. 2001). The checkpoint pathway begins when sensors bind and recognize sites of stalled replication or DNA damage, which then leads to the activation of signaling kinase effectors to initiate the response to the obstacle. At the G1/S and G2/M transition, It prevents the entrance into the subsequent phase if there is DNA damage and also prevents mitosis if there is unreplicated DNA. Furthermore, during S-phase, if the template is damaged, it reduces the replication rate and also has a role in preventing fork collapse by counteracting replisome components from dissociating at stalled forks (Trenz et al. 2006). The fork protection role is critical as replisome components are actively dissociated at stalled forks in checkpoint deficient cells (Ragland et al. 2013).

In humans, ATR is the key sensor kinase that leads to the phosphorylation of the CHK1 effector kinase at sites of replication stress upon ATRIP (ATR-interacting partner) recognition of RPA-coated ssDNA (Zou and Elledge 2003). These stretches of ssDNA may occur following impedance of the replicative polymerase and the continued procession of an uncoupled helicase still unwinding the DNA template (Lambert and Carr 2005). Sites of DSBs, on the other hand, are recognized by the ATM sensor, which facilitates a separate checkpoint pathway in humans that involves the CHK2 effector kinase. This ATM-pathway is required for the phosphorylation of MRE11 and NBS1 to initiate the resection process in recombination (Petrini 2000; D'Amours and Jackson 2002) and the phosphorylation of histone H2AX, which is critical for recruiting other repair factors and causing chromatin decondensation (Downs et al. 2000; Burma et al. 2001). ATM and ATR belong to the phosphoinositide-3 kinase-related protein kinase (PIKK) family and act as transducers of the damage signal. In fission and budding yeast, Rad3-Rad26 and Mec1-Ddc2, respectively are the ATR-ATRIP counterparts and Chk1 is the yeast CHK1 ortholog. The yeasts ATM homologs are Tel1, while the CHK2 homologs are Cds1 and Rad53 in fission and budding yeast, respectively. Interestingly, though, the effectors do not strictly have the equivalent function across all species. Specifically, whereas Cds1 responds solely to replication stress in fission yeast, its counterpart in budding yeast, Rad53, responds to both replication stress and non-S-phase related DNA damage. Furthermore, unlike ATM, Tel1 plays an active role in promoting telomere maintenance in yeast (Sabourin and Zakian 2008). In this

introduction, I will mainly focus on the S-phase checkpoint as mediated by human CHK1, fission yeast Cds1, and budding yeast Rad53.

The S-phase checkpoint serine/threonine signaling kinases serve critical roles in the response to stalled replication. The replication checkpoint slows down the replication rate by inhibiting Cdc25-dependent late origin firing and stabilizing stalled replication forks so that they can resume when the impediments are removed, whilst at the same time ensuring that entry into mitosis is delayed (Lambert et al. 2007). Rad53 is the best studied effector kinase. Its role in the maintenance of replication forks that have stalled in the presence of HU or MMS has been well documented (Lopes et al. 2001; Tercero and Diffley 2001). In Rad53's absence, replication forks collapse irreversibly and abnormal replication intermediates form, which include extensive single stranded gaps, hemi-replicated intermediates, and chicken foot structures, as revealed by electron microscopic studies, and these aberrant replication structures can then be processed by unscheduled recombination (Sogo et al. 2002). Indeed, in Rad53 mutant cells, Rad52 foci form promptly following HU treatment, despite not forming in wild-type cells treated with HU, suggesting that collapsed forks expose DNA ends that can be recognized by recombination proteins for recombination-dependent restart (Lisby et al. 2004). These observations have been replicated in fission yeast in the absence of Cds1 with the exception that origin firing may be independent of Cdc25 (Meister et al. 2005; Kommajosyula and Rhind 2006), even though Cds1 and Chk1 have been shown to phosphorylate Cdc25, and

thereby inhibit its activity (Furnari et al. 1999).

Unlike the loss of Rad53 in budding yeast, deletion of *cds1* in fission yeast does not result in lethality, however *cds1Δ* mutants do suffer from decreased viability indicating that it plays an important role in preventing potentially mutagenic replication intermediates following impeded replication even in the absence of exogenously applied genotoxic stress (Liu et al. 1999b). The importance of checkpoints stabilizing stalled forks relates to the fact that since there are multiple origins of replication in eukaryotes, replication can be completed through synthesis of the unreplicated region by the opposing fork of the adjacent origin instead of risking deleterious genomic rearrangements that may result from restart pathways. Accordingly, Cds1 and Rad53 actively block late origin firing when replication is blocked, preventing more forks being blocked and thereby allowing time for DNA lesions to be repaired (Santocanale and Diffley 1998; Shirahige et al. 1998; Kim and Huberman 2001).

Interestingly, independent of the S-phase checkpoint, the MRN complex also has a role in stabilizing the replisome during replication stress by tethering the sister chromatids to maintain their cohesion (Tittel-Elmer et al. 2009). In fact, in terms of fork stability, Rad51, along with its mediator BRCA2 and the ubiquitylated Fanconi anemia protein FANCD2, can protect newly synthesized DNA at stalled replication forks from Mre11-dependent nucleolytic degradation by preventing accumulation of ssDNA, suggesting that recombination proteins

may also have a role in fork protection (Hashimoto et al. 2010; Schlacher et al. 2011; Schlacher et al. 2012).

1.2.5.5 Pushing past barriers using accessory helicases

In addition to the MCM helicase, the replisome contains other DNA helicases that have a critical role in displacing tightly bound non-histone DNA-protein complexes that might otherwise impede the advancing replication fork. A major source of protein-DNA barriers is transcription complexes, which in *E. coli* probably account for the majority of replication fork pausing (Gupta et al. 2013). In budding yeast, Rrm3, which physically associates with the replisome through the leading strand DNA polymerase and/or PCNA, globally promotes replication of protein-bound DNA, particularly at difficult-to-replicate sites, such as the rDNA, centromere, and telomere (Ivessa et al. 2002; Schmidt et al. 2002; Ivessa et al. 2003; Azvolinsky et al. 2006). In fact, Rrm3 is required for preventing replication forks from pausing and/or breaking at an estimated 1,400 loci containing natural RFBs in the budding yeast genome (Ivessa et al. 2003). Beyond minimizing the frequency and/or duration of fork pausing, the importance of accessory helicases is underscored by their role in repressing the need for recombination-dependent restart of blocked replication forks, which could result in gross chromosomal rearrangements (Ivessa et al. 2003; Torres et al. 2004). The Rrm3 homolog in fission yeast is Pfh1, which has a similar role in promoting DNA replication through hard-to-replicate sites and suppressing genome instability (Sabouri et al. 2012; Steinacher et al. 2012).

1.2.5.6 Overcoming interstrand crosslinks

ICLs consist of covalent linkages between the two DNA template strands and can cause cell death by disrupting replication and transcription. When a replicative helicase encounters an ICL, it is unable to unwind the two parental strands, yet surprisingly, DNA combing has revealed that the replisome is still able to traverse the ICL via an unknown mechanism that is dependent on the translocase activity of the FANCM helicase, which is aided by the MHF complex, leaving the ICL behind the replisome for subsequent repair (Huang et al. 2013). In humans, the inability to repair ICLs is manifested in Fanconi anemia patients, whose cells are hypersensitive to crosslinking agents, such as cisplatin and mitomycin C (Sasaki and Tonomura 1973; Sasaki 1975). Because ICLs affect both strands, it cannot simply be repaired through excision, but instead, involves the concerted action of NER, HR, and TLS (Mirchandani and D'Andrea 2006). In short, when two replication forks converge on an ICL, a complex, which includes FANCM, MHF1, and MHF2, will recognize the stalled replication fork structure and recruit the FA core complex (FANCA, FANCB, FANCC, FANCE, FANCF, FANCG, FANCL) (Ciccia et al. 2007). In response to DNA damage or replication arrest, FANCD2 is phosphorylated by the ATR kinase (Taniguchi et al. 2002b; Andreassen et al. 2004) and then the FANCL subunit, which is an E3 ligase, monoubiquitinates FANCD2 and FANCI. The monoubiquitylation of FANCD2 and FANCI helps with the recruitment of the proteins to sites of damage by proteins with ubiquitin binding domains and leads to the recruitment of multiple nucleases, such as ERCC1-XPF and MUS81-EME1, which can

create an incision that unhooks the crosslinked nucleotides from one of the strands. TLS then bypasses the lesion through the aid of FANCJ unwinding secondary structures and coordinating the switch to the TLS polymerase (London et al. 2008; Wu et al. 2008c; Sarkies et al. 2012), and another incision is made to create a DSB, which is then repaired by HR. The link between the FA pathway and HR is through the interaction of FANCD2 with BRCA1 and RAD51 (Garcia-Higuera et al. 2001; Taniguchi et al. 2002a). Furthermore, the tumor suppressor FANCD1 (BRCA2) directly promotes the loading of RAD51 for filament formation and together with FANCN (PALB2) mediates D-loop formation following strand invasion. Interestingly, cells from Fanconi anemia patients are not severely defective in HR repair of DSBs but are profoundly defective in ICL-induced HR (Nakanishi et al. 2005; Nakanishi et al. 2011). Finally, the crosslinked nucleotides are removed by NER (Wang 2007). Following repair, FANCD2 and FANCI are deubiquitinated by the USP1-UAF1 complex, which prevents monoubiquitylated FANCD2 and FANCI accumulation and disassembles the FA core complex from the chromatin (Cohn et al. 2007; Oestergaard et al. 2007). Note that USP1-UAF1 is downregulated in response to DNA damage to allow for the increased levels of monoubiquitylated FANCD2 and FANCI. Only a subset of FANC-related proteins are conserved in yeast, and these include FANCM, MHF1, MHF2, FANCJ (Chl1) and FANCP (Slx4) (McHugh et al. 2012).

1.2.5.7 PriA-directed replication fork restart in *Escherichia coli* and recombination-dependent replication in Bacteriophage T4

The interplay between recombination and replication is best understood in *E. coli*. When a replication fork arrests in *E. coli*, the replisome is believed to collapse by default because there are no mechanisms, such as checkpoint responses, to stabilize it, which highlights the importance of an error-free recombination-dependent replication (RDR) pathway. A broken fork structure can then be generated by RuvABC cleavage of the four-way DNA junction that forms as a consequence of fork reversal (Seigneur et al. 1998; Seigneur et al. 2000). Resection of the broken DNA, followed by strand invasion into the intact homologous duplex generates a D-loop, which can be bound at the 3' end of the invading strand by the PriA helicase (McGlynn et al. 1997). This function is critical in that it allows PriA to re-load other replisome components at the site, such as the replicative helicase, DnaB, and primase, DnaG (Liu and Marians 1999; Xu and Marians 2003). A functional replication fork can then be reinitiated as DnaB can unwind the DNA template, DnaG can prime synthesis of Okazaki fragments, and the 3' end of the invading strand can become the leading strand. Interestingly, regardless of the nature of the RFB, PriA is required for the reloading of the replisome. The importance of this function is highlighted by the poor viability of *priA*$^{-}$ mutant strains (Masai et al. 1994; Sandler and Marians 2000), which in turn indicates that bacteria commonly suffer from perturbed replication and suggests that the larger genomes found in eukaryotes must inevitably have mechanisms to deal with this problem, albeit the absence of a PriA homolog suggests that they differ

from those in *E. coli*.

Bacteriophage T4 also has a well-defined link between recombination and replication as most of its genomic DNA replication depends on recombination-dependent replication. Its recombination machinery components are simple. In T4, the ssDNA-binding protein is Gp32, the recombination mediator protein is UvsY, and the recombinase is UvsX (Liu et al. 2011a). The helicase Gp41 and helicase loader Gp59 are then responsible for directly linking recombination to replication. The process proceeds in a similar manner as the PriA-system described above with DNA replication being initiated at the D-loop through extension of the invading 3' strand becoming the leading strand and lagging strand synthesis being initiated on the displaced strand of the D-loop (Kreuzer and Brister 2010; Liu and Morrical 2010).

1.2.5.8 Recombination-dependent replication restart in eukaryotes

Similar to the mechanism of BIR, HR can mediate the re-engagement of a functional replication fork if the fork breaks. This can happen when nicks in the single strand of the DNA template are accidentally converted into a one-sided DSB when it is encountered during leading strand synthesis (Harper et al. 2010). Alternatively, the structure-specific endonuclease Mus81-Eme1 can act on a stalled or collapsed replication fork structure by cleaving at the junction point to deliberately cause a one-sided DSB (Doe et al. 2002; Hanada et al. 2007; Froget et al. 2008; Forment et al. 2011; Regairaz et al. 2011). The incidentally or deliberately broken end can then become exposed to

recombinases. Thus, following resection to generate the 3' ssDNA tail and the subsequent, single-strand invasion of the nascent sister chromatid to form a D-loop, Mus81-Eme1 can cleave the three-stranded junction (Boddy et al. 2001; Doe et al. 2002; Osman and Whitby 2007). Following strand ligation, a structure resembling a DNA replication fork will be formed, and accordingly, the replication factory can be reloaded by an unknown means for the resumption of replication (Carr and Lambert 2013). In higher eukaryotes, RAD51 and MRE11 are required for reloading of replication components, such as GINS and Polε, during fork restart following fork collapse (Hashimoto et al. 2012). Interestingly, Sgs1 has also been implicated as a requirement for Polε and Polα chromatin association after replication fork stalling (Cobb et al. 2003).

If the fork remains intact, however, HR proteins can alternatively promote the regression of the stalled fork into a chicken foot structure where the nascent strands are unwound from their templates and annealed to each other. This provides a recombinogenic substrate that HR proteins can act on to generate DNA structures at which replication proteins can reload to restart replication (Liu et al. 1999a) (Figure 1.11). FANCM, Fml1, and Mph1 have been shown to be able to remodel forks and catalyze branch migration *in vitro* (Gari et al. 2008b; Sun et al. 2008; Zheng et al. 2011), while Rad54 can also catalyze branch migration and, in conjunction with Rad51, can also regress replication forks (Bugreev et al. 2006; Bugreev et al. 2011). In the case of Fml1, its ATPase activity, which has no effect on its ability to bind DNA, is required for

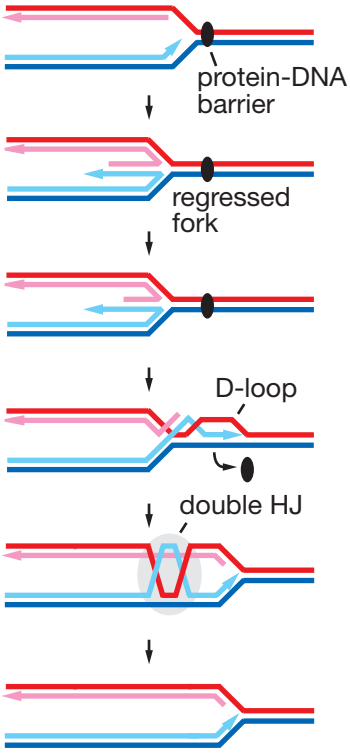


Figure 1.11 | Recombination-dependent replication restart can proceed through a remodelled fork. If a replication fork is impeded by a RFB, such as a protein-DNA barrier, and collapses, a recombination-dependent restart pathway can be used to reinitiate replication. The process can begin with the fork being remodeled into a regressed fork. This can be catalyzed by helicases, such as Fml1. The regressed fork may or may not need to be processed through resection to generate a 3' overhang at which Rad51 can then be loaded to form a nucleoprotein filament. Rad51 can promote strand invasion into the parental duplex to a form a D-loop at which replisome components can be reloaded to re-establish a replication fork. The dHJ can then be dissolved by the concerted actions of Rqh1-Top3-Rmi1.

DNA unwinding and its function in promoting recombination (Nandi and Whitby 2012). The RecQ-helicase family, which includes Rqh1 and BLM, has been shown to be capable of processing these chicken foot junctions at stalled replication forks. Although they can promote regression of a replication fork, it is believed that they are primarily responsible for dissociating these recombination intermediates by removing the HJ and limiting nonproductive recombination caused by fork cleavage (Constantinou et al. 2000; Karow et al. 2000; Doe et al. 2002; Ralf et al. 2006). Through its nuclease activity, Dna2 also prevents formation of the chicken foot structure by cleaving the leading or lagging strand following its dissociation from the template strand but before the two nascent strands become paired and form the chicken foot structure (Hu et al. 2012).

Interestingly, branch migration up and down the DNA requires no net expenditure of energy because each step involves the breaking and making of 2 bp, which illustrates the dynamic fluidity of stalled replication forks. Chicken foot structures may then be resolved through reverse branch migration or cleavage at the HJ. Thus, these structures have the potential to be interconverted between anti- and pro-recombinogenic structures and, as mentioned, are liable for Mus81-Eme1 cleavage. In fact, Mus81-Eme1 is essential for sister chromatid recombination at broken replication forks (Roseaulin et al. 2008). Note that double mutants of *mus81* and the RecQ-type helicases *rqh1* or *sgs1* in fission and budding yeast, respectively, are synthetically lethal but that the lethality can be suppressed with mutations of

rad52 (Doe et al. 2002; Bastin-Shanower et al. 2003). This may indicate that Rqh1/Sgs1 prevents regression of stalled replication forks during DNA replication, while Mus81 processes these abnormal replication intermediates. However, there is growing evidence to suggest that DSB formation at stalled forks through cleavage of the chicken foot HJ may be the last resort option and have a comparatively minor role in mediating replication restart. This is supported by the fact that fork restart requires RAD51 but not necessarily MUS81 (Petermann et al. 2010), and that DSBs are not largely detected at forks arrested at inverted repeats of the polar *RTS1* RFB at the *ura4* locus (Mizuno et al. 2009; Lambert et al. 2010) or at a single copy of the *RTS1* at the *ade6* locus (Ahn et al. 2005). In fact, in humans, the checkpoint proteins ATM and ATR prevent accumulation of DSBs and promote MRN-dependent recovery of collapsed forks (Trenz et al. 2006). Although DSBs are generated by MUS81-EME1 after long periods of replication inhibition (Saintigny et al. 2001; Hanada et al. 2007), the initiation of BIR, which involves a DSB-mediated restart, is kinetically slow and requires several hours (Malkova et al. 2005), which may suggest that replication may be rescued instead by dormant origin firing.

1.3 Aim of study

In order to understand more about the role of HR at perturbed replication forks in eukaryotes, our laboratory has placed the *RTS1* sequence and an intervening *his3*$^{+}$ marker within a direct repeat of *ade6*$^{-}$ heteroalleles positioned at the *ade6* locus on chromosome III of *S. pombe*. This site-

specific RFB has been shown to promote direct repeat recombination, dependent on Rad52 and Rad51 (Ahn et al. 2005). However, it is not known whether this recombination occurs as a default response to fork blockage when promoting its restart or only following a failure of the mechanisms that maintain stalled fork integrity. Although the role of HR in replication is to re-establish a functional replication fork, it may also occur as an accidental consequence of fork stalling due to a failure of mechanisms that normally prevent it and inadvertently, produce deleterious changes in the genome that can promote carcinogenesis. Thus, its use has to be carefully governed.

In this study, I have predominantly used time-lapse microscopy to follow recombination and replication protein dynamics in individual living cells and genetic approaches to examine the genetic factors that affect block-induced recombination at the established *RTS1* system in fission yeast. Through these experiments, I aimed to answer some fundamental questions about the role of recombination at RFBs. Specifically, I wanted to determine the frequency and rate of recombination protein recruitment following replication fork blockage, and whether this occurs following dissociation of the replication proteins from the RFB. If the latter is true, then I wanted to also be able to determine whether recombination leads to a reassociation of the replication proteins with the barrier site, which would be indicative of replication restart.

To begin, I sought to establish a system with tags to the *RTS1* RFB and the central recombination protein Rad52 for time-lapse microscopy of living cells

in order to monitor the recombinational response at the RFB (Chapter 3). After establishing the dynamics of replication and recombination proteins at the RFB in wild-type cells (Chapter 4), I changed the nature of the system by ablating an opposing replication origin to delay fork merging in order to assess whether prolonged pausing was more liable to give rise to replisome collapse and recruitment of recombination proteins (Chapter 5). I also examined the genetic factors that affected Rad52 dynamics and block-induced recombination events at the *RTS1* barrier by studying the roles and involvement of: i) Rad51 and the Rad51 mediator protein complexes, Rad55-Rad57, Swi5-Sfr1, and Rdl1-Rlp1-Sws1 (Chapter 6); ii) Fml1 helicase, Rad54 translocase, and Pfh1 sweepase (Chapter 7); and iii) the checkpoint kinase Cds1 (Chapter 8) in preserving fork integrity and aiding in replication restart at the *RTS1* barrier.

Chapter 2

Materials And Methods

2.1 Molecular biology techniques

All restriction enzymes used in this study were supplied by New England Biolabs (Ipswich, MA). Oligonucleotides for PCR amplification were custom-made, supplied by Sigma-Genosys (Dorset, England), and are listed in Table 2.1. PCR reactions were performed using either a Hybaid (OmniGene, Woburn, MA) or Biometra (Goettingen, Germany) thermocycler. Directed mutagenesis was performed with a QuikChange® Site-Directed Mutagenesis Kit (Stratagene, La Jolla, CA) following the manufacturer's manual.

2.1.1 *Escherichia coli* media

E. coli were grown in Luria-Bertani (LB) broth or on LB-agar (15 g/l agar) supplemented with ampicillin (final concentration 50 μg/ml) where appropriate at 37°C (Sambrook and Russell 2001). Ampicillin was filtered (0.2 μm Millipore syringe filters) and stored as 1000x stocks at -20°C.

2.1.2 *Escherichia coli* transformation

Competent *E. coli* DH5α or Mach1 cells were transformed with a minimum of 100 ng plasmid DNA using the standard 42°C heat shock treatment for bacterial transformation (Sambrook and Russell 2001). Cells were plated on LB medium with 50 μg/ml ampicillin and grown at 37°C overnight. For mini- and medium-scale plasmid preps, the QIAScreen Miniprep protocol and QIAprep Spin Midiprep Kits (Qiagen, Hilden, Germany) were used, respectively, following instructions from the manufacturer.

2.1.3 Cloning and subcloning DNA fragments

For plasmid construction, the appropriate DNA fragment was excised or PCR-amplified with Phusion High-Fidelity DNA Polymerase (Thermo Scientific, Loughborough, UK) or KAPA HiFi DNA Polymerase (KAPA Biosystems, Wilmington, MA) from the relevant plasmid construct and isolated from 0.8% agarose gels using a QIAquick Gel Extraction Kit (Qiagen). Fragments were ligated with T4 DNA ligase (New England Biolabs) at room temperature for a minimum of 2 hours or at 4°C overnight. Correctly constructed plasmid isolates were verified by restriction digest and sequencing. The plasmids used in this study are listed in Table 2.2.

2.1.4 One-dimensional gel electrophoresis for detection of DNA breaks

Following genomic DNA extraction in agarose plugs (see Section 2.2.4), plugs were washed three times in 1x CutSmart Buffer (New England Biolabs), melted at 65°C for 15 – 20 minutes, and then incubated with 10 µl of β-agarase I (New England Biolabs) for 2 hours at 42°C. After a centrifugation step to pellet the agarose, the supernatant was transferred into a fresh tube and incubated with 20 µl of PvuII-HF and 10 µl of RNase A overnight at 37°C. The reaction was then centrifuged at 4000 RPM for 10 minutes in a FA-45-24-11 rotor (Eppendorf, Hamburg, Germany), and the supernatant was mixed with 1 volume of isopropanol and 1/10th volume 3 M Na-acetate to precipitate the DNA. Following centrifugation at 4000 RPM for 20 minutes in a FA-45-24-11 rotor and two washes with ice cold 70% ethanol, the DNA was dissolved in

20 µl TE over two days at 4°C. DNA was loaded onto a 1% agarose gel with 0.3 µg/ml ethidium bromide to allow for visualization of DNA under UV light and was run in 1x TBE for ~ 16 hours at 60 V.

2.1.5 Southern blotting

Before blotting, gels were gently shaken at room temperature in 0.25 M HCl for 15 – 20 minutes to depurinate the DNA and then in transfer buffer (0.5 M NaOH, 1.5 M NaCl) for 10 minutes. DNA was transferred from gels onto positively-charged nylon membranes (Hybond™-XL, GE Healthcare, Little Chalfont, UK) by capillary transfer (Sambrook and Russell 2001). After dismantling the blot, membranes were briefly washed with 2x saline sodium citrate (SSC) (0.3 M sodium citrate, 0.030 M NaCl buffer) and stored at -20°C. Pre-hybridization was done at 65°C for 30 – 60 minutes in modified Church and Gilbert Buffer (0.5M Phosphate buffer [pH 7.2], 7% (w/v) SDS, 10 mM EDTA). Hybridization was performed at 65°C overnight as described (Sambrook and Russell 2001) in a Grant Boekel hybridization oven (HIR10M). Bands of interest were detected by radiolabeling the appropriate probe with [α-^{32}P]dCTP (GE Healthcare) using an Amersham™ Rediprime II Random Prime Labeling System kit following the manufacturer's instructions. Probe A is an EcoNI – XbaI restriction fragment from pFOX2. Probe B is a DNA fragment amplified from genomic DNA by PCR using primers oMW704 (5'-TGAATAATGTGCTGTGAAGC-3') and oMW705 (5'-AAGAACCTACTGAGCC TACG-3'). Following two washes with 2x SSC and 1% SDS and another wash with 0.1x SSC and 1% SDS, probed membranes were exposed to

phosphoscreens and visualized using a Fuji FLA-3000 phosphoimager (FujiFilm, Tokyo, Japan) and Image Gauge software (FujiFilm).

2.1.6 SDS-polyacrylamide gel electrophoresis

To analyze protein expression, cell extracts were mixed with SDS-PAGE loading buffer (60mM Tris-HCl [pH 6.8], 4% Beta-Mercaptoethanol, 4% Sodium Dodecyl Sulphate (SDS), 0.01% Bromophenol Blue, and 5% Glycerol) and boiled at 100°C for 3 minutes prior to loading on standard 10% SDS-polyacrylamide gels (Mini-PROTEAN 3 Cell, Bio-Rad, Hercules, CA) alongside a prestained protein marker (ColorPlus Prestained Protein Marker, Broad Range, New England Biolabs). Gels were run at constant 35 mA for approximately 1 hour and subsequently processed for western blotting. A complete list of buffers and solutions is presented in Table 2.3.

2.1.7 Western blotting

Protein gels were electroblotted onto Hybond ECL nitrocellulose membranes (GE Healthcare) using the Bio-Rad mini trans blot system (Mini-PROTEAN 3 Cell) at 100 V for 1 hour. Blots were blocked at room temperature for 1 hour in TBST-blocking buffer (5% milk powder, 2.5% Bovine Serum Albumin (BSA), 1.8% lysine in Tris-buffered saline with 1% Tween 20 (TBST)). Primary antibody incubations were carried out in fresh 0.1x TBST-blocking buffer at 4°C overnight. Blots were subsequently probed with the appropriate secondary antibody conjugated to horseradish peroxidase (1:20000 dilution) in 0.1x TBST-blocking buffer for 1 hour at room temperature. Three 10-minute

washes with 1x TBST were performed following both primary and secondary antibody incubations. Blots were visualized by enhanced chemiluminescence according to the manufacturer's instructions (ECL Western Blotting Detection Reagents, GE Healthcare) and exposed to X-ray film or visualized by a ChemiDoc XRS+ System (Bio-Rad). The primary antibody used to detect Rad52 was rabbit anti-Rad52 (1:2000) from Cosmo Bio Co., LTD (Tokyo, Japan) coupled with the secondary antibody horseradish peroxidase-conjugated anti-rabbit IgG from Sigma-Aldrich (F9887, St. Louis, MO). To control for protein levels on the gels, a mouse monoclonal anti-α-tubulin (1:500 dilution in PBST instead of TBST buffer, Sigma-Aldrich T9026) along with an anti-mouse IgG (Sigma-Aldrich A9044) was used. A complete list of buffers and solutions is presented in Table 2.3.

2.2 Protocols for the handling and genetics of *Schizosaccharomyces pombe*

General genetic techniques for *S. pombe* are based on established protocols (Sabatinos and Forsburg 2010). Strains used in this study are listed in Table 2.4.

2.2.1 Media

Yeast extract (YE) (30 g D-Glucose and 5 g Yeast Extract in 1 litre water) and YE containing all supplements (YES) (YE supplemented with 225 mg/l uracil, leucine, lysine, histidine, and adenine each) were used as complete media. Edinburgh Minimal Medium with 3.7 mg/ml L-glutamic acid monosodium salt

(EMMG) (20 ml 50x salts, 1 ml 1000x vitamins, 0.1 ml 10000x minerals, 30 g D-Glucose, 3.7 g sodium glutamate, 2.2 g anhydrous Na_2HPO_4, 3 g potassium hydrogen phthalate in 1 litre water) was used as minimal media and supplemented with amino acids as appropriate (Sabatinos and Forsburg 2010). When needed, 18 g/l Difco™ agar was added to the media.

Strains that are auxotrophic for one or more of the following: adenine, arginine, histidine, leucine, and/or uracil, required the respective supplements at 0.25 mg/ml for growth on minimal media. To differentiate between *ade*$^+$ and *ade*$^-$ colonies, cells were plated onto low adenine (LA) medium containing 0.01 mg/ml adenine, which allows *ade*$^+$ colonies to appear white and *ade*$^-$ colonies red. *Ade*$^+$ recombinants were selected on YE supplemented with 0.2 mg/ml guanine dissolved in 1 M NaOH to prevent uptake of residual adenine (Osman and Whitby 2009). To repress expression from the *nmt* promoter, 20 nM – 4 µM thiamine was added to the minimal media as indicated.

2.2.2 Integration of DNA constructs into the *Schizosaccharomyces pombe* genome

To integrate linear DNA constructs into the *S. pombe* genome, *S. pombe* was transformed by an established lithium acetate transformation protocol (Okazaki et al. 1990). Cells were washed three times in sterile Milli-Q water and resuspended 1:1 in 0.1 mM lithium acetate (pH 7.5) with 1x TE (pH 7.5). 1 – 10 µg of linear DNA for integration and 20 µg of carrier DNA (sonicated salmon sperm DNA) were mixed with 100 µl of cells and incubated at room

temperature for 10 minutes. 260 µl 0.1 mM lithium acetate, 1x TE and 40% PEG were added to the mixture at 30°C for 60 – 90 minutes. Finally, cells were heat shocked with 43 µl DMSO at 42°C for 5 minutes and plated onto the appropriate selective medium. Transformants were screened for correct integration of the DNA construct by colony PCR. Colony PCRs were performed by releasing chromosomal DNA from yeast cells by boiling a yeast colony at 100°C for 5 minutes and subsequent amplification of specific DNA fragments that would result from correct integration of the DNA construct by *Taq* DNA polymerase (New England BioLabs) using at least one primer that anneals to a unique chromosomal sequence that flanks the targeted site. Where appropriate PCR products were sequenced to confirm the presence of point mutations. Independent transformants were subsequently tested for growth and genotoxin sensitivity to determine the reproducibility of the phenotype.

2.2.3 Genetic crosses

Cells with opposite mating types were mixed and grown on Malt Extract Agar (MEA) at 25°C for 3 days. Spores were released by overnight digestion with glusulase at 30°C. Cells were then washed in sterile Milli-Q water, and plated on YES agar or directly onto the appropriate selective medium. Progeny were screened for the appropriate genetic markers and genotoxin sensitivities. For selection of strains with antibiotic resistance, Geneticin (100 mg/l), Hygromycin B (200 mg/l), or Nourseothricin (clonNAT) (100 mg/l) were added to YES.

2.2.4 Genomic DNA extraction embedded in agarose plugs

To isolate intact chromosomal DNA for running 1-D gels, 500 ml cultures of *S. pombe* were grown overnight at 37°C to a concentration of 1 x 10^7 cells/ml. Cells were then killed by adding 0.1% sodium azide (Sigma-Aldrich) and washed in water before being stored as pellets at -80°C. Subsequently, cells were spheroplasted in an equal volume of sorbital phosphate buffer (400 mM EDTA, 120 mM Na_2HPO_4, 40 mM citric acid, 1.2 M sorbitol, 10 mM NaN_3, 5 mM DTT) containing 1 mg/ml yeast lysing enzymes from *Trichoderma harzianum* (Sigma-Aldrich) and 5 mg/ml lyticase from *Arthrobacter luteus* (Sigma-Aldrich) for 1 hour at 37°C. Spheroplasted cells were embedded in 1% agarose plugs as described (Hyppa and Smith 2009) using Bio-Rad Low Melt Agarose (Bio-Rad). To degrade proteins, plugs were incubated two times overnight in 3 ml NDS buffer (485 mM EDTA, 10 mM Tris-HCl [pH 7.5], 10 mM NaN_3, 1% N-Lauroylsarcosine) with 1 mg/ml Proteinase K at 50°C. To inactivate residual Proteinase K, plugs were incubated in 10 ml TE with 0.5 mM PMSF on a rocking platform for 1 hour at room temperature and subsequently washed three times in 15 ml TE for 1 hour each on a rocking platform before being stored in 15 ml TE at 4°C.

2.2.5 Alkaline lysis for protein extraction

Proteins were extracted by an established alkaline lysis protocol (Matsuo et al. 2006). Overnight logarithmically growing cultures were harvested, washed, and resuspended in STOP buffer (5% 1 M NaF, 3% 5 M NaCl, 5% 0.2 M EDTA, pH 8.0, and 0.01% sodium azide in sterile water). Following

centrifugation at 3000 RPM for 3 minutes in an A-4-62 rotor (Eppendorf), the samples were resuspended in 0.3 ml sterile water and 0.3 ml 0.6 M NaOH and incubated at room temperature for 10 minutes. Following centrifugation at 13000 RPM for 10 seconds in an F45-24-11 rotor (Eppendorf), the pellets were washed with sterile water and processed for loading onto a SDS-PAGE gel for further analysis as previously described.

2.2.6 Genotoxin sensitivity spot assays

Exponentially growing cells from liquid cultures were harvested, washed, and initially diluted to 1 x 10^7 cells/ml. Subsequent tenfold dilutions from 1 x 10^6 cells/ml to 1 x 10^4 cells/ml were made in water. Aliquots (10 μl) of the cell suspensions were spotted onto YES plates containing various concentrations of chemical genotoxins (CPT, HU, MMS) or irradiated with various doses of UV light using a Stratalinker (Stratagene) as specified. In each spot assay, the undiluted spot (designated 1 in each of the figures) represents 1 x 10^5 cells, whereas the 0.1, 0.001, and 0.001 spots represent 1 x 10^4, 1 x 10^3, and 1 x 10^2 cells, respectively. Plates were incubated at 30°C for up to 6 days and were normally photographed on each day, starting from day 2, in order to monitor differences in growth rates between the strains. The length of incubation for the spot assays shown in the figures is typically 3 days unless otherwise indicated. The spot assays reveal relative differences in survival and growth following a single (acute) exposure to UV or prolonged (chronic) exposure to CPT, HU, and MMS, which generate DNA lesions that can variously cause replication fork stalling, blockage and breakage.

2.2.7 Direct repeat recombination assays

Strains were initially grown on minimal media (EMMG supplemented with 225 mg/l uracil, leucine, lysine, histidine, and adenine each and 1 μM thiamine unless otherwise specified) or YES plates. 10 – 20 single colonies from these plates were then resuspended in sterile Milli-Q water. Approximately 10^5 – 10^6 cells were plated onto plates lacking adenine to score *ade*$^+$ recombinants, and 10^2 – 10^3 cells were plated on non-selective plates of YE with supplements containing low adenine to assess cell viability. The frequency of recombinants was calculated by counting the colonies on the plates after 4 – 6 days of incubation at 30°C. Plates with *ade*$^+$ recombinants were then replica-plated onto EMMG lacking both adenine and histidine to estimate the proportion of conversion-type recombinants (*ade*$^+$*his*$^+$). After 1 – 2 days of incubation at 30°C, the frequency of conversion-type recombinants was calculated by counting colonies.

2.2.8 Microscopy

For time-lapse imaging experiments, cells were grown overnight in 30°C EMMG lacking histidine. 1 μM thiamine was also included in the media unless stated otherwise. Cells were mounted with soybean lectin (Sigma-Aldrich) in a glass bottom culture dish (MatTek Corp., Ashland, MA) and observed in the appropriate medium in a thermally insulated temperature-controlled chamber at 30°C. Live cells were imaged on an inverted Olympus IX71 microscope controlled by a DV Elite Core using DeltaVision softWoRx 5.5.0 software using either CFP/YFP/mCherry or GFP/mCherry filters (Applied Precision Inc.,

Issaquah, WA). Images were taken with an Evolve^{TM} 512 EMCCD camera (Photometrics, Tucson, AZ) using an oil-immersed Olympus 100X UPlanSApo objective with a NA of 1.40. A stack of 16 focal planes at a step-size of 0.3 μm was taken every 5 minutes for 4 hours. Brightfield images of cells and LacI-tdKatushka2 were imaged with a 100 ms exposure time and 10% neutral density filter. Rad52-YFP and Rad54-GFP were imaged with a 100 ms exposure time and 5% neutral density filter. Rad11-GFP, Pcn1-CFP, and Pol12-YFP were imaged with a 25 ms exposure time and 5% neutral density filter, 25 ms exposure time and 2% neutral density filter, and 100 ms exposure time and 5% neutral density filter, respectively.

Microscopic analysis with cells fixed in 70% ethanol was done using a 100x/1.30 UPlanFl objective of an Olympus BX50 epifluorescence microscope equipped with the appropriate filter sets to detect red and yellow fluorescence (Chroma Technology Corp., Bellows Falls, VT). Black-and-white images were taken with a CoolSNAP HQ^2 CCD camera (Photometrics) controlled by MetaMorph v7.7.3.0 software (Molecular Devices Inc., Sunnyvale, CA). Single channel pictures were pseudo-colored and overlayed using Adobe Photoshop CS5 v12 (Adobe Systems Inc., San Jose, CA).

2.3 Analysis

2.3.1 Image processing and analysis

Raw images from the DV Elite Core were subsequently denoised with Priism with the dimensionality set to “3D: xyz” for three iterations (Buades et al.

2005). Denoised images were then deconvolved with softWoRx 5.5.0 software with the Additive method for 12 cycles (Applied Precision). Foci were scored manually and separately for each fluorescent channel. Foci were distinguished as being a minimum of three to five times brighter than background intensity levels with a minimum of a 2 x 2 pixel volume. Co-localization was manually assessed and scored as foci in separate channels overlapping in xyz by a minimum of 2 pixels. Fluorescent signals were quantified using Volocity (Improvision, Coventry, England) or Imaris (Bitplane, South Windsor, CT).

2.3.2 Statistics

All statistical analysis was performed on SPSS Statistics (IBM, Armonk, NY). Data was tested for normal distribution by the Shapiro-Wilk normality test. In accordance with the distribution of the data, means were compared by the appropriate independent-samples T-test. *P* values below 0.05 were considered significant.

Table 2.1 List of primers used in this study

Name	Primer Sequence (5'→3')	Details
oMW285	AATGTACGGGCGACAGTC	Sequencing; upstream of *natMX4* promoter of pAG25-derived plasmids
oMW862	GGGCTGGCTTAACTATGC	Sequencing; upstream *lys1* in pSHA4-derived plasmids
oMW1040	ATCCCGCACCCGTCTACG	Sequencing; downstream of multicloning site in pREP-plasmids; Used to make pMN3
oMW1105	CCGTCAGGACATTGTTGG	Sequencing; within *hphMX4* in pSHA4-derived plasmids
oMW1202	ATATCCATGGGATTTAAC AAAGCGACTATAAGTC	Sequencing; upstream of P_{nmt} of pREP-plasmids
oMW1410	ATGAATTCATGGGAAGTC CTAAGAAG	Sequencing; upstream of *NLS-lacI* in pZN9-derived plasmids
oMW1411	ATGAATTCCAACTCGAGA CCTGAGCCCAG	Sequencing; downstream of *lacI* in pZN9-derived plasmids
oMW1418	TATGGCGCGCCCTGCAG GTCGATCGACTC	Upstream of P_{nmt} in pREP-plasmids with an inserted AscI site; Used to make pMN2 and pMN3
oMW1465	CAGGTCTCGAGTTGGAAT TCG	Sequencing; downstream of *lacI* in pZN9-derived plasmids
oMW1477	TATGGCGCGCCCGAATTC GAGCTCGCATTAC	Downstream of multicloning site in pREP-plasmids with an inserted AscI site; Used to make pMN2
oMW1493	GGCCTCTTCGCTATTACG	Colony PCR to amplify *lacO* array
oMW1494	CAGCACATCCCCCTTTCG	Colony PCR to amplify *lacO* array
oMW1521	GTGGCACAGCAACTGGC GGACAAAGGTGGCGGAT CGTTGCTGATTGGCGTTG CCTCCT	Site directed mutagenesis with base changes and insertions to change pZN9 to a LacI variant, LacI**; Used to make pMN4
oMW1522	AGGAGGCAACGCCAATC AGCAACGATCCGCCACCT TTGTCCGCCAGTTGCTGT GCCAC	Site directed mutagenesis with base changes and insertions to change pZN9 to a LacI variant, LacI**; Used to make pMN4
oMW1530	TATAGGATCCTCAAGATC TGAGTCCGGAGC	3' end of tdKatushka2 in pTEC22 with an inserted BamHI site; Used to make pMN7 and pMN8

oMW1531	TATACTCGAGGAAGGAGA TATACATATGGTG	5' end of tdKatushka2 in pTEC22 with an inserted XhoI site; Used to make pMN7 and pMN8
oMW1577	ATAAAGCTTTAACCATCA GGTTATTCTC	Forward primer for amplifying downstream flanking region of *ori-1253* with a natural HindIII site; used to make pBU1
oMW1578	TTTGGATCCGAGGAAATC ACAAGCATTTCC	Reverse primer for amplifying downstream flanking region of *ori-1253* with an inserted BamHI site; used to make pBU1
oMW1579	TTTGAGCTCTTGTTCAGA GCTAGGATTCG	Forward primer for amplifying upstream flanking region of *ori-1253* with an inserted SacI site; used to make pBU2
oMW1580	ATAGAATTCACGACGAAA ACGCGGACATTC	Reverse primer for amplifying upstream flanking region of *ori-1253* with an inserted EcoRI site; used to make pBU2

Table 2.2 List of plasmids used in this study

Name	Vector	*E. coli* Marker	*S. pombe* Marker	Description	Purpose
pSHA4	pAG32	Ampicillin	*hphMX4*	PCR amplified 3' (oMW1424, oMW1425) and 5' (oMW1422, oMW1423) ends of the open reading frame of *lys1;* cloned as a SacI-ClaI and PvuII-PacI fragment, respectively, into pAG32; [pAG32 + 5'*lys1* + 3'*lys1*]	Targeting construct for integrating a Hygromycin B resistance gene at *S. pombe lys1*, disrupting *lys1*'s gene function.
pZN8	pREP41	Ampicillin	*S.c.LEU2*$^{+}$	PCR amplified (oMW1420, oMW1421) *NLS-lacI-mCherry* from pROD23; cloned as a SalI-BamHI fragment into pREP41; [pREP41 + *NLS-lacI-mCherry*]	Overexpressing NLS-LacI-mCherry from the inducible *nmt41*-promoter in *S. pombe*.
pZN9	pAG32	Ampicillin	*hphMX4*	PCR amplified (oMW1418, oMW1477) P_{nmt41}-*NLS-lacI-mCherry* from pZN8; cloned as an AscI fragment into pSHA4; [pAG32 + 5'*lys1* + P_{nmt41}-*NLS-lacI-mCherry* + 3'*lys1*]	Targeting *NLS-lacI-mCherry* with the inducible *nmt41*-promoter in *S. pombe* to the *lys1* ORF on chromosome I.
pMN1	pREP81	Ampicillin	*S.c.LEU2*$^{+}$	*NLS-lacI-mCherry* from pZN8; cloned as a SalI-BamHI fragment into pREP81; [pREP81 + *NLS-lacI-mCherry*]	Overexpressing NLS-LacI-mCherry from the inducible *nmt81*-promoter in *S. pombe*.

pMN2	pAG32	Ampicillin	*hphMX4*	PCR amplified (oMW1418, oMW1477) P_{nmt81}-*NLS-lacI-mCherry* from pMN1; cloned as an AscI fragment into pSHA4; [pAG32 + 5'*lys1* + P_{nmt81}-*NLS-lacI-mCherry* + 3'*lys1*]	Targeting *NLS-lacI-mCherry* with the inducible *nmt81*-promoter in *S. pombe* to the *lys1* ORF on chromosome I.
pMN3	pAG32	Ampicillin	*hphMX4*	PCR amplified (oMW1040, oMW1418) P_{nmt1} from pREP1; cloned as an AscI-SalI fragment into pMN2; [pAG32 + 5'*lys1* + P_{nmt1}-*NLS-lacI-mCherry* + 3'*lys1*]	Targeting *NLS-lacI-mCherry* with the inducible *nmt1*-promoter in *S. pombe* to the *lys1* ORF on chromosome I.
pMN4	pAG32	Ampicillin	*hphMX4*	Directed mutagenesis (oMW1521, oMW1522) on pZN9 to change to a LacI variant (LacI**); [pAG32 + 5'*lys1* + P_{nmt41}-*NLS-lacI**-mCherry* + 3'*lys1*]	Targeting *NLS-lacI**-mCherry* with the inducible *nmt41*-promoter in *S. pombe* to the *lys1* ORF on chromosome I.
pMN5	pUC8	Ampicillin	$his3^+$	XhoI cleaved 4.5 kb *lacO* array from pLAU43 (Lau et al. 2003), blunt-ended with Klenow; cloned into PvuII site downstream of $his3^+$ in pMW701 [pUC8 + 4.5 kb *lacO* + $his3^+$ + *RTS1-AO* + *ade6-L469*]	Construct for creating a recombination substrate consisting of nontandem direct repeats of *ade6* heteroalleles, interspersed by a $his3^+$ gene, 4.5 kb *lacO* array, and *RTS1-AO*.

pMN6	pUC8	Ampicillin	*his3*$^{+}$	4.5 kb *lacO* array from pMN5; cloned as a SapI-PstI fragment into pMW700 [pUC8 + 4.5 kb *lacO* + *his3*$^{+}$ + *RTS1-IO* + *ade6-L469*]	Construct for creating a recombination substrate consisting of nontandem direct repeats of *ade6* heteroalleles, interspersed by a *his3*$^{+}$ gene, 4.5 kb *lacO* array, and *RTS1-IO*.
pMN7	pAG32	Ampicillin	*hphMX4*	PCR amplified (oMW1530, oMW1531) *tdKatushka2* from pTEC22 (Takaki et al. 2012); cloned as an XhoI-BamHI fragment into pZN9; [pAG32 + 5'*lys1* + P_{nmt41}-*NLS-lacI-tdKatuska2* + 3'*lys1*]	Targeting *NLS-lacI-tdKatushka2* with the inducible *nmt41*-promoter in *S. pombe* to the *lys1* ORF on chromosome I.
pMN8	pAG32	Ampicillin	*hphMX4*	PCR amplified (oMW1530, oMW1531) *tdKatushka2* from pTEC22 (Takaki et al. 2012); cloned as an XhoI-BamHI fragment into pMN4; [pAG32 + 5'*lys1* + P_{nmt41}-*NLS-lacI**-tdKatuska2* + 3'*lys1*]	Targeting *NLS-lacI**-tdKatushka2* from the inducible *nmt41*-promoter in *S. pombe* to the *lys1* ORF on chromosome I.

pMN9	pUC8	Ampicillin	*his3*$^{+}$	PvuII cleaved 4.2 kb lambda DNA, cloned into PvuII site downstream of *his3*$^{+}$ in pMW701 [pUC8 + 4.2 kb lambda DNA + *his3*$^{+}$ + *RTS1-AO* + *ade6-L469*]	Construct for creating a recombination substrate consisting of nontandem direct repeats of *ade6* heteroalleles, interspersed by a *his3*$^{+}$ gene, 4.2 kb non-repetitive DNA spacer, and *RTS1-AO*.
pBU1	pAG25	Ampicillin	*natMX4*	PCR amplified downstream (oMW1577, oMW1578) region flanking *ori-1253*; cloned as a BamHI-HindIII fragment into pAG25	First part of targeting construct for deleting *ori-1253*
pBU2	pAG25	Ampicillin	*natMX4*	PCR amplified upstream (oMW1579, oMW1580) region flanking *ori-1253*; cloned as SacI-EcoRI fragment into pBU1	Targeting construct for deleting *ori-1253*
pBU5	pFOX2	Ampicillin	*natMX4*	*TER2/3* from pJ204-TER; cloned as a SalI fragment into pFOX2 (orientation 1)	Construct for creating a recombination substrate consisting of nontandem direct repeats of *ade6* heteroalleles, interspersed by a *his3*$^{+}$ gene and *TER2/3-IO*.

pBU6	pFOX2	Ampicillin	*natMX4*	*TER2/3* from pJ204-TER; cloned as a SalI fragment into pFOX2 (orientation 2)	Construct for creating a recombination substrate consisting of nontandem direct repeats of *ade6* heteroalleles, interspersed by a *his3*$^{+}$ gene and *TER2/3-AO*.

Table 2.3 Buffers and solutions for SDS-PAGE and Western Blotting

Stop buffer (per 100 ml)	3 ml 5 M NaCl 5 ml 1 M NaF 5 ml 0.2 M EDTA 0.1% Na_3N Add sterile Milli-Q water up to 100 ml
SP buffer (per 100 ml)	5 ml 1 M Tris-HCl (pH 7.5) 15 ml 0.1 M EGTA 0.5 ml 0.2 M EDTA 30 ml 350 mM Sodium vandate 10 ml 10% Triton X-100 68 ml sterile Milli-Q water
Stacking buffer (pH 6.8) (per 200 ml)	12 g Tris 96 ml 1 M HCl 80 ml sterile Milli-Q water
Resolving buffer (pH 8.8) (per 100 ml)	36.3 g Tris Add sterile Milli-Q water up to 100 ml
Stacking gel (for 2 gels)	1.25 ml Ultra pure protogel 2.5 ml Stacking buffer 0.1 ml 10% SDS 0.5 ml 1.5% AMPS 0.075 ml TEMED 5.56 ml sterile Milli-Q water
12.5% Resolving gel (for 2 gels)	6.25 ml Ultra pure protogel 1.88 ml Resolving buffer 0.15 ml 10% SDS 0.75 ml 1.5% AMPS 0.125 ml TEMED 5.98 ml sterile Milli-Q water
SDS-PAGE Loading dye (~ 8 ml)	1 ml Stacking buffer 0.8 ml 100% Glycerol 1.6 ml 10% SDS 4 ml 1% Bromophenol Blue 0.5 ml 0.2 M DTT
10x SDS-PAGE Running buffer (per litre)	30.3 g Tris-HCl 144 g Glycine 10 g SDS Add sterile Milli-Q water up to 1 litre
10x Tris Buffered Saline pH 7.6 (per litre)	24.23 g Tris-HCl 80.06 g NaCl Add sterile Milli-Q water up to 1 litre
10x Native buffer (per litre)	30 g Tris-HCl 144 g Glycine Add sterile Milli-Q water up to 1 litre

10X TBS, pH 7.6 – 7.8 (Tris buffered saline) (per litre)	6.06 g Tris-HCl 1.39 g Tris base 8.77 g NaCl Add sterile Milli-Q water up to 1 litre
Blot buffer (1 litre)	100 ml 10x Native buffer 200 ml Methanol 2 ml 10% SDS Add sterile Milli-Q water up to 1 litre

Table 2.4 List of *S. pombe* strains used in this study

Name	Genotype	Source
FO645	*h+ ade6-L469/pUC8/his3+/ade6-M375 ura4-D18 leu1-32 his3-D1 arg3-D4*	Lab strain
FO1458	*h+ rad52Δ::ura4+ rad51Δ::arg3+ ura4-D18 leu1-32 his3-D1 arg3-D4*	Lab strain
FO1751	*h- rad52+::YFP-kanMX6 ura4-D18 leu1-32 his3-D1 arg3-D4*	This study
FO1752	*h+ rad52+::YFP-kanMX6 ura4-D18 leu1-32 his3-D1*	This study
FO1791	*h- ade6-L469/pUC8/1.7 kb lacO/his3+/RTS1-IO/ade6-M375 ura4-D18 leu1-32 his3-D1 arg3-D4*	This study
FO1792	*h- ade6-L469/pUC8/1.7 kb lacO/his3+/RTS1-AO/ade6-M375 ura4-D18 leu1-32 his3-D1 arg3-D4*	This study
MCW1088	*h+ rad51Δ::arg3+ ura4-D18 leu1-32 his3-D1 arg3-D4*	Lab strain
MCW1221	*h+ ura4-D18 leu1-32 his3-D1 arg3-D4*	Lab strain
MCW1230	*rad54Δ::ura4+ ura4-D18 leu1-32 his3-D1 arg3-D4*	This study
MCW1433	*h- ade6-L469/pUC8/his3+/RTS1-AO/ade6-M375 ura4-D8 leu1-32 his3-D1 arg3-D4*	Lab strain
MCW1691	*h+ rad51Δ::arg3+ ade6-L469/pUC8/his3+/RTS1-IO/ade6-M375 ura4-D18 leu1-32 his3-D1 arg3-D4*	Lab strain
MCW1692	*h+ rad51Δ::arg3+ ade6-L469/pUC8/his3+/RTS1-AO/ade6-M375 ura4-D18 leu1-32 his3-D1 arg3-D4*	Lab strain
MCW1779	*h+ mus81Δ::arg3+ ura4-D18 leu1-32 his3-D1 arg3-D4*	Lab strain
MCW2220	*h+ cds1Δ::ura4+ ade6-L469/pUC8/his3+/RTS1-IO/ade6-M375 ura4-D18 leu1-32 his3-D1 arg3-D4*	This study
MCW2222	*h+ cds1Δ::ura4+ ade6-L469/pUC8/his3+/RTS1-AO/ade6-M375 ura4-D18 leu1-32 his3-D1 arg3-D4*	This study
MCW2647	*h+ swi5Δ::ura4+ ade6-L469/pUC8/his3+/RTS1-IO/ade6-M375 ura4-D18 leu1-32 his3-D1 arg3-D4*	This study
MCW2650	*h+ rad55Δ::arg3+ ade6-L469/pUC8/his3+/RTS1-IO/ade6-M375 ura4-D18 leu1-32 his3-D1 arg3-D4*	This study
MCW2651	*h+ rad54Δ::ura4+ ade6-L469/pUC8/his3+/RTS1-IO/ade6-M375 ura4-D18 leu1-32 his3-D1 arg3-D4*	This study
MCW2653	*h+ swi5Δ::ura4+ ade6-L469/pUC8/his3+/RTS1-AO/ade6-M375 ura4-D18 leu1-32 his3-D1 arg3-D4*	This study
MCW2655	*h+ rad55Δ::arg3+ ade6-L469/pUC8/his3+/RTS1-AO/ade6-M375 ura4-D18 leu1-32 his3-D1 arg3-D4*	This study
MCW2656	*h+ rad54Δ::ura4+ ade6-L469/pUC8/his3+/RTS1-AO/ade6-M375 ura4-D18 leu1-32 his3-D1 arg3-D4*	This study
MCW2726	*h+ rad52+::YFP-kanMX6 ade6-L469/pUC8/1.7 kb lacO/his3+/RTS1-IO/ade6-M375 ura4-D18 leu1-32 his3-D1 arg3-D4*	This study
MCW2728	*h+ rad52+::YFP-kanMX6 ade6-L469/pUC8/1.7 kb lacO/his3+/RTS1-AO/ade6-M375 ura4-D18 leu1-32 his3-D1 arg3-D4*	This study

MCW2906	*h+ mus81Δ::arg3+ cds1Δ::ura4+ ade6-L469/pUC8/his3+/RTS1-IO/ade6-M375 ura4-D18 leu1-32 his3-D1 arg3-D4*	This study
MCW2907	*h+ mus81Δ::arg3+ cds1Δ::ura4+ ura4-D18 leu1-32 his3-D1 arg3-D4*	This study
MCW2910	*h+ mus81Δ::arg3+ cds1Δ::ura4+ ade6-L469/pUC8/his3+/RTS1-AO/ade6-M375 ura4-D18 leu1-32 his3-D1 arg3-D4*	This study
MCW2912	*h+ rad55Δ::arg3+ swi5Δ::ura4+ ade6-L469/pUC8/his3+/RTS1-IO/ade6-M375 ura4-D18 leu1-32 his3-D1 arg3-D4*	This study
MCW2916	*h+ rad55Δ::arg3+ swi5Δ::ura4+ ade6-L469/pUC8/his3+/RTS1-AO/ade6-M375 ura4-D18 leu1-32 his3-D1 arg3-D4*	This study
MCW3059	*h+ fml1Δ::natMX4 ade6-L469/pUC8/his3+/RTS1-IO/ade6-M375 ura4-D18 leu1-32 his3-D1 arg3-D4*	This study
MCW3061	*h+ fml1Δ::natMX4 ade6-L469/pUC8/his3+/RTS1-AO/ade6-M375 ura4-D18 leu1-32 his3-D1 arg3-D4*	This study
MCW3329	*h+ mus81T239A::13myc-kanMX6 ade6-L469/pUC8/his3+/RTS1-AO/ade6-M375 ura4-D18 leu1-32 his3-D1 arg3-D4*	This study
MCW3374	*h+ rad51Δ::arg3+ cds1Δ::ura4+ ade6-L469/pUC8/his3+/RTS1-IO/ade6-M375 ura4-D18 leu1-32 his3-D1 arg3-D4*	This study
MCW3376	*h+ rad51Δ::arg3+ mus81Δ::kanMX6 ade6-L469/pUC8/his3+/RTS1-IO/ade6-M375 ura4-D18 leu1-32 his3-D1 arg3-D4*	This study
MCW3377	*h+ rad51Δ::arg3+ mus81Δ::kanMX6 cds1Δ::ura4+ ade6-L469/pUC8/his3+/RTS1-IO/ade6-M375 ura4-D18 leu1-32 his3-D1 arg3-D4*	This study
MCW3379	*h+ rad51Δ::arg3+ cds1Δ::ura4+ ade6-L469/pUC8/his3+/RTS1-AO/ade6-M375 ura4-D18 leu1-32 his3-D1 arg3-D4*	This study
MCW3380	*h+ rad51Δ::arg3+ mus81Δ::kanMX6 ade6-L469/pUC8/his3+/RTS1-AO/ade6-M375 ura4-D18 leu1-32 his3-D1 arg3-D4*	This study
MCW3381	*h+ rad51Δ::arg3+ mus81Δ::kanMX6 cds1Δ::ura4+ ade6-L469/pUC8/his3+/RTS1-AO/ade6-M375 ura4-D18 leu1-32 his3-D1 arg3-D4*	This study
MCW3790	*h+ rad51Δ::arg3+ fml1Δ::natMX4 ade6-L469/pUC8/his3+/RTS1-IO/ade6-M375 ura4-D18 leu1-32 his3-D1 arg3-D4*	This study
MCW3794	*h+ rad51Δ::arg3+ fml1Δ::natMX4 ade6-L469/pUC8/his3+/RTS1-AO/ade6-M375 ura4-D18 leu1-32 his3-D1 arg3-D4*	This study
MCW4643	*h+ eCFP-rad51+::kanMX6 ura4+ leu1-32 his3-D1 arg3-D4*	This study

MCW4712	*h$^+$ ade6-L469/pUC8/his3$^+$/RTS1-IO/ade6-M375 ura4-D8 leu1-32 his3-D1 arg3-D4*	Lab strain
MCW4713	*h$^+$ ade6-L469/pUC8/his3$^+$/RTS1-AO/ade6-M375 ura4-D8 leu1-32 his3-D1 arg3-D4*	Lab strain
MCW4859	*h$^+$ leu1-32::pJK148-leu1$^+$-pfh1-m21 pfh1Δ::kanMX6 ura4-D18 his3-D1 arg3-D4*	This study
MCW4861	*h$^+$ leu1-32::pJK148-leu1$^+$-pfh1-mt* pfh1Δ::kanMX6 ura4-D18 his3-D1 arg3-D4*	This study
MCW5146	*h$^+$ eCFP-rad51$^+$::kanMX6 ura4$^-$::rad51$^+$ leu1-32 his3-D1 arg3-D4*	This study
MCW5277	*h$^+$ rad51Δ::arg3$^+$ leu1-32::pJK148-leu1$^+$-pfh1-m21 pfh1Δ::kanMX6 ura4-D18 his3-D1 arg3-D4*	This study
MCW5281	*h$^+$ rad51Δ::arg3$^+$ leu1-32::pJK148-leu1$^+$-pfh1-mt* pfh1Δ::kanMX6 ura4-D18 his3-D1 arg3-D4*	This study
MCW5447	*h$^+$ leu1-32::pJK148-leu1$^+$-pfh1$^+$ pfh1Δ::hphMX4 ura4-D8 leu1-32 his3-D1 arg3-D4*	This study
MCW5686	*h$^+$ rad52$^+$::YFP-kanMX6 lys1$^-$::P$_{nmt41}$-NLS-lacI-mCherry-hphMX4 ade6-L469/pUC8/1.7 kb lacO/his3$^+$/RTS1-IO/ade6-M375 ura4-D18 leu1-32 his3-D1 arg3-D4*	This study
MCW6443	*h$^+$ cds1Δ::ura4$^+$ fml1Δ::natMX4 ade6-L469/pUC8/his3$^+$/RTS1-AO/ade6-M375 ura4-D18 leu1-32 his3-D1 arg3-D4*	This study
MCW6446	*h$^+$ rad54Δ::ura4$^+$ leu1-32::pJK148-leu1$^+$-pfh1-m21 pfh1Δ::hphMX4 ade6-L469/pUC8/his3$^+$/RTS1-IO/ade6-M375 ura4-D18 leu1-32 his3-D1 arg3-D4*	This study
MCW6447	*h$^+$ rad54Δ::ura4$^+$ leu1-32::pJK148-leu1$^+$-pfh1-m21 pfh1Δ::hphMX4 ade6-L469/pUC8/his3$^+$/RTS1-AO/ade6-M375 ura4-D18 leu1-32 his3-D1 arg3-D4*	This study
MCW6448	*h$^+$ rad54Δ::ura4$^+$ leu1-32::pJK148-leu1$^+$-pfh1-m21 pfh1Δ::hphMX4 ura4-D18 leu1-32 his3-D1 arg3-D4*	This study
MCW6454	*h$^+$ rad57Δ::LEU2$^+$ ade6-L469/pUC8/his3$^+$/RTS1-AO/ade6-M375 ura4-D18 leu1-32 his3-D1 arg3-D4*	This study
MCW6468	*h$^+$ rdl1D-25::natMX6 ade6-L469/pUC8/his3$^+$/RTS1-AO/ade6-M375 ura4-D18 leu1-32 his3-D1 arg3-D4*	This study
MCW6470	*h$^+$ sws1D-23::kanMX6 ade6-L469/pUC8/his3$^+$/RTS1-AO/ade6-M375 ura4-D18 leu1-32 his3-D1 arg3-D4*	This study
MCW6497	*h$^+$ sfr1D-11::hphMX4 ade6-L469/pUC8/his3$^+$/RTS1-IO/ade6-M375 ura4-D18 leu1-32 his3-D1 arg3-D4*	This study
MCW6499	*h$^+$ sfr1D-11::hphMX4 ade6-L469/pUC8/his3$^+$/RTS1-AO/ade6-M375 ura4-D18 leu1-32 his3-D1 arg3-D4*	This study
MCW6501	*h$^+$ rdl1D-25::natMX6 ade6-L469/pUC8/his3$^+$/RTS1-IO/ade6-M375 ura4-D18 leu1-32 his3-D1 arg3-D4*	This study
MCW6503	*h$^+$ sws1D-23::kanMX6 ade6-L469/pUC8/his3$^+$/RTS1-IO/ade6-M375 ura4-D18 leu1-32 his3-D1 arg3-D4*	This study

MCW6505	*h$^+$ rlp1D-7::natMX6 ade6-L469/pUC8/his3$^+$/RTS1-IO/ade6-M375 ura4-D18 leu1-32 his3-D1 arg3-D4*	This study
MCW6507	*h$^+$ rlp1D-7::natMX6 ade6-L469/pUC8/his3$^+$/RTS1-AO/ade6-M375 ura4-D18 leu1-32 his3-D1 arg3-D4*	This study
MCW6539	*h$^+$ rad57Δ::LEU2$^+$ ade6-L469/pUC8/his3$^+$/RTS1-IO/ade6-M375 ura4-D18 leu1-32 his3-D1 arg3-D4*	This study
MCW6540	*h$^+$ rad54Δ::ura4$^+$ leu1-32::pJK148-leu1$^+$-pfh1$^+$ pfh1Δ::hphMX4 ade6-L469/pUC8/his3$^+$/RTS1-IO/ade6-M375 ura4-D18 his3-D1 arg3-D4*	This study
MCW6541	*h$^+$ rad54Δ::ura4$^+$ leu1-32::pJK148-leu1$^+$-pfh1$^+$ pfh1Δ::hphMX4 ade6-L469/pUC8/his3$^+$/RTS1-AO/ade6-M375 ura4-D18 his3-D1 arg3-D4*	This study
MCW6542	*h$^+$ rad54Δ::ura4$^+$ leu1-32::pJK148-leu1$^+$-pfh1$^+$ pfh1Δ::hphMX4 ura4-D18 his3-D1 arg3-D4*	This study
MCW6543	*h$^+$ rad54Δ::ura4$^+$ leu1-32::pJK148-leu1$^+$-pfh1-mt* pfh1Δ::hphMX4 ade6-L469/pUC8/his3$^+$/RTS1-IO/ade6-M375 ura4-D18 his3-D1 arg3-D4*	This study
MCW6544	*h$^+$ rad54Δ::ura4$^+$ leu1-32::pJK148-leu1$^+$-pfh1-mt* pfh1Δ::hphMX4 ade6-L469/pUC8/his3$^+$/RTS1-AO/ade6-M375 ura4-D18 his3-D1 arg3-D4*	This study
MCW6545	*h$^+$ rad54Δ::ura4$^+$ leu1-32::pJK148-leu1$^+$-pfh1-mt* pfh1Δ::hphMX4 ura4-D18 his3-D1 arg3-D4*	This study
MCW6910	*h$^+$ rad54$^+$::natMX4 ura4-D18 leu1-32 his3-D1 arg3-D4*	This study
MCW6911	*h$^+$ rad54^{K300A}::natMX4 ura4-D18 leu1-32 his3-D1 arg3-D4*	This study
MCW6955	*h$^+$ rad55Δ::arg3$^+$ ade6-L469/pUC8/4.5 kb lacO/his3$^+$/RTS1-IO/ade6-M375 lys1$^-$::P$_{nmt41}$-NLS-lacI-tdKatushka2-hphMX4 rad52$^+$::YFP-kanMX6 ura4-D18 leu1-32 his3-D1 arg3-D4*	This study
MCW6958	*h$^+$ rad55Δ::arg3$^+$ ade6-L469/pUC8/4.5 kb lacO/his3$^+$/RTS1-AO/ade6-M375 lys1$^-$::P$_{nmt41}$-NLS-lacI-tdKatushka2-hphMX4 rad52$^+$::YFP-kanMX6 ura4-D18 leu1-32 his3-D1 arg3-D4*	This study
MCW6961	*h$^+$ swi5Δ::ura4$^+$ ade6-L469/pUC8/4.5 kb lacO/his3$^+$/RTS1-IO/ade6-M375 lys1$^-$::P$_{nmt41}$-NLS-lacI-tdKatushka2-hphMX4 rad52$^+$::YFP-kanMX6 ura4-D18 leu1-32 his3-D1 arg3-D4*	This study
MCW6964	*h$^+$ swi5Δ::ura4$^+$ ade6-L469/pUC8/4.5 kb lacO/his3$^+$/RTS1-AO/ade6-M375 lys1$^-$::P$_{nmt41}$-NLS-lacI-tdKatushka2-hphMX4 rad52$^+$::YFP-kanMX6 ura4-D18 leu1-32 his3-D1 arg3-D4*	This study
MCW6967	*h$^+$ fml1Δ::natMX4 rad55Δ::arg3$^+$ ade6-L469/pUC8/his3$^+$/RTS1-IO/ade6-M375 ura4-D18 leu1-32 his3-D1 arg3-D4*	This study

MCW6982	*h⁺ fml1Δ::natMX4 rad55Δ::arg3⁺ ura4-D18 leu1-32 his3-D1 arg3-D4 ade6-L469/pUC/his3⁺/RTS1-AO/ade6-M375*	This study
MCW6985	*h⁺ rdl1D-25::natMX6 ade6-L469/pUC8/4.5 kb lacO/his3⁺/RTS1-IO/ade6-M375 lys1⁻::P$_{nmt41}$-NLS-lacI-tdKatushka2-hphMX4 rad52⁺::YFP-kanMX6 ura4-D18 leu1-32 his3-D1 arg3-D4*	This study
MCW6988	*h⁺ rdl1D-25::natMX6 ade6-L469/pUC8/4.5 kb lacO/his3⁺/RTS1-AO/ade6-M375 lys1⁻::P$_{nmt41}$-NLS-lacI-tdKatushka2-hphMX4 rad52⁺::YFP-kanMX6 ura4-D18 leu1-32 his3-D1 arg3-D4*	This study
MCW7028	*h⁺ rad54⁺::natMX4 ade6-L469/pUC8/his3⁺/RTS1-IO/ade6-M375 ura4-D18 leu1-32 his3-D1 arg3-D4*	This study
MCW7031	*h⁺ rad54⁺::natMX4 ade6-L469/pUC8/his3⁺/RTS1-AO/ade6-M375 ura4-D18 leu1-32 his3-D1 arg3-D4*	This study
MCW7034	*h⁺ rad54^{K300A}::natMX4 ade6-L469/pUC8/his3⁺/RTS1-IO/ade6-M375 ura4-D18 leu1-32 his3-D1 arg3-D4*	This study
MCW7037	*h⁺ rad54^{K300A}::natMX4 ade6-L469/pUC8/his3⁺/RTS1-AO/ade6-M375 ura4-D18 leu1-32 his3-D1 arg3-D4*	This study
MCW7045	*h⁺ ade6-L469/pUC8/his3⁺/Ter2/3-IO/ade6-M375 ura4-D18 leu1-32 his3-D1 arg3-D4*	This study
MCW7046	*h⁺ ade6-L469/pUC8/his3⁺/Ter2/3-AO/ade6-M375 ura4-D18 leu1-32 his3-D1 arg3-D4*	This study
MCW7088	*h⁺ fml1Δ::natMX4 rad54Δ::ura4⁺ ade6-L469/pUC8/his3⁺/RTS1-IO/ade6-M375 ura4-D18 leu1-32 his3-D1 arg3-D4*	This study
MCW7091	*h⁺ fml1Δ::natMX4 rad54Δ::ura4⁺ ade6-L469/pUC8/his3⁺/RTS1-AO/ade6-M375 ura4-D18 leu1-32 his3-D1 arg3-D4*	This study
MCW7159	*h⁺ fml1Δ::natMX4 rad52Δ::ura4⁺ ade6-L469/pUC8/his3⁺/RTS1-AO/ade6-M375 ura4-D18 leu1-32 his3-D1 arg3-D4*	This study
MCW7161	*h⁺ fml1Δ::natMX4 rad52Δ::ura4⁺ ade6-L469/pUC8/his3⁺/RTS1-IO/ade6-M375 ura4-D18 leu1-32 his3-D1 arg3-D4*	This study
MCW7165	*h⁺ fml1Δ::natMX4 rad52Δ::ura4⁺ rad51Δ::arg3⁺ ade6-L469/pUC8/his3⁺/RTS1-AO/ade6-M375 ura4-D18 leu1-32 his3-D1 arg3-D4*	This study
MCW7169	*h⁺ fml1Δ::natMX4 rad52Δ::ura4⁺ rad51Δ::arg3⁺ ade6-L469/pUC8/his3⁺/RTS1-IO/ade6-M375 ura4-D18 leu1-32 his3-D1 arg3-D4*	This study
MON1	*h⁺ rad52⁺::YFP-kanMX6 ade6-L469/pUC8/1.7 kb lacO/his3⁺/RTS1-AO/ade6-M375 lys1⁻::P$_{nmt41}$-NLS-lacI-mCherry-hphMX4 ura4-D18 leu1-32 his3-D1 arg3-D4*	This study

MON2	*h⁺ rad52⁺::YFP-kanMX6 ade6-L469/pUC8/1.7 kb lacO/his3⁺/RTS1-AO/ade6-M375 lys1⁻::P$_{nmt41}$-NLS-lacI-mCherry-hphMX4 ura4-D18 leu1-32 his3-D1 arg3-D4*	This study
MON3	*h⁺ rad52⁺::YFP-kanMX6 ade6-L469/pUC8/1.7 kb lacO/his3⁺/RTS1-AO/ade6-M375 lys1⁻::P$_{nmt41}$-NLS-lacI-mCherry-hphMX4 ura4-D18 leu1-32 his3-D1 arg3-D4*	This study
MON4	*h⁺ rad52⁺::YFP-kanMX6 ade6-L469/pUC8/1.7 kb lacO/his3⁺/RTS1-IO/ade6-M375 lys1⁻::P$_{nmt81}$-NLS-lacI-mCherry-hphMX4 ura4-D18 leu1-32 his3-D1 arg3-D4*	This study
MON5	*h⁺ rad52⁺::YFP-kanMX6 ade6-L469/pUC8/1.7 kb lacO/his3⁺/RTS1-IO/ade6-M375 lys1⁻::P$_{nmt81}$-NLS-lacI-mCherry-hphMX4 ura4-D18 leu1-32 his3-D1 arg3-D4*	This study
MON6	*h⁺ rad52⁺::YFP-kanMX6 ade6-L469/pUC8/1.7 kb lacO/his3⁺/RTS1-IO/ade6-M375 lys1⁻::P$_{nmt81}$-NLS-lacI-mCherry-hphMX4 ura4-D18 leu1-32 his3-D1 arg3-D4*	This study
MON7	*h⁺ rad52⁺::YFP-kanMX6 ade6-L469/pUC8/1.7 kb lacO/his3⁺/RTS1-AO/ade6-M375 lys1⁻::P$_{nmt81}$-NLS-lacI-mCherry-hphMX4 ura4-D18 leu1-32 his3-D1 arg3-D4*	This study
MON8	*h⁺ rad52⁺::YFP-kanMX6 ade6-L469/pUC8/1.7 kb lacO/his3⁺/RTS1-AO/ade6-M375 lys1⁻::P$_{nmt81}$-NLS-lacI-mCherry-hphMX4 ura4-D18 leu1-32 his3-D1 arg3-D4*	This study
MON9	*h⁺ rad52⁺::YFP-kanMX6 ade6-L469/pUC8/1.7 kb lacO/his3⁺/RTS1-AO/ade6-M375 lys1⁻::P$_{nmt81}$-NLS-lacI-mCherry-hphMX4 ura4-D18 leu1-32 his3-D1 arg3-D4*	This study
MON10	*h⁺ rad52⁺::YFP-kanMX6 ade6-L469/pUC8/1.7 kb lacO/his3⁺/RTS1-IO/ade6-M375 lys1⁻::P$_{nmt41}$-NLS-lacI-mCherry-hphMX4 ura4-D18 leu1-32 his3-D1 arg3-D4*	This study
MON31	*h⁺ ade6-L469/pUC8/1.7 kb lacO/his3⁺/RTS1-IO/ade6-M375 lys1⁻::P$_{nmt41}$-NLS-lacI-mCherry-hphMX4 ura4-D18 leu1-32 his3-D1 arg3-D4*	This study
MON37	*h⁺ ade6-L469/pUC8/1.7 kb lacO/his3⁺/RTS1-AO/ade6-M375 lys1⁻::P$_{nmt41}$-NLS-lacI-mCherry-hphMX4 ura4-D18 leu1-32 his3-D1 arg3-D4*	This study
MON51	*h⁺ rad52⁺::YFP-kanMX6 ade6-L469/pUC8/1.7 kb lacO/his3⁺/RTS1-IO/ade6-M375 lys1⁻::P$_{nmt1}$-NLS-lacI-mCherry-hphMX4 ura4-D18 leu1-32 his3-D1 arg3-D4*	This study

MON54	*h+ rad52+::YFP-kanMX6 ade6-L469/pUC8/1.7 kb lacO/his3+/RTS1-AO/ade6-M375 lys1-::Pnmt1-NLS-lacI-mCherry-hphMX4 ura4-D18 leu1-32 his3-D1 arg3-D4*	This study
MON86	*h+ ade6-L469/pUC8/4.5 kb lacO/his3+/RTS1-IO/ade6-M375 ura4-D18 leu1-32 his3-D1 arg3-D4*	This study
MON90	*h+ ade6-L469/pUC8/4.5 kb lacO/his3+/RTS1-AO/ade6-M375 ura4-D18 leu1-32 his3-D1 arg3-D4*	This study
MON97	*h+ ade6-L469/pUC8/4.5 kb lacO/his3+/RTS1-IO/ade6-M375 lys1-::Pnmt41-NLS-lacI-tdKatushka2-hphMX4 ura4-D18 leu1-32 his3-D1 arg3-D4*	This study
MON102	*h+ ade6-L469/pUC8/4.5 kb lacO/his3+/RTS1-IO/ade6-M375 lys1-::Pnmt41-NLS-lacI**-tdKatushka2-hphMX4 ura4-D18 leu1-32 his3-D1 arg3-D4*	This study
MON110	*h+ ade6-L469/pUC8/4.5 kb lacO/his3+/RTS1-IO/ade6-M375 lys1-::Pnmt41-NLS-lacI-tdKatushka2-hphMX4 rad52+::YFP-kanMX6 ura4-D18 leu1-32 his3-D1 arg3-D4*	This study
MON129	*h+ rad51Δ::arg3+ rad55Δ::hphMX4 ade6-L469/pUC8/his3+/RTS1-IO/ade6-M375 ura4-D18 leu1-32 his3-D1 arg3-D4*	This study
MON138	*h+ rad54Δ::ura4+ rad51Δ::arg3+ ade6-L469/pUC8/his3+/RTS1-IO/ade6-M375 ura4-D18 leu1-32 his3-D1 arg3-D4*	This study
MON140	*h+ rad54Δ::ura4+ rad51Δ::arg3+ ade6-L469/pUC8/his3+/RTS1-AO/ade6-M375 ura4-D18 leu1-32 his3-D1 arg3-D4*	This study
MON143	*h+ ade6-L469/pUC8/4.5 kb lacO/his3+/RTS1-AO/ade6-M375 lys1-::Pnmt41-NLS-lacI-tdKatushka2-hphMX4 ura4-D18 leu1-32 his3-D1 arg3-D4*	This study
MON148	*h+ ade6-L469/pUC8/4.5 kb lacO/his3+/RTS1-AO/ade6-M375 lys1-::Pnmt41-NLS-lacI-tdKatushka2-hphMX4 rad52+::YFP-kanMX6 ura4-D18 leu1-32 his3-D1 arg3-D4*	This study
MON149	*h+ rad51Δ::arg3+ rad55Δ::hphMX4 ade6-L469/pUC8/his3+/RTS1-AO/ade6-M375 ura4-D18 leu1-32 his3-D1 arg3-D4*	This study
MON163	*h+ rad51Δ::arg3+ ade6-L469/pUC8/4.5 kb lacO/his3+/RTS1-IO/ade6-M375 lys1-::Pnmt41-NLS-lacI-tdKatushka2-hphMX4 rad52+::YFP-kanMX6 ura4-D18 leu1-32 his3-D1 arg3-D4*	This study
MON167	*h+ rad51Δ::arg3+ ade6-L469/pUC8/4.5 kb lacO/his3+/RTS1-AO/ade6-M375 lys1-::Pnmt41-NLS-lacI-tdKatushka2-hphMX4 rad52+::YFP-kanMX6 ura4-D18 leu1-32 his3-D1 arg3-D4*	This study

MON172	*h⁺ fml1Δ::natMX4 ade6-L469/pUC8/4.5 kb lacO/his3⁺/RTS1-IO/ade6-M375 lys1⁻::P$_{nmt41}$-NLS-lacI-tdKatushka2-hphMX4 rad52⁺::YFP-kanMX6 ura4-D18 leu1-32 his3-D1 arg3-D4*	This study
MON177	*h⁺ fml1Δ::natMX4 ade6-L469/pUC8/4.5 kb lacO/his3⁺/RTS1-AO/ade6-M375 lys1⁻::P$_{nmt41}$-NLS-lacI-tdKatushka2-hphMX4 rad52⁺::YFP-kanMX6 ura4-D18 leu1-32 his3-D1 arg3-D4*	This study
MON190	*h⁺ cds1Δ::ura4⁺ ade6-L469/pUC8/4.5 kb lacO/his3⁺/RTS1-IO/ade6-M375 lys1⁻::P$_{nmt41}$-NLS-lacI-tdKatushka2-hphMX4 rad52⁺::YFP-kanMX6 ura4-D18 leu1-32 his3-D1 arg3-D4*	This study
MON196	*h⁺ cds1Δ::ura4⁺ ade6-L469/pUC8/4.5 kb lacO/his3⁺/RTS1-AO/ade6-M375 lys1⁻::P$_{nmt41}$-NLS-lacI-tdKatushka2-hphMX4 rad52⁺::YFP-kanMX6 ura4-D18 leu1-32 his3-D1 arg3-D4*	This study
MON198	*h⁺ cds1Δ::ura4⁺ mus81Δ::arg3⁺ ade6-L469/pUC8/4.5 kb lacO/his3⁺/RTS1-IO/ade6-M375 lys1⁻::P$_{nmt41}$-NLS-lacI-tdKatushka2-hphMX4 rad52⁺::YFP-kanMX6 ura4-D18 leu1-32 his3-D1 arg3-D4*	This study
MON202	*h⁺ cds1Δ::ura4⁺ mus81Δ::arg3⁺ ade6-L469/pUC8/4.5 kb lacO/his3⁺/RTS1-AO/ade6-M375 lys1⁻::P$_{nmt41}$-NLS-lacI-tdKatushka2-hphMX4 rad52⁺::YFP-kanMX6 ura4-D18 leu1-32 his3-D1 arg3-D4*	This study
MON207	*h⁺ ade6-L469/pUC8/4.5 kb lacO/his3⁺/RTS1-IO/ade6-M375 lys1⁻::P$_{nmt41}$-NLS-lacI-tdKatushka2-hphMX4 pol12⁺::YFP-kanMX6 ura4⁻::pECFP-PCNA⁺ leu1-32 his3-D1 arg3-D4*	This study
MON213	*h⁺ ade6-L469/pUC8/4.5 kb lacO/his3⁺/RTS1-AO/ade6-M375 lys1⁻::P$_{nmt41}$-NLS-lacI-tdKatushka2-hphMX4 pol12⁺::YFP-kanMX6 ura4⁻::pECFP-PCNA⁺ leu1-32 his3-D1 arg3-D4*	This study
MON217	*h⁺ ade6-L469/pUC8/4.5 kb lacO/his3⁺/RTS1-IO/ade6-M375 lys1⁻::P$_{nmt41}$-NLS-lacI-tdKatushka2-hphMX4 eCFP-rad51⁺::kanMX6 ura4⁻::rad51⁺ leu1-32 his3-D1 arg3-D4*	This study
MON222	*h⁺ ade6-L469/pUC8/4.5 kb lacO/his3⁺/RTS1-AO/ade6-M375 lys1⁻::P$_{nmt41}$-NLS-lacI-tdKatushka2-hphMX4 eCFP-rad51⁺::kanMX6 ura4⁻::rad51⁺ leu1-32 his3-D1 arg3-D4*	This study
MON227	*h⁺ ade6-L469/pUC8/4.5 kb lacO/his3⁺/RTS1-IO/ade6-M375 lys1⁻::P$_{nmt41}$-NLS-lacI-tdKatushka2-hphMX4 ura4⁻::pECFP-PCNA⁺ leu1-32 his3-D1 arg3-D4*	This study

MON232	*h$^+$ ade6-L469/pUC8/4.5 kb lacO/his3$^+$/RTS1-AO/ade6-M375 lys1$^-$::P$_{nmt41}$-NLS-lacI-tdKatushka2-hphMX4 ura4$^-$::pECFP-PCNA$^+$ leu1-32 his3-D1 arg3-D4*	This study
MON236	*h$^+$ ade6-L469/pUC8/4.5 kb lacO/his3$^+$/RTS1-IO/ade6-M375 lys1$^-$::P$_{nmt41}$-NLS-lacI-tdKatushka2-hphMX4 rad52$^+$::YFP-kanMX6 ura4$^-$::pECFP-PCNA$^+$ leu1-32 his3-D1 arg3-D4*	This study
MON240	*h$^+$ ade6-L469/pUC8/4.5 kb lacO/his3$^+$/RTS1-AO/ade6-M375 lys1$^-$::P$_{nmt41}$-NLS-lacI-tdKatushka2-hphMX4 rad52$^+$::YFP-kanMX6 ura4$^-$::pECFP-PCNA$^+$ leu1-32 his3-D1 arg3-D4*	This study
MON243	*h$^+$ ade6-L469/pUC8/4.5 kb lacO/his3$^+$/RTS1-IO/ade6-M375 lys1$^-$::P$_{nmt41}$-NLS-lacI-tdKatushka2-hphMX4 pol12$^+$::YFP-kanMX6 leu1-32 his3-D1 arg3-D4*	This study
MON248	*h$^+$ ade6-L469/pUC8/4.5 kb lacO/his3$^+$/RTS1-AO/ade6-M375 lys1$^-$::P$_{nmt41}$-NLS-lacI-tdKatushka2-hphMX4 pol12$^+$::YFP-kanMX6 leu1-32 his3-D1 arg3-D4*	This study
MON257	*h$^+$ ori-1253Δ::natMX4 ade6-L469/pUC8/his3$^+$/RTS1-AO/ade6-M375 ura4-D8 leu1-32 his3-D1 arg3-D4*	This study
MON259	*h$^+$ ori-1253Δ::natMX4 ade6-L469/pUC8/4.5 kb lacO/his3$^+$/RTS1-AO/ade6-M375 lys1$^-$::P$_{nmt41}$-NLS-lacI-tdKatushka2-hphMX4 rad52$^+$::YFP-kanMX6 ura4-D18 leu1-32 his3-D1 arg3-D4*	This study
MON263	*h$^+$ rdl1D-25::natMX6 rad51Δ::arg3$^+$ ade6-L469/pUC8/his3$^+$/RTS1-IO/ade6-M375 ura4-D18 leu1-32 his3-D1 arg3-D4*	This study
MON269	*h$^+$rdl1D-25::natMX6 rad51Δ::arg3$^+$ ade6-L469/pUC8/his3$^+$/RTS1-AO/ade6-M375 ura4-D18 leu1-32 his3-D1 arg3-D4*	This study
MON275	*h$^+$ rdl1D-25::natMX6 rad55Δ::hphMX ade6-L469/pUC8/his3$^+$/RTS1-IO/ade6-M375 ura4-D18 leu1-32 his3-D1 arg3-D4*	This study
MON279	*h$^+$ rdl1D-25::natMX6 rad55Δ::hphMX ade6-L469/pUC8/his3$^+$/RTS1-AO/ade6-M375 ura4-D18 leu1-32 his3-D1 arg3-D4*	This study
MON283	*h$^+$ swi5Δ::ura4$^+$ rad51Δ::arg3$^+$ ade6-L469/pUC8/his3$^+$/RTS1-IO/ade6-M375 ura4-D18 leu1-32 his3-D1 arg3-D4*	This study
MON289	*h$^+$ swi5Δ::ura4$^+$ rad51Δ::arg3$^+$ ade6-L469/pUC8/his3$^+$/RTS1-AO/ade6-M375 ura4-D18 leu1-32 his3-D1 arg3-D4*	This study
MON293	*h$^+$ ori-1253Δ::natMX4 ade6-L469/pUC8/his3$^+$/RTS1-IO/ade6-M375 ura4-D8 leu1-32 his3-D1 arg3-D4*	This study

MON297	*h⁻ ori-1253Δ::natMX4 ade6-L469/pUC8/4.5 kb lacO/his3⁺/RTS1-IO/ade6-M375 lys1⁻::P$_{nmt41}$-NLS-lacI-tdKatushka2-hphMX4 rad52⁺::YFP-kanMX6 ura4-D18 leu1-32 his3-D1 arg3-D4*	This study
MON301	*h⁺ cds1Δ::ura4⁺ ura4-D18 leu1-32 his3-D1 arg3-D4*	This study
MON303	*h⁺ ade6-L469/pUC8/4.5 kb lacO/his3⁺/RTS1-AO/ade6-M375 rad51Δ::arg3⁺ ura4-D18 leu1-32 his3-D1 arg3-D4*	This study
MON307	*h⁺ ade6-L469/pUC8/4.5 kb lacO/his3⁺/RTS1-IO/ade6-M375 lys1⁻::P$_{nmt41}$-NLS-lacI-tdKatushka2-hphMX4 rad52⁺::YFP-kanMX6 mus81Δ::arg3⁺ ura4-D18 leu1-32 his3-D1 arg3-D4*	This study
MON309	*h⁺ ade6-L469/pUC8/4.5 kb lacO/his3⁺/RTS1-AO/ade6-M375 lys1⁻::P$_{nmt41}$-NLS-lacI-tdKatushka2-hphMX4 rad52⁺::YFP-kanMX6 mus81Δ::arg3⁺ ura4-D18 leu1-32 his3-D1 arg3-D4*	This study
MON315	*h⁻ rad54Δ::ura4⁺ rad52Δ::kanMX6 ade6-L469/pUC8/his3⁺/RTS1-IO/ade6-M375 ura4-D18 leu1-32 his3-D1 arg3-D4*	This study
MON317	*h⁺ rad54Δ::ura4⁺ rad52Δ::kanMX6 ade6-L469/pUC8/his3⁺/RTS1-AO/ade6-M375 ura4-D18 leu1-32 his3-D1 arg3-D4*	This study
MON320	*h⁺ rad52⁺::YFP-kanMX6 ade6-L469/pUC8/his3⁺/RTS1-IO/ade6-M375 ura4-D8 leu1-32 his3-D1 arg3-D4*	This study
MON323	*h⁺ rad52⁺::YFP-kanMX6 ade6-L469/pUC8/his3⁺/RTS1-AO/ade6-M375 ura4-D8 leu1-32 his3-D1 arg3-D4*	This study
MON326	*h⁺ ori-1253Δ::natMX4 rad52⁺::YFP-kanMX6 ade6-L469/pUC8/his3⁺/RTS1-AO/ade6-M375 ura4-D8 leu1-32 his3-D1 arg3-D4*	This study
MON330	*h⁺ rad11⁺::GFP-kanMX6 ade6-L469/pUC8/4.5 kb lacO/his3⁺/RTS1-IO/ade6-M375 lys1⁻::P$_{nmt41}$-NLS-lacI-tdKatushka2-hphMX4 ura4-D18 leu1-32 his3-D1 arg3-D4*	This study
MON335	*h⁺ rad11⁺::GFP-kanMX6 ade6-L469/pUC8/4.5 kb lacO/his3⁺/RTS1-AO/ade6-M375 lys1⁻::P$_{nmt41}$-NLS-lacI-tdKatushka2-hphMX4 ura4-D18 leu1-32 his3-D1 arg3-D4*	This study
MON339	*h⁺ ade6-L469/pUC8/4.2 kb lambda DNA/his3⁺/RTS1-AO/ade6-M375 ura4-D18 leu1-32 his3-D1 arg3-D4*	This study
MON341	*h⁺ ade6-L469/pUC8/4.5 kb lacO/his3⁺/RTS1-IO/ade6-M375 lys1⁻::P$_{nmt41}$-NLS-lacI-tdKatushka2-hphMX4 rad54⁺::GFP-kanMX6 ura4-D18 leu1-32 his3-D1 arg3-D4*	This study

MON342	*h⁻ ade6-L469/pUC8/4.5 kb lacO/his3⁺/RTS1-AO/ade6-M375 lys1⁻::P$_{nmt41}$-NLS-lacI-tdKatushka2-hphMX4 rad54⁺::GFP-kanMX6 ura4-D18 leu1-32 his3-D1 arg3-D4*	This study

Chapter 3

Establishing a System for Visualizing Replication Restart at a Site-Specific Replication Fork Barrier

3.1 Introduction

To visualize the localization of *RTS1* in the nucleus of living cells, I needed to tag the genomic locus where our laboratory had ectopically positioned *RTS1* on chromosome III of *S. pombe* (Ahn et al. 2005). A common molecular strategy for following loci during live cell imaging studies involves using arrays of *lac operator* (*lacO*) sequences bound by a fluorescently tagged version of the *lac* repressor protein LacI. In *E. coli*, *S. pombe*, and mammalian cells, such *lacO*-LacI arrays can impede DNA replication by acting as a persistent non-programmed bi-directional protein-DNA barrier (Payne et al. 2006; Possoz et al. 2006; Jacome and Fernandez-Capetillo 2011; Sofueva et al. 2011; Beuzer et al. 2014). Our laboratory has shown that *lacO*-LacI RFBs can lead to under-replication and DNA breakage that induces recombination-dependent SSA annealing (Sofueva et al. 2011). However, this problem can be avoided by using low levels of LacI expression, such that the *lacO*-LacI array can be used as an inert cytological marker. Therefore, the first stage of my work was to introduce a *lacO*-LacI array downstream of the *RTS1* that: i) could be tracked during time-lapse microscopy and ii) did not act as an undesirable second RFB.

To monitor recombination dynamics at *RTS1*, I wanted to primarily use a fluorescently tagged version of Rad52. As Rad52 plays fundamental roles in promoting both Rad51-dependent strand invasion of a homologous duplex DNA and Rad51-independent strand annealing to a complementary DNA strand (San Filippo et al. 2008) and also is required for all *RTS1*-induced

direct-repeat recombination (Ahn et al. 2005), it serves as a key protein for tracking recombination at *RTS1*. In fact, fluorescently tagged versions of Rad52 have been used extensively to study HR processes in both *S. pombe* and *S. cerevisiae* (Lisby et al. 2001; Lisby et al. 2003; Meister et al. 2003; Lisby et al. 2004). Therefore, in addition to inserting an inert *lacO*-LacI array, I sought to confirm that the Rad52-YFP fusion protein, which was first characterized by Meister et al. (2003), is: i) biologically functional and ii) does not form foci in response to the *lacO*-LacI array.

3.2 Results

3.2.1 Effect of adding *lac* operator sequences between direct repeats on direct repeat recombination

To measure *RTS1*-stimulated inter/intra-chromosomal recombination in *S. pombe*, our laboratory has placed the *RTS1* sequence and an intervening *his3*$^{+}$ marker within a direct repeat of *ade6*$^{-}$ heteroalleles positioned at the *ade6* locus (Figure 3.1). As *RTS1* is a polar RFB, it blocks replication in an orientation-dependent manner. Due to the positions of the putative origins of replication (Heichinger et al. 2006; Siow et al. 2012), there is a predicted bias in replication proceeding across the *ade6* locus towards the centromere (*cen3*). Thus, the orientation of *RTS1* that blocks forks moving toward the centromere will be referred to as the 'active orientation' (*RTS1-AO*), whereas the opposite orientation of *RTS1* that does not block forks moving toward the centromere will be referred to as the 'inactive orientation' (*RTS1-IO*). With the direct repeat system, *ade6*$^{+}$ recombinants can be distinguished from each

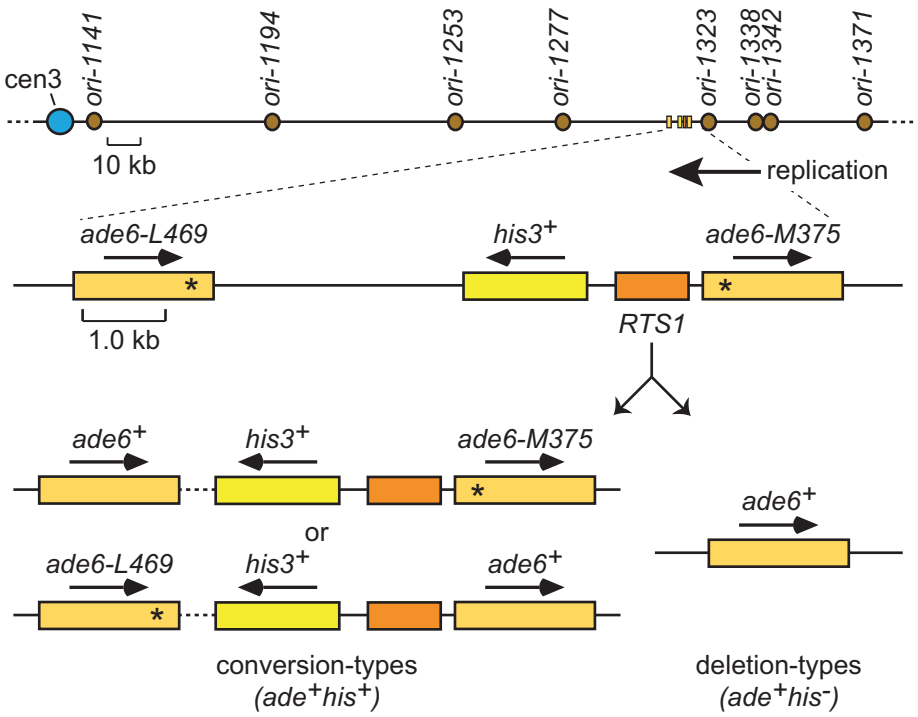


Figure 3.1 | Direct repeat recombination can lead to conversion- and deletion-types. Schematic showing the position of the *ade6*$^{-}$ intrachromosomal recombination substrate along with an intervening *his3*$^{+}$ gene and *RTS1* polar RFB in relation to nearby replication origins on chromosome III (Siow et al. 2012). Replication across the *ade6* locus occurs in the centromere-proximal direction. Thus, depending on the orientation of *RTS1*, it will either block (*RTS1-AO*) or not block (*RTS1-IO*) forks emanating from the centromere-proximal direction. Possible *ade6*$^{+}$ recombinant products that may arise spontaneously or be induced by the perturbed replication fork at *RTS1-AO* include conversion- and deletion-types. Asterisks indicate the positions of the point mutations in *ade6-L469* and *ade6-M375*.

other as either retaining the intervening marker (conversion-types) or losing it (deletion-types) (Figure 3.1). As this assay measures ectopic recombination, it is not representative of the total recombination occurring at the site, as it does not select for the recombinants that are not *ade*$^{+}$ and are therefore, genetically silent. Nevertheless, it provides a readout of a subclass of recombination events occurring at the site and has been used by our lab to demonstrate that the *RTS1-AO* stimulates recombination (Ahn et al. 2005).

To mark the genomic locus where we positioned *RTS1*, I inserted either a 40 x or 115 x *lacO* array, which both contain random, heterologous 10 bp sequences interspersed between every operator (Lau et al. 2003), downstream of the *RTS1* within the recombination substrate. As this changed the spacing between the *ade6*$^{-}$ heteroalleles (Figure 3.2A), I determined its effect on the frequency of recombination between the repeats. In strains with *RTS1-IO* and a 115 x *lacO* array, the frequency of Ade^{+} recombinants is not significantly different from that in a strain with *RTS1-IO* and no *lacO* array (Figure 3.2B, Table 3.1). However, while strains with *RTS1-AO* and a 40 x or 115 x *lacO* array produce similar levels of conversion-type recombinants compared to strains with *RTS1-AO* and no added spacing element, they also produce more deletion-type recombinants, a ~ 1.7- and ~ 4.4-fold increase, respectively, (Figure 3.2C, Table 3.1). This suggests that changing the distance between the direct repeats influences direct repeat recombination.

To see whether this effect was due to the added spacing between the direct

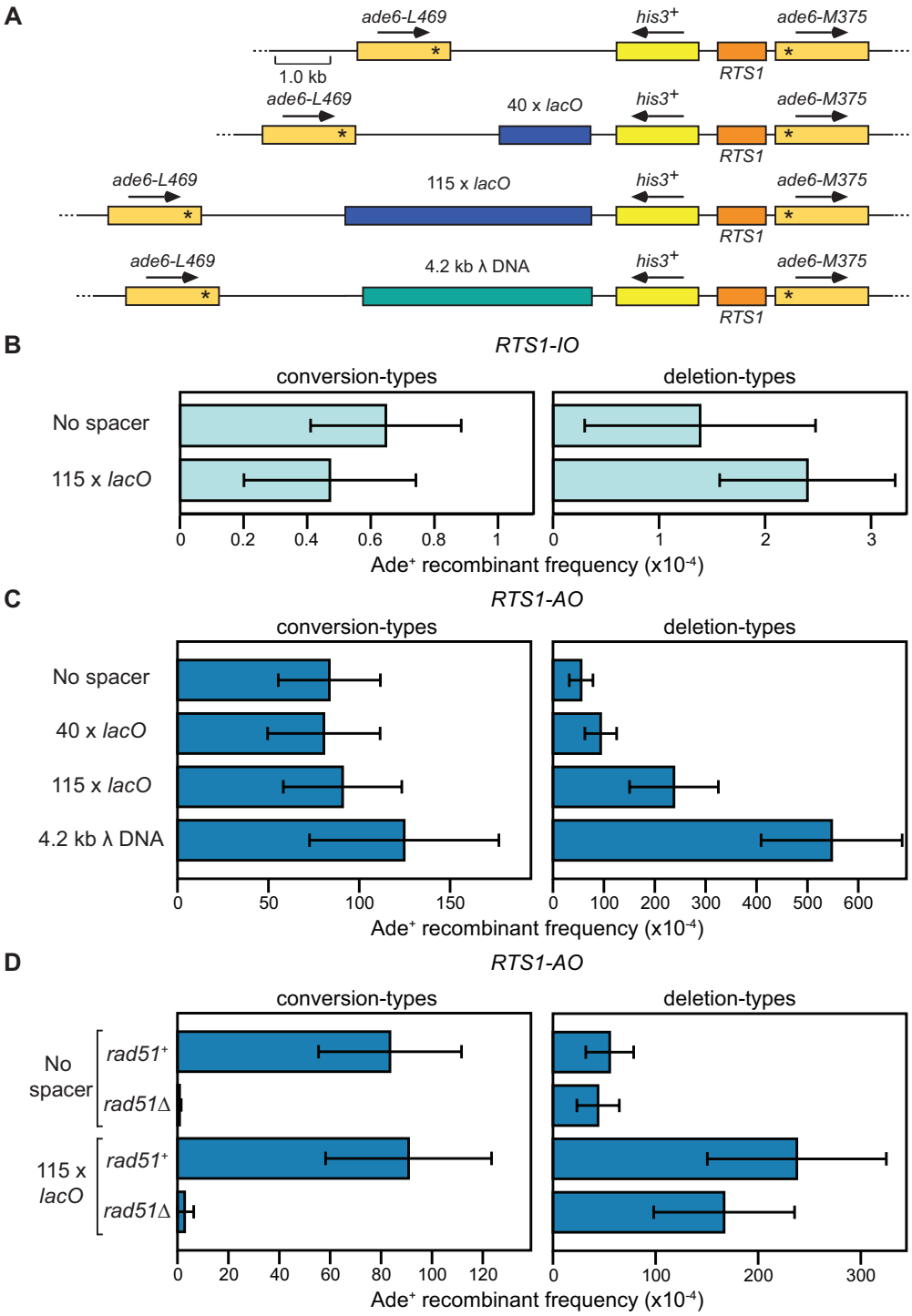


Figure 3.2 | Effect of spacing on direct repeat recombination. (A) Schematic showing the *ade6*$^{-}$ intrachromosomal recombination substrate with and without 40 x *lacO*, 115 x *lacO* and 4.2 kb λ DNA that is drawn to scale. Bar charts showing the frequency of Ade^{+} recombinants in: (B) *RTS1-IO* strains with and without 115 x *lacO* repeats; (C) *RTS1-AO* strains with and without 40 x *lacO*, 115 x *lacO*, and 4.2 kb λ DNA; and (D) *rad51*$^{+}$ and *rad51Δ* *RTS1-AO* strains with and without 115 x *lacO* repeats. Error bars represent ± one standard deviation. In order of presentation, the strains are MCW4712, MON86, MCW4713, FO1792, MON90, MON339, MCW4713, MCW1692, MON90, and MON303.

Table 3.1 | **Effect of spacing on direct repeat recombination**. Direct repeat recombination data presented in the same order as Figure 3.2B, C, and D. All means are presented with ± one standard deviation in parenthesis. P-values are derived from independent-sample t-tests comparing the mean values of the respective mutant to the corresponding mean value found in the control strain.

Genotype	Number of Colonies Analyzed	$Ade^+ His^+$ recombinant frequency (x 10^{-4})		$Ade^+ His^-$ recombinant frequency (x 10^{-4})	
		Mean	P-value	Mean	P-value
RTS1-IO					
No spacer	16	0.65 (±0.24)	-	1.39 (±1.09)	-
115 x *lacO*	27	0.47 (±0.27)	0.037	2.40 (±0.83)	0.001
RTS1-AO					
No spacer	20	85.01 (±28.55)	-	53.14 (±21.23)	-
40 x *lacO*	17	80.52 (±30.94)	0.739	93.78 (±31.17)	<0.001
115 x *lacO*	22	90.82 (±32.61)	0.400	237.65 (±87.26)	<0.001
4.2 kb λ DNA	14	124.73 (±52.12)	0.002	547.53 (±138.67)	<0.001
No spacer, *rad51*$^+$	20	85.01 (±28.55)	-	53.14 (±21.23)	-
No spacer, *rad51Δ*	15	0.83 (±0.61)	<0.001	43.91 (±20.66)	0.120
115 x *lacO*, *rad51*$^+$	22	90.82 (±32.61)	-	237.65 (±87.26)	-
115 x *lacO*, *rad51Δ*	17	2.80 (±3.56)	<0.001	166.80 (±68.63)	0.009

repeats or the repetitive nature of *lacO* arrays, I inserted a 4.2 kb lambda DNA sequence, which did not contain any repetitive elements, in the same position where I placed the *lacO* arrays. In strains with *RTS1-AO* and a 4.2 kb lambda DNA spacer, both conversion- and deletion-type recombinants increase by ~ 1.5- and ~ 9.9-fold, respectively, compared to strains with *RTS1-AO* and no added spacing element (Figure 3.2C, Table 3.1). Therefore, the effects of spacers on the frequency of direct repeat deletions are likely to be due to the change in the distance between the *ade6*$^{-}$ heteroalleles rather than the actual DNA sequence of the spacers themselves.

Our lab has previously shown that all conversion-type recombinants and a proportion of deletion-type recombinants that are induced by the *RTS1* RFB are dependent on Rad51 (Ahn et al. 2005). To see whether the increase in deletion-type recombinants in strains with *RTS1-AO* and *lacO* arrays are Rad51-dependent or -independent, I assessed Ade^{+} recombinant formation in *RTS1-AO* strains with and without a 115 x *lacO* array in a *rad51Δ* background (Figure 3.2D, Table 3.1). In both cases, loss of Rad51 abolished all conversion-types, while also reducing the amount of deletion-types by ~ 1.2-fold in strains with *RTS1-AO* and no added spacer element and ~ 1.4-fold in strains with *RTS1-AO* and a 115 x *lacO* array. These data indicate that although some of the induced deletion-type recombinants in strains with *RTS1-AO* and a 115 x *lacO* array are dependent on Rad51, the majority of the induced deletion-type recombinants are Rad51-independent. Although the frequency of ectopic recombination is different in *RTS1-AO* strains with and

without a *lacO* array, the overall frequency of recombination is unlikely to be different (see Section 3.3).

3.2.2 Expressing fluorescently tagged LacI at levels that produce a detectable *lacO*-LacI focus and do not induce recombination

Our laboratory has previously expressed LacI from a thiamine-repressible *nmt* promoter on a plasmid, which induces recombination at high levels of LacI expression. Because plasmid copy number can vary between cells, I decided to integrate a copy of the *lacI* gene into the *S. pombe* genome in order to obtain more consistent levels of LacI. The version of *lacI* that was integrated also encoded an N-terminal nuclear localization signal (NLS) and C-terminal mCherry fluorescent protein tag. In order to produce a robust *lacO*-LacI focus, I first sought to test various LacI expression levels with the 40 x *lacO* array. I expressed LacI-mCherry from the thiamine repressible *nmt* promoter using either *nmt1* or one of two mutated versions, *nmt41* and *nmt81*, to achieve different levels of expression ranging from *nmt1* to approximately 100-fold lower with *nmt81* (Basi et al. 1993; Forsburg 1993) (Figure 3.3). As LacI expression driven by the *nmt1* promoter, even when it is fully repressed with 4 *μ*M thiamine, gives pan-nuclear fluorescence (Figure 3.3), which our laboratory has observed as being high enough levels of LacI expression to induce recombination (Sofueva et al. 2011), I discounted using *nmt1* driven expression of LacI. I also discounted using *nmt81* driven expression of LacI as it does not give robust *lacO*-LacI foci (Figure 3.3). In contrast, *nmt41* driven expression of LacI produces discernible foci that are not associated with pan-

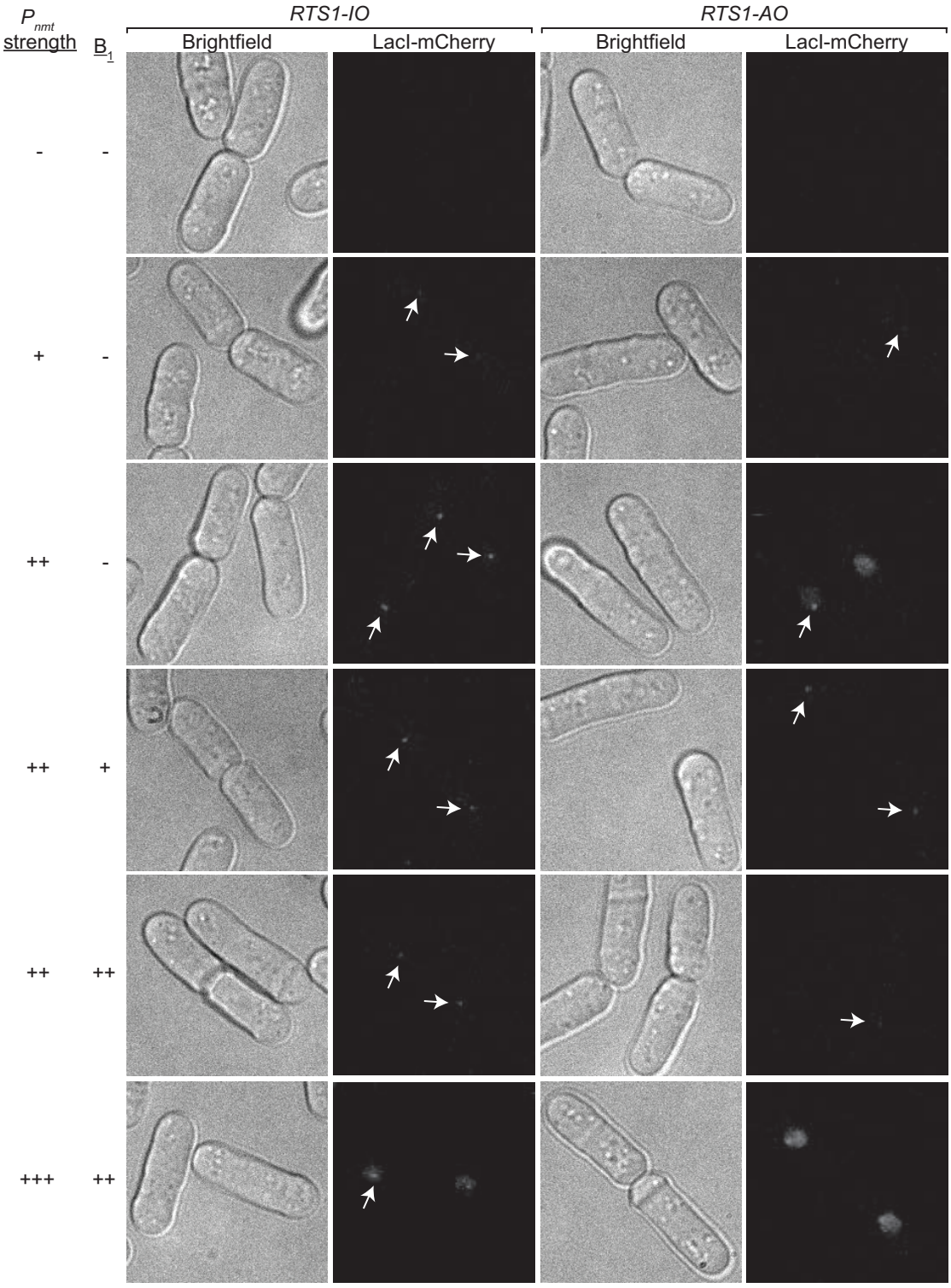


Figure 3.3 | **Appearance of LacI-mCherry foci with different *nmt* promoter strengths**. Representative images of cells with LacI-mCherry expression driven under low (+, P_{nmt81}), medium (++, P_{nmt41}), and full strength (+++, P_{nmt1}) promoters under fully repressed (++, 4 μM thiamine), partially repressed (+, 20 nM thiamine), and non-repressed (-, no thiamine) conditions. In order of presentation, *RTS1-IO strains* are: MCW2726, MON5, MON10, and MON51; and *RTS1-AO* strains are: MCW2728, MON7, MON1, and MON54.

nuclear fluorescence when it is partially repressed with 20 nM thiamine (Figure 3.3). As discussed later, partially repressed *nmt41* levels of LacI do not induce recombination, and therefore, the further development of the *lacO*-LacI system for tracking *RTS1* focused on using this promoter.

In order to monitor *RTS1* in the course of a cell cycle through time-lapse microscopy, I needed a *lacO*-LacI focus that I could track robustly for several hours. When I attempted to track a 40 x or 115 x *lacO* array bound by LacI-mCherry, however, I found that the focus could not reliably be tracked through an entire four-hour time course in most cells. As this was not a result of an accumulation of cells with a contracting *lacO* array (Figure S3.1C), this may be a consequence of the fluorophore photobleaching. To compensate for the loss of fluorescence caused by photobleaching, I tried using higher levels of protein expression, with a LacI variant, LacI**, which carries mutations that reduces its binding affinity for *lacO* and therefore should lessen its potential to form a RFB (Falcon and Matthews 1999; Dubarry et al. 2011), and partially repressing its expression with different thiamine levels. However, LacI** did not produce detectable foci and gave rise to pan-nuclear fluorescence when combined with either a 40 x or 115 x *lacO* array (data not shown). I next tried changing the fluorophore linked to LacI from mCherry to the far-red fluorescent tag, tdKatushka2, which is three times brighter than mCherry and as bright as eYFP (Shcherbo et al. 2009; Takaki et al. 2012). After trying various permutations and further optimizing the imaging conditions, I found that the tdKatuska2 tagged LacI bound to a 115 x *lacO* array gives the most

robust focus that can be tracked in a majority of cells during the time-lapse microscopy (Figure 3.4). Furthermore, I found that the 115 x *lacO*-LacI array did not contract in most cells under the imaging conditions I sought to use, even when LacI-tdKatushka2 expression was driven by the non-repressed *nmt41* promoter (Figure S3.2).

Having established that a 115 x *lacO* array together with expression of tdKatushka2 tagged LacI generated a focus that could be robustly tracked during live cell imaging, I next needed to find a level of LacI expression that would not induce recombination between the repeats in order for the *lacO*-LacI array to not act as a RFB. In strains with the *RTS1-IO* and 115 x *lacO* array, I tested various levels of LacI-tdKatushka2 expression by repressing the *nmt41* promoter with different amounts of thiamine (Figure 3.5A, Table 3.2). When the *nmt41* promoter is repressed with 0.1 μM thiamine, conversion- and deletion-type recombinants increase by ~ 21- and ~ 78-fold, respectively, compared to the equivalent strain with no LacI expression. As the deletion-types consisted of ~ 95% of total recombinants, this was consistent with published work showing that the *lacO*-LacI array induces recombination that mainly arises by SSA (Sofueva et al. 2011). However, when thiamine levels were increased to 0.5 μM, 1 μM, 2 μM, or 4 μM to decrease LacI expression, conversion- and deletion-type recombinants did not vary significantly compared to the equivalent strain with no LacI expression, indicating that these thiamine levels are sufficient for preventing the high levels of LacI that are needed for the *lacO*-LacI array to perturb

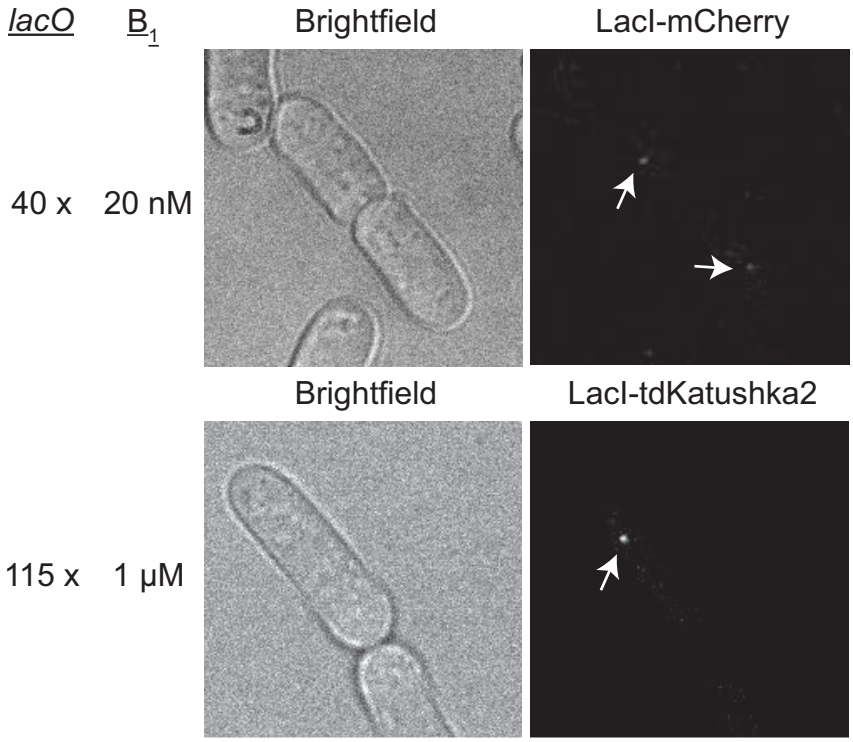


Figure 3.4 | 115 x *lacO*-LacI-tdKatushka2 foci are more detectable than 40 x *lacO*-LacI-mCherry foci. Representative images of cells expressing LacI from P_{nmt41}. In the top panel, the cells (MON10) have a 40 x *lacO* array and express LacI tagged with mCherry that is partially repressed with 20 nM thiamine. In the bottom panel, the cell (MON148) has a 115 x *lacO* array and expresses LacI tagged with tdKatushka2 that is partially repressed with 1 μM thiamine.

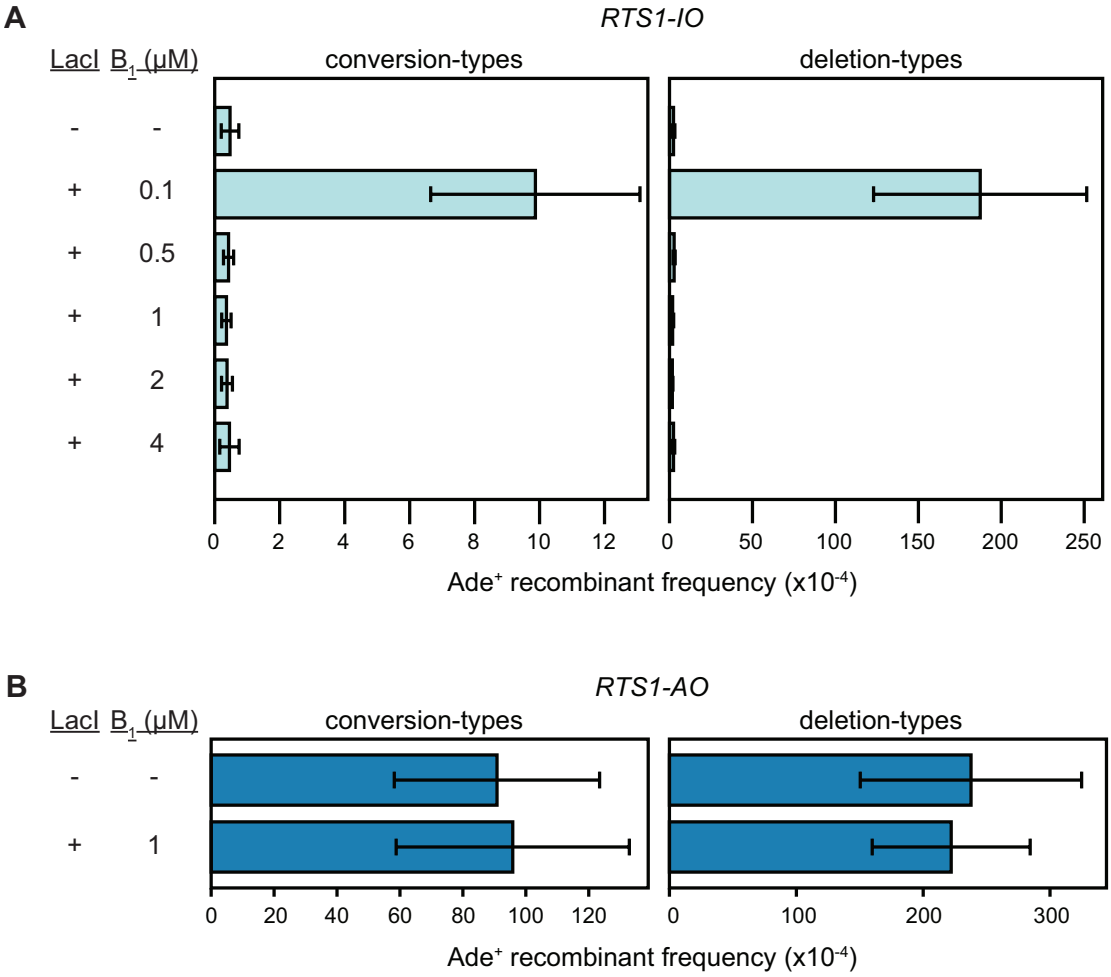


Figure 3.5 | Effect of LacI expression on direct repeat recombination. Bar charts showing the frequency of Ade$^+$ recombinants in *RTS1-IO* (A) and *RTS1-AO* (B) strains with and without P_{nmt41} driven expression of LacI. LacI expression is repressed with 0.1, 0.5, 1, 2, and 4 μM thiamine as indicated. Error bars represent ± one standard deviation. The *RTS1-IO* strains are MON86 (- LacI) and MON97 (+ LacI). The *RTS1-AO* strains are MON90 (- LacI) and MON143 (+ LacI).

Table 3.2 | Effect of LacI expression on direct repeat recombination. Direct repeat recombination data presented in the same order as Figure 3.5A and B. All means are presented with ± one standard deviation in parenthesis. P-values are derived from independent-sample t-tests comparing the mean values of the respective mutant to the corresponding mean value found in the control strain.

Genotype	Number of Colonies Analyzed	$Ade^+ His^+$ recombinant frequency (x 10^{-4})		$Ade^+ His^-$ recombinant frequency (x 10^{-4})	
		Mean	P-value	Mean	P-value
RTS1-IO					
- LacI, - μM B_1	27	0.47 (±0.27)	-	2.40 (±0.83)	-
+ LacI, 0.1 μM B_1	10	9.87 (±3.22)	<0.001	187.28 (±64.27)	<0.001
+ LacI, 0.5 μM B_1	10	0.42 (±0.16)	0.611	2.76 (±0.65)	0.226
+ LacI, 1 μM B_1	19	0.36 (±0.15)	0.107	1.83 (±0.66)	0.016
+ LacI, 2 μM B_1	10	0.38 (±0.17)	0.319	1.64 (±0.39)	0.001
+ LacI, 4 μM B_1	9	0.45 (±0.30)	0.863	2.43 (±0.65)	0.909
RTS1-AO					
- LacI, - μM B_1	22	90.82 (±32.61)	-	237.65 (±87.26)	-
+ LacI, 1 μM	17	95.87 (±37.06)	0.654	222.08 (±62.28)	0.520

replication. To see whether these low levels of LacI expression also did not induce direct repeat recombination in the equivalent strains with *RTS1-AO*, I assessed Ade^+ recombinant formation in strains with and without LacI-tdKatushka2 repressed at 1 μM thiamine (Figure 3.5B, Table 3.2). As the levels of conversion- and deletion-type recombinants were similar in strains with and without LacI, this suggested that when LacI expression is repressed with 1 μM thiamine, the *lacO*-LacI array does not induce additional recombination beyond the levels induced by the *RTS1* RFB. Altogether, the data in Section 3.2.2 indicate that the 115 x *lacO* array in combination with the LacI-tdKatushka2 expression levels driven by the *nmt41* promoter and repressed by 1 μM thiamine do not trigger recombination and can form foci that can be tracked through four-hour time-lapse microscopy studies.

3.2.3 Rad52-YFP is biologically functional

To visualize recombination protein activity at *RTS1*, I decided to first use Rad52 tagged on its C-terminus with YFP (Meister et al. 2003). Although previous studies had confirmed that Rad52-YFP is fully functional with respect to conferring resistance to IR, its ability to promote resistance to other genotoxins had not been tested. This is relevant because *rad52Δ* mutants are hypersensitive to a range of genotoxins, including CPT, HU, MMS, and UV (Doe et al. 2004). The sensitivity of two different isolates of a strain with Rad52-YFP were compared to wild-type and a *rad52Δrad51Δ* double mutant that exhibits identical sensitivities as a *rad52Δ* single mutant (Doe et al. 2004) (Figure 3.6). Unlike *rad52Δrad51Δ* strains that are hypersensitive to the low

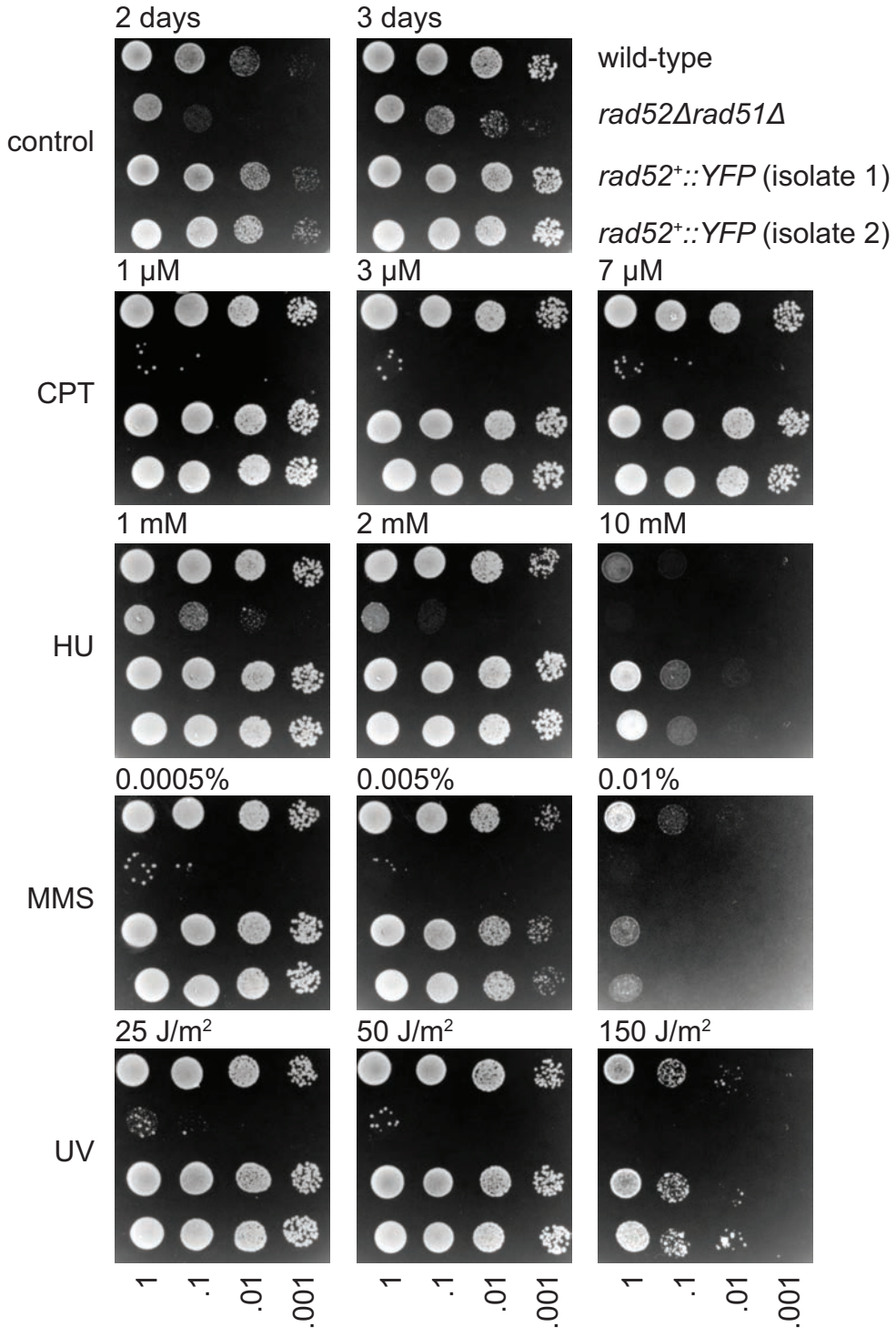


Figure 3.6 | Rad52-YFP strains are not sensitive to CPT, HU, MMS, or UV. Spot assays comparing the growth and sensitivity of wild-type (MCW1221), *rad52Δrad51Δ* (FO1458), and two independent isolates of *rad52⁺::YFP* (FO1751 - top and FO1752 - bottom) to different genotoxins. Strains were grown on complete media for 3 days at 30°C before being photographed. The control plate is also shown after 2 days of incubation.

doses of CPT, HU, MMS, and UV tested, both of the isolates with Rad52-YFP did not show sensitivity, similar to the wild-type strain. Even at higher doses of genotoxins, the Rad52-YFP isolates were as resistant as the wild-type. Altogether, this suggests that the YFP tag does not interfere with Rad52's function in repairing lesions induced by CPT, HU, MMS, or UV.

To confirm that the level of Rad52-YFP protein is equal to that of untagged Rad52 in wild-type mitotic cells, I did a western blot analysis of Rad52 in whole cell extracts (Figure 3.7). In wild-type strains with *RTS1-IO* or *RTS1-AO*, Rad52 protein levels are similar. Likewise, strains with Rad52-YFP and either *RTS1-IO* or *RTS1-AO*, exhibit similar levels of Rad52-YFP, which are comparable to the levels of untagged Rad52 in the equivalent strain backgrounds. These data show that the YFP tag does not alter the level of protein *in vivo*.

To confirm that strains with Rad52-YFP are proficient in direct repeat recombination, I made a comparison of Ade^+ recombinant frequencies in *rad52*$^+$ and *rad52-YFP* strains either with *RTS1-IO* or *RTS1-AO*. All strains contained the 115 x *lacO* array and *nmt41*-LacI-tdKatushka2, and recombinant frequencies were determined in colonies grown on minimal media containing 1 μM thiamine (i.e. equivalent conditions to those used for live cell imaging). Both *rad52*$^+$ and *rad52-YFP* strains exhibited similar frequencies of conversion- and deletion-type recombinants according to whether *RTS1* was *IO* or *AO* (Figure 3.8, Table 3.3). As deletion of *rad52*

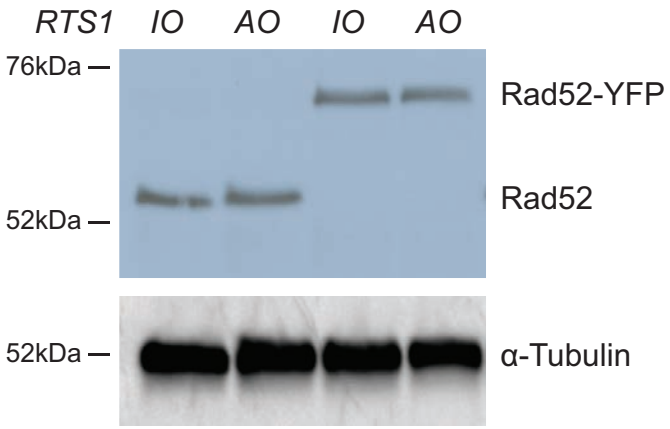


Figure 3.7 | Tagging Rad52 with YFP does not affect Rad52 protein levels. Western blot analysis of Rad52 expression levels from logarithmically growing cultures. The blot was probed with anti-Rad52 antibody. From left to right, the first two strains (MON31 and MON37), express Rad52 with no tags, while the last two strains (MON10 and MON1) express Rad52 tagged with YFP.

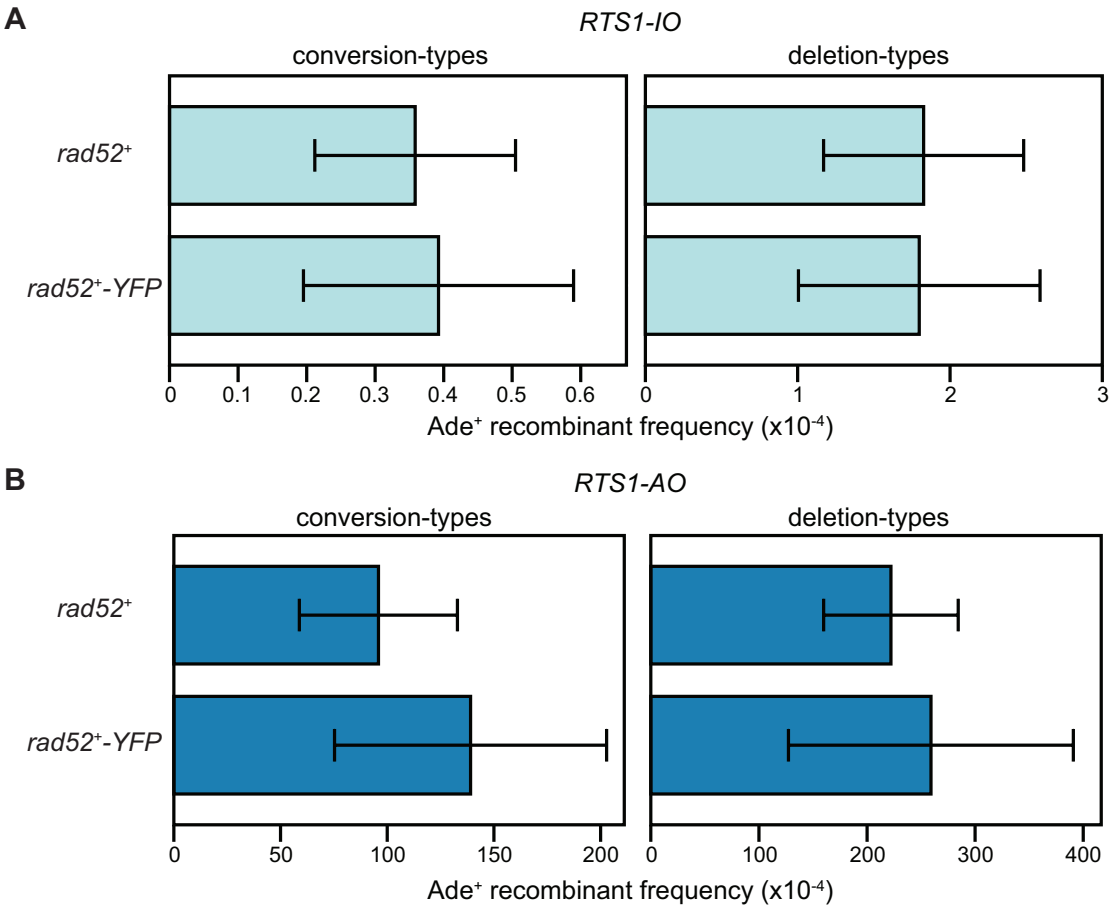


Figure 3.8 | Effect of Rad52-YFP on direct repeat recombination. Bar charts showing the frequency of Ade$^+$ recombinants in *RTS1-IO* (A) and *RTS1-AO* (B) strains with untagged Rad52 or Rad52-YFP. Error bars represent ± one standard deviation. The *RTS1-IO* strains are MON97 (Rad52) and MON110 (Rad52-YFP). The *RTS1-AO* strains are MON143 (Rad52) and MON148 (Rad52-YFP).

Table 3.3 | Effect of Rad52-YFP on direct repeat recombination. Direct repeat recombination data presented in the same order as Figure 3.8A and B. All means are presented with ± one standard deviation in parenthesis. P-values are derived from independent-sample t-tests comparing the mean values of the respective mutant to the corresponding mean value found in the control strain.

Genotype	Number of Colonies Analyzed	$Ade^+ His^+$ recombinant frequency (x 10^{-4})		$Ade^+ His^-$ recombinant frequency (x 10^{-4})	
		Mean	P-value	Mean	P-value
RTS1-IO					
rad52⁺	20	0.36 (±0.15)	-	1.83 (±0.66)	-
rad52⁺-YFP	28	0.39 (±0.20)	0.524	1.80 (±0.79)	0.894
RTS1-AO					
rad52⁺	17	95.87 (±37.06)	-	222.08 (±62.28)	-
rad52⁺-YFP	14	139.08 (±63.77)	0.025	259.12 (±131.79)	0.311

would result in loss of nearly all recombinants, these data show that Rad52-YFP remains fully functional for promoting both spontaneous and *RTS1*-induced direct repeat recombination. Altogether, these data indicate that the YFP tag on the C-terminus of Rad52 does not interfere with the biological functions of Rad52.

3.2.4 The *lacO*-LacI array does not induce Rad52-YFP foci in strains with either *RTS1-IO* or *RTS1-AO*

As *lacO*-LacI RFBs have previously been shown to induce Rad52-YFP foci (Sofueva et al. 2011), I determined whether the appearance of Rad52-YFP foci during time-lapse images of strains with either *RTS1-IO* or *RTS1-AO* depended on the *lacO*-LacI array. In an asynchronous population of cells, I followed a minimum of 65 cells for a minimum of 90 minutes following anaphase and recorded the number of time points that Rad52-YFP foci appeared in individual cells during five-minute intervals. In both cases of strains with *RTS1-IO* or *RTS1-AO*, the distribution of the number of time points cells exhibit a Rad52-YFP focus in the first 90 minutes after anaphase does not change significantly when the *lacO*-LacI array is introduced into the respective strain (Figure 3.9A). Similarly, the mean number of time points cells exhibit a Rad52-YFP focus in the first 90 minutes does not increase in strains with *lacO*-LacI arrays compared to the respective strains that do not have *lacO*-LacI arrays in either *RTS1-IO* or *RTS1-AO* backgrounds (Figure 3.9B). The orientation of *RTS1* does have an effect that is independent of the *lacO*-LacI array, though, as the mean number increases from approximately

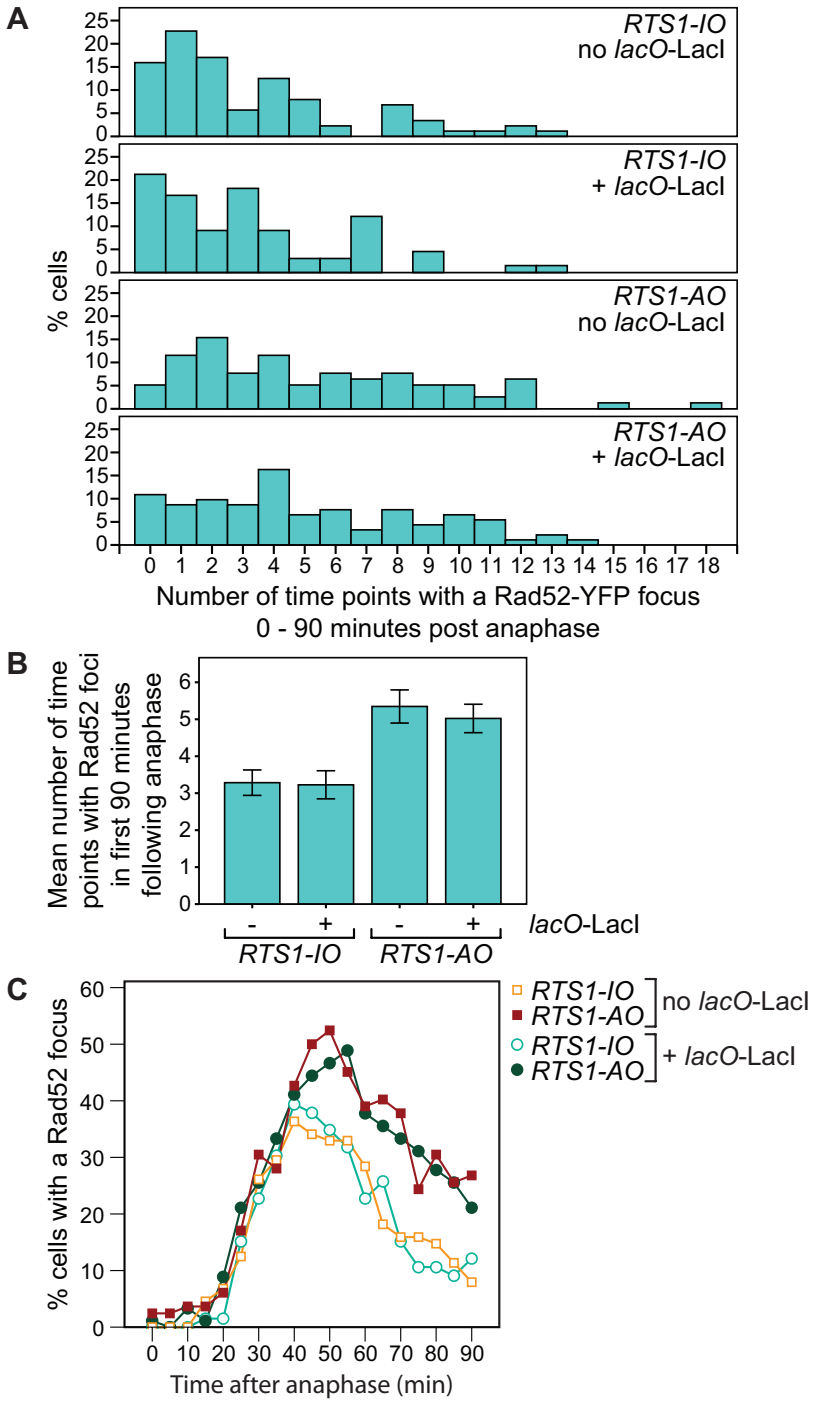


Figure 3.9 | Appearance of Rad52-YFP foci in *RTS1-IO* and *RTS1-AO* cells do not depend on *lacO*-LacI. (A) Histogram showing the percentage of cells with a given number of time points in which a Rad52-YFP focus is detected within the first 90 minutes following anaphase. (B) Bar chart of the mean number of time points cells have a Rad52-YFP focus in the first 90 minutes following anaphase. Error bars represent ± one standard error of the mean. (C) Line graph of the percentage of cells with a Rad52-YFP focus during the first 90 minutes following anaphase. The strains without *lacO*-LacI are MON320 (*RTS1-IO*, n = 88) and MON323 (*RTS1-AO*, n = 83). The strains with *lacO*-LacI are MON110 (*RTS1-IO*, n = 66) and MON148 (*RTS1-AO*, n = 92).

three time points with a Rad52-YFP focus in strains with *RTS1-IO* to five time points with a Rad52-YFP focus in strains with *RTS1-AO* (Figure 3.9B). To see whether there is a change in the timing of when Rad52-YFP foci are appearing in strains with and without a *lacO*-LacI array, I plotted the percentage of cells with a Rad52-YFP focus through the first 90 minutes following anaphase at five-minute intervals (Figure 3.9C). Rad52-YFP foci start appearing at approximately 20 minutes post anaphase regardless of whether the *lacO*-LacI array is present or absent and whether *RTS1* is *AO* or *IO*. A higher proportion of cells with *RTS1-AO* exhibit Rad52-YFP foci than those with *RTS1-IO*, with the peak occurring at 50 – 55 minutes compared to 40 minutes in *RTS1-IO* strains. Crucially, the presence of the *lacO*-LacI array has no effect on either the timing, persistence, or frequency of Rad52-YFP foci. The only differences that are observed can be attributed solely to the orientation of *RTS1*.

3.3 Discussion

In this chapter, I presented the groundwork that has demonstrated that the *lacO*-LacI array is an inert cytological marker and that the YFP tag on Rad52 does not interfere with its biological functions under the equivalent conditions to those used for live cell imaging. Below, I discuss two unexpected findings of this foundation work.

Increasing the distance between direct repeats has previously been found to influence direct repeat recombination in different ways without affecting the

frequency of recombination (Chedin et al. 1994; Lovett et al. 1994; Delviks and Pathak 1999; Rocha 2003; Kappeler et al. 2008). In our system, increasing the space between the direct repeats leads to an increase in the amount of deletion-type recombinants induced by the *RTS1* RFB. It is likely that the increase in deletions is related to the fork being arrested at *RTS1* since there is no equivalent increase in deletion-type recombinants in strains with *RTS1-IO* and the 115 x *lacO* array. These deletions are largely Rad51-independent, suggesting that they are probably arising from a Rad52-dependent strand-annealing pathway. There are potentially two different Rad52-dependent mechanisms that could promote deletion-type recombinants: DSB-induced SSA and a template-mispairing that could occur at an arrested fork (Figure 3.10). The frequency of DSB-induced SSA-dependent recombinants, however, tends to decrease exponentially with increasing distances between direct repeats (Chedin et al. 1994; Lovett et al. 1994; Kappeler et al. 2008). Therefore, it is unlikely that the increase in deletion-types in strains with *RTS1-AO* and increasing spacing elements arise from DSB-induced SSA. The more likely scenario that could explain the increased deletion-types involves Rad52 at the arrested fork annealing the direct repeats when the incoming fork arrives. In fact, increased distances between direct repeats has been found to increase deletion-types that arise from a template-switching mechanism, and this was predicted to be due to the increased distance between the direct repeats relieving a structural constraint associated with the template (Delviks and Pathak 1999). In a similar manner, the increased distance between the direct repeats in our system may lead to a

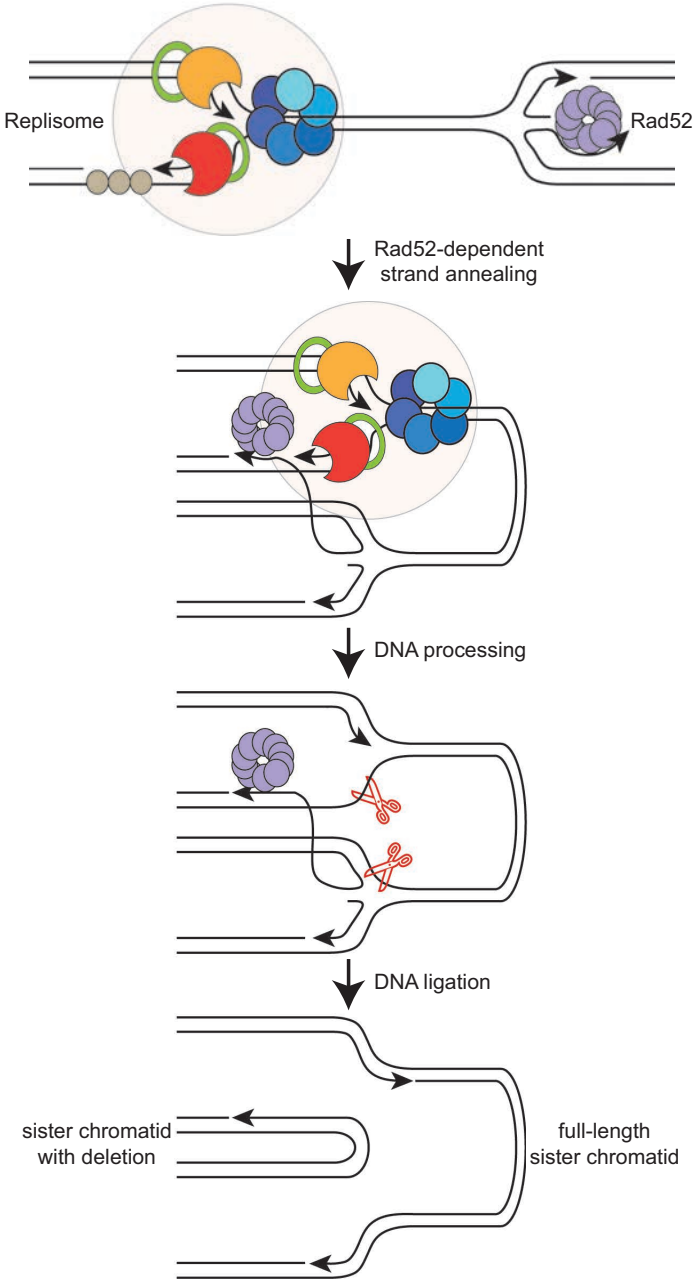


Figure 3.10 | Model for Rad52-dependent annealing at an arrested fork. If Rad52 is loaded at an arrested fork, it may promote annealing between homologous sequences when a converging fork is arriving. If Rad52 promotes annealing between the homologous sequences, DNA replication may terminate and endonucleases may process the DNA, such that ligation can complete DNA replication. This leads to one sister chromatid with a deletion and one full-length sister chromatid.

localized increase in the flexibility of the DNA duplex or a change in the chromosomal structure that increases the likelihood that the two direct repeats are spatially positioned closer to each other such that Rad52 can promote annealing between the repeats. Conversely, when the distance between the direct repeats is decreased, a structural constraint in the DNA may exist that constrains the alignment between the homologous sequences that is needed to promote these interactions, such that these particular Rad52-dependent deletion-type recombinant events occur at much lower rates.

Intriguingly, our laboratory has also found that the frequency of direct repeat recombination can also be influenced by media conditions as strains grown on minimal media (EMMG) have a lower frequency of direct repeat recombination than the equivalent strain grown on complete media (YES) (Lorenz et al. 2009). All recombination data shown in this chapter are from strains grown on minimal media, which are the exact same conditions that are used for all of the strains in the time-lapse microscopy studies presented in the subsequent chapters. However, I have also assessed the effect that the 40 x *lacO* array has on the recombinant frequency in strains with either *RTS1-IO* or *RTS1-AO* grown in complete media and found that there is a similar increase in deletion-types in the *RTS1-AO* strain, although this is accompanied with a slight increase in conversion-types so the ratio of the two types of recombinants is not the same as observed under minimal media conditions (Figure S3.1, Table S3.1).

Interestingly, I also found that strains expressing Rad52-YFP in complete media have increased levels of *RTS1*-induced direct repeat recombination frequencies compared to the equivalent strains with untagged Rad52 (Figure S3.1B, Table S3.1). This elevated recombination seems to impact conversion- and deletion-type recombinants equally without skewing the balance towards one or the other. The reason for the difference in direct repeat recombination in strains with Rad52-YFP in complete and minimal media is unknown. Further work is needed to understand why complete media causes this effect. One possibility is that strains growing in complete media may have a different balance of certain proteins, either an increase or decrease in their expression levels, that leads to a differentially regulated interaction with Rad52-YFP. However because all of the subsequent work with strains expressing Rad52-YFP presented in this thesis is done in minimal media, this difference was not a concern for the present study.

Chapter 4

Spatio-Temporal Dynamics of Recombination and Replication Foci During the Cell Cycle in Cells Containing *RTS1-IO* and *RTS1-AO*

4.1 Introduction

Our laboratory and others have exploited a site-specific polar RFB in fission yeast termed *RTS1* to investigate the consequences of perturbing a single replication fork (Ahn et al. 2005; Lambert et al. 2005; Sun et al. 2008; Lorenz et al. 2009; Lambert et al. 2010; Iraqui et al. 2012). When the progression of a replication fork is impeded at *RTS1*, the stalled fork could in theory simply be held in a competent state to merge with the opposing fork to complete replication. Despite this, fork blockage at *RTS1* triggers a strong recombinational response that is able to restart DNA synthesis, which at least initially is highly error prone and as a consequence, can produce deleterious changes in the genome. Therefore, the use of recombination-dependent replication restart (RDR) has to be carefully governed. It is not known, however, whether RDR at *RTS1* occurs as a default response to fork blockage or only following a failure of the mechanisms that maintain stalled fork integrity. It is also unclear how quickly recombination occurs following fork blockage, its frequency, and what the molecular basis is for the infidelity of the restarted fork. In this chapter, I will present live cell imaging data of recombination at the RFB to address these questions.

4.2 Results

4.2.1 Tracking the timing of replication foci during the cell cycle

In eukaryotic cells, DNA replication occurs in discrete subnuclear domains that can be microscopically visualized as replication foci (Chagin et al. 2010). Replication foci are associated with numerous DNA replication factors and

nascent DNA from several replication forks, and they form distinct patterns of localization over the course of S-phase. Because previous research has established that PCNA (*S. pombe* Pcn1) foci correspond to sites of genomic DNA replication in *S. pombe*, I introduced the previously characterized replication marker, Pcn1 fused to CFP, in strains containing *RTS1* to determine the timing of replication in living fission yeast under the time-lapse microscopy conditions detailed in Chapter 3 (Meister et al. 2007). These time-lapse analyses involved imaging an asynchronously growing population of cells every five minutes for four hours at 30˚C. Under these conditions, Pcn1-CFP foci formed a reproducible sequence of patterns as described previously be Meister et al. (2007) (Figure 4.1A). In early S-phase, Pcn1 foci appeared in the entire extranucleolar region, while toward the end of S-phase, one bright Pcn1 focus would remain in or around the nucleolus. To monitor when S-phase is occurring in the cell, I recorded the timing of when Pcn1 foci appeared relative to the timing of anaphase and tracked the duration of Pcn1 foci in individual cells containing either *RTS1-IO* or *RTS1-AO* (Figure 4.1B). The appearance and duration of Pcn1 foci does not differ significantly in cells containing either *RTS1-IO* or *RTS1-AO*, indicative that the *RTS1* RFB does not alter global replication foci patterns. In both cases, Pcn1-CFP foci begin appearing as early as 10 minutes following anaphase and by 15 minutes after anaphase, nearly 100% of cells have Pcn1 foci. Approximately all cells continue to exhibit Pcn1 foci until at least about 40 minutes after anaphase. By 45 minutes after anaphase, only 80% of cells have Pcn1 foci. This decreases to 42% of cells with Pcn1 foci by 55 minutes and fewer than 16%

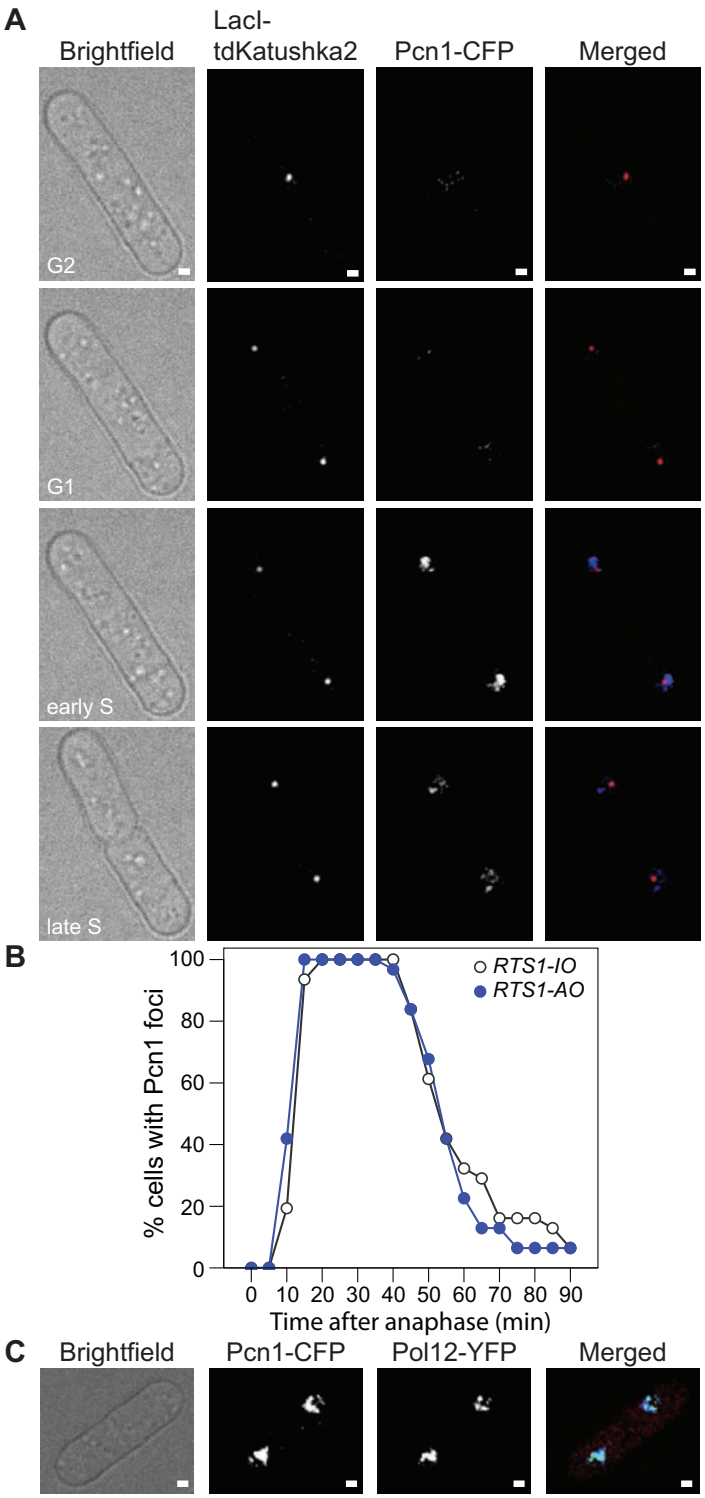


Figure 4.1 | Determining the timing of replication foci during the cell cycle. (A) Example of images taken from a time-lapse movie of a cell with Pcn1-CFP and LacI-tdKatushka2. (B) Line graphs of the percentage of cells with a Pcn1-CFP focus in the first 90 minutes following anaphase. The *RTS1-IO* strain is MON227 (n = 31), and the *RTS1-AO* strain is MON232 (n = 31). (C) Example of images taken from a time-lapse movie of a cell with Pcn1-CFP and Pol12-YFP. The strain pictured is MON213. The scale bar in all images represents 1 μM.

of cells with Pcn1 foci by 70 minutes after anaphase. On average, Pcn1 foci persist for approximately 40 minutes in an individual cell. To confirm that these Pcn1 foci are reflective of replication foci, I also looked at the dynamics of the YFP tag on the second subunit of DNA polymerase α (Pol12), which had been previously characterized (Meister et al. 2007). As expected, Pol12-YFP foci co-localize with Pcn1-CFP foci (Figure 4.1C) (Meister et al. 2007). Altogether, these data suggest that the vast majority of cells begin DNA replication within 10 or 15 minutes following anaphase under these imaging conditions and that S-phase is normally completed between 45 – 60 minutes following anaphase.

4.2.2 The *RTS1* replication fork barrier stimulates the recruitment of Rad52-YFP to the *ade6* locus

Our laboratory has previously shown that the *RTS1* RFB induces recombination that is dependent on Rad52 (Ahn et al. 2005). To determine the frequency and timing of recruitment of Rad52, I monitored Rad52-YFP foci in live cells containing either *RTS1-IO* or *RTS1-AO* by time-lapse microscopy. In addition to recording spontaneous Rad52-YFP foci, I also marked the time points when the Rad52-YFP focus co-localized with the *lacO*-LacI focus that visually marks the position of the *RTS1* in the nucleus (Figures 4.2 and 4.3). Rad52 is recruited to the *RTS1* RFB as early as 20 to 25 minutes following anaphase, as indicated by a subset of cells (8%) containing *RTS1-AO* exhibiting a Rad52 focus that co-localized with the *lacO*-LacI focus (Figure 4.4A). At 50 minutes post anaphase, 32% of the cells within the population

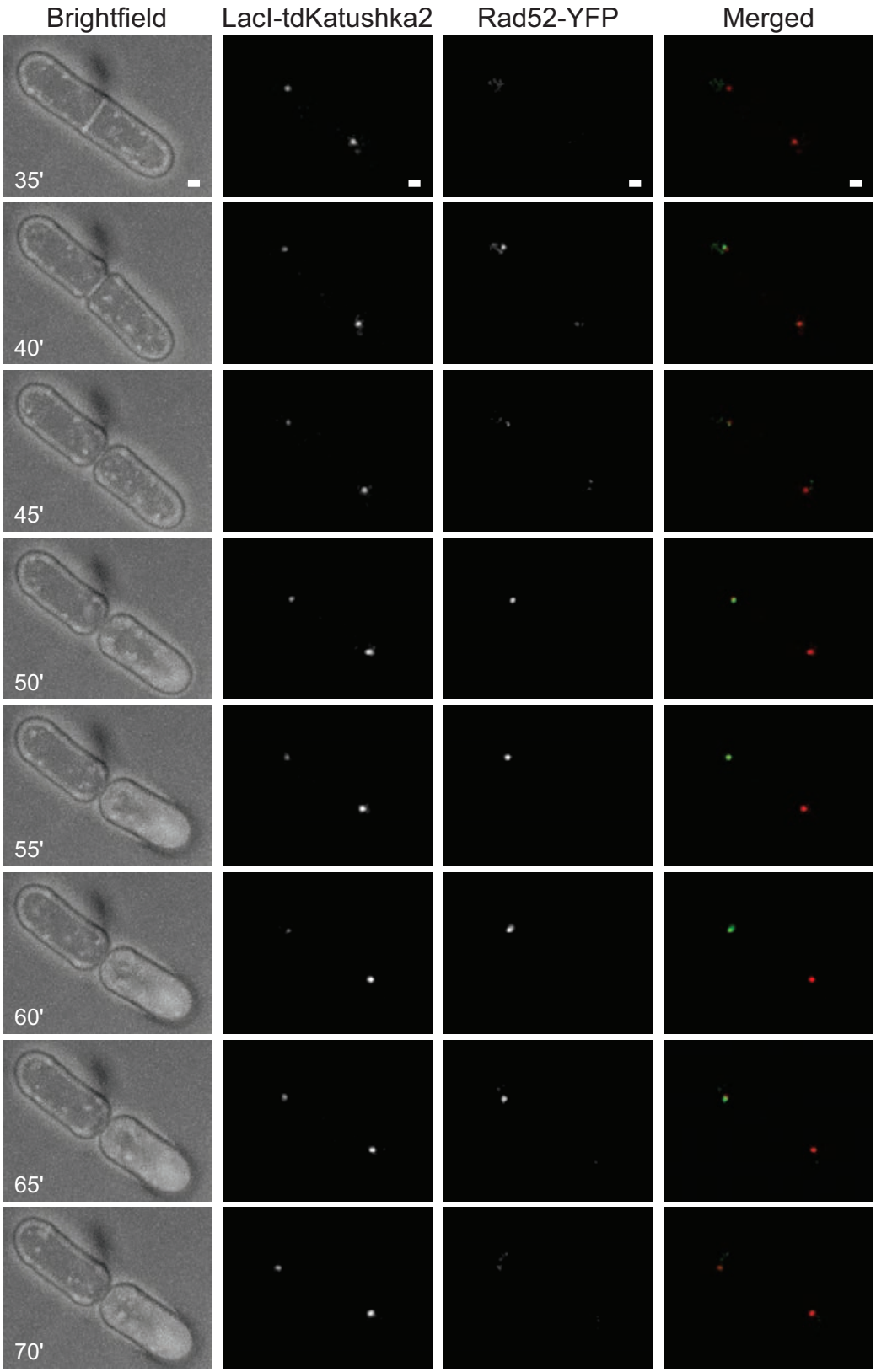


Figure 4.2 | A Rad52-YFP focus co-localizes with the *lacO*-LacI focus in one daughter. Example of images taken from a time-lapse movie of a cell with *RTS1-AO*, LacI-tdKatushka2 and Rad52-YFP. Scale bars represent 1 μM. The strain shown is MON148.

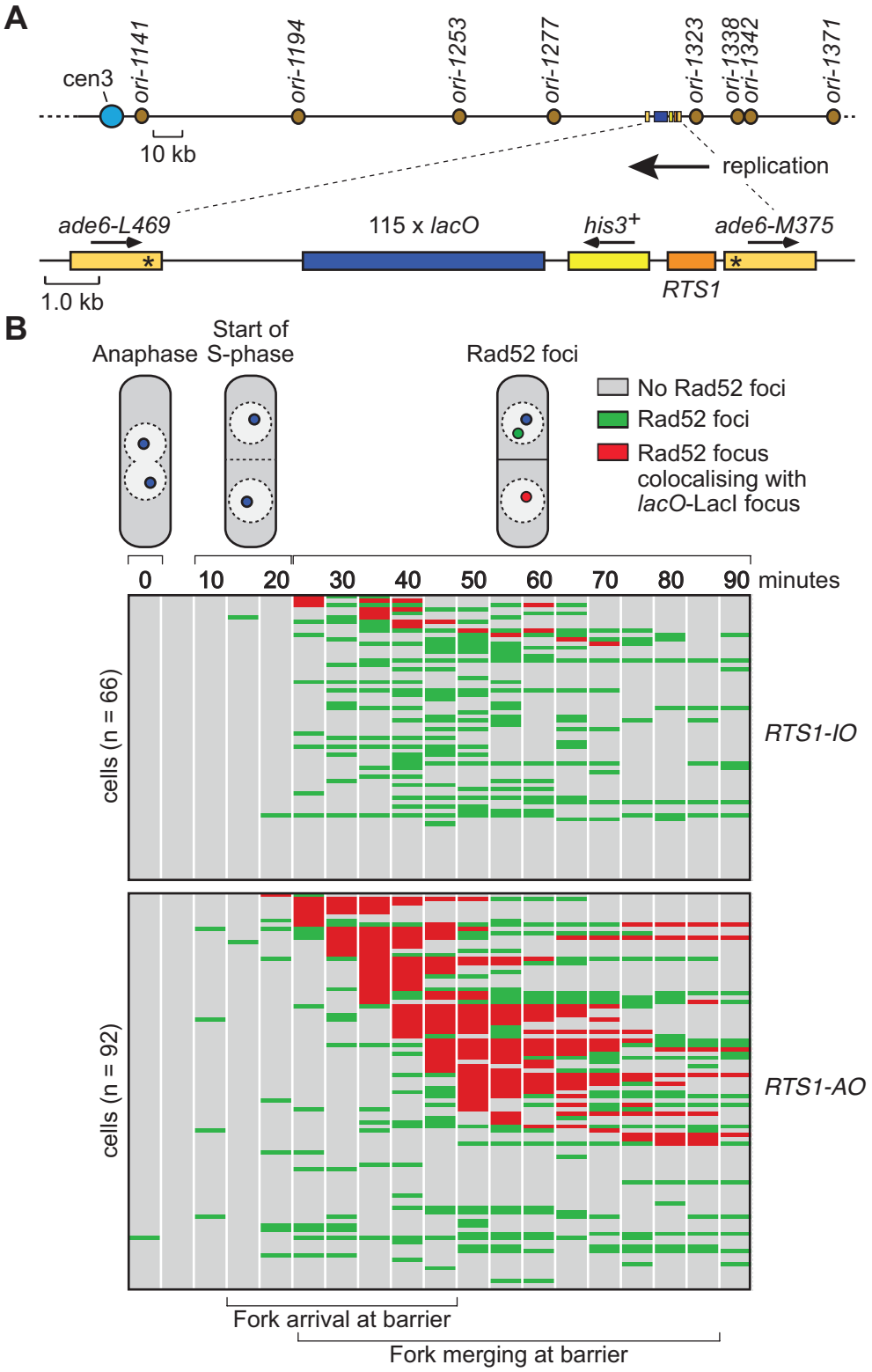


Figure 4.3 | Cells with *RTS1-AO* exhibit a Rad52-YFP focus that co-localizes with the *lacO*-LacI focus. (A) Schematic showing the chromosomal region where the *lacO* array is inserted within the recombination substrate on chromosome III. (B) Analysis of time-lapse movies. The *RTS1-IO* strain is MON110, and the *RTS1-AO* strain is MON148.

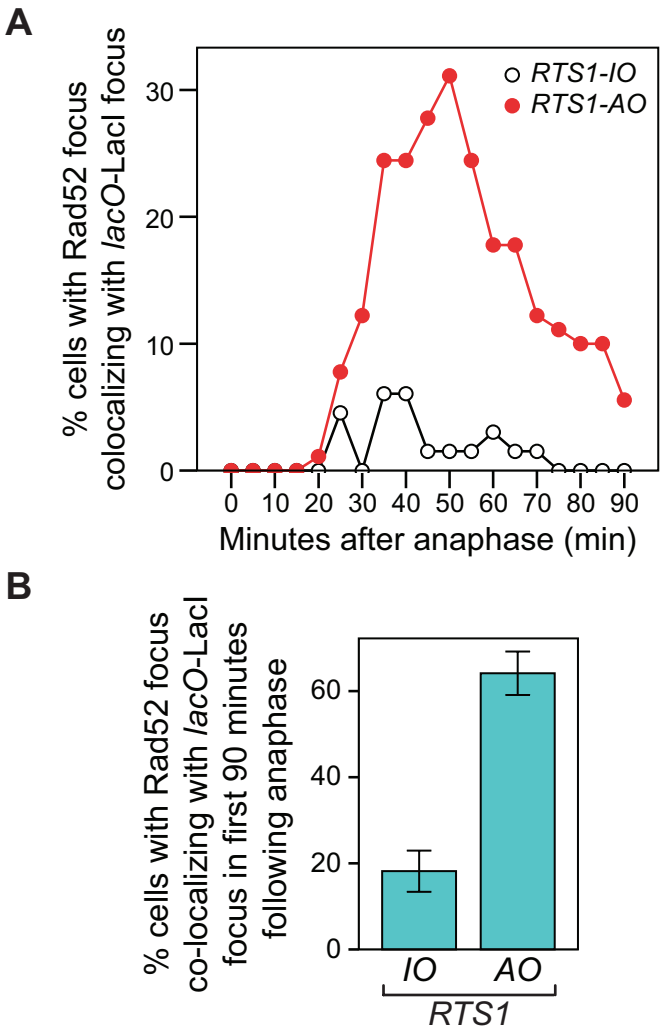


Figure 4.4 | **The *RTS1* RFB induces Rad52-YFP foci**. (A) Line graph of the percentage of cells with a Rad52-YFP focus that co-localize with the *lacO*-LacI focus during the first 90 minutes following anaphase at five-minute intervals. (B) Bar chart of the percentage of cells that exhibit at least one Rad52-YFP focus that co-localizes with the *lacO*-LacI focus in the first 90 minutes following anaphase. Error bars represent ± one standard error of the mean. The *RTS1-IO* strain is MON110 and the *RTS1-AO* strain is MON148.

exhibit a co-localizing Rad52 focus and by 90 minutes, this has reduced to 5%. Overall 64% of cells containing *RTS1-AO* exhibit at least one Rad52 focus that co-localizes with a *lacO*-LacI focus in the first 90 minutes following anaphase compared to 18% of cells containing *RTS1-IO*. If one discounts single time point co-localizations, which may occur by chance, and only considers cells in which Rad52-*lacO*-LacI co-localization is observed in two consecutive time points then the value for *RTS1-AO* cells only drops to 52%, whereas for *RTS1-IO* cells it drops to 5% (Figure 4.5A). Overall these data indicate that the majority of cells within a population mount a recombinational response to replication fork stalling at *RTS1*. Moreover, based on the timing of Pcn1-CFP foci (Figure 4.1B), Rad52 is recruited to *RTS1* during S-phase, and at least in some cells within ~ 10 minutes of the replication fork encountering the barrier.

4.2.3 Temporal dynamics of the Rad52-YFP focus at *RTS1* during the cell cycle

Time-lapse microscopy of individual cells revealed that the Rad52-YFP focus persists at the *RTS1* RFB. In cells with *RTS1-AO*, the number of time points cells have a co-localized Rad52 focus ranges from one to ten time points, albeit the cells with over six time points with a co-localized Rad52 represent a very small minority of total cells. On average, an individual cell with *RTS1-AO* has ~ 2.41 time points with a co-localized Rad52 focus in the first 90 minutes following anaphase compared to ~ 0.27 time points in cells with *RTS1-IO* (Figure 4.5B). To investigate whether these time points of co-localized Rad52

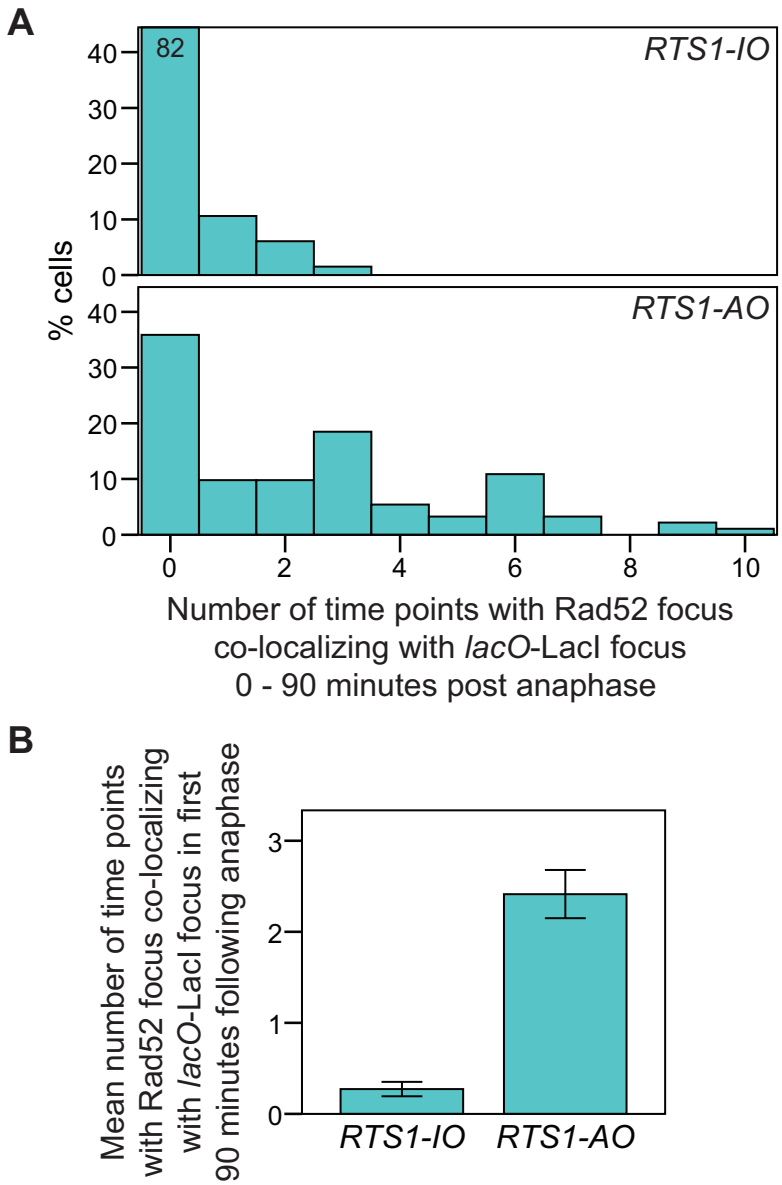


Figure 4.5 | Cells exhibit a prolonged Rad52-YFP focus at the *RTS1* RFB. (A) Histogram showing the percentage of cells with a given number of time points in which a Rad52-YFP focus co-localizes with a *lacO*-LacI focus within the first 90 minutes following anaphase. (B) Bar chart of the mean number of time points cells have a Rad52-YFP focus that co-localizes with a *lacO*-LacI focus during the first 90 minutes following anaphase. Error bars represent ± one standard error of the mean. The *RTS1-IO* strain is MON110, and the *RTS1-AO* strain is MON148.

occurred consecutively, I also plotted the longest track of consecutive time points in which Rad52 co-localization with *lacO*-LacI was observed for each cell (Figure 4.6A). These histograms look similar to those in Figure 4.5A, indeed the mean numbers for the longest track of consecutive time points with a co-localized Rad52 focus are only slightly less than those for the total time points with a co-localized Rad52 focus (Figures 4.5B and 4.6B). These data suggest that Rad52 is recruited to *RTS1-AO* once, presumably following replication fork blockage, and then persists there possibly until replication is complete. The mean number of consecutive time points with a co-localizing Rad52 focus is ~ 2.2 and therefore, on average, Rad52 remains at *RTS1-AO* for ~ 5 – 15 minutes, with the caveat being that due to the limitations of the cells being imaged every five minutes, it is possible, although unlikely, that Rad52 may dissociate before re-associating with the site in the intervals between imaging.

4.2.4 Rad52 focus assembly at *RTS1* has a random distribution in daughter cells

To investigate whether there is a propensity for paired daughter cells to both experience Rad52 recruitment to the *RTS1* RFB, I also analyzed the percentage of paired daughter cells with a co-localizing Rad52 focus in neither, one, or both daughters (Figure 4.7). In this analysis, I was able to follow 56 cells that had a paired daughter out of the 66 total *RTS1-IO* cells and 68 cells that had a paired daughter out of the 92 total *RTS1-AO* cells. Of these 68 *RTS1-AO* cells, 70.6% of cells exhibited a co-localized Rad52 focus,

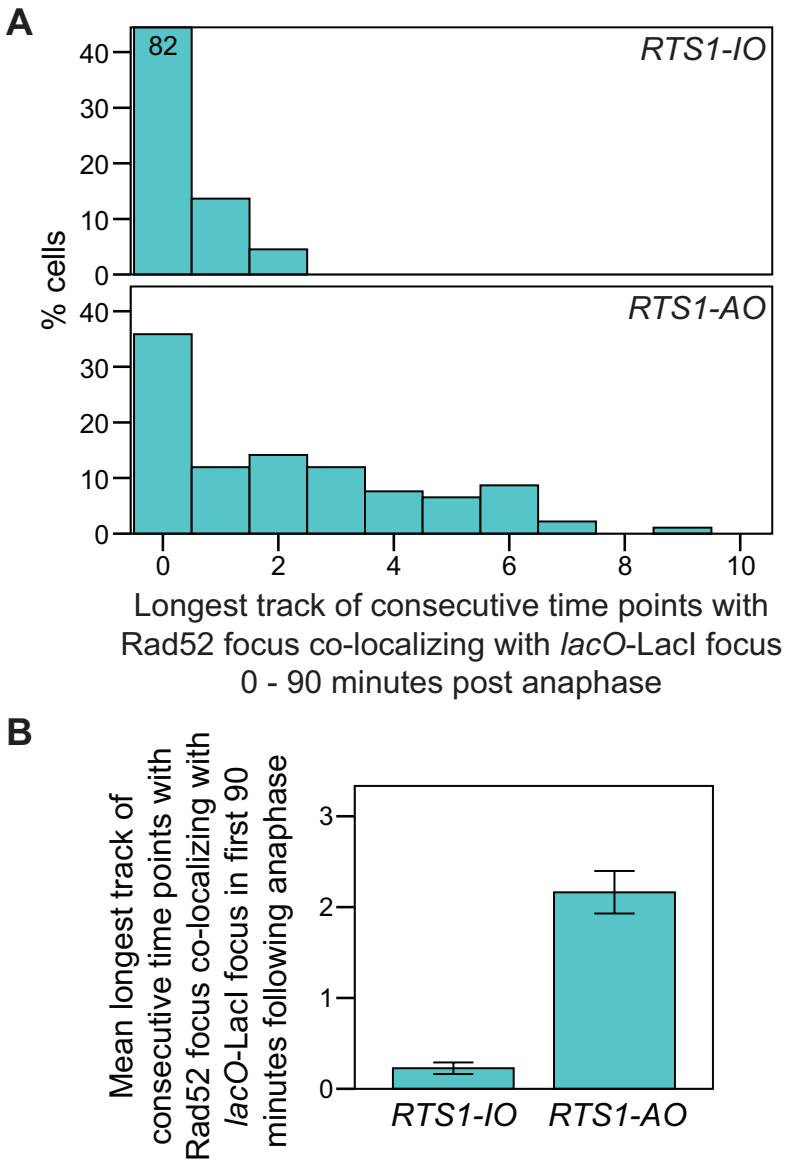


Figure 4.6 | Cells exhibit tracks of a Rad52-YFP focus at the *RTS1* RFB that are uninterrupted. (A) Histogram showing the percentage of cells with a given number of uninterrupted time points in which a Rad52-YFP focus co-localizes with a *lacO*-LacI focus within the first 90 minutes following anaphase. (B) Bar chart of the mean number of uninterrupted time points cells have a Rad52-YFP focus that co-localizes with a *lacO*-LacI focus during the first 90 minutes following anaphase. Error bars represent ± one standard error of the mean. The *RTS1-IO* strain is MON110, and the *RTS1-AO* strain is MON148.

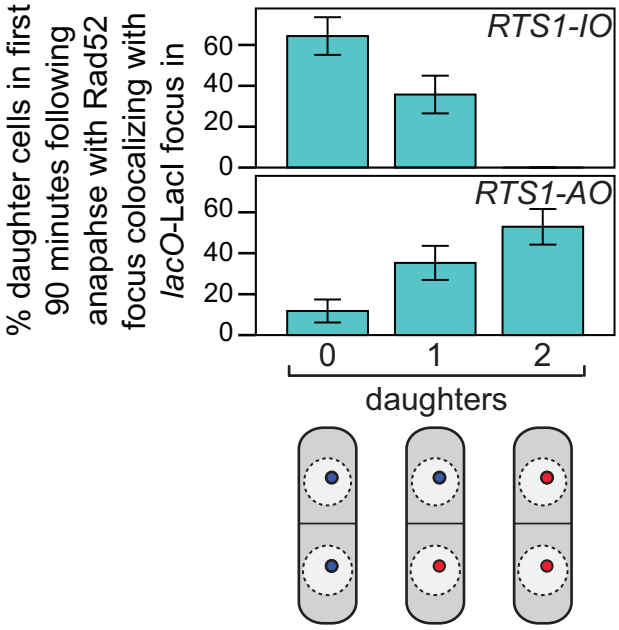


Figure 4.7 | Cells that exhibit a Rad52-YFP focus are randomly distributed amongst daughter cells with *RTS1-AO*. Histogram showing the percentage of daughter cells in the first 90 minutes following anaphase with neither, one, or both paired daughters having a Rad52-*lacO*-LacI co-localization. Error bars represent ± one standard error of the mean. The *RTS1-IO* strain is MON110, and the *RTS1-AO* strain is MON148.

which is a slightly higher proportion than seen in the 64% of cells of the 92 total cells analyzed. In cells with the *RTS1-IO*, over 60% of paired daughter cells did not have a co-localized Rad52 focus in either daughter, just under 40% of paired daughter cells had a co-localized Rad52 focus in one daughter, and there were no instances in which both daughters had a co-localized Rad52 focus. In contrast, in cells with *RTS1-AO*, only 12% of paired daughters did not have a co-localized Rad52 focus whereas 35% and 53% of paired daughter cells had a co-localized Rad52 focus in one or both daughters, respectively. Intriguingly, the distribution of the *RTS1-AO* paired daughter cells is similar to one that is predicted by chance based on a 70.6% chance of a cell exhibiting a co-localized Rad52 focus. In this scenario based on a random distribution, 8.6% of paired daughter cells should not have a co-localized Rad52 focus whereas 41.4% and 50% of paired daughter cells should have a co-localized Rad52 focus in one or both daughters, respectively. The predicted random distribution does not differ significantly from the empirical data. This indicates that Rad52 co-localization at *RTS1-AO* has no bearing on whether Rad52 is recruited to *RTS1* in the paired daughter cell, which in turn suggests that Rad52's localization to *RTS1* is stochastic.

4.2.5 Comparison between the temporal dynamics of spontaneous and *RTS1*-induced Rad52 foci during the cell cycle

The data in Figures 4.3B and 3.9A (Chapter 3) reveal that most cells have a minimum of one Rad52-YFP focus during the first 90 minutes following anaphase regardless of *RTS1* orientation or presence. Rad52 foci can occur

in response to DSBs and replication perturbation. To see whether the appearance of Rad52 at *RTS1* is distinct from spontaneous Rad52, I compared the time when spontaneous Rad52-YFP foci first occurred in cells containing *RTS1-IO* to the time when co-localized Rad52 foci first occur in cells containing *RTS1-AO* (Figure 4.8A). In both cases, the majority of spontaneous and co-localized Rad52 foci occur within 25 to 50 minutes post anaphase and normally are not evident within the first 15 minutes when S-phase is starting. On average, a Rad52 focus is first observed 40 minutes after anaphase regardless of whether it co-localizes with *RTS1* or not (Figure 4.8B). The fact that spontaneous Rad52 foci occur with similar timing to foci that co-localize with *RTS1* may be consistent with the notion that spontaneous foci mainly arise in response to replication perturbation.

4.2.6 Rad51-CFP does not form detectable foci at *RTS1*

Having established that Rad52 is recruited to stalled forks at *RTS1* in most cells during S-phase, I next investigated whether its recruitment led to detectable Rad51 foci at the *RTS1* RFB. This is relevant because Rad52 is believed to promote the nucleation of Rad51 onto RPA-coated ssDNA and our lab has previously shown that replication fork blockage by *RTS1* results in a strong stimulation in Ade^+ recombinant formation that is dependent on Rad51 (Ahn et al. 2005). Dr. Fikret Osman had previously constructed strains in our laboratory that expressed a fluorescently tagged Rad51 protein either alone or in tandem with an untagged Rad51 protein. The untagged Rad51 protein is expressed from the endogenous Rad51 promoter and integrated at the *ura4*

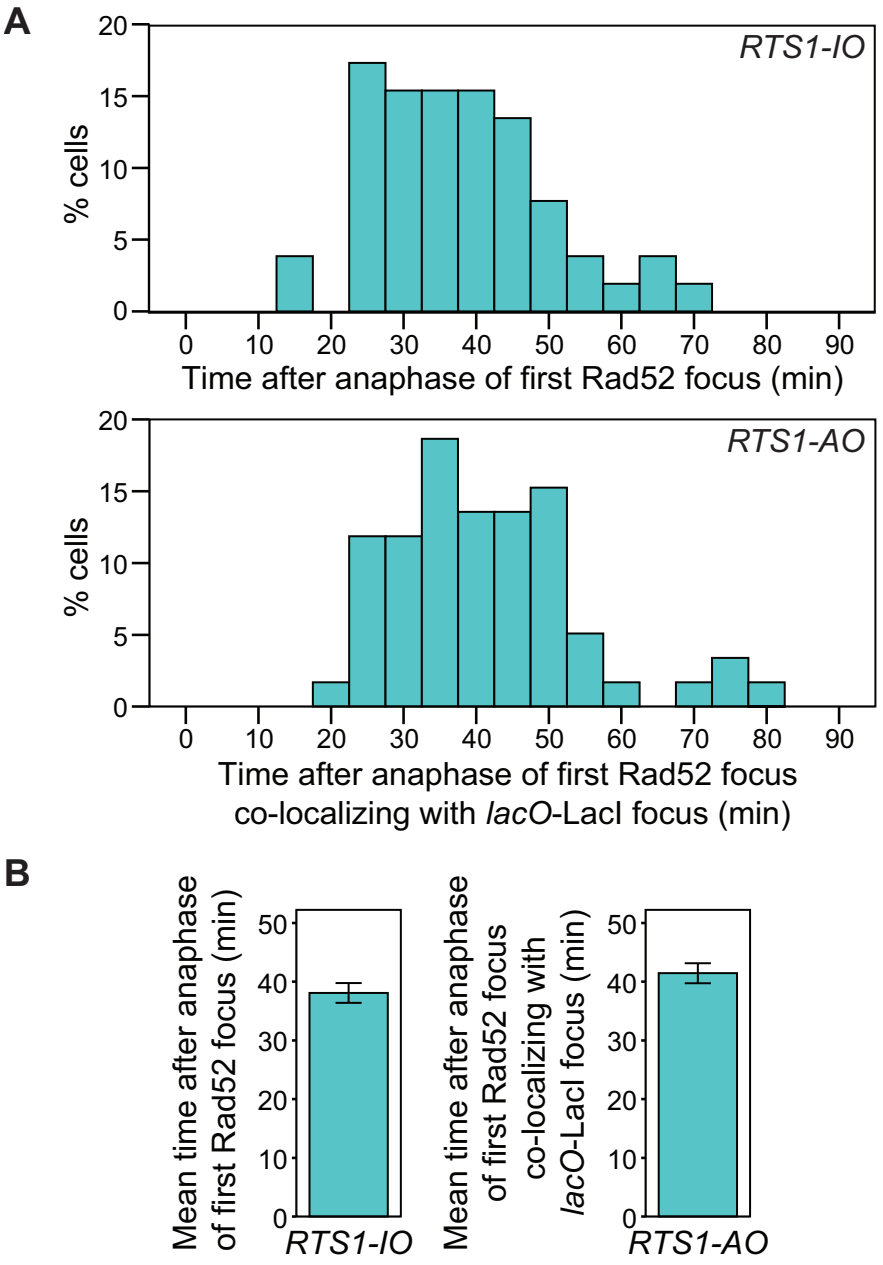


Figure 4.8 | The Rad52-YFP focus is induced at the *RTS1* RFB at a similar time as when spontaneous Rad52-YFP foci are detected in unperturbed cells. (A) Histogram showing the percentage of cells at a given time after anaphase in which the first Rad52-YFP focus is detected (top panel) or the first Rad52-YFP focus co-localizes with a *lacO*-LacI focus (bottom panel). (B) Bar chart of the mean time after anaphase of when the first Rad52-YFP focus is detected (left panel) or the first Rad52-YFP focus co-localizes with a *lacO*-LacI focus (right panel). Error bars represent ± one standard error of the mean. The *RTS1-IO* strain is MON110, and the *RTS1-AO* strain is MON148.

locus on chromosome III. The tagged Rad51 protein is fused with eCFP on its N-terminus, expressed from the endogenous Rad51 promoter, and integrated at the endogenous *rad51* locus.

As *rad51Δ* mutants are hypersensitive to a range of genotoxins, including CPT, HU, MMS, and UV, I tested the sensitivity of the strains with the fluorescently tagged Rad51 with and without untagged Rad51 and compared them to wild-type and a *rad51Δ* mutant (Figure 4.9). Strains that express the fusion Rad51 protein without the untagged Rad51 protein are hypersensitive to CPT, HU, MMS, and UV compared to the wild-type strain, but they are not as sensitive as a *rad51Δ* single mutant. On the other hand, strains that express both the fusion Rad51 protein and the untagged Rad51 protein did not show sensitivity to either the lower or higher dosages of genotoxins, similar to the wild-type strain. Altogether, this suggests that Rad51-CFP may not efficiently substitute for untagged Rad51 in repairing damage-induced lesions but is sufficiently active to function together with untagged Rad51 in repairing CPT-, HU-, MMS-, and UV-induced lesions when they are expressed together. For this reason, to visualize Rad51 activity at *RTS1*, I decided to use strains that expressed both untagged and fluorescently tagged Rad51.

To determine the frequency and timing of recruitment of Rad51 at *RTS1*, I monitored Rad51-CFP foci in an asynchronous population of live cells containing either *RTS1-IO* or *RTS1-AO* by time-lapse microscopy. When I attempted to track Rad51-CFP foci, however, I found that most cells did not

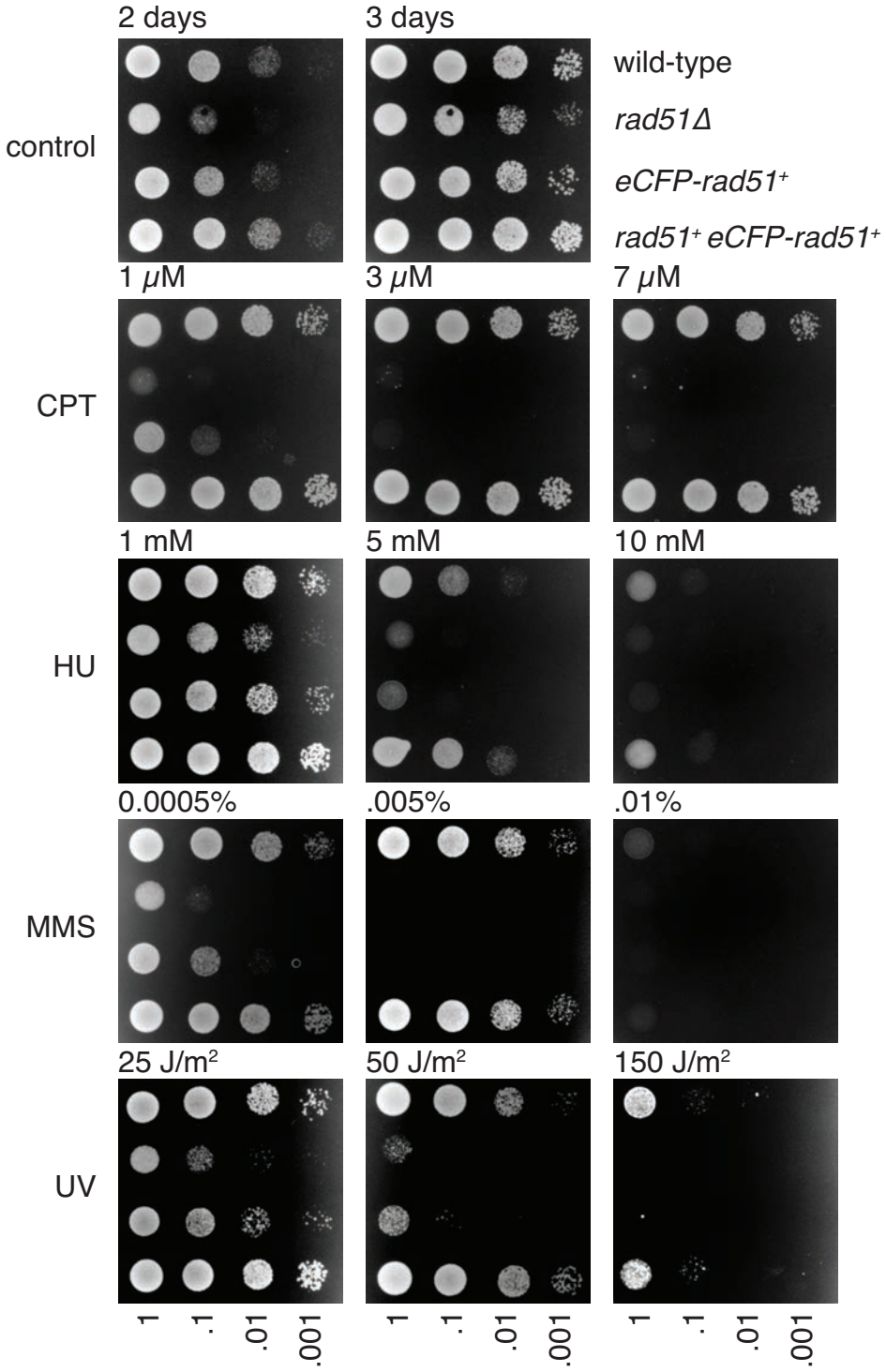


Figure 4.9 | Cells with both untagged and tagged Rad51 are not sensitive to CPT, HU, MMS, or UV. Spot assays comparing the growth and sensitivity of wild-type (MCW1221), *rad51Δ* (MCW1088), *eCFP-rad51*$^{+}$ (MCW4643), and *rad51*$^{+}$ *eCFP-rad51*$^{+}$ (MCW5146) to different genotoxins. Strains were grown on complete media for 3 days at 30°C before being photographed. The control plate is also shown after 2 days of incubation.

exhibit either a detectable spontaneous or *RTS1*-induced Rad51 focus through an entire four-hour time course. This contrasts with how most cells will exhibit a Rad52-YFP focus spontaneously within the first 90 minutes following anaphase under the same imaging conditions. To see whether Rad51-CFP is capable of forming detectable foci in response to replication fork blockage and/or breakage, I next analyzed Rad51-CFP focus formation in cells exposed to 10 μM CPT for four hours. Under the same imaging conditions, exposure to CPT results in a single Rad51 focus in the majority of cells (Figure 4.10). These data suggest that Rad51 form foci in response to damage-induced lesions; however, Rad51 does not form detectable foci during spontaneous or *RTS1*-induced Rad51-mediated recombination events under my imaging conditions.

4.2.7 Rad54-GFP does not form detectable foci at *RTS1*

As an alternative to Rad51 as a recombination marker downstream of Rad52, I next investigated whether Rad54 could form detectable foci at *RTS1* in live cells. Similar to Rad51 and Rad52, I found that Rad54 is required for promoting replication fork block-induced gene conversions at *RTS1* (see Chapter 7). To follow the spatio-temporal dynamics of Rad54 foci, I sought to use a Rad54-GFP fusion protein with the GFP tag on the C-terminus of Rad54, which had previously been characterized and shown to be fully functional with respect to conferring resistance to replication lesions that are induced by CPT and MMS (Maki et al. 2011).

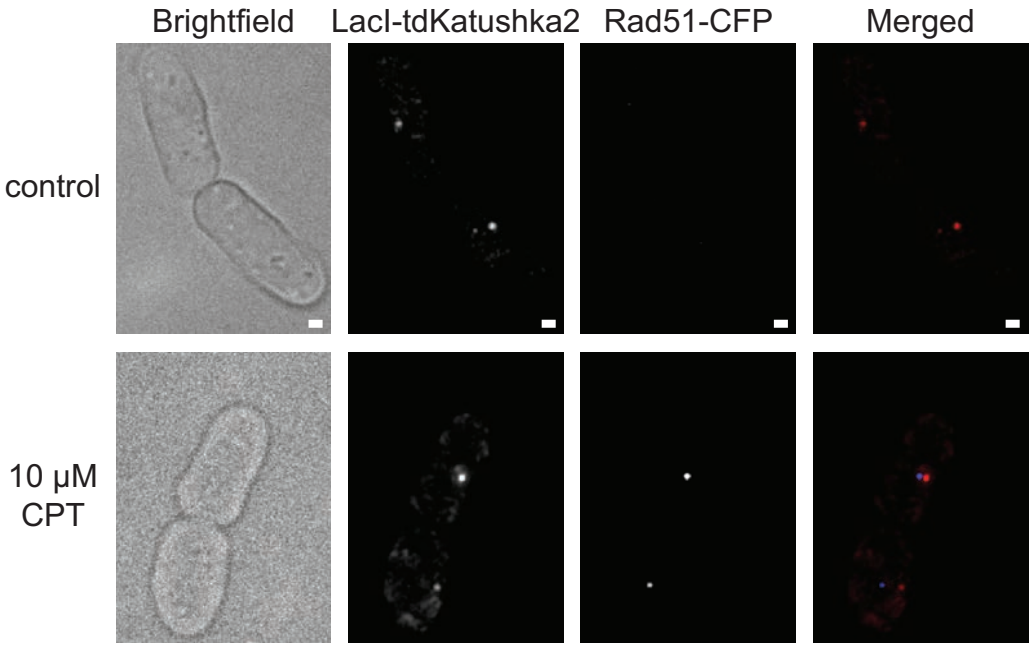


Figure 4.10 | Rad51-CFP foci are not detected at the *RTS1* RFB but are detected in cells treated with CPT. Example of images of a cell with *RTS1-AO*, LacI-tdKatushka2 and Rad51-CFP. The scale bar in all images represents 1 μM. The strain shown is MON222.

To determine the frequency and timing of recruitment of Rad54 at *RTS1*, I monitored Rad54-GFP foci in an asynchronous population of live cells containing either *RTS1-IO* or *RTS1-AO* by time-lapse microscopy. Similar to Rad52, most cells exhibit a spontaneous Rad54 focus in the first 90 minutes following anaphase; however, unlike Rad52, many cells exhibit 2 – 4 Rad54-GFP foci simultaneously across multiple time points (data not shown and Figure 4.11A). Despite this, there is no clear and logical difference in the percentage of cells displaying a Rad54 focus that co-localizes with the *lacO*-LacI focus in the first 90 minutes following anaphase in strains with *RTS1-AO* compared to strains with *RTS1-IO* (Figure 4.11B). In both *RTS1-IO* and *RTS1-AO* strains, over 60% of cells do not exhibit a Rad54-GFP focus that co-localizes with a *lacO*-LacI focus, and in the majority of cells, the co-localizing Rad54-GFP focus does not persist at the site beyond one time point (Figure 4.11C). These data suggests that there is no significant difference in Rad54-GFP foci patterns in *RTS1-AO* strains compared to *RTS1-IO* strains. Intriguingly, when strains with Rad54-GFP are exposed to 10 μM CPT for four hours, Rad54 forms damage-induced foci that are brighter than the Rad54-GFP foci that arise spontaneously (data not shown). Altogether, these data indicate that, similar to Rad51, Rad54 does not form detectable foci in response to replication fork blockage at *RTS1* under these imaging conditions and that damage-induced Rad54 foci formation is different than the Rad54 foci that arise spontaneously.

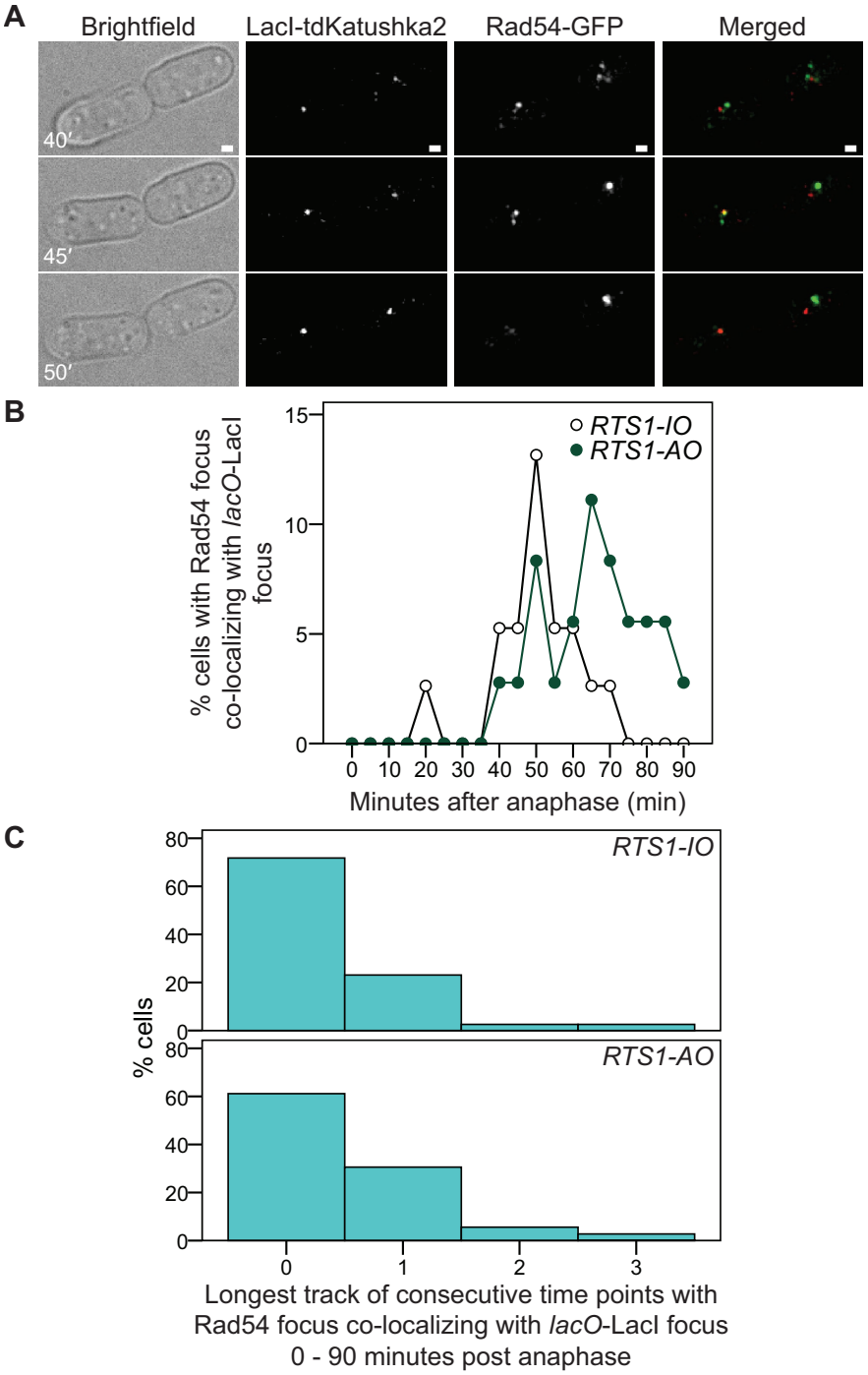


Figure 4.11 | Rad54-GFP foci do not persist at the *RTS1* RFB. (A) Example of images taken from a time-lapse of a cell with *RTS1-AO*, LacI-tdKatushka2 and Rad54-GFP. The scale bar in all images represents 1 μM. (B) Line graph of the percentage of cells with a Rad54-GFP focus that co-localize with the *lacO*-LacI focus during the first 90 minutes following anaphase at five-minute intervals. (C) Histogram showing the percentage of cells with a given number of uninterrupted time points in which a Rad54-GFP focus co-localizes with a *lacO*-LacI focus within the first 90 minutes following anaphase. The *RTS1-IO* strain is MON341 (n = 39), and the *RTS1-AO* strain is MON342 (n = 36).

4.2.8 Rad11-GFP is recruited to the *RTS1* replication fork barrier

The binding of the heterotrimeric ssDNA-binding protein RPA, an essential factor in DNA replication and DNA damage repair, to ssDNA is known to precede the binding of Rad52 at recombination sites. As arrested replication forks can accumulate a patch of ssDNA that RPA may bind to, I investigated whether Rad11, the large subunit of RPA, forms detectable foci at the *RTS1* RFB in live cells. To this end, I made use of strains expressing a Rad11-GFP fusion protein (Tomita and Cooper 2008; Cavero et al. 2010; Takahashi et al. 2011). Rad11-GFP foci were imaged every five minutes during a four-hour time-lapse experiment (Figure 4.12). To see whether there is a difference between *RTS1-AO* and *RTS1-IO* cells in the recruitment and/or timing of Rad11-GFP foci co-localization with the *lacO*-LacI array, I assessed the percentage of cells with a co-localizing Rad11-GFP focus through the first 90 minutes following anaphase (Figure 4.13A). This analysis reveals that a higher proportion of cells with *RTS1-AO* display a Rad11-GFP focus that co-localizes with the *lacO*-LacI focus than those with *RTS1-IO* and that RPA (Rad11-GFP) is recruited to the *RTS1* RFB as early as 40 to 45 minutes following anaphase (Figure 4.13A).

On an individual cell-by-cell basis, 77% of cells containing *RTS1-AO* have a minimum of one Rad11-GFP focus that co-localizes with a *lacO*-LacI focus in the first 90 minutes following anaphase whereas in the *RTS1-IO* strain, only 23.5% of cells exhibit this (Figure 4.13B). As these co-localization events can represent both chance and meaningful co-localization at *RTS1*, I also

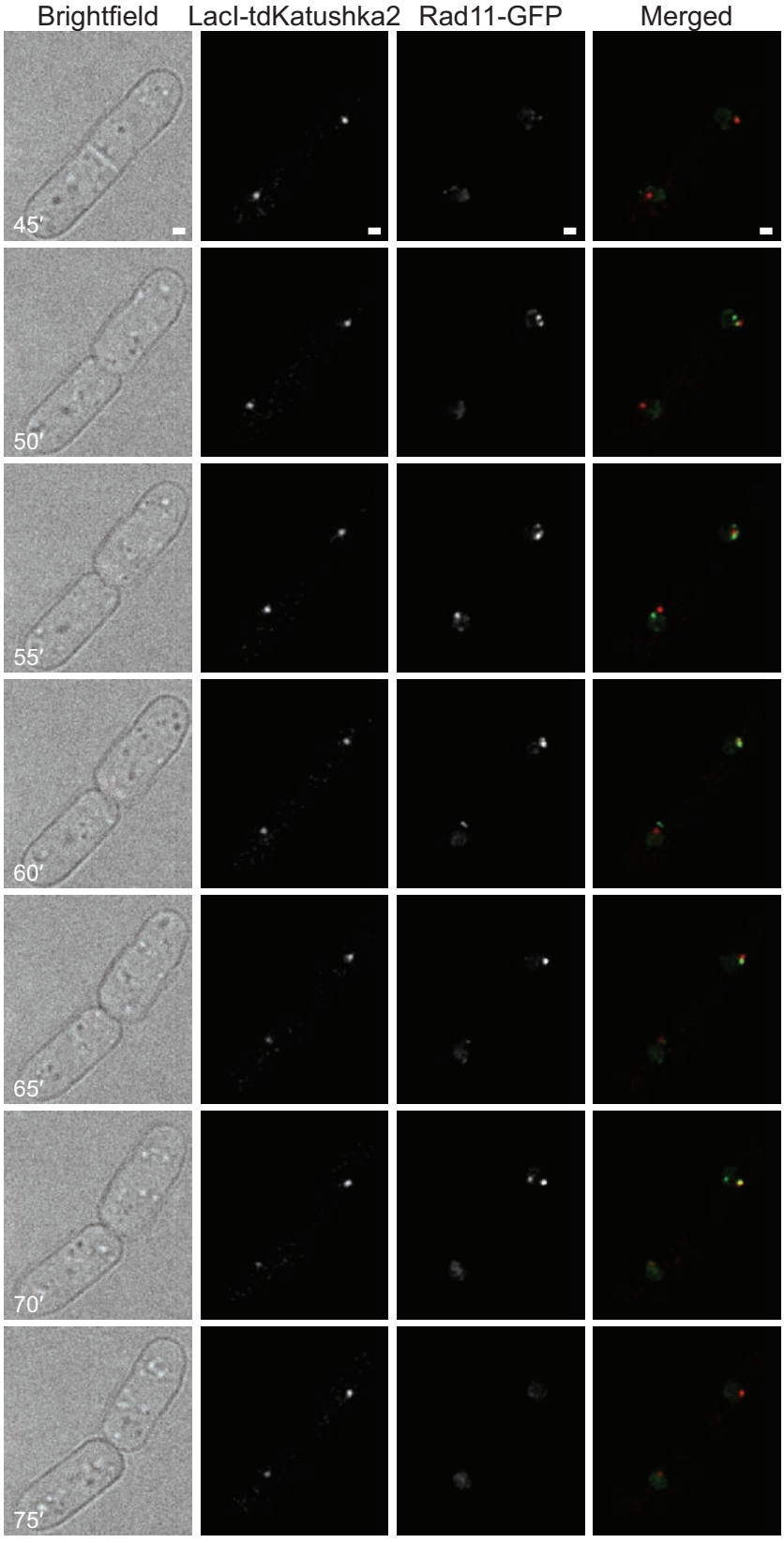


Figure 4.12 | A Rad11-GFP focus co-localizes with the *lacO*-LacI focus in one daughter. Example of images taken from a time-lapse movie of a cell with *RTS1-AO*, LacI-tdKatushka2 and Rad11-GFP. The scale bar in all images represents 1 μM. The strain shown is MON335.

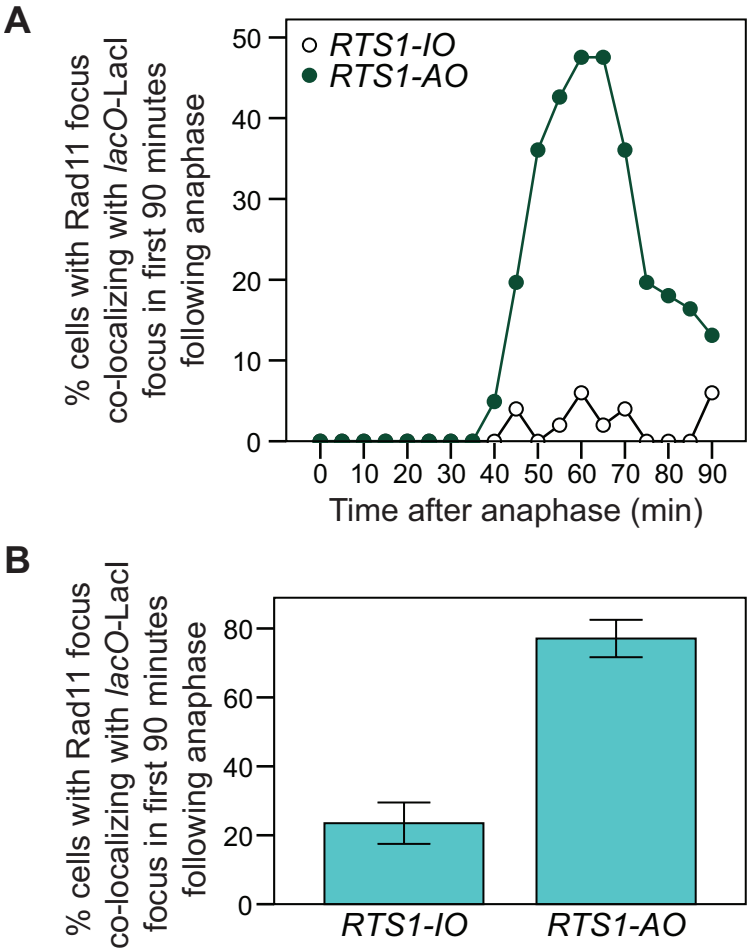


Figure 4.13 | The *RTS1* RFB induces Rad11-GFP foci. (A) Line graph of the percentage of cells with a Rad11-GFP focus that co-localize with the *lacO*-LacI focus during the first 90 minutes following anaphase at five-minute intervals. (B) Bar chart of the percentage of cells that exhibit at least one Rad11-GFP focus that co-localizes with the *lacO*-LacI focus in the first 90 minutes following anaphase. Error bars represent ± one standard error of the mean. The *RTS1-IO* strain is MON330 (n = 51) and the *RTS1-AO* strain is MON335 (n = 61).

investigated the total number of time points an individual cell has a Rad11 focus co-localizing with the *lacO*-LacI focus in the first 90 minutes following anaphase. In the *RTS1-AO* strain, over 70% of cells have a minimum of two time points with a Rad11-GFP focus co-localizing with a *lacO*-LacI focus compared to less than 3% in *RTS1-IO* cells (Figure 4.14A). In fact, in the *RTS1-AO* strain, the number of time points cells have a co-localized Rad11 focus ranges from one to eight time points. On average, an individual *RTS1-AO* cell has ~ 3 time points with a co-localized Rad11 focus in the first 90 minutes following anaphase compared to ~ 0.25 time points in a *RTS1-IO* cell (Figure 4.14B). To investigate whether these time points of co-localized Rad11 occur consecutively, I also determined the longest track of consecutive time points with a co-localized Rad11 focus in each cell (Figure 4.14C). The similarity of the *RTS1-AO* histograms in Figures 4.14A and 4.14C indicates that in most cases when Rad11 co-localizes with *RTS1-AO*, it does so through a series of consecutive time points. Based on these data, I can also conclude that, on average, Rad11 persists at *RTS1-AO* for approximately 10 to 15 minutes.

4.2.9 Timing of Rad11-GFP focus formation at *RTS1-AO* during the cell cycle

To determine the timing of the appearance of Rad11 at *RTS1*, I examined the first time point when a Rad11 focus first co-localized with a *lacO*-LacI focus in *RTS1-AO* cells (Figure 4.15A). The majority of co-localized Rad11 foci occur between 40 to 65 minutes post anaphase, with the mean time being ~ 54

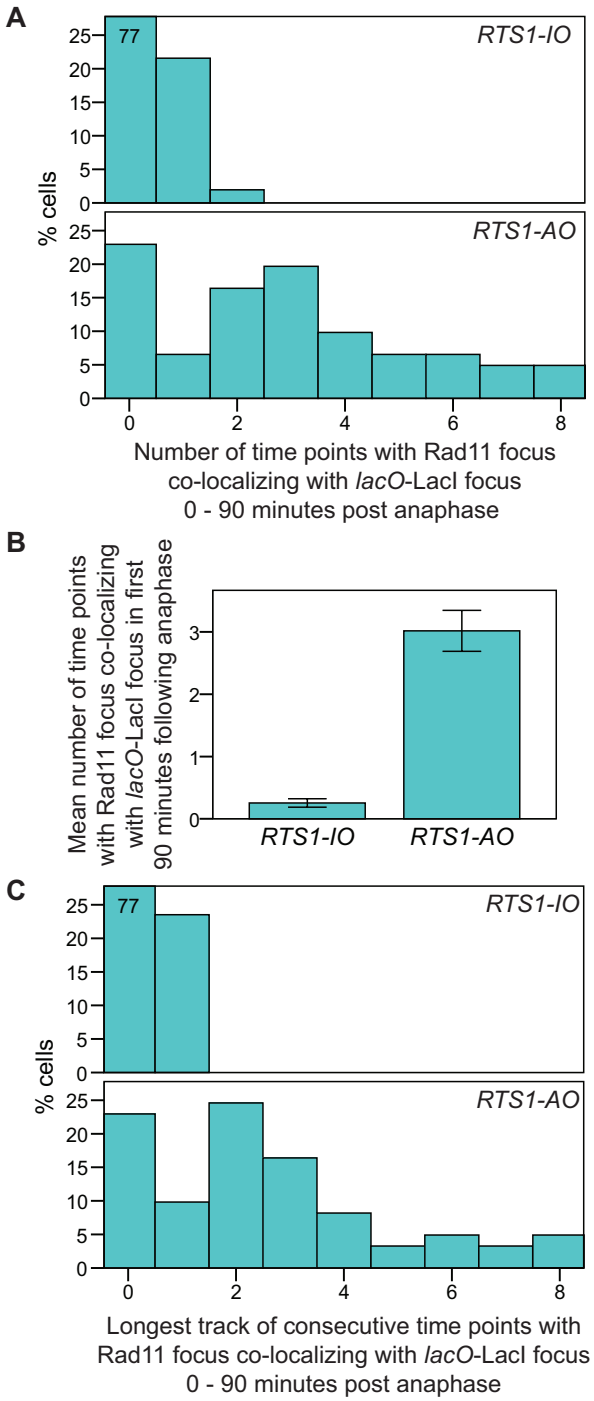


Figure 4.14 | Cells exhibit a prolonged Rad11-GFP focus at the *RTS1* RFB. (A) Histogram showing the percentage of cells with a given number of time points in which a Rad11-GFP focus co-localizes with a *lacO*-LacI focus within the first 90 minutes following anaphase. (B) Bar chart of the mean number of time points cells have a Rad11-GFP focus that co-localizes with a *lacO*-LacI focus during the first 90 minutes following anaphase. Error bars represent ± one standard error of the mean. (C) Histogram showing the percentage of cells with a given number of uninterrupted time points in which a Rad11-GFP focus co-localizes with a *lacO*-LacI focus within the first 90 minutes following anaphase. The *RTS1-IO* strain is MON330, and the *RTS1-AO* strain is MON335.

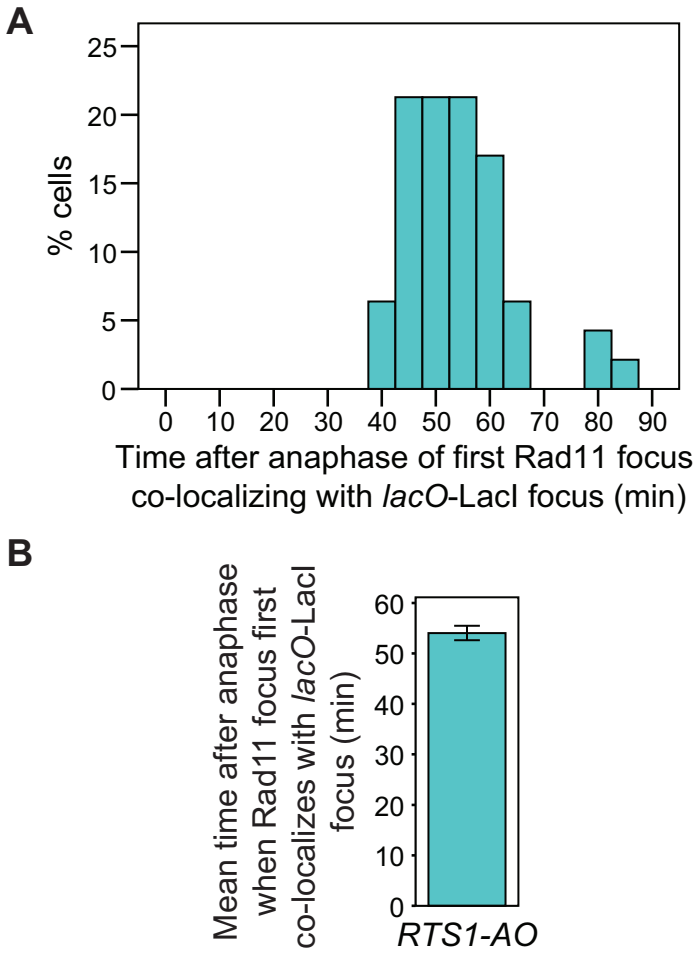


Figure 4.15 | Timing of when the first Rad11-GFP focus co-localizes at the *RTS1* RFB. (A) Histogram showing the percentage of cells at a given time after anaphase in which the first Rad11-GFP focus co-localizes with a *lacO*-LacI focus. (B) Bar chart of the mean time after anaphase of when the first Rad11-GFP focus co-localizes with a *lacO*-LacI focus. Error bars represent ± one standard error of the mean. The *RTS1-AO* strain is MON335.

minutes (Figure 4.15B). Altogether, these data suggest that RPA is recruited to the *RTS1* RFB and that Rad11 begins to form detectable foci at *RTS1* at a later time point than when Rad52-YFP foci are first observed.

4.3 Discussion

4.3.1 Dynamics of Rad52 foci at replication forks blocked at *RTS1*

Our laboratory previously found that recombination is stimulated at forks blocked by *RTS1*. However, it was unclear to what extent recombination is initiated directly at the stalled/blocked fork. In this chapter, I have shown that recombination is triggered in a majority of cells that have a fork blocked by *RTS1* as indicated by the prevalence of cells exhibiting a Rad52-YFP focus co-localizing with a *lacO*-LacI focus. In *S. cerevisiae*, Rad52 has been shown to be recruited to replication forks that collapse but not to those that simply stall (Lisby et al. 2004). If the same is true in *S. pombe*, then the majority of forks that encounter *RTS1* collapse. Interestingly, there is no detectable difference in the growth or viability of recombination-deficient (e.g., *rad52Δ*) strains with either *RTS1-IO* or *RTS1-AO* (Ahn et al. 2005). This suggests that recombinase activity at forks blocked at *RTS1* is unnecessary for growth and survival. Despite this, the induction of recombination at *RTS1* generally occurs during S-phase and in some cells, is observed as early as 5 – 10 minutes following its initiation, as determined by the timing of when Pcn1-CFP foci appear. This indicates that recombination is triggered within a few minutes of fork blockage by *RTS1*, suggesting that recombination may be initiated as a default response to arrested forks at *RTS1* even when it is unnecessary for

viability and despite its propensity to generate genome rearrangements.

Interestingly, there is variability in the occurrence, timing, and duration of a co-localized Rad52-YFP focus even among paired daughter cells. This variability may be explained by the stochastic nature of origin firing, which would lead to differences between *RTS1-AO* cells in which origins of replication are firing and consequently, the timings of when fork blockage and fork convergence are occurring at *RTS1* relative to anaphase. The influence this has on recombination will be explored in Chapter 5. From the data described in this chapter, it is also unclear what leads to the curtailment of the Rad52-YFP focus at *RTS1*. Possible explanations include: a restarted fork that moves away from *RTS1*; a converging fork that arrives at the site and displaces the Rad52 protein; and/or the recruitment of downstream recombination factors. The latter two ideas will be explored in Chapters 5 and 6, respectively. Finally, as every *RTS1-AO* cell does not exhibit a Rad52-YFP focus at *RTS1*, it is also possible that recombination may be constrained in some cells under certain circumstances, such that Rad52 is not recruited at *RTS1* in every cell. This idea will be explored in Chapter 8.

4.3.2 Involvement of recombinases at replication forks blocked at *RTS1*

Recombination proteins may be directly loaded at the blocked fork for various reasons. For example, it is possible that recombinases may be recruited to arrested forks at *RTS1* to help maintain fork stability by promoting sister

chromatid interactions. Alternatively, recombination factors may load at gaps between the arrested fork and a converging fork that are generated during fork merging. We prefer the idea, however, that recombinases load directly at the blocked fork to aid in RDR.

To disentangle the possible reasons for why recombination occurs at blocked forks at *RTS1*, I attempted to track when replication across the *lacO* array occurred with respect to the timing of the appearance and disappearance of a co-localized Rad52-YFP focus through two different approaches. In the first method, I sought to follow the reduction and recovery in the intensity of the *lacO*-LacI focus, which is expected to occur during the transition from anaphase to replication of the locus during S-phase. Previous work has shown in budding yeast that the intensity of a *lacO*-LacI focus doubles following replication of the array (Kitamura et al. 2006). In my experiments, I sought to determine the difference in the timing of replication across the locus between cells with either *RTS1-IO* or *RTS1-AO*. Although I was able to reproducibly detect a reduction in the intensity of the *lacO*-LacI focus following anaphase, I could not robustly see the recovery in the intensity of the *lacO*-LacI focus to ascertain the timing at which the locus was replicated (data not shown). If I had been able to do this, I could have compared the time of recovery to that of Rad52-YFP focus appearance and disappearance at *RTS1*, and in so doing, obtain evidence that Rad52's presence was directly leading to replication restart. For example, if the intensity of the *lacO*-LacI focus consistently doubled following Rad52-YFP co-localization, this would

have been indicative of the recombinase having a role in restart since the *lacO* array is downstream of *RTS1* with respect to the direction of the restarted fork. Conversely, if the intensity of the *lacO*-LacI focus doubled before the appearance of a co-localized Rad52-YFP focus, then this would be suggestive of recombination arising in response to fork merging at *RTS1*. There are various reasons for why I may have been unable to track the recovery in the intensity of the *lacO*-LacI focus. For example, this analysis could be complicated by photobleaching of the LacI fluorophore or the possibility that LacI may not bind to all of the *lacO* repeats within the array under my imaging conditions.

In a second approach to understand why recombination occurs at *RTS1*, I also tried to determine when a Pcn1-CFP focus co-localized with the *lacO*-LacI focus in cells with either *RTS1-IO* or *RTS1-AO* during time-lapse imaging in strains that also expressed Rad52-YFP. Due to time restrictions, however, I decided to collaborate with Dr. Carl Morrow in our laboratory in order to carry out this analysis, which is still ongoing. Preliminary data in *RTS1-AO* cells suggests that there may be a loss of replisome association with the *RTS1* site based on how the *lacO*-LacI focus tends to transition from being in a cloud of Pcn1-CFP foci to associating with a Rad52-YFP focus that does not initially co-localize with a Pcn1-CFP focus. Intriguingly, the site appears to reassociate with a Pcn1-CFP focus following Rad52-YFP association, which could be indicative of replication restart.

4.3.3 Comparison of recombination responses to forks blocked at *RTS1* and spontaneous lesions

The timing of Rad52 recruitment to *RTS1* during the cell cycle appears to be similar to its response to spontaneous lesions that occur under our laboratory growth conditions. The overall increase in Rad52-YFP foci in *RTS1-AO* cells compared to *RTS1-IO* cells indicates that a single collapsed replication fork is capable of inducing a Rad52 focus, which is equivalent to what has been observed for a single DSB in *S. cerevisiae* (Lisby et al. 2001). However, the total number of Rad52-YFP foci in *RTS1-AO* cells is less than would be expected form a simple addition of spontaneous foci (determined in *RTS1-IO* cells) and *RTS1* co-localizing foci (determined in *RTS1-AO* cells). Moreover, *RTS1-AO* cells rarely exhibit more than one Rad52-YFP focus at any time. These observations suggest that the single co-localizing Rad52-YFP focus at *RTS1* may often be dealing with other problem replication forks and/or DNA lesions, and therefore acts as a “repair factory”. Interestingly, many *RTS1-AO* cells exhibit Rad52-YFP foci that appear to persist following loss of co-localization with *lacO*-LacI, suggesting that after Rad52 has dealt with the replication fork blocked at *RTS1* it continues to process other lesions that have been recruited to the “repair factory”.

4.3.4 Failure to detect Rad51 and Rad54 foci at blocked forks

Intriguingly, forks blocked at *RTS1* do not induce detectable Rad51-CFP or Rad54-GFP foci. There are several possible reasons that could explain this. First, the proteins may not be recruited to the same extent as Rad52, such

that there may be insufficient protein to form a focus that can be detected under my imaging conditions. Second, the proteins may only transiently localize to the blocked fork at *RTS1* such that greater temporal resolution would be needed to detect them. Alternatively, it is possible that Rad52 does not load Rad51 (and Rad54 indirectly) either because of a posttranslational modification, such as SUMOylation, that alters its interaction with Rad51 (Esta et al. 2013) or it does not have time to load Rad51 before forks converge at the site. However, I found that some cells exhibit a co-localized Rad52 focus for over 30 minutes, which based on current understanding, should provide adequate time for Rad52 to help load Rad51.

Although I was not able to detect Rad51 foci at *RTS1* during my time-lapse experiments, this does not exclude the idea that Rad51 is still functioning in a pathway with Rad52 in promoting the recombinational response at *RTS1*. In fact, the majority of Rad52-mediated direct repeat recombinants that are induced by *RTS1* depend on Rad51. Furthermore, Rad51 foci are also not detected spontaneously in *RTS1-IO* cells even though most cells must be dependent on Rad51, particularly in response to replication stress, as indicated by the relatively poor growth and heightened checkpoint response of *rad51Δ* mutant cells under normal laboratory growth conditions. Thus, if the *RTS1* barrier is representative of a subclass of a “DNA lesion” that arises spontaneously, we would not expect to see it induce a Rad51 focus. Under my imaging conditions, I am only able to detect a Rad51-CFP focus after cells have been exposed to 10 μM CPT, which causes a large accumulation of

replication stress to cells. When our laboratory previously used a more sensitive approach involving immunostaining of spread nuclei, Rad52-dependent Rad51 foci were detected both spontaneously and at *RTS1* (Lorenz et al. 2009). This is consistent with the idea that Rad51 is likely to be acting downstream of Rad52 at *RTS1*.

Although I was not able to detect Rad54-GFP foci at *RTS1* during my time-lapse experiments, Rad54 is also likely to be acting downstream of Rad52 at *RTS1*. Interestingly, Rad54-GFP, unlike Rad51-CFP, does form spontaneous foci (often multiple foci in a single cell) that appear during late S-phase and G2. However, very few of these foci co-localize with *RTS1-AO*, and even those that do appear to do so by chance as there is little difference between *RTS1-AO* and *RTS1-IO* cells in terms of the extent of co-localization. Exactly what is inducing the spontaneous Rad54-GFP foci is unclear, but from their lack of co-localization with *RTS1-AO* and multiplicity in each cell, it would appear that most of them would not co-localize with either spontaneous or *RTS1*-induced Rad52-YFP foci, and therefore would not be part of the “repair factory”. Because Rad54 has various roles in recombination, including the removal of Rad51 from dsDNA (Shah et al. 2010), the spontaneous Rad54-GFP foci are presumably representative of only a subset of its activity within the cell, and one that is not needed at *RTS1*. In order to detect Rad54 (and Rad51) at *RTS1*, improvements in our imaging experiments will need to be made, including the use of more sensitive and higher resolution microscopes.

4.3.5 Dynamics of Rad11 foci at the *RTS1* replication fork barrier

Unlike Rad51-CFP and Rad54-GFP, Rad11-GFP forms foci that co-localize with *lacO*-LacI foci predominately in *RTS1-AO* cells. Similar to Rad52, the variability of the occurrence, timing, and duration of Rad11-GFP at *RTS1* may be influenced by the stochastic nature of origin firing. Despite this, there is a clear difference in the timing of when Rad11-GFP foci appear compared to the timing of when Rad52-YFP foci appear at *RTS1*. Unexpectedly, RPA foci at *RTS1* are first detected at a later time than when Rad52 foci are detected. This is surprising because, although RPA foci can form in the absence of Rad52, Rad52 foci cannot form without the presence of RPA (Lisby et al. 2004). This suggests that the RPA that is loaded at blocked forks before Rad52 may not form detectable foci. In fact, the pattern of RPA foci is similar to that of Pcn1 foci, which is consistent with RPA's role in replication. In early S-phase, there is an induction of RPA fluorescence such that there is a cloud of RPA foci. As the cell cycle progresses, RPA forms fewer foci, such that each cell typically exhibits between one to three foci at any one time. The later instances of Rad11 co-localization suggests that forks blockage at *RTS1* leads to an accumulation of ssDNA, which in turn results in sufficient Rad11 being recruited for it to be detectable as a focus. This ssDNA may arise as a result of fork convergence. To confirm whether Rad11 forms detectable foci that co-localize with *RTS1* after Rad52 does, a strain that expresses both Rad11-CFP and Rad52-YFP is being constructed to enable the detection of both proteins in the same cell.

Chapter 5

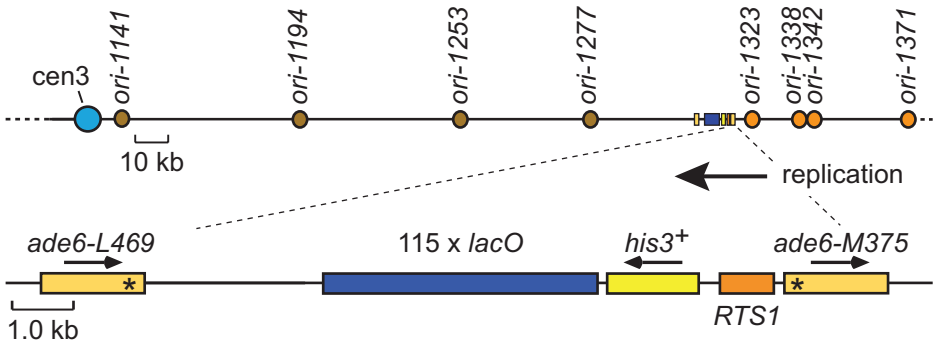
The Effect of Delaying Fork Merging at *RTS1* on Direct Repeat Recombination and Rad52-YFP Foci

5.1 Introduction

The variability of the first appearance of a Rad52-YFP focus at the *RTS1* RFB, its duration, and absence in some cells may be explained by the stochastic nature of origin firing. Since origins of replication fire with different efficiencies, a specific origin will fire in some but not all cell cycles (Patel et al. 2006). The eight origins immediately flanking the ectopically positioned *RTS1* (Figure 5.1A) have previously been documented as having firing efficiencies ranging from 23 – 56% in mitotic S-phase (Heichinger et al. 2006). Therefore, depending on which nearby origin of replication fires, replication fork blockage and convergence at the *RTS1* RFB will occur at different times during the cell cycle, corresponding to the varied distances the forks must travel to arrive at the site (Figures 5.1B and 5.1C).

To explore what influence the stochastic nature of origin firing has on recombination at the *RTS1* RFB, I deleted *ori-1253*, an origin on the centromere-proximal side of *RTS1*. This involved replacing the 500 bp intergenic region between a *tRNA* gene and the *sndI* gene, which defines *ori-1253* and is comprised of discrete A-T rich content that characterizes *S. pombe* origins of replication, with a *natMX4* marker (Segurado et al. 2003; Siow et al. 2012). *ori-1253* is one of four origins of replication between *cen3* and the ectopically positioned *RTS1* and is the nearest centromere-proximal located origin that has been identified by a minimum of two microarray studies (Feng et al. 2006; Heichinger et al. 2006; Hayashi et al. 2007). Note that although *ori-1277* is located closer to the *RTS1* than *ori-1253*, it is regarded

A



B

Origin	Distance from barrier (bp)	Time from barrier (min)
ori-1141	186,731	62.2
ori-1194	134,208	44.7
ori-1253	75,154	25.1
ori-1277	51,031	17.0
ori-1323	7,735	2.6
ori-1338	23,098	7.7
ori-1342	27,172	9.1
ori-1371	55,444	18.5

C

	ori-1323	*ori-1338*	*ori-1342*	*ori-1371*
ori-1277	14.4 min	9.3 min	7.9 min	-1.5 min
ori-1253	22.5 min	17.4 min	16 min	6.6 min
ori-1194	42.1 min	37 min	35.6 min	26.2 min
ori-1141	59.6 min	54.5 min	53.1 min	43.7 min

Figure 5.1 | Timing of replication fork blockage and convergence at *RTS1*. (A) Schematic showing the chromosomal region where the *RTS1* RFB is positioned within the recombination substrate in respect to positions of the adjacent origins of replication on chromosome III. (B) Table of the distances between different adjacent origins of replication to the *RTS1* barrier based on the midpoint of the origin coordinates (Siow et al. 2012), and therefore the time taken for replication forks emanating from the respective origins to reach the barrier based on a replication fork velocity of 3.0 kb/min (Heichinger et al. 2006). (C) Table of the time after fork blockage until fork merging. Values may be ± 10 minutes depending on the relative timing of firing of the two origins. These origins have previously been characterized as early firing origins with differences in firing time normally less than 10 minutes (Heichinger et al. 2006).

as a “dubious” origin of replication because it has only been found in one microarray study and its firing efficiency has not been quantified (Feng et al. 2006). On the other hand, *ori-1253* is estimated to have a firing efficiency of 56% in mitotic S-phase (Heichinger et al. 2006). By deleting *ori-1253*, the subset of cells that relied on the converging fork from *ori-1253* to merge with the restarted or arrested fork at *RTS1* will instead be dependent on a fork emanating from a more distant origin of replication to arrive at the site and complete DNA replication. Accordingly, in this subset of *ori-1253Δ* cells, the timing of fork convergence at *RTS1* will be delayed. Therefore, by deleting *ori-1253*, I was aiming to assess whether prolonged pausing at *RTS1*: i) is more liable to give rise to replisome collapse and the early recruitment of recombination proteins, supportive of a model for RDR at the barrier or ii) delayed fork convergence, such that recombinases are recruited at a later time in the cell cycle, supportive of a model for recombination aiding in fork merging at the barrier.

5.2 Results

5.2.1 Deleting *ori-1253* increases direct repeat recombination at the *RTS1* replication fork barrier

To investigate whether delaying fork merging at *RTS1* has an influence on stimulating recombination, I determined the effect of *ori-1253* deletion on the frequency of direct repeat recombination (Figure 5.2). In *ori-1253Δ* strains with *RTS1-IO*, the frequency of conversion- and deletion-type recombinants is not significantly different than wild-type. In both cases, ~ 30% of these

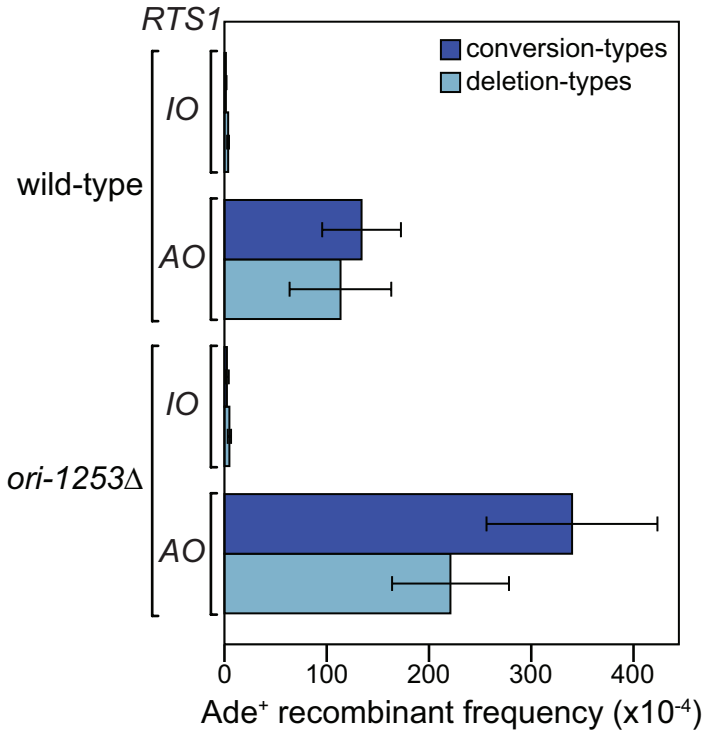


Figure 5.2 | Direct repeat recombination increases at the *RTS1* RFB in *ori-1253Δ* strains. Bar chart showing the frequency of conversion- and deletion-type Ade$^+$ recombinants in wild-type and *ori-1253Δ* strains with either *RTS1-IO* or *RTS1-AO*. Error bars represent ± one standard deviation. In order of presentation, the strains are MCW4712, MCW4713, MON293, and MON257. The values in this chart are also presented with statistical analysis in Tables S1 and S2 in the appendix.

recombinants are conversion-types. However, with *RTS1-AO*, deleting *ori-1253* further increases the already high frequency of Ade$^+$ recombinants in wild-type strains. This increase is 2.5- and 2-fold in conversion- and deletion-type recombinants, respectively, over the wild-type strain. These differences are both statistically significant (both P = < 0.001). The percentage of these recombinants that are conversion-types in an *ori-1253Δ* mutant also increases from wild-type from 55% to 60% (P = 0.049). These data show that the fork emanating from *ori-1253* limits the recombination that is induced by the *RTS1* RFB and, in particular, it limits both the production of conversion- and deletion-type recombinants to a similar extent.

To see if I could get evidence that recombination was being initiated at a site downstream of the blocked replication fork, I monitored the conversion-types to see which of the two *ade6* heteroalleles converted to *ade$^+$* in the wild-type and *ori-1253Δ* strains (data not shown). In our assay system, *ade6-L469* to *ade$^+$* conversion-types can be distinguished from *ade6-M375* to *ade$^+$* conversion-types by colony color. The former appear as pale pink colonies, whereas the latter form white colonies (Osman et al. 1996). Our laboratory has previously shown that 100% of conversion-types are *ade6-M375* to *ade$^+$* in wild-type *RTS1-AO* strains (Ahn et al. 2005). If there was an increase in *ade6-L469* to *ade$^+$* conversions in *ori-1253Δ* strains, then the restarted fork could in theory be prone to invading homologous sequences immediately behind the fork. However, after screening over 1,000 colonies, I found that there was no evidence for increased *ade6-L469* to *ade$^+$* conversions in *ori-*

1253Δ cells compared to wild-type cells with *RTS1-AO*. In all, 100% of conversion-types are *ade6-M375* to *ade*$^{+}$ irrespective of the presence or absence of *ori-1253*. These data are consistent with the increased direct repeat recombination in *ori-1253Δ* cells being initiated at the site of the blocked replication fork.

5.2.2 Deleting *ori-1253* increases the recruitment of Rad52-YFP to the *RTS1* replication fork barrier

Having established that deleting *ori-1253* increases *RTS1*-induced direct repeat recombination, I determined its effect on the frequency and timing of recruitment of Rad52 to *RTS1* in an asynchronous population of cells in the first 90 minutes following anaphase (Figures 5.3 and 5.4). I found that deleting *ori-1253* has an effect that is dependent on the orientation of *RTS1*, such that a higher percentage of *ori-1253Δ* cells with *RTS1-AO* exhibit a Rad52-YFP focus that co-localizes with a *lacO*-LacI focus than wild-type *RTS1-AO* cells while there is no significant change in *RTS1-IO* strains following *ori-1253* deletion (Figure 5.4A). Overall 80% of *ori-1253Δ* cells containing *RTS1-AO* exhibit at least one Rad52-*lacO*-LacI co-localization compared to 64% of wild-type cells containing *RTS1-AO* (Figure 5.4B). This difference is statistically significant ($P = 0.02$). Altogether, these data are consistent with the idea that more cells are mounting a recombinational response to replication fork stalling at *RTS1* when *ori-1253* is deleted.

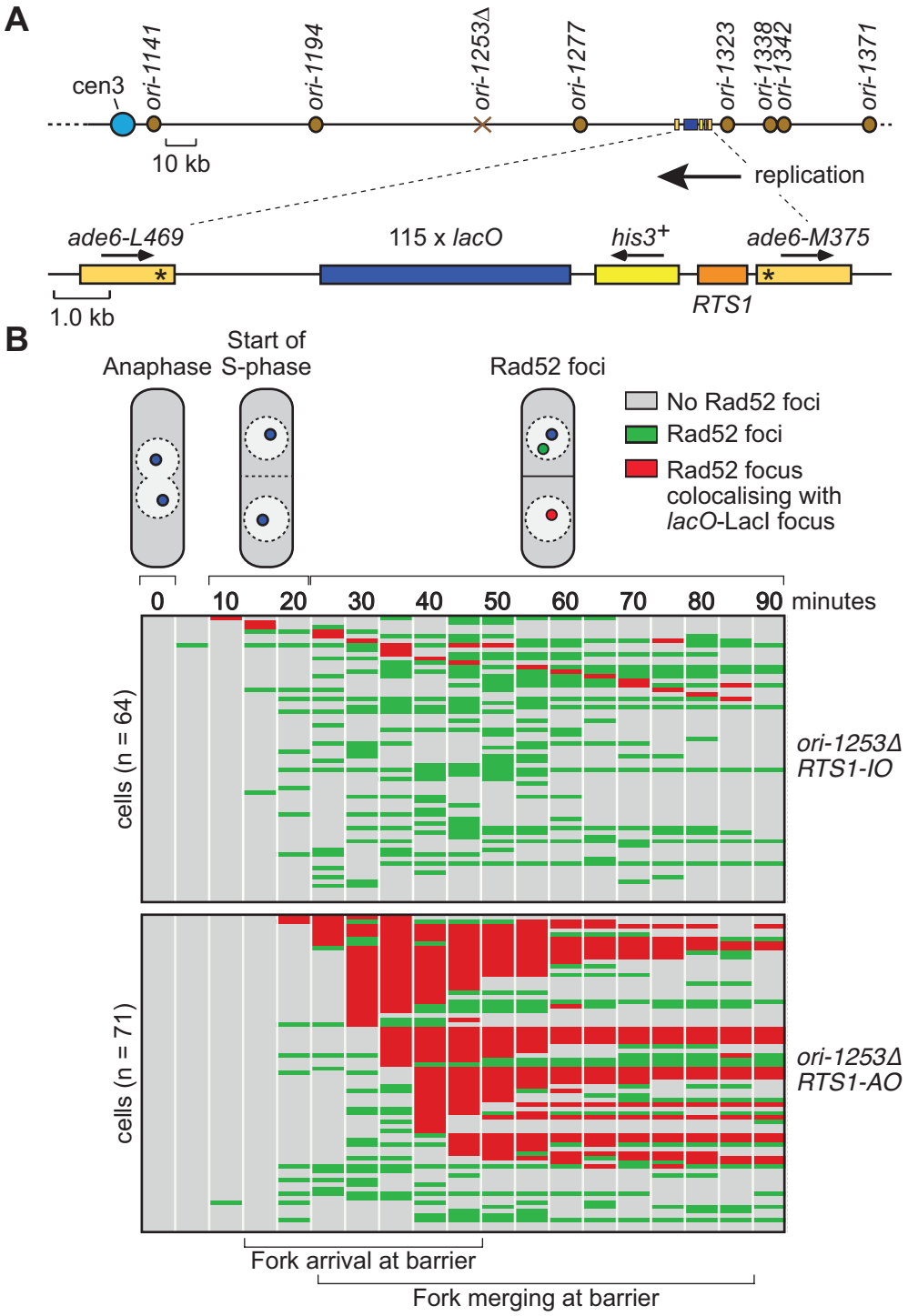


Figure 5.3 | *ori-1253Δ* cells with *RTS1-AO* exhibit a Rad52-YFP focus that co-localizes with the *lacO*-LacI focus. (A) Schematic showing the chromosomal region where the recombination substrate is positioned on chromosome III in relation to the region where *ori-1253* has been deleted. (B) Analysis of time-lapse movies of *ori-1253Δ* cells with either *RTS1-IO* or *RTS1-AO*. The *RTS1-IO* strain is MON297, and the *RTS1-AO* strain is MON259.

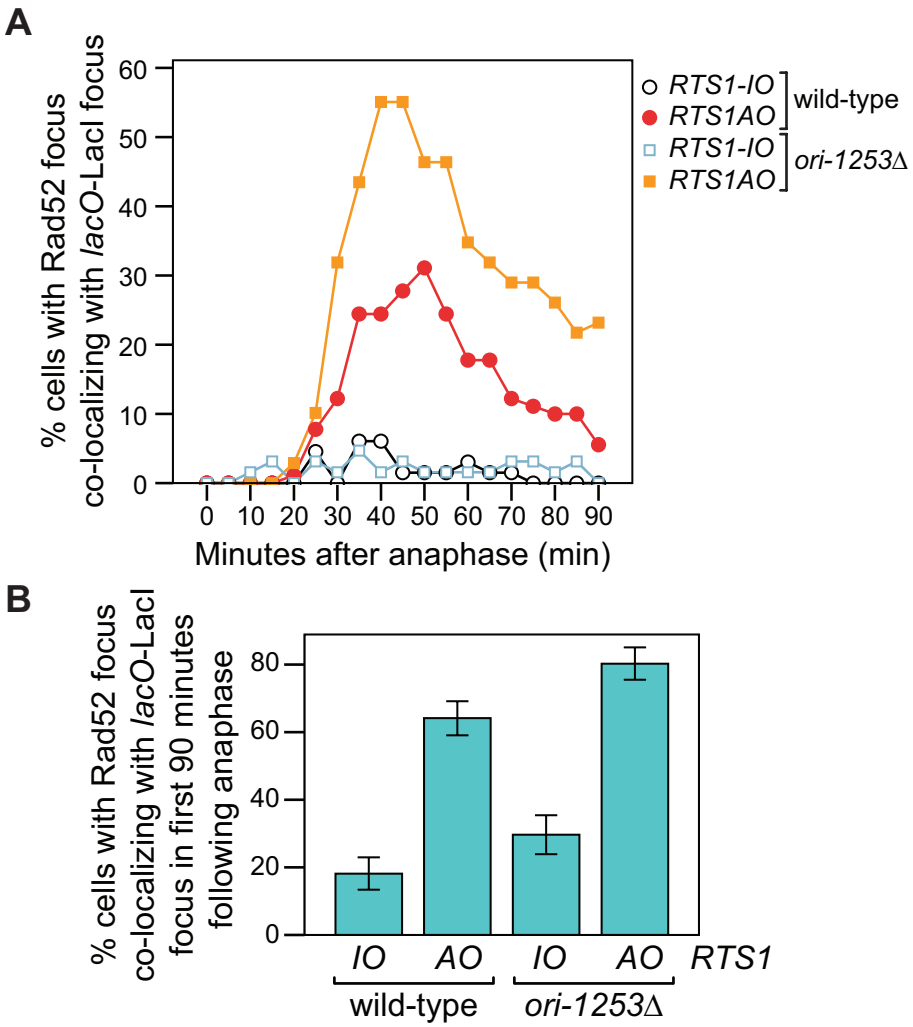


Figure 5.4 | Deleting *ori-1253Δ* in cells leads to an increased frequency of Rad52-YFP foci co-localizing with the *RTS1* RFB. (A) Line graph of the percentage of cells with a Rad52-YFP focus that co-localizes with the *lacO*-LacI focus during the first 90 minutes following anaphase at five-minute intervals. (B) Bar chart of the percentage of cells that exhibit at least one Rad52-YFP focus that co-localizes with the *lacO*-LacI focus in the first 90 minutes following anaphase. Error bars represent ± one standard error of the mean. The *RTS1-IO* strains are MON110 (wild-type) and MON297 (*ori-1253Δ*). The *RTS1-AO* strains are MON148 (wild-type) and MON259 (*ori-1253Δ*).

5.2.3 Deleting *ori-1253* increases the duration of Rad52 localization at the *RTS1* replication fork barrier

To investigate whether delaying fork convergence has an effect on the duration of Rad52-YFP foci at *RTS1-AO*, I assessed tracks of consecutive time points with Rad52-*lacO*-LacI co-localization in each cell (Figure 5.5A). In *RTS1-IO* strains, less than 5% of cells exhibit a Rad52-*lacO*-LacI co-localization that persists beyond one time point regardless of whether *ori-1253* is deleted or not. In contrast, the majority of *RTS1-AO* cells, irrespective of *ori-1253* deletion, have a Rad52 focus that co-localizes with a *lacO*-LacI focus for at least two time points. Deleting *ori-1253* results in a significant ($P = < 0.001$) increase in the average track length of co-localization from ~ 2.4 time points in wild-type to ~ 4.9 time points in *ori-1253Δ* cells (Figure 5.5B). These data suggest that replication forks emanating from *ori-1253* frequently curtail Rad52's association with the *RTS1* barrier, presumably by the incoming fork in some way displacing the Rad52 protein from DNA during the process of fork merging.

Intriguingly, there is a subset of *RTS1-AO ori-1253Δ* cells (~ 15%) that each exhibits a very long (> 2 hours) uninterrupted track of Rad52 focus co-localization with *lacO*-LacI (i.e. Rad52-*lacO*-LacI co-localization that persists for a minimum of 25 consecutive time points) (Figure 5.5C). Such long-lived tracks are typically not observed in wild-type cells with *RTS1-AO* (Figure 5.5C). In addition to scoring the longest track of Rad52-*lacO*-LacI co-localization in each cell, I also assessed the total number of time points in

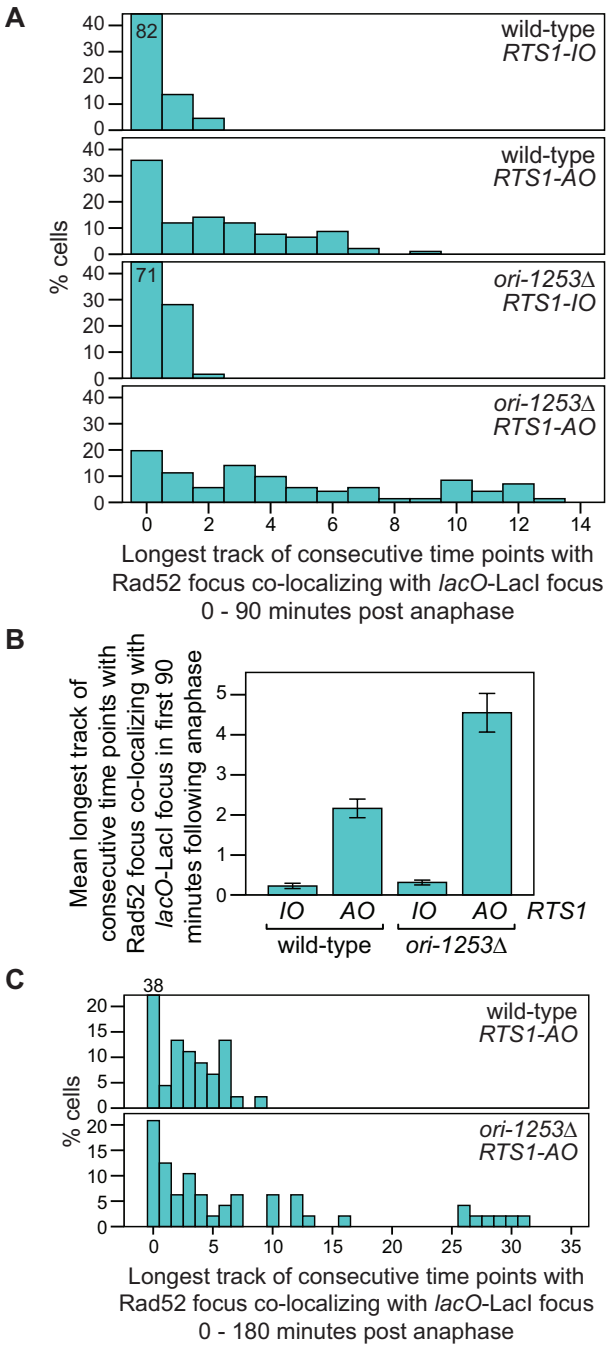


Figure 5.5 | *ori-1253Δ* cells exhibit enhanced tracks of a prolonged Rad52-YFP focus at the *RTS1* RFB. (A) Histogram showing the percentage of cells with a given number of uninterrupted time points in which a Rad52-YFP focus co-localizes with a *lacO*-LacI focus within the first 90 minutes following anaphase. (B) Bar chart of the mean number of uninterrupted time points cells display a Rad52-YFP focus that co-localizes with a *lacO*-LacI focus during the first 90 minutes following anaphase. (C) Histogram showing the percentage of cells with a given number of uninterrupted time points in which a Rad52-YFP focus co-localizes with a *lacO*-LacI focus within the first 180 minutes following anaphase. The *RTS1-IO* strains are MON110 (wild-type) and MON297 (*ori-1253Δ*). The *RTS1-AO* strains are MON148 (wild-type) and MON259 (*ori-1253Δ*).

each cell in which a co-localization was observed (Figure S5.1). This analysis reveals little difference to the data in Figure 5.5 indicating that a Rad52-YFP focus tends to be recruited to *RTS1* only once per cell cycle. Overall these data suggest that in a subpopulation of cells lacking *ori-1253*, the other available origins between *RTS1* and the centromere fail to fire. Consequently, the completion of DNA replication might depend on RDR with the restarted fork having to travel at least as far as the centromere.

5.2.4 Slightly more cells with *ori-1253* deleted exhibit early Rad52 recruitment to *RTS1*-AO than wild-type cells

Having established that deleting *ori-1253* changes the persistence of Rad52 at the *RTS1* RFB, I wanted to next investigate whether it led to a change in the timing of when Rad52 is recruited to forks blocked at *RTS1* during the cell cycle. In *RTS1-AO* cells, the majority of co-localized Rad52 foci occur within 25 to 50 minutes post anaphase even when *ori-1253* is deleted (Figure 5.6A). However, there is a slightly greater percentage of cells with earlier appearing co-localizing Rad52 foci. On average, a co-localizing Rad52 focus is first observed 35.4 minutes after anaphase in cells with *ori-1253* deleted compared to 41.4 minutes after anaphase in wild-type cells (Figure 5.6B). This difference is statistically significant ($P = 0.004$). If deleting *ori-1253* only removes incoming forks, then fork convergence is occurring at a later time point, on average, in *ori-1253Δ* cells compared to wild-type cells. The fact that Rad52 co-localization is detected earlier in *ori-1253Δ* cells, instead of at a similar or later time point, may relate to how deleting *ori-1253* could affect the

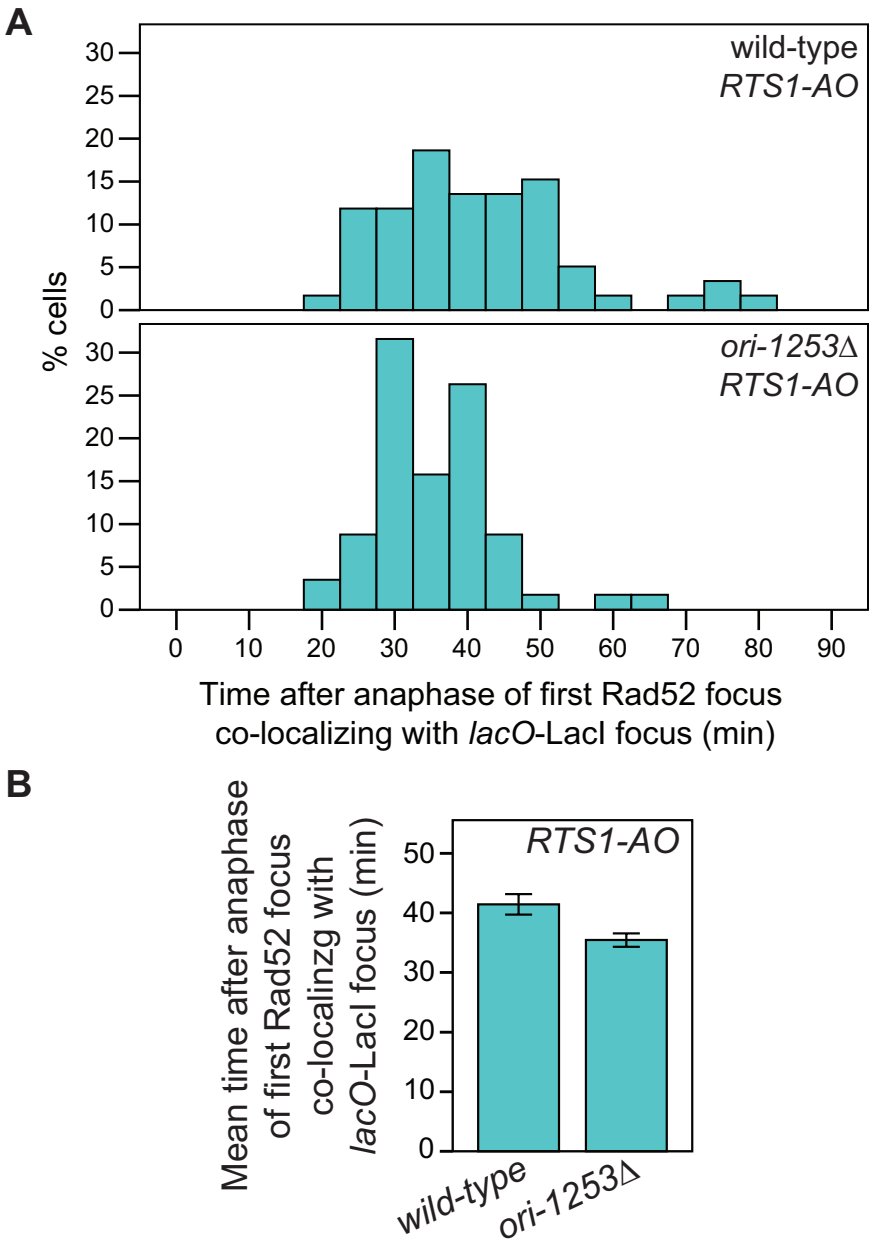


Figure 5.6 | Rad52-YFP is recruited to the *RTS1* RFB earlier in the cell cycle in cells with *ori-1253* deleted. (A) Histogram showing the percentage of cells at a given time after anaphase in which the first Rad52-YFP focus co-localizes with a *lacO*-LacI focus. (B) Bar chart of the mean time after anaphase of when the first Rad52-YFP focus co-localizes with a *lacO*-LacI focus. Error bars represent ± one standard error of the mean. The *RTS1-AO* strains are MON148 (wild-type) and MON259 (*ori-1253Δ*).

firing efficiency of the replication origins that flank *RTS1*. If the nearest origins of replication on the telomere proximal side of *RTS1* were firing with an increased frequency when *ori-1253* is absent, then fork blockage at *RTS1* and consequently, Rad52 co-localization, would be occurring earlier in a subpopulation of cells.

5.3 Discussion

5.3.1 Delaying fork merging increases the percentage of *RTS1-AO* cells performing recombination-dependent replication restart

In this chapter, I have shown that the variability in the first appearance of a Rad52-YFP focus at the *RTS1* RFB, its duration, and absence in some cells is influenced, at least partly, by the stochastic nature of origin firing. By deleting *ori-1253*, I delayed fork merging at *RTS1* in the subset of cells in which *ori-1253* would have fired if it were present. This led to increases in both direct repeat recombination and Rad52 foci assembly at forks blocked at *RTS1*, consistent with the notion that in a subpopulation of cells, recombination is constrained by the arrival of the converging fork. The increase in recombinant activity in *ori-1253Δ* cells also does not support the idea that recombinases are recruited during fork merging at *RTS1-AO* since presumably fewer forks are now terminating at the site in *ori-1253Δ* strains. These data are more consistent with the idea that recombinases load directly at the blocked fork and act before fork convergence, presumably to aid in RDR. Furthermore, deleting *ori-1253* led to increases in the mean track length of Rad52-*lacO*-LacI co-localization in cells with *RTS1-AO*, indicating that RDR is curtailed by

the arrival of the opposing fork. It is currently unclear, however, how the incoming fork may displace the recombinases. It is presumably not simply due to the physical removal of recombinases by the incoming replicative and accessory helicases, particularly if recombination proteins, such as Rad52, are positioned behind *RTS1*.

5.3.2 Local and global effects of deleting an individual origin of replication

It is unknown what effect deleting an individual origin of replication has on the firing efficiency of adjacent origins of replication and on global genome stability. Intriguingly, deleting *ori-1253* leads to 15% of cells experiencing atypically long-lived tracks of Rad52-*lacO*-LacI co-localization that are not observed in wild-type cells. This may suggest that the stochastic nature of origin firing may not be efficiently reprogrammed in a manner that would proficiently compensate for the loss of a single origin of replication and/or that dormant origin firing is not an effective strategy for overcoming replication stress at this locus. A study by Heichinger et al. (2006) previously showed that late origins are not common in fission yeast and that on chromosome III, where the ectopic *RTS1* has been positioned, there are no late origins. Additionally, another study showed that of the 189 dormant origins that fired in a *rif1Δ* mutant that deregulates origin firing, only one dormant origin was located on chromosome III (Hayano et al. 2012). This may suggest that dormant origin firing might not be a strategy that is commonly used on chromosome III in *S. pombe*. In effect, the deletion of *ori-1253* in a subset of

cells may have created a fragile site when combined with *RTS1-AO*. In this subset of *ori-1253Δ* cells, the three other available origins between *RTS1* and the centromere may fail to fire and the forks coming through the centromere may not arrive in a timely manner as replication forks pause at yeast centromeres due to the protein-DNA complexes required for centromeric function (Greenfeder and Newlon 1992). Thus, the completion of DNA replication might depend on RDR with the restarted fork having to travel at least as far as the centromere.

Unexpectedly, deleting an individual origin may have a global effect on genome stability. In *RTS1-IO* strains, the mean number of time points cells exhibit a Rad52-YFP focus in the first 90 minutes, irrespective of whether or not it co-localizes with the *lacO*-LacI focus, slightly increases from 3.2 to 4.6 time points in strains with *ori-1253* deleted compared to the respective wild-type strain (Figure S5.2) (P = 0.03). This suggests that *ori-1253Δ* cells have increased spontaneous Rad52 foci that are not related to the *RTS1* RFB. A recent study in *Haloferax volcanii* also observed that the deletion of a single origin led to reduced growth and perturbed replication dynamics (Hawkins et al. 2013). This study also highlighted that when all origins of replication are deleted in *H. volcanii*, the archael RecA/Rad51 homolog, RadA, becomes essential for viability. Our laboratory is now investigating whether *ori-1253Δ* strains with *RTS1-AO* may also have some dependency on recombination factors for viability.

5.3.3 Restarted replication forks remain associated with Rad52 and prone to template switching

As mentioned above, one unanticipated finding of this study is the detection of very long-lived, uninterrupted tracks of Rad52-*lacO*-LacI co-localization in a subset of *ori-1253Δ* cells. This suggests that either the initiation of RDR is slow, in a similar manner to BIR (Malkova et al. 2005), and/or that the Rad52 protein may remain associated with the restarted fork. 2D-gel analysis of replication intermediates in wild-type strains with *RTS1-AO* from our laboratory indicates, however, that the restarted fork does move downstream of the RFB. To determine how far the restarted fork travels and, at the same time, assess whether Rad52's presence with the restarted fork may correlate with a propensity for DNA template switching, Manisha Jalan, a doctoral student in our laboratory, inserted a direct repeat recombination reporter at sites 10 kb and 140 kb downstream of the *RTS1* RFB. So far, she has preliminary data at the 10 kb site, which shows that replication fork blockage at *RTS1* induces recombination (predominantly deletion-type recombinants) 45-fold downstream of the barrier compared to when there is no fork blockage, consistent with the notion that the restarted fork is prone to template switching. Deletion of *ori-1253* increases recombination downstream of the barrier by 7.4-fold, indicating that more forks are traveling at least as far as 10 kb downstream of the *RTS1* RFB in *ori-1253Δ* cells. This suggests that the restarted fork continues to have a mutagenic property even as it progresses away from the site where the fork collapsed, at least as far as 10 kb downstream of the RFB. Our laboratory is currently investigating whether

template switching may remain active over a more extensive region than has been observed for BIR in budding yeast (Smith et al. 2007).

5.3.4 Examining the effect of inserting a pausing site to delay fork merging at *RTS1*

As an alternative to studying the effect of delaying fork merging at *RTS1* by deleting an individual origin, I also began work on inserting a pausing site that would delay the arrival of all opposing forks at *RTS1*. To investigate whether the pausing site would induce a recombinational response in its own right, I created a strain with three copies of the ribosomal DNA fork barrier sequence, *TER2/3*, positioned between direct repeats of *ade6*$^{-}$ heteroalleles on chromosome III (Figure S5.3A). I found that *TER2/3* does not significantly induce direct repeat recombination in either its blocking or non-blocking orientation compared to when *TER2/3* is not present within the direct repeats (Figure S5.3B, Table S5.1), consistent with the idea that forks pause transiently at *TER2/3* and do not require HR for resumption (Krings and Bastia 2004; Sanchez-Gorostiaga et al. 2004; Mizuno et al. 2013). Our laboratory has now placed *TER2/3* at a site 10 kb downstream of the *RTS1* RFB to pause converging replication forks and provide more time for cells to perform RDR. These studies are in progress but thus far, preliminary analysis from Dr. Fikret Osman indicates that delaying fork merging with *TER2/3* also increases direct repeat recombination, similar to *ori-1253Δ* cells. This would seem to support the idea that the timely arrival of the opposing fork at *RTS1* is an important factor in influencing how many cells initiate RDR and how far the

restarted fork must travel to complete DNA replication.

Chapter 6

Role of Rad51 and Rad51 Mediators in Replication Restart at *RTS1*

6.1 Introduction

It is thought that the reengagement of the nascent strands at the collapsed fork with the parental DNA duplex is central to the process of RDR. Although the exact mechanism that facilitates the reloading of replisome components has yet to be determined in eukaryotes, Rad51 is proposed to play a key role in catalyzing the strand invasion into the parental DNA duplex. Rad51 requires a number of other proteins, including the Rad51 mediators, to promote the formation and stability of its nucleoprotein filament, which is fundamentally necessary for the strand invasion step *in vivo*; however, it is unknown which of these factors are required for the recombinational repair of stalled replication forks. In the case of *S. pombe*, there are three so-called Rad51 mediator complexes – Rad55-Rad57, Swi5-Sfr1, and Rdl1-Rlp1-Sws1. Each mediator is believed to facilitate Rad51 assembly via a different mechanism, but it is currently unclear what distinguishes their functions. To gain further insights into Rad51 and its mediators, I assessed their roles in RDR to ascertain: i) which of the mediators are involved, ii) whether the mediators functioned in the same pathway and/or had redundant roles, iii) whether they are genetically required for Rad52 focus assembly and persistence at *RTS1-AO*, and if they were not, iv) whether these downstream factors displaced Rad52 at the *RTS1 RFB*.

6.2 Results

6.2.1 Rad55 and Rad57 are required for replication fork block-induced gene conversion and the majority of deletion events

To determine the role of the Rad55-Rad57 complex in spontaneous and *RTS1*-induced recombination, I assessed the effect of *rad55Δ* and *rad57Δ* on the frequency of direct repeat recombination (Figure 6.1). Deletion of either *rad55* or *rad57* abolished both spontaneous (Figure 6.1A) and *RTS1*-induced gene conversions (Figure 6.1B). Contrastingly, *rad55Δ* and *rad57Δ* single mutants exhibited a ~ 3.8-fold increase in spontaneous deletion-type recombinants (both $P = < 0.001$) and a ~ 3.2-fold decrease in *RTS1*-induced deletion-type recombinants (both $P = < 0.001$) compared to wild-type cells (Figure 6.1). Both of the effects on gene conversions and deletions are similar to a *rad51Δ* mutant with the exception that there is a lower frequency of deletions in a *rad55Δ* and a *rad57Δ* single mutant compared to a *rad51Δ* single mutant (both $P = < 0.001$) (Ahn et al. 2005). These data suggest that Rad55-Rad57 is required for Rad51-mediated recombination that occurs spontaneously or in response to replication fork blockage at *RTS1* (the difference in the frequency of deletion-type recombinants in *rad51Δ* and *rad55Δ RTS1-AO* strains is discussed in Section 6.2.5). The increased spontaneous deletions in *rad55Δ* and *rad57Δ* cells with *RTS1-IO* indicate that the repair of spontaneous lesions is occurring through a more mutagenic pathway, such as SSA, which is a Rad51-independent process (Doe et al. 2004). At blocked replication forks, however, SSA may account for only a minority of recombination events.

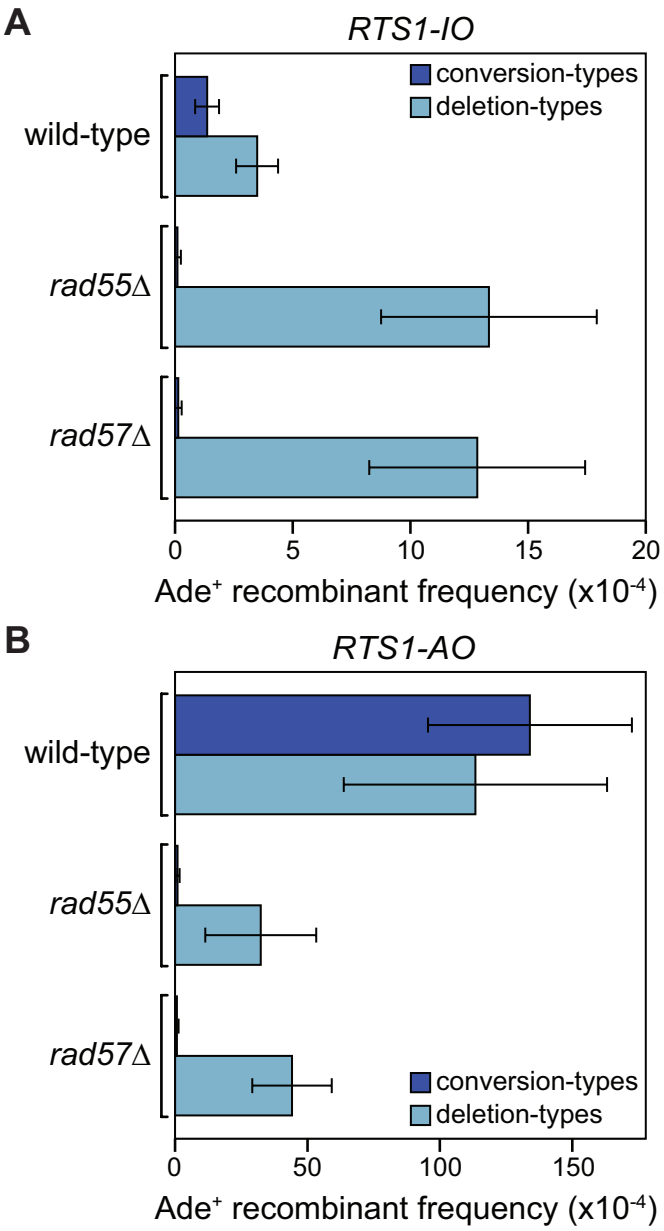


Figure 6.1 | Rad55 and Rad57 are required for replication fork block-induced gene conversion and the majority of deletion events. Bar chart showing the frequency of conversion- and deletion-type Ade$^+$ recombinants in wild-type, *rad55Δ,* and *rad57Δ* strains with either *RTS1-IO* (A) or *RTS1-AO* (B). Error bars represent ± one standard deviation. In order of presentation, the strains are MCW4712, MCW2650, MCW6539, MCW4713, MCW2655, and MCW6454. The recombination assay values presented in this chart and the remaining charts in this chapter are also listed in Tables S1 and S2 with statistical analysis in the appendix.

6.2.2 Rdl1, Rlp1, and Sws1 have critical roles in promoting replication fork block-induced gene conversions and deletions

To see whether the Rdl1-Rlp1-Sws1 complex affects HR spontaneously and at blocked replication forks, I also investigated the effect of *rdl1Δ, rlp1Δ* and *sws1Δ* single mutants on the frequency of direct repeat recombination (Figure 6.2). In the absence of *rdl1*, *rlp1* or *sws1*, the normal low frequency of spontaneous conversion-types is significantly reduced by ~ 1.7-fold in each of the mutants compared to wild-type (all P = < 0.003) (Figure 6.2A). However, this reduction is even greater (~ 16-fold in *rdl1Δ* and *rlp1Δ* single mutants and ~ 4.5-fold in *sws1Δ* mutants relative to wild-type) when forks are blocked at *RTS1* (all P = < 0.001) (Figure 6.2B). In contrast, there is a ~ 1.5-fold increase in *rdl1Δ* and *rlp1Δ* single mutants (both P = < 0.001) and a slight reduction in the *sws1Δ* mutant (P = 0.03) in the frequency of deletions in *RTS1-IO* cells compared to wild-type (Figure 6.2A). On the other hand, there is a significant reduction (~ 3.8-fold relative to wild-type) in the frequency of deletions when forks are blocked at *RTS1* in the absence of *rdl1*, *rlp1*, or *sws1* (all P = < 0.001) (Figure 6.2B). Taken together, these data suggest that the Rdl1-Rlp1-Sws1 complex has a relatively minor role in promoting Rad51-dependent recombinational repair of spontaneous lesions that occur during normal growth, but has a more important role in promoting Rad51-dependent recombinational repair of blocked replication forks. These data also suggest that Rdl1 and Rlp1 may retain some ability to act without Sws1 in promoting the activity of the Rad51 nucleoprotein filament or, conversely, that Sws1 may have an additional role in suppressing gene conversions.

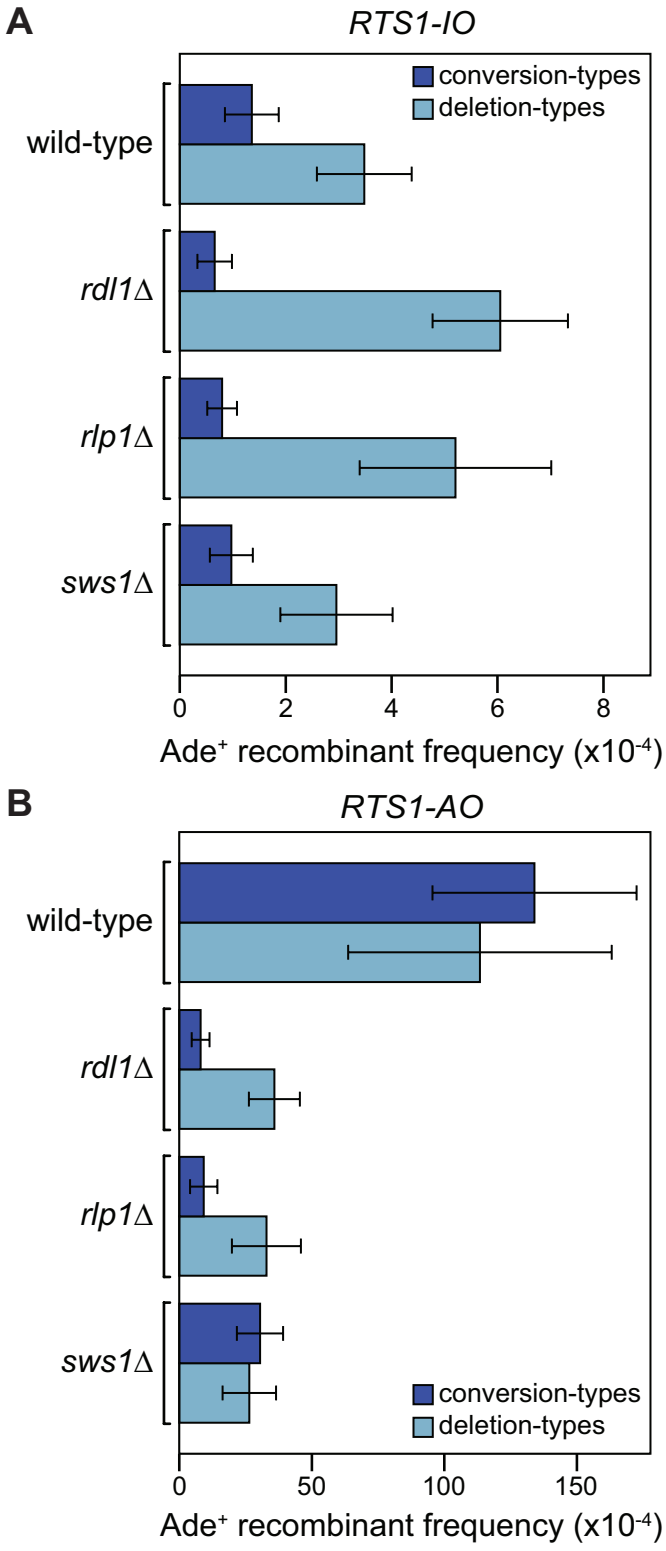


Figure 6.2 | Rdl1, Rlp1, and Sws1 have critical roles in promoting replication fork block-induced gene conversions and deletions. Bar chart showing the frequency of conversion- and deletion-type Ade$^+$ recombinants in wild-type, *rdl1Δ, rlp1Δ*, and *sws1Δ* strains with either *RTS1-IO* (A) or *RTS1-AO* (B). Error bars represent ± one standard deviation. In order of presentation, the strains are MCW4712, MCW6501, MCW6505, MCW6503, MCW4713, MCW6468, MCW6507, and MCW6470.

6.2.3 Sfr1 and Swi5 have minor roles in promoting replication fork block-induced recombination

To investigate whether the Sfr1-Swi5 complex plays a role in promoting Rad51-dependent recombination spontaneously and at blocked replication forks, I also determined the effect of *sfr1Δ* and *swi5Δ* single mutants on the frequency of direct repeat recombination in cells with either *RTS1-IO* or *RTS1-AO* (Figure 6.3). In the absence of *sfr1* or *swi5*, spontaneous gene conversions are slightly reduced (P = 0.003 and 0.002, respectively) and spontaneous deletions are slightly increased (P = 0.03 and < 0.001, respectively) relative to wild-type (Figure 6.3A). Similarly, there is a comparatively modest effect on *RTS1*-induced recombination in *sfr1Δ* and *swi5Δ* single mutants compared to wild-type, with a slight reduction in total Ade^+ recombinants (P = 0.006 and < 0.001, respectively) and conversion-type recombinants still accounting for over 45% of total recombinants in both mutants (Figure 6.3B). Altogether, these data suggest that the Sfr1-Swi5 complex has a relatively minor role in promoting Rad51-dependent recombinational repair of spontaneous lesions and collapsed forks at *RTS1*.

6.2.4 Epistasis analysis reveals that the Rad51 mediators function in the same pathway for promoting replication fork block-induced recombination

To determine whether the Rad51 mediators work in the same pathway to promote Rad51-dependent recombination, I compared the frequency of direct repeat recombination in *rad55Δ, rdl1Δ* and *swi5Δ* single and double mutant

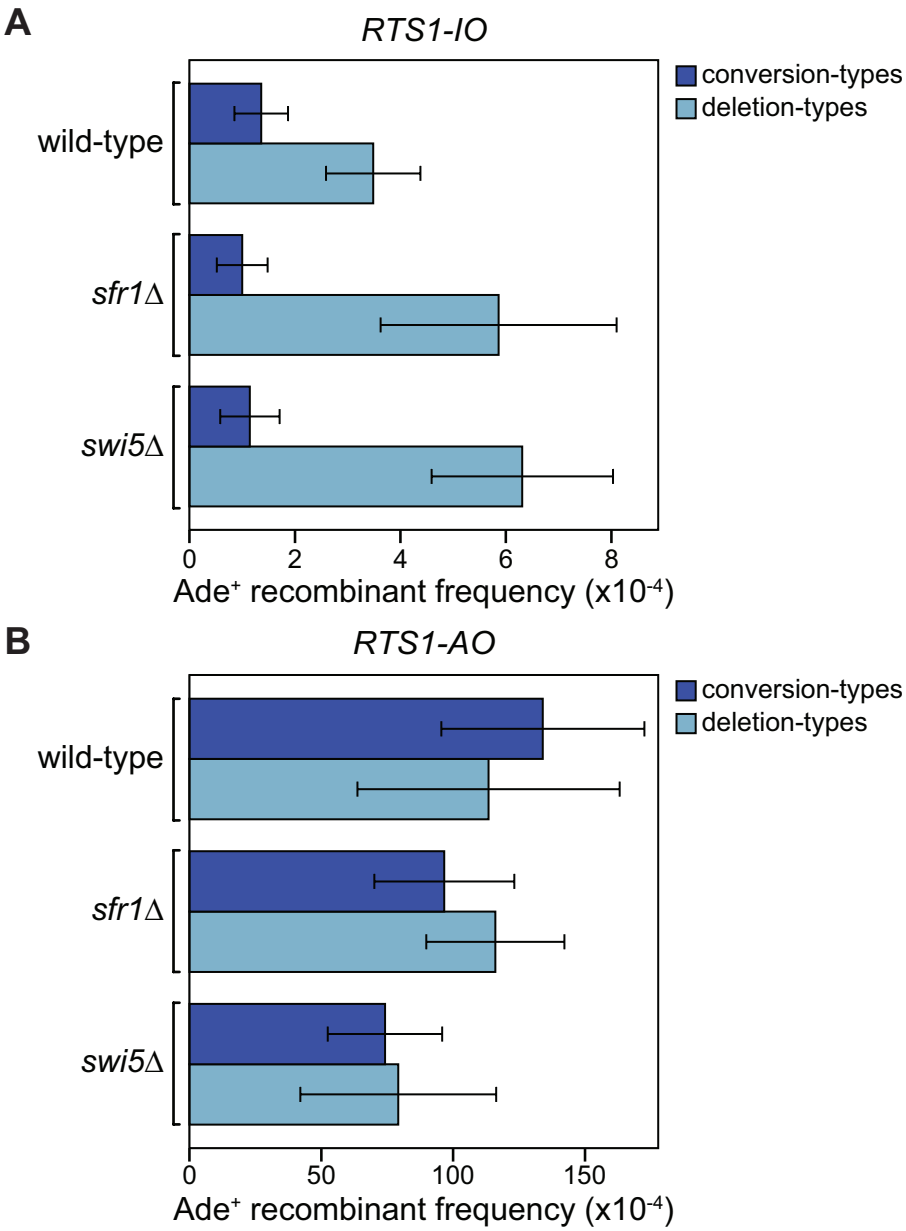


Figure 6.3 | Swi5 and Sfr1 have minor roles in promoting replication fork block-induced gene conversions and deletions. Bar chart showing the frequency of conversion- and deletion-type Ade$^+$ recombinants in wild-type, *sfr1Δ,* and *swi5Δ* strains with either *RTS1-IO* (A) or *RTS1-AO* (B). Error bars represent ± one standard deviation. In order of presentation, the strains are MCW4712, MCW6497, MCW2647, MCW4713, MCW6499, and MCW2653.

strains (Figures 6.4 and 6.5). I found that similar to a *rad55Δ* single mutant, both *rad55Δrdl1Δ* and *rad55Δswi5Δ* double mutants are totally deficient for the production of either spontaneous or *RTS1*-induced conversion-type recombinants (Figures 6.4 and 6.5). Interestingly both double mutants also exhibited at least an additive increase in spontaneous deletions compared to their respective single mutant strains (all $P = < 0.001$), which was not apparent for recombination induced by *RTS1-AO*. Together these data provide further evidence that Rad55, like Rad51, is essential for the production of conversion-type recombinants. The data also shows that Rad55 plays an important role in the formation of deletions that are induced following replication fork blockage at *RTS1*. The epistasis for *RTS1*-induced deletion formation observed between *rad55Δ* and *swi5Δ*, and *rad55Δ* and *rdl1Δ*, suggests that Rad55 works in the same pathway as Swi5 and Rdl1 in promoting Rad51-dependent recombination at blocked replication forks. In contrast, the increase in spontaneous deletions observed in all single mutants, which is further heightened in the two double mutants, indicates that Rad55, Swi5, and Rdl1 can each play an independent role in suppressing deletion events that are triggered by 'lesions' that occur under normal laboratory growth conditions. Moreover, the synergistic increase in deletions observed in the *rad55Δswi5Δ* double mutant suggests that there may be some overlap in the mechanism by which Rad55 and Swi5 suppress deletions.

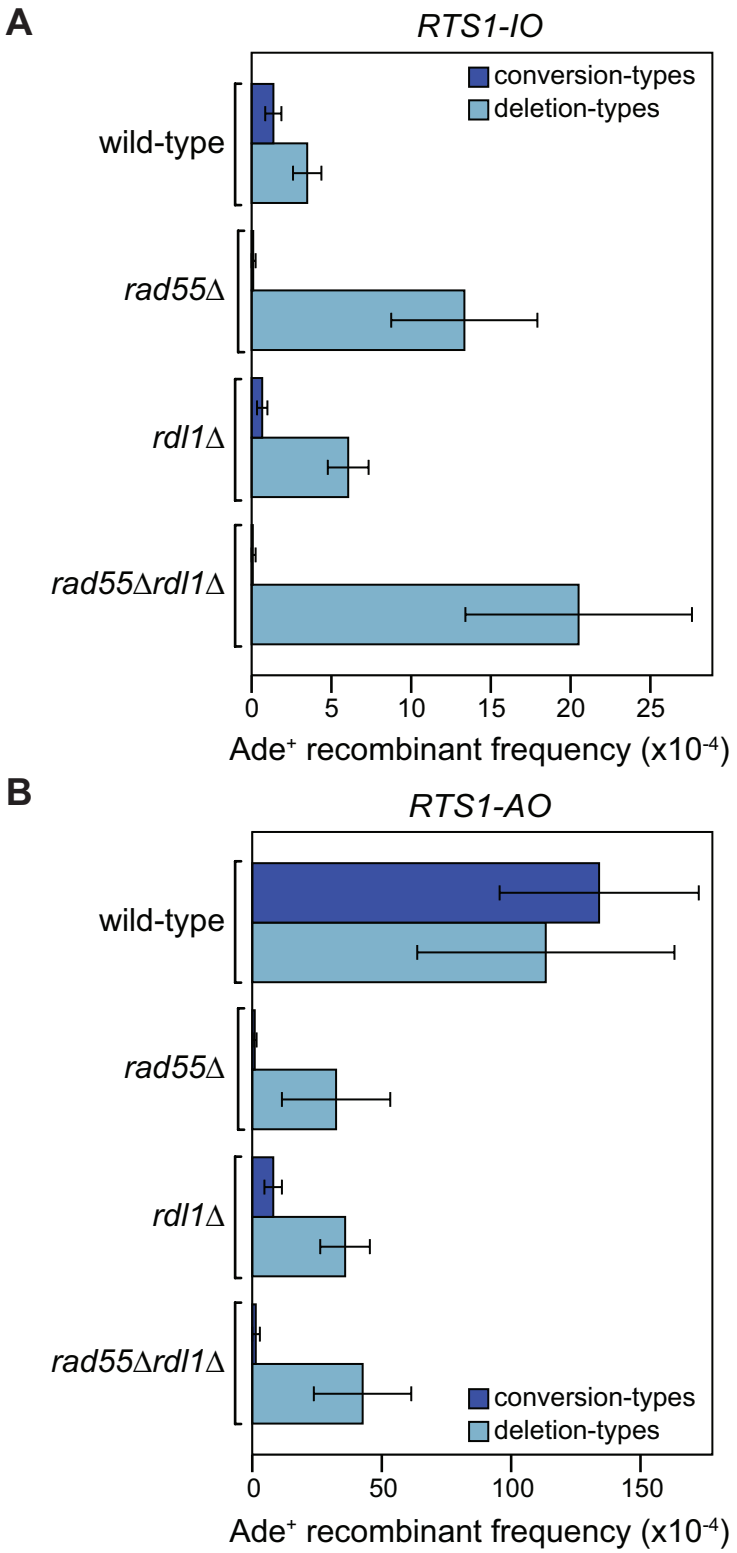


Figure 6.4 | Rad55 and Rdl1 function in the same pathway for promoting replication fork block-induced recombination. Bar chart showing the frequency of conversion- and deletion-type Ade$^+$ recombinants in wild-type, *rad55Δ, rdl1Δ*, and *rad55Δrdl1Δ* strains with either *RTS1-IO* (A) or *RTS1-AO* (B). Error bars represent ± one standard deviation. In order of presentation, the strains are MCW4712, MCW2650, MCW6501, MON275, MCW4713, MCW2655, MCW6468, and MON279.

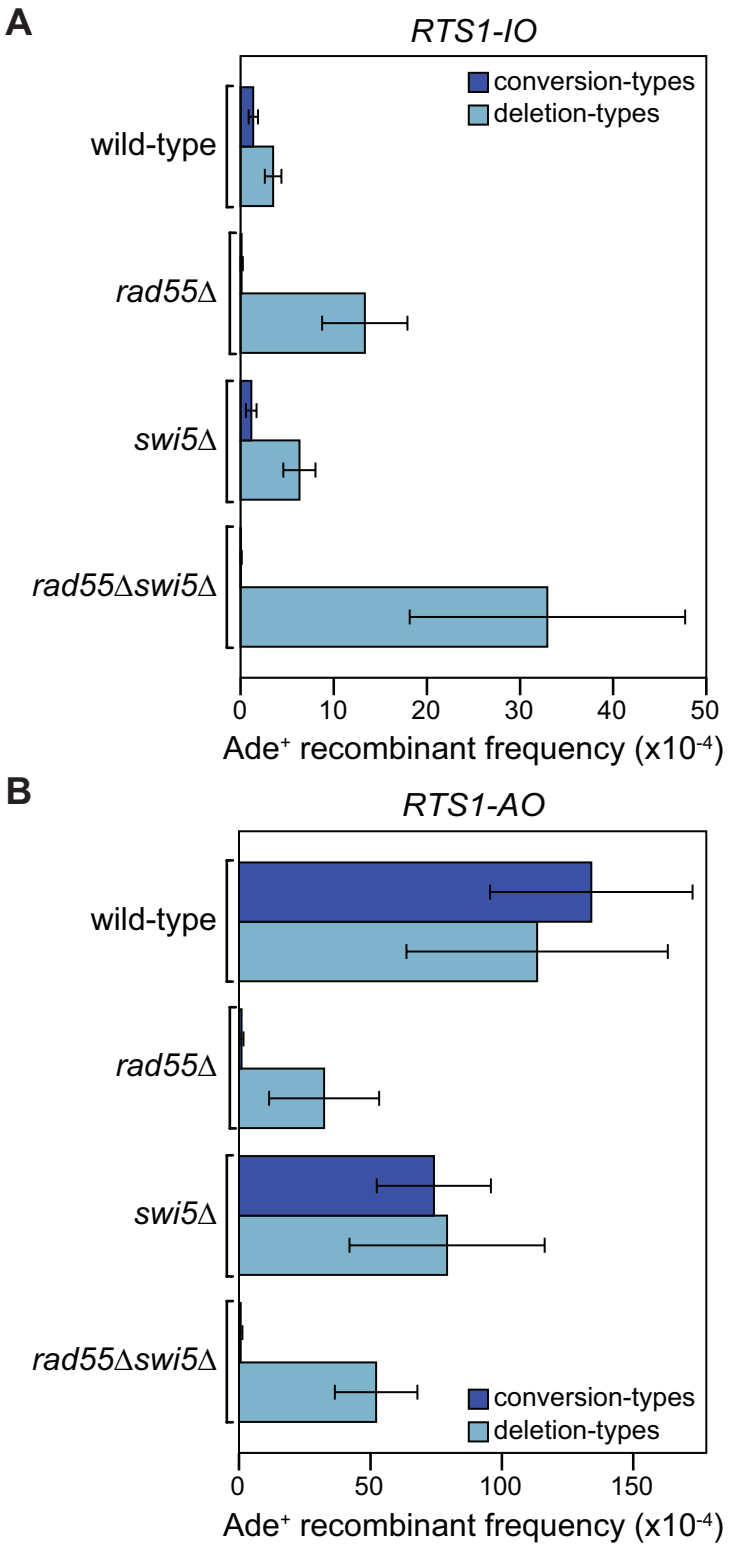


Figure 6.5 | Rad55 and Swi5 function in the same pathway for promoting replication fork block-induced recombination. Bar chart showing the frequency of conversion- and deletion-type Ade$^+$ recombinants in wild-type, *rad55Δ, swi5Δ*, and *rad55Δswi5Δ* strains with either *RTS1-IO* (A) or *RTS1-AO* (B). Error bars represent ± one standard deviation. In order of presentation, the strains are MCW4712, MCW2650, MCW2647, MCW2912, MCW4713, MCW2655, MCW2653, and MCW2916.

6.2.5 Rad51 and its mediators have a role in preventing replication fork block-induced deletions

To investigate whether the Rad51 mediators could have a Rad51-independent role, I determined the frequency of direct repeat recombination in *rad55Δ*, *rdl1Δ*, *swi5Δ*, and *rad51Δ* single and double mutant strains (Figures 6.6 – 6.8). In *rad51Δ* single mutants, the frequency of conversion-type recombinants is essentially zero (Figure 6.6), whereas spontaneous deletions increase ~ 4.5-fold (~ 15.7 x 10^{-4} recombinants) and *RTS1*-induced deletions decrease by ~ 1.5-fold (~ 74.7 x 10^{-4} recombinants) compared to wild-type (all P = < 0.001) (Figure 6.6). As expected when *rad51Δ* is combined with *rad55Δ*, *rdl1Δ,* or *swi5Δ*, the resultant double mutant strains exhibit essentially no spontaneous or *RTS1*-induced conversion-type recombinants (Figures 6.6 – 6.8). In *rad51Δrad55Δ* and *rad51Δswi5Δ* double mutants, the frequency of spontaneous deletions, however, increases to ~ 30 x 10^{-4} Ade^{+} recombinants, which is significantly higher than any of the single mutants (all P = < 0.003) (Figures 6.6A and 6.8A). The *rad51Δrdl1Δ* double mutant, on the other hand, is epistatic to *rad51Δ* in the frequency of spontaneous deletions (Figure 6.7A). At forks blocked at *RTS1*, the low frequency of deletions that is seen in a *rad55Δ* single mutant increases by ~ 2.5-fold when it is combined with *rad51Δ* (P = < 0.001) (Figure 6.6B). This is a similar frequency to that observed in a *rad51Δ* single mutant with *RTS1-AO*. Similarly, combining *rad51Δ* with either *rdl1Δ* or *swi5Δ* in cells with *RTS1-AO* increases the frequency of deletions in the double mutants to levels higher than any of the single mutants (all P = < 0.004). Altogether, these data suggest that the loading of Rad51 onto DNA

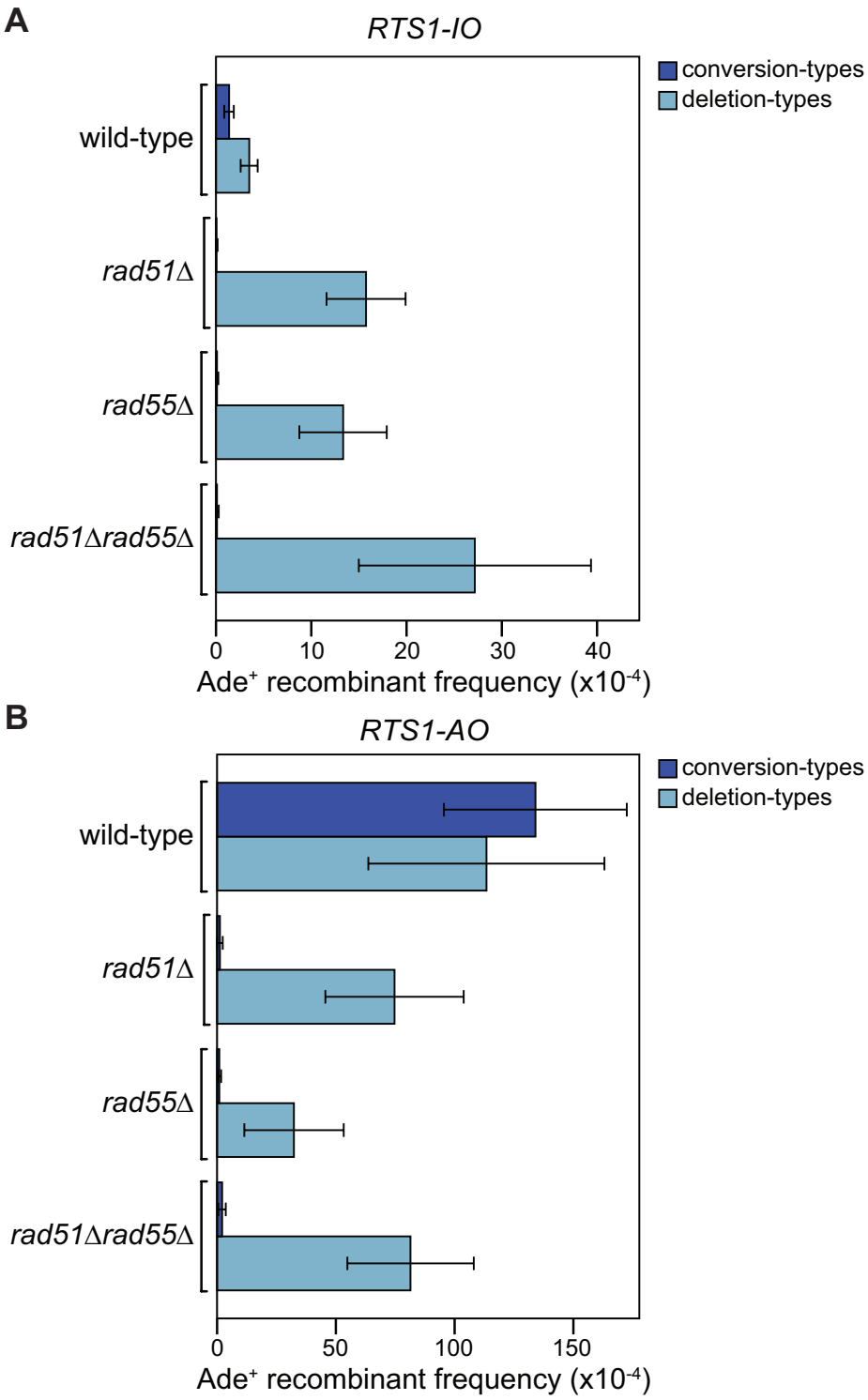


Figure 6.6 | Rad51 has a role in preventing replication fork block-induced deletions independent of its role in promoting gene conversion. Bar chart showing the frequency of conversion- and deletion-type Ade$^+$ recombinants in wild-type, *rad51Δ, rad55Δ*, and *rad51Δrad55Δ* strains with either *RTS1-IO* (A) or *RTS1-AO* (B). Error bars represent ± one standard deviation. In order of presentation, the strains are MCW4712, MCW1691, MCW2650, MON129, MCW4713, MCW1692, MCW2655, and MON149.

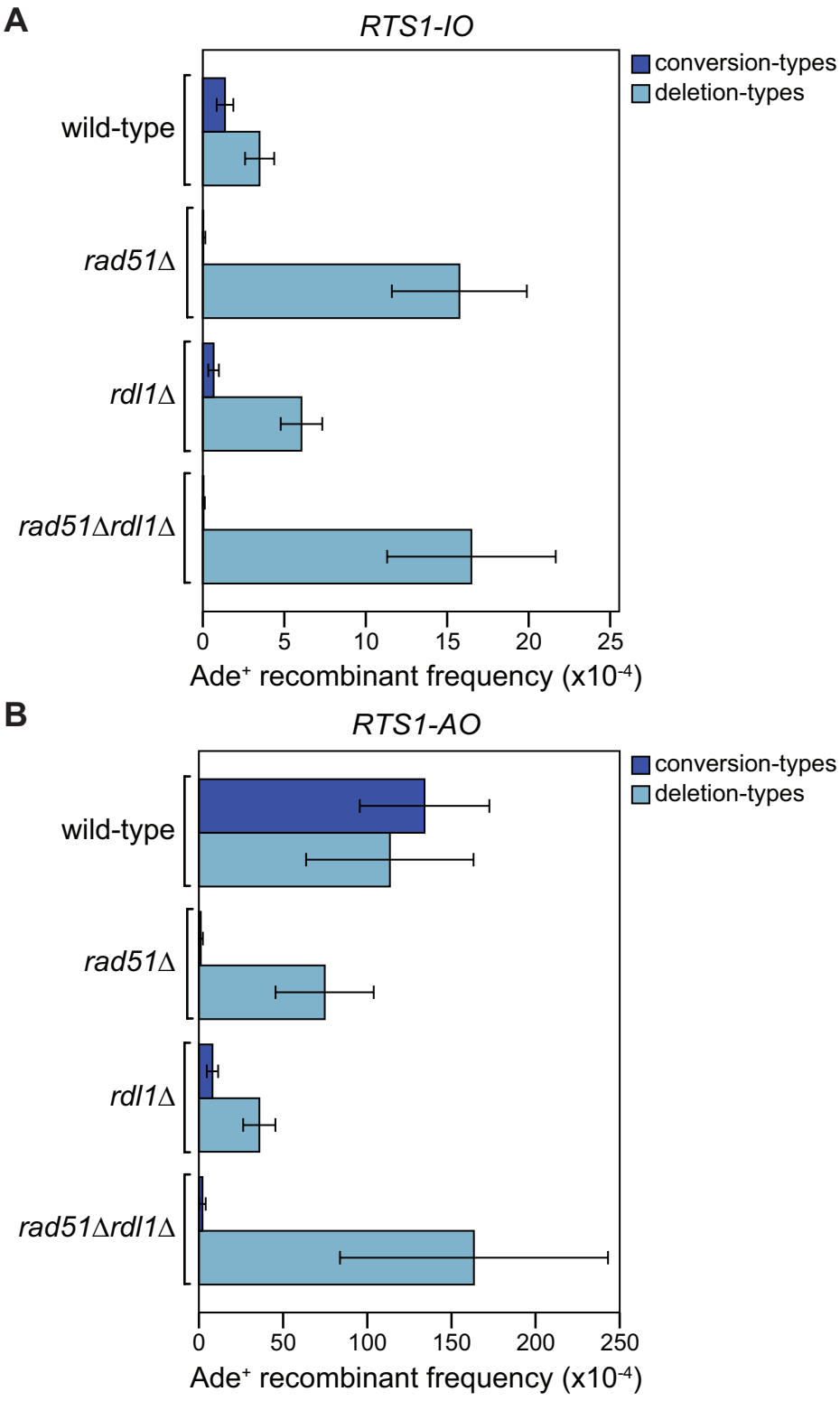


Figure 6.7 | Rdl1 has a Rad51-independent role in limiting replication fork block-induced deletions. Bar chart showing the frequency of conversion- and deletion-type Ade$^+$ recombinants in wild-type, *rad51Δ, rdl1Δ*, and *rad51Δrdl1Δ* strains with either *RTS1-IO* (A) or *RTS1-AO* (B). Error bars represent ± one standard deviation. In order of presentation, the strains are MCW4712, MCW1691, MCW6501, MON263, MCW4713, MCW1692, MCW6468, and MON269.

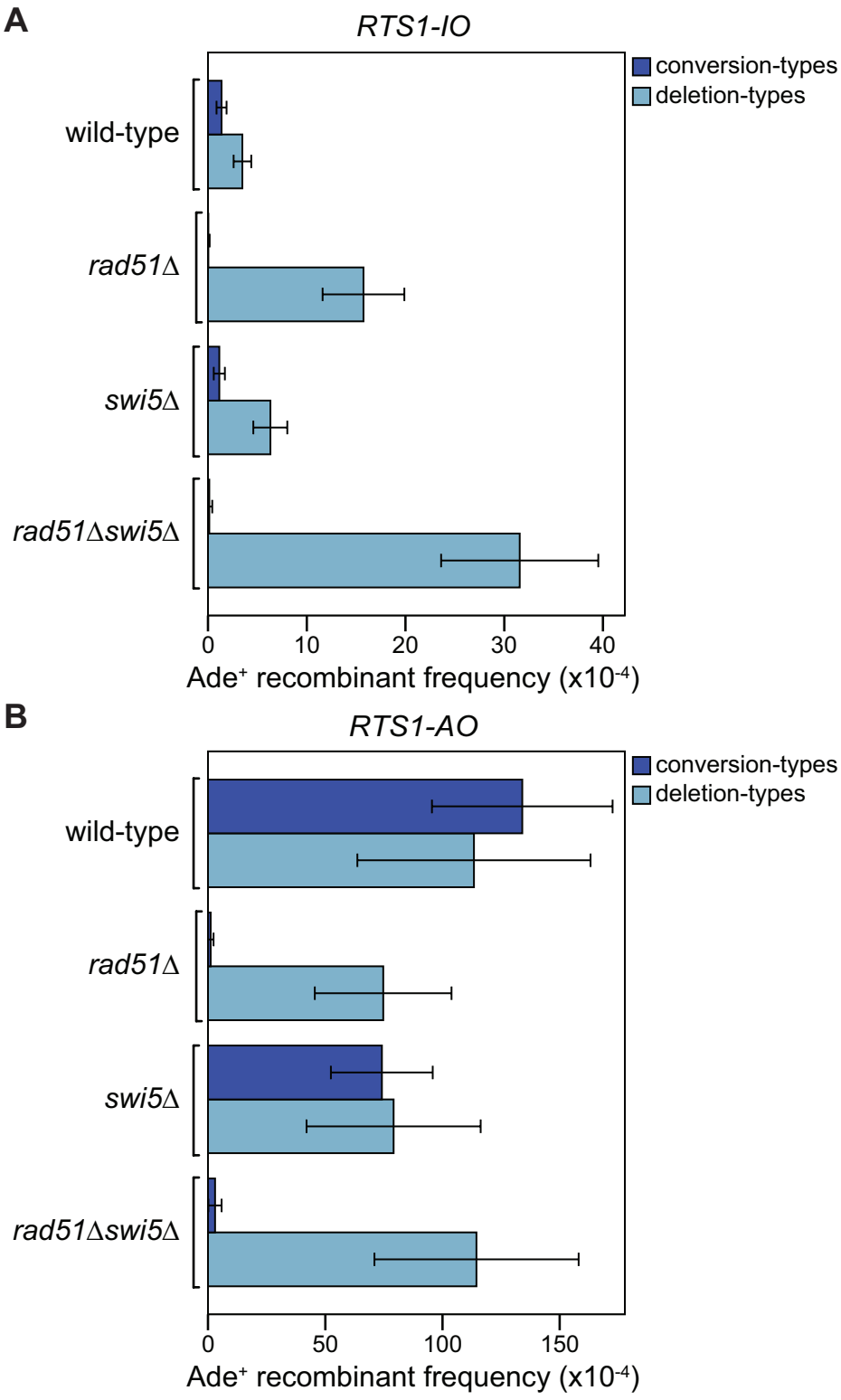


Figure 6.8 | Swi5 has a Rad51-independent role in limiting both spontaneous and replication fork block-induced deletions. Bar chart showing the frequency of conversion- and deletion-type Ade$^+$ recombinants in wild-type, *rad51Δ, swi5Δ*, and *rad51Δswi5Δ* strains with either *RTS1-IO* (A) or *RTS1-AO* (B). Error bars represent ± one standard deviation. In order of presentation, the strains are MCW4712, MCW1691, MCW2647, MON283, MCW4713, MCW1692, MCW2653, and MON289.

may have a role in suppressing Rad51-independent deletions even when its ability to promote gene conversions is impaired. Furthermore, the increase in the frequency of deletions observed in some of the double mutant strains relative to a *rad51Δ* single mutant suggests that the mediators may also play a role in suppressing deletions when Rad51 is absent.

6.2.6 Recruitment of Rad52-YFP to *RTS1-AO* is not affected by the loss of Rad51 or its mediators

Having established that the loss of Rad51 or its mediators impairs replication fork block-induced recombination, I performed a genetic analysis of Rad52's focus formation to determine whether Rad52's recruitment and retention at forks blocked at *RTS1* depended on Rad51 or its mediators. Rad52 foci form efficiently in *rad51Δ*, *rad55Δ*, *rdl1Δ*, and *swi5Δ* strains (Figures S6.1 – S6.4). I found that the overall frequency of spontaneous Rad52-YFP foci in the 90-minute interval following anaphase increased significantly in *rad51Δ*, *rad55Δ*, *rdl1Δ*, or *swi5Δ* single mutants compared to wild-type irrespective of the orientation of *RTS1* (all $P = < 0.006$) (Figure 6.9). This increase was most marked in a *rad51Δ* mutant, with > 95% of cells exhibiting at least one Rad52-YFP focus (Figure 6.9A), and an average of ~ 2- to 3-fold increases in the number of time points in which a focus was detected (Figure 6.9B). A subset of *rad51Δ* cells (~ 15 – 21%) also exhibited a Rad52 focus immediately following anaphase (Figure S6.1), which is normally not seen in wild-type or any of the mediator mutants. Of the mediators, the *rad55Δ* mutant exhibited the highest increase in spontaneous Rad52 foci, while *rdl1Δ* and *swi5Δ* single

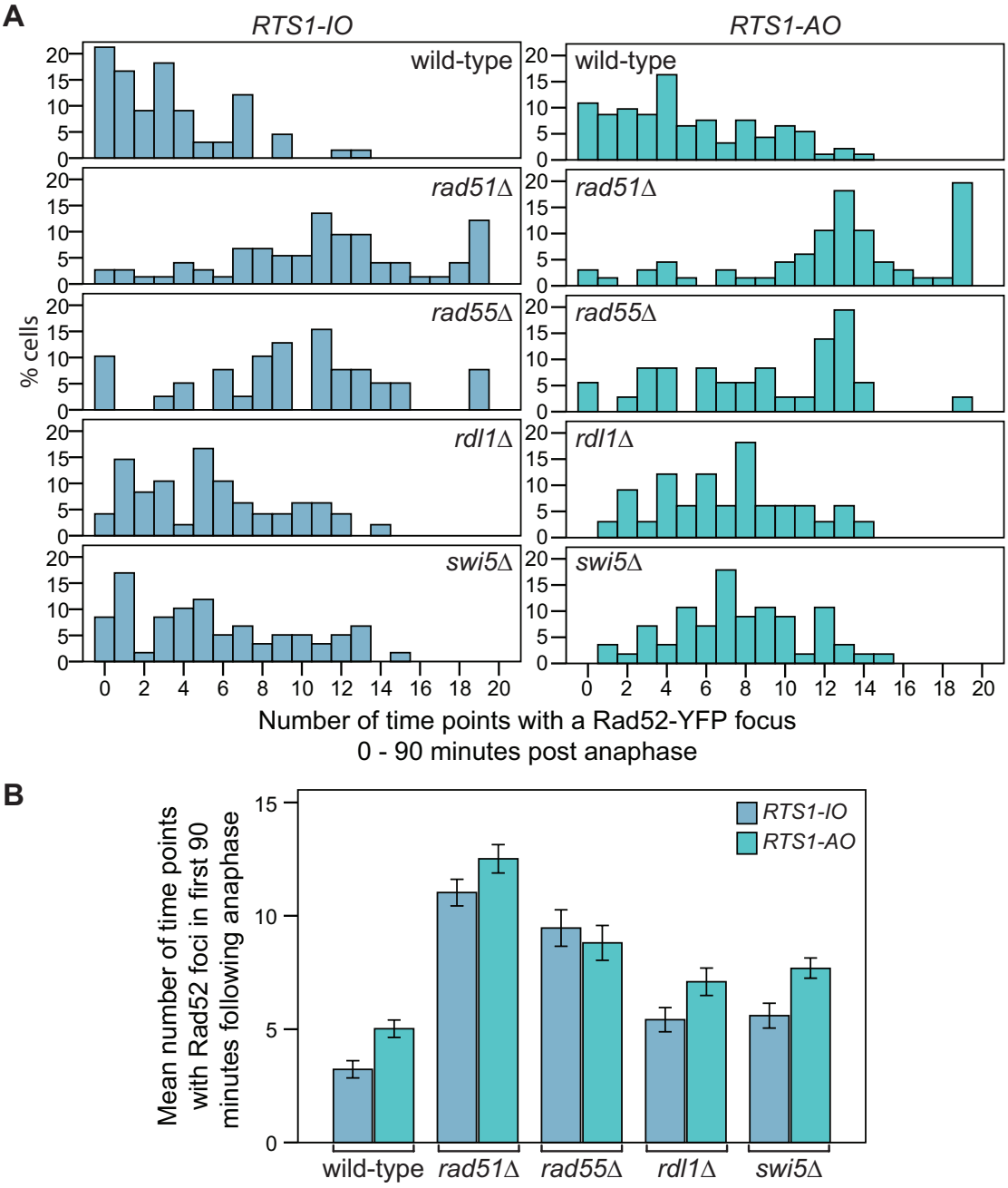


Figure 6.9 | Rad52 foci increase when Rad51 and its mediators are deleted. (A) Histogram showing the percentage of cells with a given number of time points in which a Rad52-YFP focus is detected within the first 90 minutes following anaphase. (B) Bar chart of the mean number of time points cells display a Rad52-YFP focus in the first 90 minutes following anaphase. Error bars represent ± one standard error of the mean. The *RTS1-IO* strains are MON110 (wild-type), MON163 (*rad51Δ*), MCW6955 (*rad55Δ*), MCW6985 (*rdl1Δ*), and MCW6961 (*swi5Δ*). The *RTS1-AO* strains are MON148 (wild-type), MON167 (*rad51Δ*), MCW6958 (*rad55Δ*), MCW6988 (*rdl1Δ*), and MCW6964 (*swi5Δ*).

mutants displayed a more modest increase compared to wild-type cells (Figure 6.9). At forks blocked at *RTS1*, Rad52 focus assembly and persistence was not disrupted by the loss of Rad51 or its mediators (Figure 6.10). On average, Rad52 remained associated at *RTS1-AO* for a similar duration in *rad51Δ*, *rad55Δ*, and *rdl1Δ* single mutants compared to wild-type (Figure 6.10B). Curiously, Rad52 persists slightly longer in a *swi5Δ* mutant compared to wild-type ($P = < 0.001$) (Figure 6.10B). Taken together, these data indicate that Rad52 focus formation at the *RTS1* RFB does not depend on Rad51, Rad55, Rdl1, or Swi5 and that Rad52 is not typically displaced at *RTS1-AO* by downstream recombination proteins. One exception to this latter point seems to be Swi5, which, based on the data in Figure 6.10, appears to promote the displacement of Rad52 from *RTS1-AO* in a manner that presumably does not require Rad51, Rad55, or Rdl1. How it does this is unclear and will require further investigation to determine.

6.2.7 Timing of Rad52 recruitment to forks blocked at *RTS1* is not affected by the loss of downstream recombination proteins

Having established that Rad52 focus formation is not impaired by the loss of Rad51 or its mediators, I also assessed the timing at which Rad52 is recruited to the *RTS1-AO* (Figure 6.11). Similar to wild-type, the majority of co-localized Rad52 foci occur within 25 to 55 minutes post anaphase in *rad51Δ*, *rad55Δ*, *rdl1Δ*, and *swi5Δ* single mutants (Figure 6.11A). A subset of *rad51Δ* cells (4 of 46 cells with a co-localized Rad52 focus) exhibit a co-localized Rad52 focus before 20 minutes post anaphase, which is not typically observed in wild-type

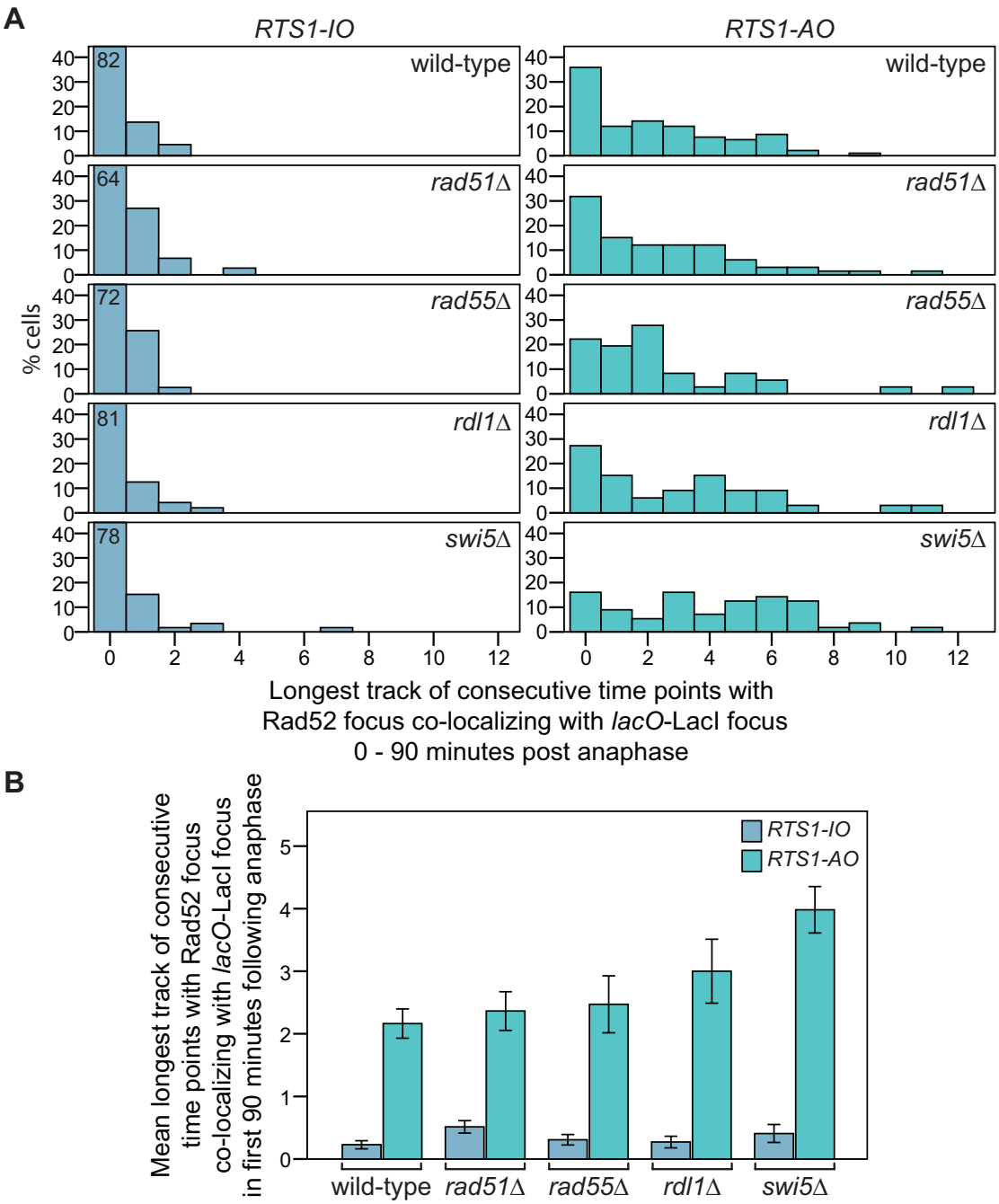


Figure 6.10 | Rad52 is not displaced at *RTS1-AO* by downstream recombination proteins. (A) Histogram showing the percentage of cells with a given number of uninterrupted time points in which a Rad52-YFP focus co-localizes with a *lacO*-LacI focus within the first 90 minutes following anaphase. (B) Bar chart of the mean number of uninterrupted time points cells display a Rad52-YFP focus that co-localizes with a *lacO*-LacI focus during the first 90 minutes following anaphase. Error bars represent ± one standard error of the mean. The *RTS1-IO* strains are MON110 (wild-type), MON163 (*rad51Δ*), MCW6955 (*rad55Δ*), MCW6985 (*rdl1Δ*), and MCW6961 (*swi5Δ*). The *RTS1-AO* strains are MON148 (wild-type), MON167 (*rad51Δ*), MCW6958 (*rad55Δ*), MCW6988 (*rdl1Δ*), and MCW6964 (*swi5Δ*).

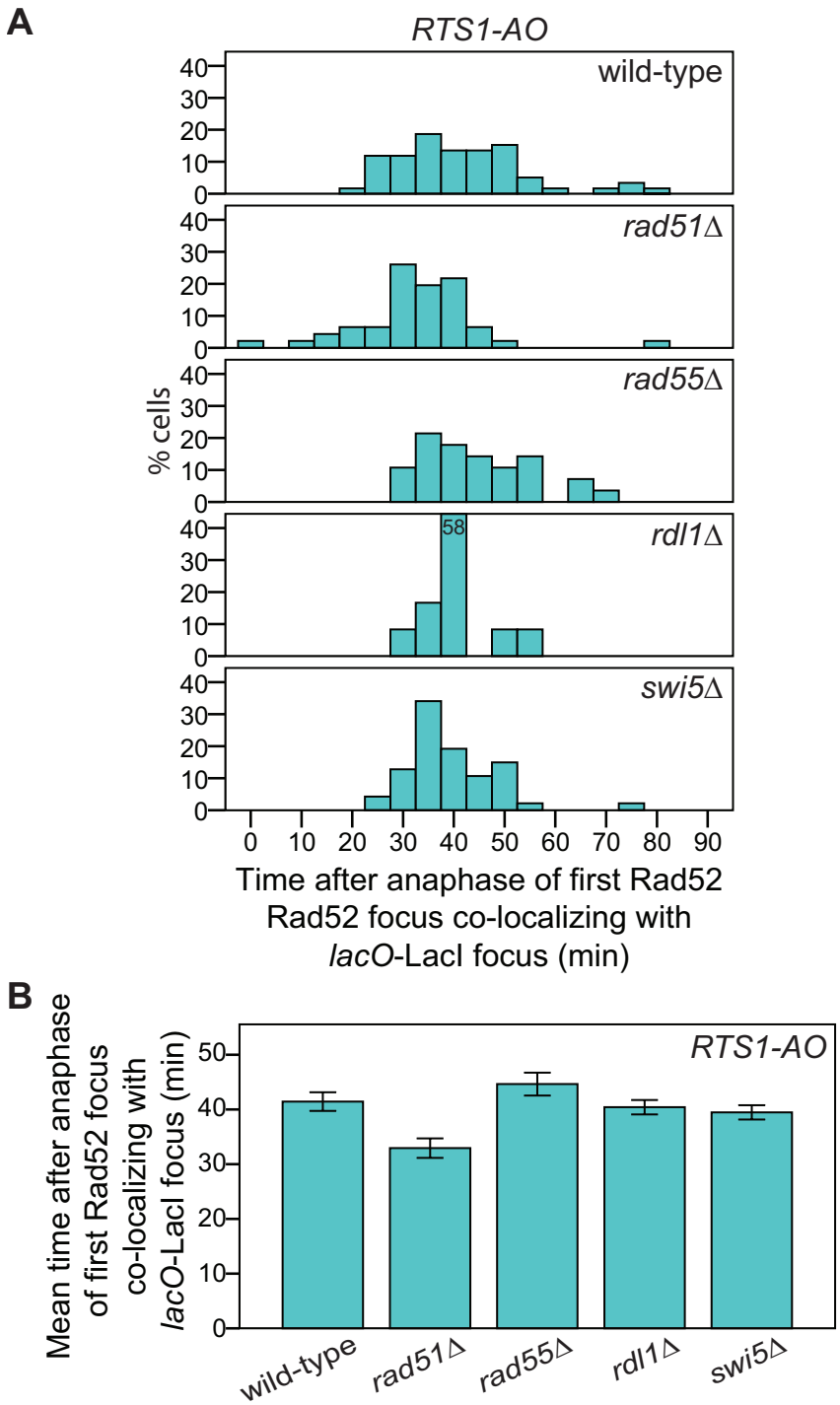


Figure 6.11 | Recruitment of Rad52-YFP to *RTS1-AO* is not significantly affected by the loss of Rad51 or its mediators. (A) Histogram showing the percentage of cells at a given time after anaphase in which the first Rad52-YFP focus co-localizes with a *lacO*-LacI focus. (B) Bar chart of the mean time after anaphase of when the first Rad52-YFP focus co-localizes with a *lacO*-LacI focus. Error bars represent ± one standard error of the mean. The *RTS1-IO* strains are MON110 (wild-type), MON163 (*rad51Δ*), MCW6955 (*rad55Δ*), MCW6985 (*rdl1Δ*), and MCW6961 (*swi5Δ*). The *RTS1-AO* strains are MON148 (wild-type), MON167 (*rad51Δ*), MCW6958 (*rad55Δ*), MCW6988 (*rdl1Δ*), and MCW6964 (*swi5Δ*).

cells. However, in three out of four cases, co-localization at this early stage post anaphase was observed in only one time point, and, as similar early co-localizations are seen in *RTS1-IO rad51Δ* cells, it is likely that they result from chance co-localizations, which become more prevalent with the overall heightened frequency of Rad52 foci in *rad51Δ* cells. These early chance co-localizations partly explain why the mean time for Rad52 appearance at *RTS1-AO* post anaphase is earlier than in wild-type (P = 0.001) (Figure 6.11B). In contrast, the absence of Rad55, Rdl1, or Swi5, has no significant effect on the timing of Rad52 recruitment to *RTS1-AO*. Together, these data indicate that the timing of Rad52 recruitment to blocked forks at *RTS1* is not significantly affected by the loss of downstream recombination proteins.

6.3 Discussion

In this chapter, I have shown that the loss of Rad51 or its mediators has different effects on the proficiency of spontaneous and *RTS1*-induced direct repeat recombination. The normal low frequency of spontaneous Ade^+ recombinants, which may arise from fork stalling at lesions that occur during normal laboratory growth conditions, leads to a significant reduction in conversion-type recombinants and a significant increase in deletion-type recombinants in the absence of *rad51* or its mediators. This suggests that the repair of spontaneous damage shifts from a more precise homology directed repair towards a more mutagenic pathway. Our laboratory has previously shown that deletion-type recombinants are largely abolished in the absence of *rad52*, irrespective of *RTS1* orientation (Ahn et al. 2005). This is consistent

with the idea that the increased spontaneous deletion-type recombinants in the absence of *rad51* or its mediators occur through a Rad51-independent, Rad52-dependent process, such as SSA.

Similar to Rad51, Rad55-Rad57 is essential for gene conversion and the majority of deletions that stem from replication fork blockage at *RTS1*. Likewise, the Rdl1-Rlp1-Sws1 complex is required for Rad51 activity at blocked forks, albeit not to the same extent as Rad55-Rad57. In contrast, Swi5-Sfr1 appears to play a relatively minor role in the early stage of promoting Rad51-dependent recombination. Interestingly, the relative requirement for each mediator in *RTS1*-induced recombination does not in every case correlate with its requirement for the repair of DNA damage induced by agents such as CPT, MMS, HU, and UV. For example, *rdl1Δ*, *rlp1Δ*, and *sws1Δ* mutants exhibit relatively little hyper-sensitivity to these agents, compared to *rad55Δ*, *rad57Δ*, *swi5Δ* and *sfr1Δ* mutants (data not shown) (Martin et al. 2006), yet they exhibit deficiencies in *RTS1*-induced recombination that are similar to *rad55Δ* and *rad57Δ* mutants and greater than *swi5Δ* and *sfr1Δ* mutants. If the readout of *RTS1*-induced direct repeat recombination is truly a measure of RDR proficiency, then one must suppose that RDR is unnecessary for the tolerance/repair of damage induced by CPT, MMS, HU and UV.

Interestingly, at forks blocked at *RTS1*, the residual deletion-type recombinants is lower in *rad55Δ*, *rad57Δ*, *rdl1Δ*, *rlp1Δ*, and *sws1Δ* single

mutant strains than in *rad51Δ* mutants. This suggests that either Rad51 is less important for the production of deletions than its mediators or has a more prominent role in suppressing their formation. As it is unclear how the mediators could promote deletion-type formation without Rad51 I favor the latter idea. Loading of Rad51 onto DNA could help protect the fork (Hashimoto et al. 2010; Schlacher et al. 2011; Schlacher et al. 2012), possibly even without the stabilization afforded by its mediators, which are perhaps only needed to make the Rad51 nucleofilament competent for catalyzing strand invasion. In the absence of Rad51, Rad52's persistence at the site may promote deletion-type formation by annealing the unwound nascent strands with a homologous template in the vicinity of the collapsed fork, as previously depicted in Figure 3.10. A model for replication fork block-induced recombination that summarizes the findings in this chapter is presented in Figure 6.12.

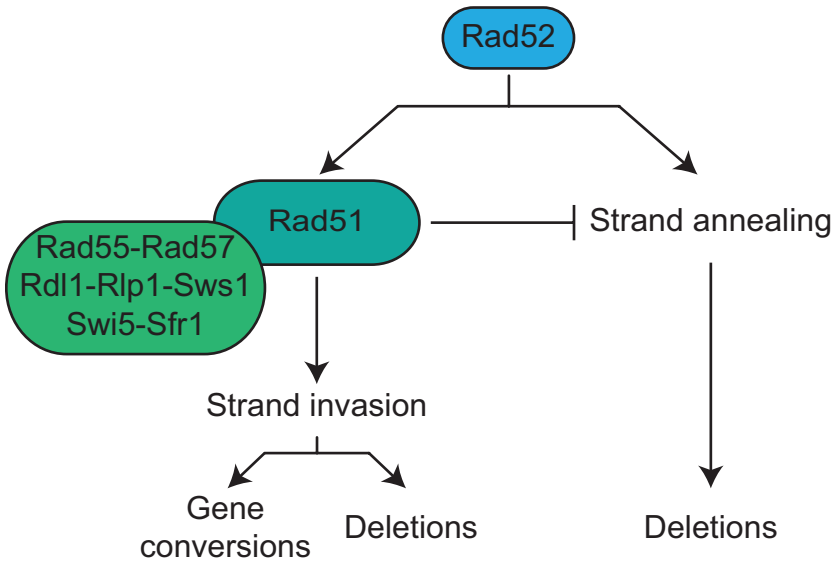


Figure 6.12 | Rad51 and its mediators promote Rad51-dependent strand invasion and block Rad52-dependent strand annealing at forks blocked at *RTS1*. Model for replication fork block-induced recombination. Following Rad52 recruitment to the *RTS1* RFB, it can load Rad51 or perform its strand annealing activities, which can lead to the production of deletion-types. Rad51, aided by its mediators – Rad55-Rad57, Rdl1-Rlp1-Sws1, and Swi5-Sfr1 – promotes strand invasions that can lead to gene conversions and deletions while it also blocks Rad52's ability to anneal homologous strands.

Chapter 7

Consequences of Pathological Fork Merging at *RTS1*

7.1 Introduction

DNA helicases and translocases play critical roles in the rescue of blocked replication forks. In this chapter, I will examine the role of three evolutionarily conserved factors – Fml1, Rad54, and Pfh1 – in promoting RDR and fork merging at the *RTS1* RFB.

In the first part of this chapter, I conducted genetic experiments to analyze the importance of Fml1 in restart. Fml1 is part of the FANCM family of DNA helicases that *in vitro* can catalyze fork remodeling, HJ branch migration and D-loop dissociation (Gari et al. 2008a; Gari et al. 2008b; Sun et al. 2008; Prakash et al. 2009; Nandi and Whitby 2012). At collapsed replication forks, Fml1 is thought to drive replication fork reversal to generate a substrate at which recombinases can load to promote RDR. I investigated its role *in vivo* to see whether its loss would impair recombination at blocked replication forks and to determine if it is a genetic requirement for Rad52 focus formation at *RTS1*.

In the second part of this chapter, I focused on Rad54, a member of the Snf2 family of DNA-dependent ATPases. Rad54 is a DNA translocase that has multiple roles in recombination (Tan et al. 2003; Thoma et al. 2005; Heyer et al. 2006; Mazin et al. 2010). These include the stimulation of Rad51 DNA strand exchange activity, chromatin remodeling, branch migration of Holliday junctions, and the dissociation of Rad51 from DNA following strand exchange to allow DNA polymerase to prime DNA synthesis on the invading 3' end

(Petukhova et al. 1998; Mazin et al. 2000; Van Komen et al. 2000; Solinger et al. 2002; Alexeev et al. 2003; Mazin et al. 2003; Bugreev et al. 2006; Li and Heyer 2009). To learn more about its role at blocked replication forks, I assessed whether its absence lead to a reduction in RDR and whether its ATPase activity is critical for its roles in restart.

Lastly, as there are likely to be factors that control the orderly merging between a restarted fork and an oncoming fork, I further explored Pfh1's role in replication fork merging at *RTS1*. Pfh1, which is part of the Pif1 family of DNA helicases, promotes replication fork progression past DNA-protein barriers and fork merging at replication termination sites (Sabouri et al. 2012; Steinacher et al. 2012). Because there may be times when the recombination machinery at the restarted fork collides with an oncoming fork, I investigated whether there was a consequence of fork merging in Pfh1 mutants when the converging fork arrives at an arrested fork in which the Rad51 filament has been loaded for RDR but its turnover is impaired by the loss of Rad54.

7.2 Results

7.2.1 Fml1 has a dual role in modulating replication fork block-induced recombination

Fml1 promotes spontaneous and *RTS1*-induced Rad51-dependent conversion-types between a direct repeat of *ade6*$^{-}$ heteroalleles (Sun et al. 2008). However, unlike in the absence of other HR factors, such as Rad51 or Rad55, *fml1Δ* mutants continue to exhibit high levels of deletion-type events at

forks blocked at *RTS1* that are similar to wild-type levels. To further examine this, I compared the frequency of *ade*$^{+}$ deletion- and conversion-types in *fml1Δ*, *rad51Δ*, *rad55Δ*, and *rad52Δ* single and double mutants (Figure 7.1). In the absence of *fml1*, the low frequency of spontaneous conversion-types is reduced 2.6-fold compared to wild-type (P = <0.001), while there is no significant effect of *fml1Δ* on the frequency of spontaneous deletion-types compared to wild-type (Figure 7.1A). The absence of *fml1* when forks are blocked at *RTS1*, however, leads to an even greater reduction in conversion-types compared to wild-type (7.8-fold, P = < 0.001), yet it also has no significant effect on the frequency of deletion-types compared to wild-type (Figure 7.1B). When *fml1Δ* is combined with either *rad51Δ* or *rad55Δ* mutants, the residual conversion-types in a *fml1Δ* single mutant are lost irrespective of *RTS1* orientation (Figure 7.1). Both *fml1Δrad51Δ* and *fml1Δrad55Δ* double mutants exhibit increases in spontaneous deletion-types compared to a *fml1Δ* single mutant (both P = < 0.001) that are epistatic to *rad51Δ* and *rad55Δ* single mutants, respectively (Figure 7.1A). At forks blocked at *RTS1*, however, the frequency of deletion-types in *fml1Δrad51Δ* and *fml1Δrad55Δ* double mutants significantly increase compared to *rad51Δ* and *rad55Δ* single mutants, respectively (both P = < 0.001). This suggests that Fml1 can function independently of Rad51 and Rad55 in modulating replication fork block-induced recombination to prevent deletions. The deletion-types in a *fml1Δ* mutant are largely dependent on Rad52 (Figure 7.1B). This suggest that in addition to promoting Rad51-dependent gene-conversions, presumably by catalyzing fork reversal, Fml1 also has a role in constraining Rad52-

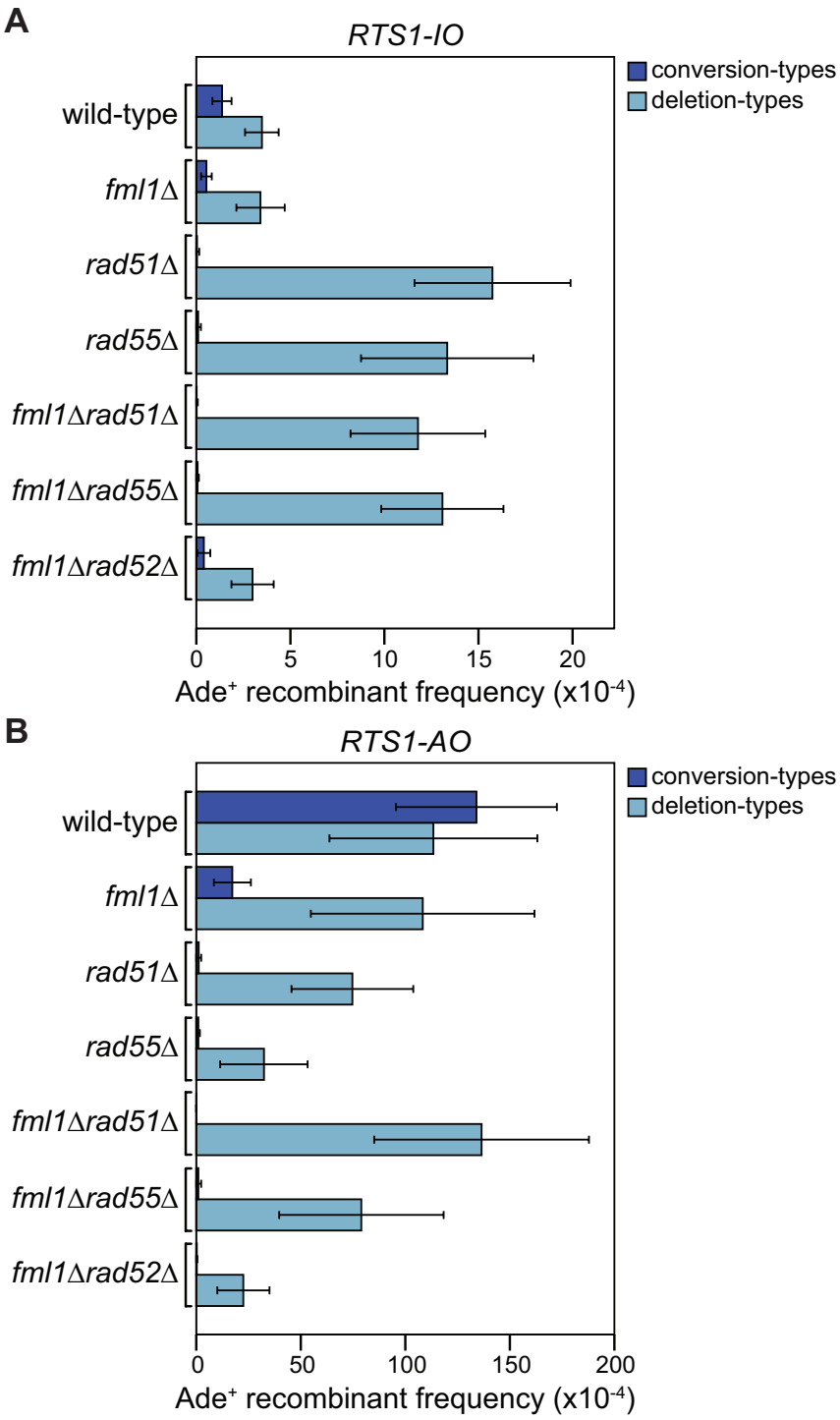


Figure 7.1 | Fml1 has a dual role in modulating replication fork block-induced recombination. Bar chart showing the frequency of conversion- and deletion-type Ade$^+$ recombinants in wild-type, *fml1Δ, rad51Δ*, *rad55Δ*, *fml1Δrad51Δ*, *fml1Δrad55Δ*, and *fml1Δrad52Δ* strains with either *RTS1-IO* (A) or *RTS1-AO* (B). Error bars represent ± one standard deviation. In order of presentation, the strains are MCW4712, MCW3059, MCW1691, MCW2650, MCW3790, MCW6967, MCW7161, MCW4713, MCW3061, MCW1692, MCW2655, MCW3794, MCW6982, and MCW7159. The recombination assay values presented in this chart and the remaining charts in this chapter are also listed in Tables S1 and S2 with statistical analysis in the appendix.

dependent deletions at blocked forks.

7.2.2 Rad52-YFP foci persist longer at *RTS1-AO* in the absence of *fml1*

Because one of Fml1's functions is believed to involve the catalysis of fork reversal at stalled replication forks to generate the dsDNA that can act as an entry point for recombinases, I sought to determine whether Fml1 is a genetic requirement for Rad52 focus assembly at *RTS1-AO*. In the absence of *fml1*, however, I found that Rad52 foci continue to form efficiently at forks blocked at *RTS1* (Figure S7.1). Unexpectedly, a subset of *fml1Δ RTS1-AO* cells (~ 28%) exhibited a Rad52-YFP focus that persisted for 7 to 13 consecutive time points, which was not typically observed in wild-type *RTS1-AO* cells (Figure 7.2A). On average, Rad52 remained associated at *RTS1-AO* in *fml1Δ* cells for approximately twice as long as wild-type ($P = < 0.001$) (Figure 7.2B). Altogether, these data suggest that Rad52 is able to accumulate enough protein to form foci at replication forks that are blocked at *RTS1* independently of Fml1 and moreover, that Fml1 has a role in displacing Rad52 from *RTS1-AO*.

7.2.3 Rad52's recruitment to forks blocked at *RTS1* is not significantly delayed in the absence of *fml1*

Having established that Fml1 is not required for Rad52's association at blocked replication forks, I also assessed whether its absence led to a delay in the timing of when Rad52 foci formed at *RTS1-AO* (Figure 7.3). Similar to wild-type, however, the majority Rad52-*lacO*-LacI co-localizations occurred

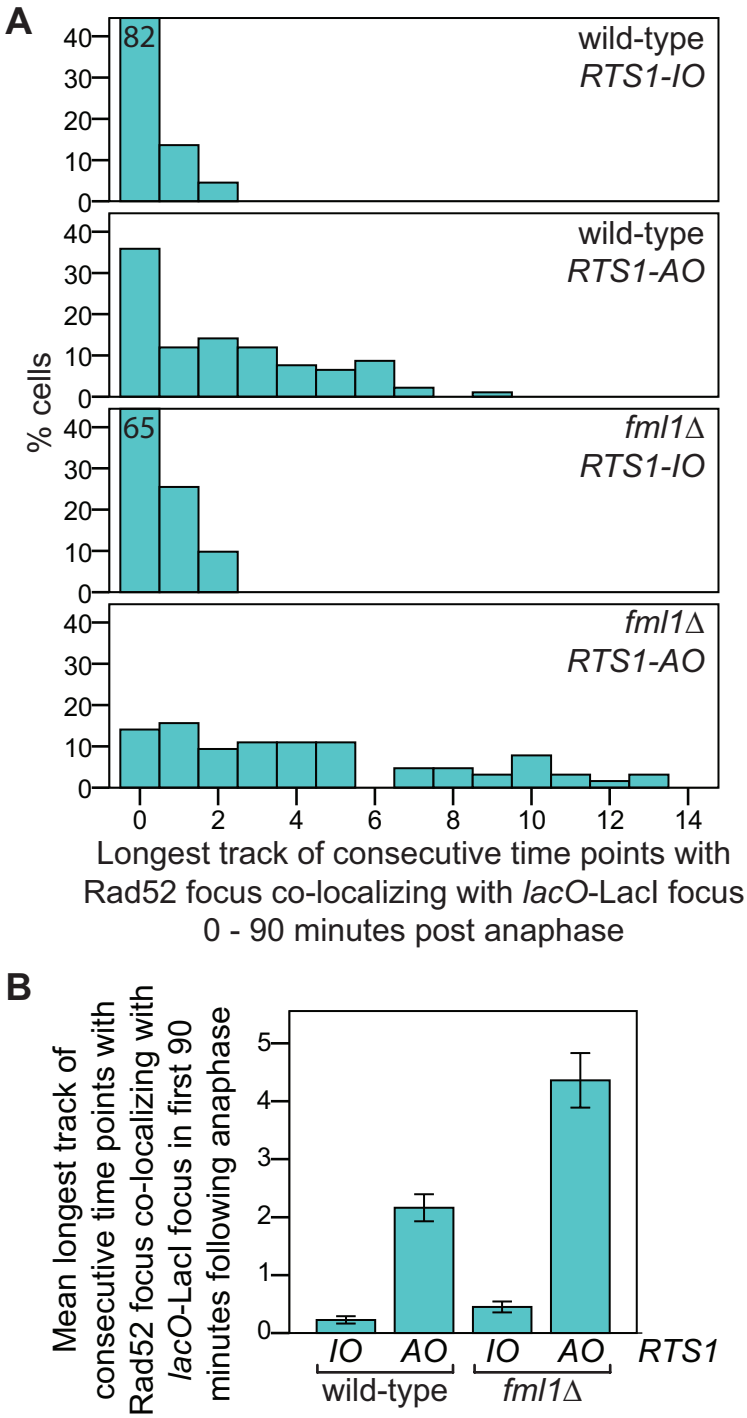


Figure 7.2 | Rad52 persistence at *RTS1-AO* increases in the absence of *fml1*. (A) Histogram showing the percentage of cells with a given number of uninterrupted time points in which a Rad52-YFP focus co-localizes with a *lacO*-LacI focus within the first 90 minutes following anaphase. (B) Bar chart of the mean number of uninterrupted time points cells display a Rad52-YFP focus that co-localizes with a *lacO*-LacI focus during the first 90 minutes following anaphase. Error bars represent ± one standard error of the mean. The *RTS1-IO* strains are MON110 (wild-type) and MON172 (*fml1Δ*). The *RTS1-AO* strains are MON148 (wild-type) and MON177 (*fml1Δ*).

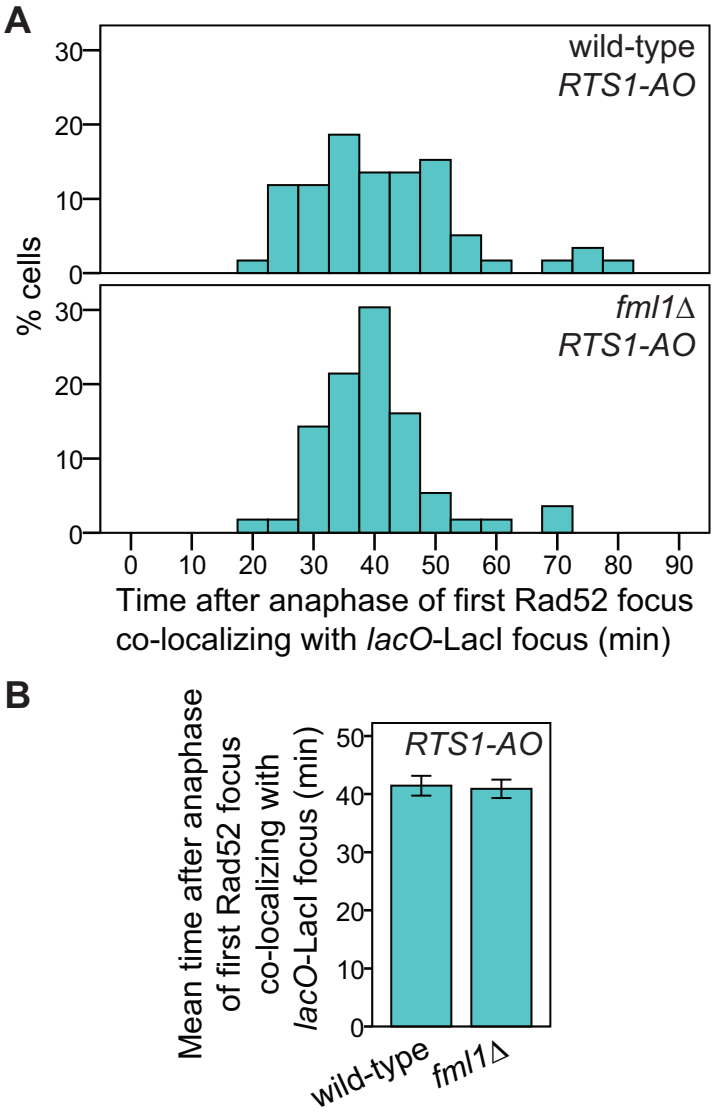


Figure 7.3 | Rad52 recruitment to forks blocked at *RTS1-AO* is not significantly delayed in the absence of *fml1*. (A) Histogram showing the percentage of cells at a given time after anaphase in which the first Rad52-YFP focus co-localizes with a *lacO*-LacI focus. (B) Bar chart of the mean time after anaphase of when the first Rad52-YFP focus co-localizes with a *lacO*-LacI focus. Error bars represent ± one standard error of the mean. The *RTS1-AO* strains are MON148 (wild-type) and MON177 (*fml1Δ*).

within 30 to 50 minutes post anaphase in *RTS1-AO fml1Δ* cells (Figure 7.3A). In fact, on average, the timing of Rad52 foci at *RTS1-AO* was not significantly delayed in *fml1Δ* compared to wild-type (Figure 7.3B). These results suggest that Rad52 may be able to load at blocked forks in a timely manner regardless of whether Fml1 has promoted their reversal.

7.2.4 Rad54 has a role in promoting gene conversions and preventing deletions during replication fork block-induced recombination

To determine the role of Rad54 in spontaneous and *RTS1*-induced recombination, I assessed the effect of *rad54Δ* on the frequency of direct repeat recombination (Figure 7.4). Deletion of *rad54* eliminated both spontaneous (Figure 7.4A) and *RTS1*-induced gene conversions (Figure 7.4B). In contrast, there is a small increase in the frequency of spontaneous deletion-types (~ 1.6-fold) and an even greater increase in the frequency of deletion-types when forks are blocked at *RTS1* (~ 2.3-fold) in *rad54Δ* mutants compared to wild-type (both $P = < 0.001$). I also tested whether these deletions are dependent on Rad51 and/or Rad52. Unexpectedly, the *rad54Δrad51Δ* double mutant exhibited higher levels of spontaneous deletion-types than either single mutant (both $P = < 0.001$) and is epistatic to a *rad54Δ* single mutant in the frequency of deletion-types induced by *RTS1-AO*. In comparison, the *rad54Δrad52Δ* double mutant exhibits virtually zero recombinants irrespective of *RTS1* orientation. Together, these data suggest that Rad54 plays a critical role in promoting Rad51-dependent gene conversions at spontaneous lesions and blocked forks. Furthermore, it also

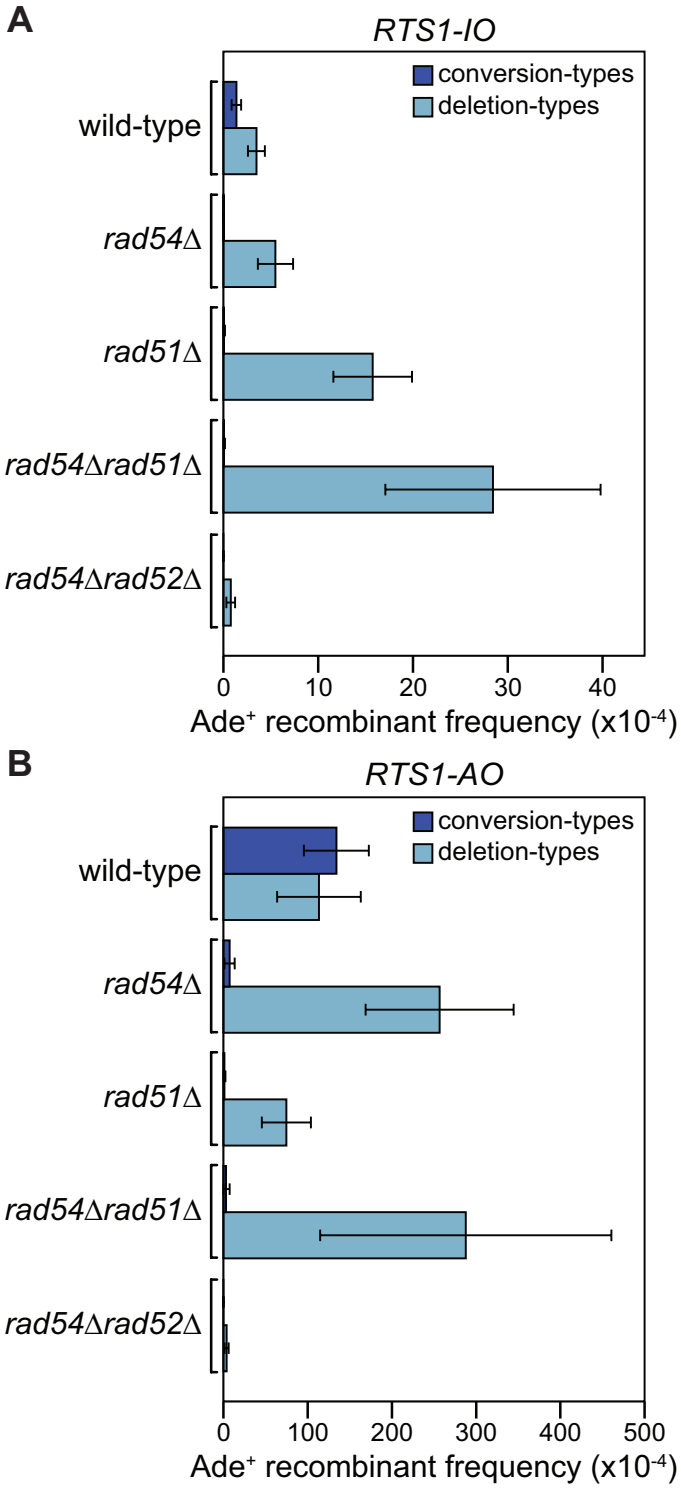


Figure 7.4 | Rad54 has a role in promoting gene conversions and preventing deletions during replication fork block-induced recombination. Bar chart showing the frequency of conversion- and deletion-type Ade$^+$ recombinants in wild-type, *rad54Δ*, *rad51Δ*, *rad54Δrad51Δ*, and *rad54Δrad52Δ* strains with either *RTS1-IO* (A) or *RTS1-AO* (B). Error bars represent ± one standard deviation. In order of presentation, the strains are MCW4712, MCW2651, MCW1691, MON138, MON315, MCW4713, MCW2656, MCW1692, MON140, and MON317.

suggests that Rad54 has a Rad51-independent role in limiting the formation of deletion-types, particularly at blocked forks.

7.2.5 Rad54's ATPase activity is essential in promoting gene conversions and some deletions during replication fork block-induced recombination

Rad54's dual role in modulating replication fork block-induced recombination may be dependent on its ATPase activities. To test this, Claire Bryer, a research technician in our laboratory, generated strains in which the endogenous *rad54* gene was replaced by a *rad54*^{K300A} allele. In this Rad54 mutant, the highly conserved lysine residue (lysine 300) in the Walker A ATPase domain is substituted with alanine. Based on work on the equivalent mutants in both budding yeast and mice, this Rad54 variant is expected to be defective in its interaction with ATP (Clever et al. 1999; Petukhova et al. 1999b; Agarwal et al. 2011). Indeed, similar to budding yeast, Claire found that strains with the *rad54*^{K300A} allele exhibited similar DNA damage sensitivity as strains with a *rad54* gene deletion (unpublished data). To determine whether Rad54's ATPase activity is critical to its role in promoting HR spontaneously and at blocked replication forks, I investigated the effect of *rad54*^{K300A} on the frequency of direct repeat recombination (Figure 7.5). Because this allele is linked to a *natMX4* marker, I also determined the effect of positioning the *natMX4* marker next to a wild-type copy of *rad54*$^{+}$. I found that the *rad54*$^{+}$*::natMX4* allele had a relatively minor effect on the total frequency of spontaneous and *RTS1*-induced *ade*$^{+}$ recombinants compared to

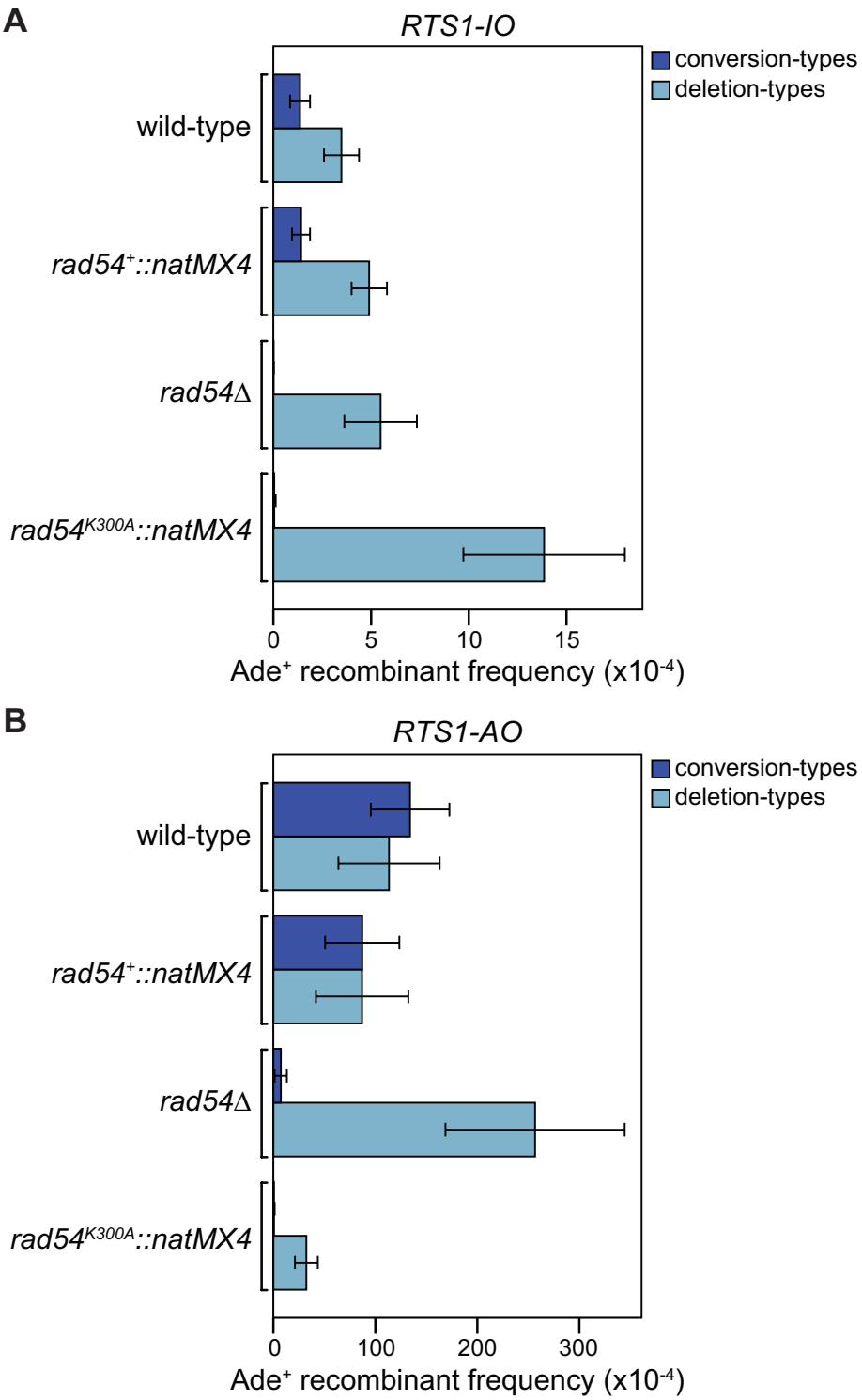


Figure 7.5 | Rad54's ATPase activity is essential in promoting gene conversions and some deletions during replication fork block-induced recombination. Bar chart showing the frequency of conversion- and deletion-type Ade$^+$ recombinants in wild-type, *rad54$^+$::natMX4, rad54Δ*, and *rad54^{K300A}::natMX4* strains with either *RTS1-IO* (A) or *RTS1-AO* (B). Error bars represent ± one standard deviation. In order of presentation, the strains are MCW4712, MCW7028, MCW2651, MCW7034, MCW4713, MCW7031, MCW2656, and MCW7037.

wild-type; however, this did not significantly affect the percentage of conversion-types in cells with either *RTS1-IO* or *RTS1-AO* (Figure 7.5). Similar to a *rad54* null mutant, *rad54*^{K300A} mutants cannot produce conversion-types regardless of *RTS1* orientation (Figure 7.5). In cells with *RTS1-IO*, *rad54*^{K300A} mutants exhibit an increase in the frequency of deletion-types compared to wild-type (P = < 0.001) (Figure 7.5A). This heightened deletion-type level is similar to that of *rad51Δ* and *rad55Δ* single mutants with *RTS1-IO* (refer to Table S1 in the appendix). At forks blocked at *RTS1*, the deletion-types in *rad54*^{K300A} mutants significantly decrease compared to wild-type (P = < 0.001) (Figure 7.5B). This is in contrast to the high levels found in a *rad54* null mutant. The relatively low frequency of deletion-types in *rad54*^{K300A} is similar to a *rad55Δ* single mutant (refer to Table S2 in the appendix). Altogether, these data indicate that Rad54's ATPase activity is critical for promoting Rad51-dependent recombination. They also indicate that Rad54's ATPase activity is not required for suppressing Rad52-dependent deletions. Similar to the Rad51 mediators (discussed in Chapter 6), Rad54's role in suppressing deletions may be through its ability to promote Rad51 nucleofilament formation, which occurs independently of its ATPase activity (Agarwal et al. 2011).

7.2.6 Fml1 and Rad54 have an additive effect in suppressing deletions during replication fork block-induced recombination

Having established that Fml1 and Rad54 suppress deletion-types at *RTS1-AO*, I also determined whether they worked in the same pathway to suppress

block-induced deletion-types. I found that *fml1Δrad54Δ* double mutants exhibited an additive increase in *RTS1*-induced deletion-types compared to *fml1Δ* and *rad54Δ* single mutants (both P = < 0.012), while it did not have a significant effect on spontaneous deletion-type formation compared to a *rad54Δ* single mutant (Figure 7.6). Because the loss of both Fml1 and Rad54 results in an additive effect at blocked replication forks, these data suggest that Fml1 and Rad54 may suppress deletions by distinct and independent mechanisms.

7.2.7 Investigating the consequence of fork merging during replication restart in Pfh1 mutants

Pfh1 mutants exhibit a hyperrecombinant phenotype that is largely dependent on Rad51 (Steinacher et al. 2012). Because Rad54 has a role in the turnover of Rad51, I wanted to see whether Rad51 loading at blocked replication forks could become toxic in a *rad54Δ* mutant during fork merging if the oncoming replisome lacked the sweepase function of Pfh1. As *pfh1* has an essential mitochondrial role in *S. pombe*, I used two different mutant alleles (*pfh1-m21* and *pfh1-mt**) where the Pfh1 protein is depleted in the nucleus but unaffected in the mitochondria (Pinter et al. 2008). The difference between *pfh1-m21* and *pfh1-mt** is that *pfh1-m21* has very low levels of residual nuclear Pfh1 whereas *pfh1-mt** has no nuclear Pfh1 (Pinter et al. 2008). To test whether Rad54 and Pfh1 have a genetic interaction, I tested the sensitivity of *rad51Δ*, *rad54Δ* and *pfh1* single and double mutants under a range of genotoxins, including CPT, HU, MMS, UV, and the microtubule-

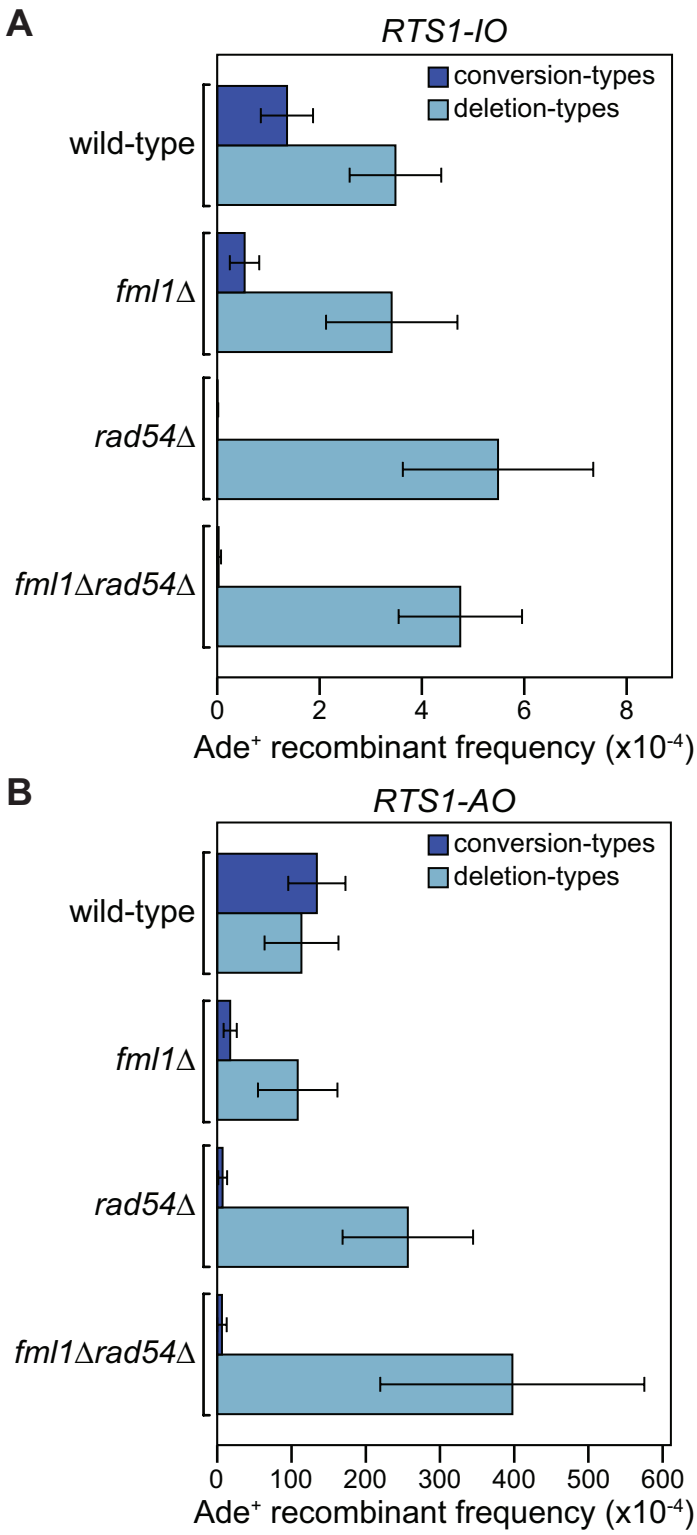


Figure 7.6 | Fml1 and Rad54 have an additive effect in suppressing deletions during replication fork block-induced recombination. Bar chart showing the frequency of conversion- and deletion-type Ade$^+$ recombinants in wild-type, *fml1Δ, rad54Δ*, and *fml1Δrad54Δ* strains with either *RTS1-IO* (A) or *RTS1-AO* (B). Error bars represent ± one standard deviation. In order of presentation, the strains are MCW4712, MCW3059, MCW2651, MCW7088, MCW4713, MCW3061, MCW2656, and MCW7091.

destabilizing drug thiabendazole (TBZ) (Figure 7.7 and 7.8). I found that when either *pfh1* mutant allele was combined with *rad54Δ*, the double mutant exhibited sensitivities to these genotoxins that were comparable to a *rad54Δ* single mutant. In contrast, when either of these *pfh1* mutants was combined with *rad51Δ*, they were more sensitive than either single mutant. These data suggest that the loss of Rad54 in a *pfh1* mutant does not lead to any further toxic intermediates that would cause viability issues, even when challenged with genotoxins that perturb replication. On the other hand, the synergistic increase in hypersensitivity to genotoxins in a *rad51Δpfh1* double mutant indicates that Pfh1 and Rad51 can promote DNA repair/damage tolerance via alternative pathways. Most likely these are Rad51-mediated replication restart and/or lesion bypass and Pfh1-mediated removal of RFBs, i.e. in the absence of barrier removal, there would be a greater requirement for RDR.

7.2.8 The hyperrecombination at forks blocked at *RTS1* in the absence of Pfh1 is partly dependent on Rad54

To further test the idea that the absence of both Rad54 and Pfh1 could lead to pathological fork merging at a restarted fork, I assessed the direct repeat recombinant frequencies in *rad54Δ* mutants combined with either of the two *pfh1* mutant alleles (Figure 7.9). Our laboratory previously reported that the *pfh1-mt** mutant exhibited hyperrecombinant levels spontaneously and at forks blocked at *RTS1* (an *ade*$^{+}$ recombinant frequency of ~ 6 x 10^{-4} and ~ 2000 x 10^{-4}, respectively) (Steinacher et al. 2012). Instead of causing a further increase in recombinants, however, deletion of *rad54Δ* in either *pfh1* mutants

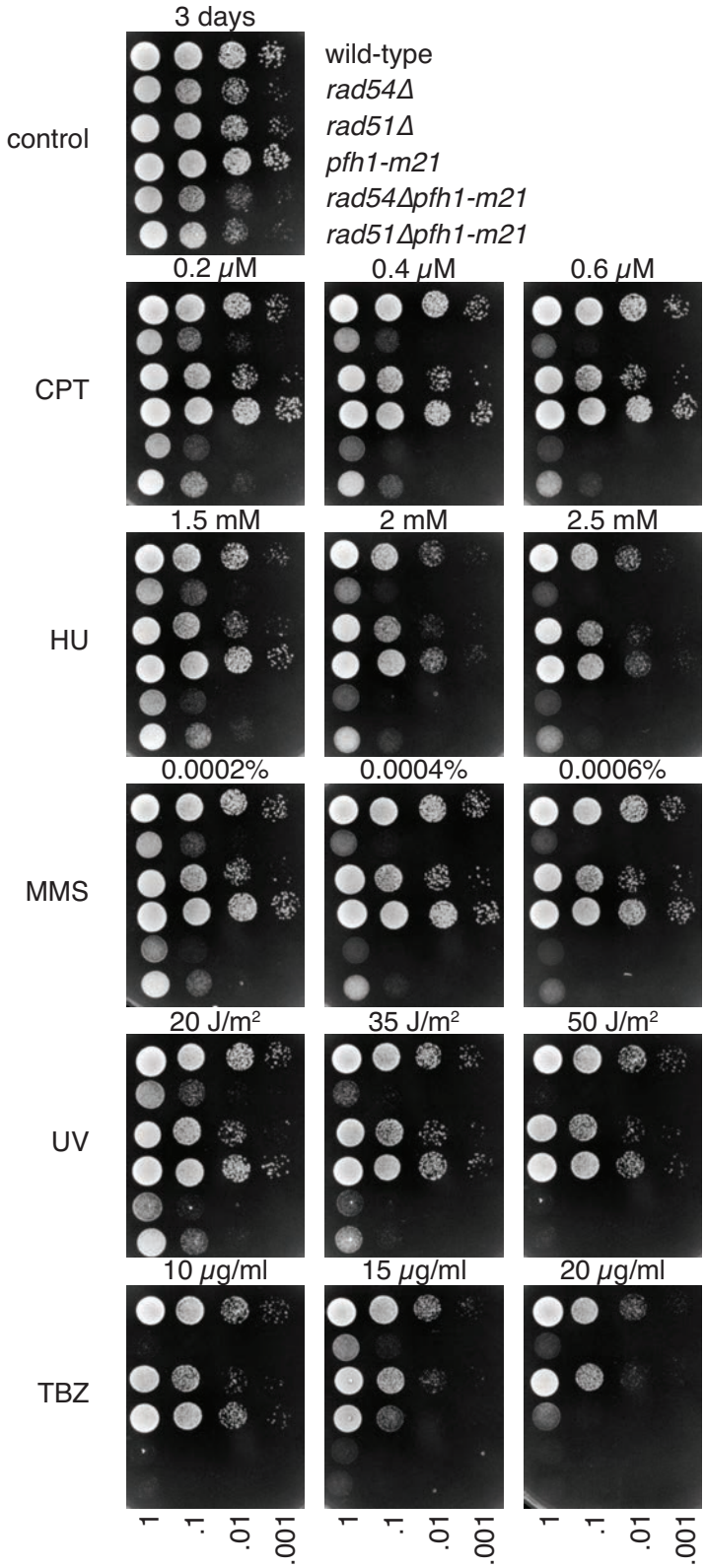


Figure 7.7 | Loss of Rad51 in *pfh1-m21* cells leads to increased genotoxin sensitivity. Spot assays comparing the sensitivity of wild-type (MCW1221), *rad54Δ* (MCW1230), *rad51Δ* (MCW1088), *pfh1-m21* (MCW4859), *rad54Δpfh1-m21* (MCW6448), and *rad51Δpfh1-m21* (MCW5277) to different genotoxins. Strains were grown on complete media for 3 days at 30°C before being photographed.

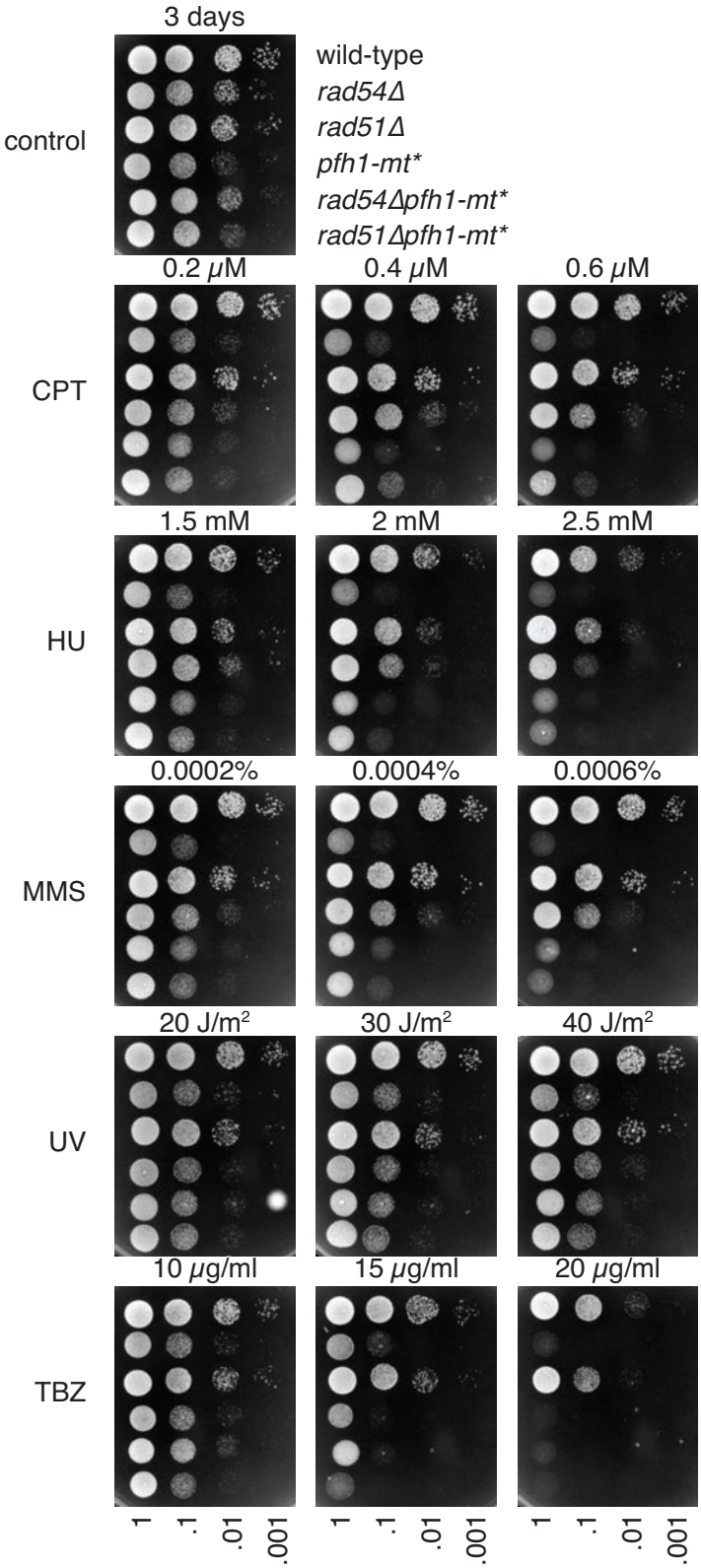


Figure 7.8 | Loss of Rad51 in *pfh1-mt cells does leads to increased genotoxin sensitivity**. Spot assays comparing the sensitivity of wild-type (MCW1221), *rad54Δ* (MCW1230), *rad51Δ* (MCW1088), *pfh1-mt** (MCW4861), *rad54Δpfh1-mt** (MCW6545), and *rad51Δpfh1-mt** (MCW5281) to different genotoxins. Strains were grown on complete media for 3 days at 30°C before being photographed.

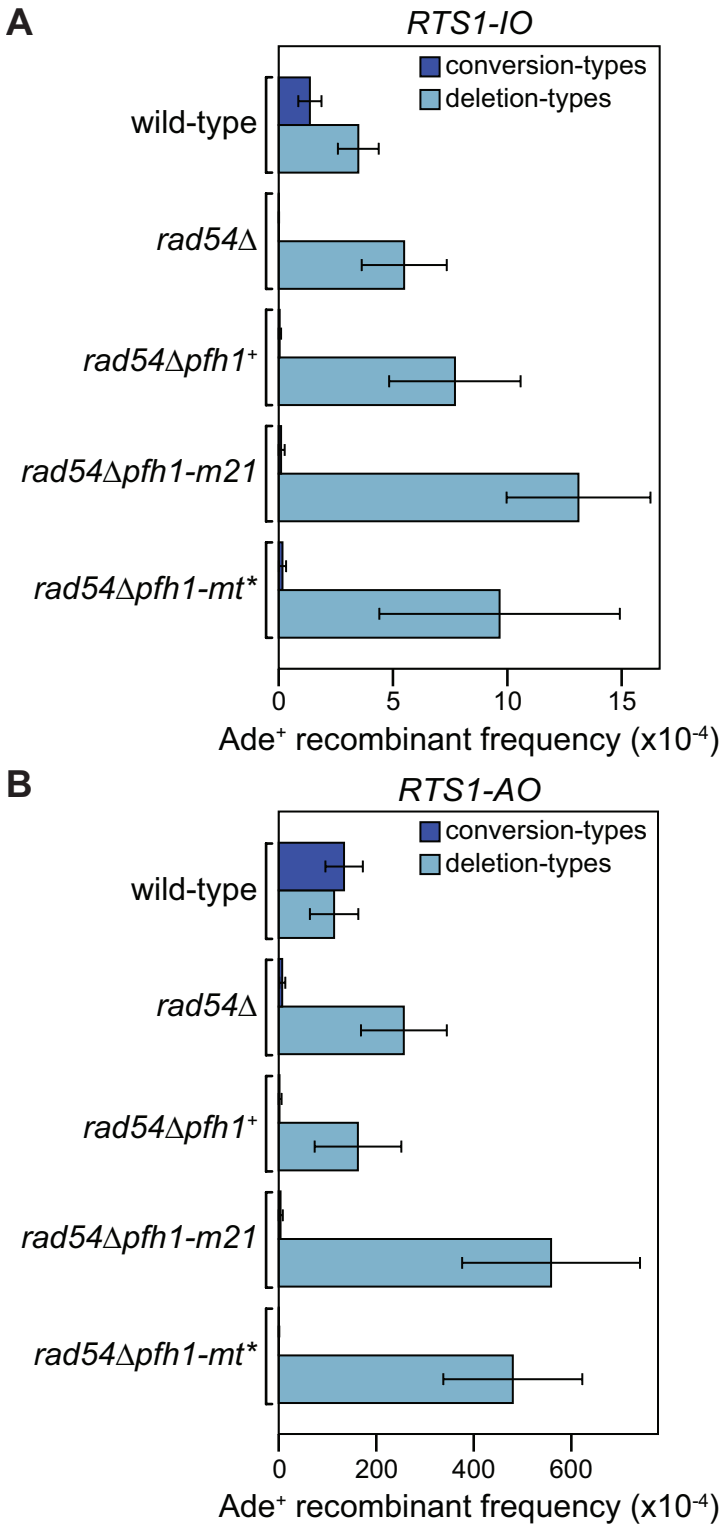


Figure 7.9 | The hyperrecombination at forks blocked at *RTS1* in the absence of Pfh1 is partly dependent on Rad54. Bar chart showing the frequency of conversion- and deletion-type Ade$^+$ recombinants in wild-type, *rad54Δ*, *rad54Δpfh1$^+$*, *rad54Δpfh1-m21*, *rad54Δphf1-mt** strains with either *RTS1-IO* (A) or *RTS1-AO* (B). Error bars represent ± one standard deviation. In order of presentation, the strains are MCW4712, MCW2651, MCW6540, MCW6446, MCW6543, MCW4713, MCW2656, MCW6541, MCW6447, and MCW6544.

leads to a reduction in *RTS1*-induced recombinant frequency (Figure 7.9B). These levels are comparable to *RTS1-AO rad51Δ pfh1-mt** double mutants (Steinacher et al. 2012). These data suggest that the high levels of recombinants in *pfh1* mutant strains are partly dependent on Rad54. Therefore, instead of creating a situation where the Rad51 nucleoprotein filament may have caused a problematic situation during fork convergence in the absence of Pfh1, the loss of Rad54 may have alleviated some of these potential problems as it has an early role in promoting the loading of the Rad51 nucleoprotein filament.

7.3 Discussion

7.3.1 Fml1 and Rad54's role in modulating recombination at blocked replication forks

In this chapter, I showed that both Fml1 and Rad54 have dual roles in promoting Rad51-dependent conversions-types and suppressing Rad52-dependent deletion-types at blocked replication forks. Both Fml1 and Rad54 are dependent on their ATPase activities in promoting their roles in HR (Petukhova et al. 1998; Bugreev et al. 2006; Bugreev et al. 2007; Nandi and Whitby 2012). Interestingly, however, mutations that impair the ATPase activity of Fml1 and Rad54 reveal a key difference between the functions of these proteins at blocked replication forks. Our laboratory previously reported that ATPase mutants of *fml1* exhibit similar frequencies of conversion- and deletion-types at *RTS1-AO* as a *fml1* deletion (Nandi and Whitby 2012). In contrast, I showed that while *rad54*^{K300A} and *rad54Δ* mutants both produce

essentially zero conversion-types, the frequency of deletion-types in a *rad54*^{K300A} mutant is significantly lower than that of a *rad54Δ* mutant (~ 8-fold). Taken together, this suggests that whereas Fml1's ATPase activity is essential in Fml1's role in suppressing deletions, Rad54's role in suppressing deletion-types is not completely dependent on its ATPase activity.

Furthermore, as the *fml1Δrad54Δ* double mutant has an additive effect on deletion-type formation compared to its single mutants, Fml1 and Rad54 may be acting differently in preventing Rad52-dependent deletions. Besides aiding in the loading of Rad51, it is currently unclear how Rad54 could additionally prevent the high frequency of *RTS1*-induced deletions that are seen in a *rad54Δ* mutant, which is ~ 3.5-fold higher than in a *rad51Δ* mutant, in a manner that does not depend on its ATPase activity. Further work is needed to uncover this function. On the other hand, Fml1's suppression of deletions may relate to its ability to promote branch migration, which could be used to reset regressed forks in addition to stimulating their regression. This may be critical during fork convergence as the positive supercoiling in DNA ahead of a converging fork may drive fork regression of the opposing fork (Postow et al. 2001). In the presence of Fml1, the chicken foot structure at the stalled fork that is created by the oncoming fork may be reset by Fml1 to promote fork termination (Figure 7.10A). In the absence of Fml1, however, the regressed fork could give rise to free single stranded DNA at which RPA, and subsequently Rad52, could load (Figure 7.10B). Rad52's presence could then catalyze strand annealing between homologous sequences that could lead

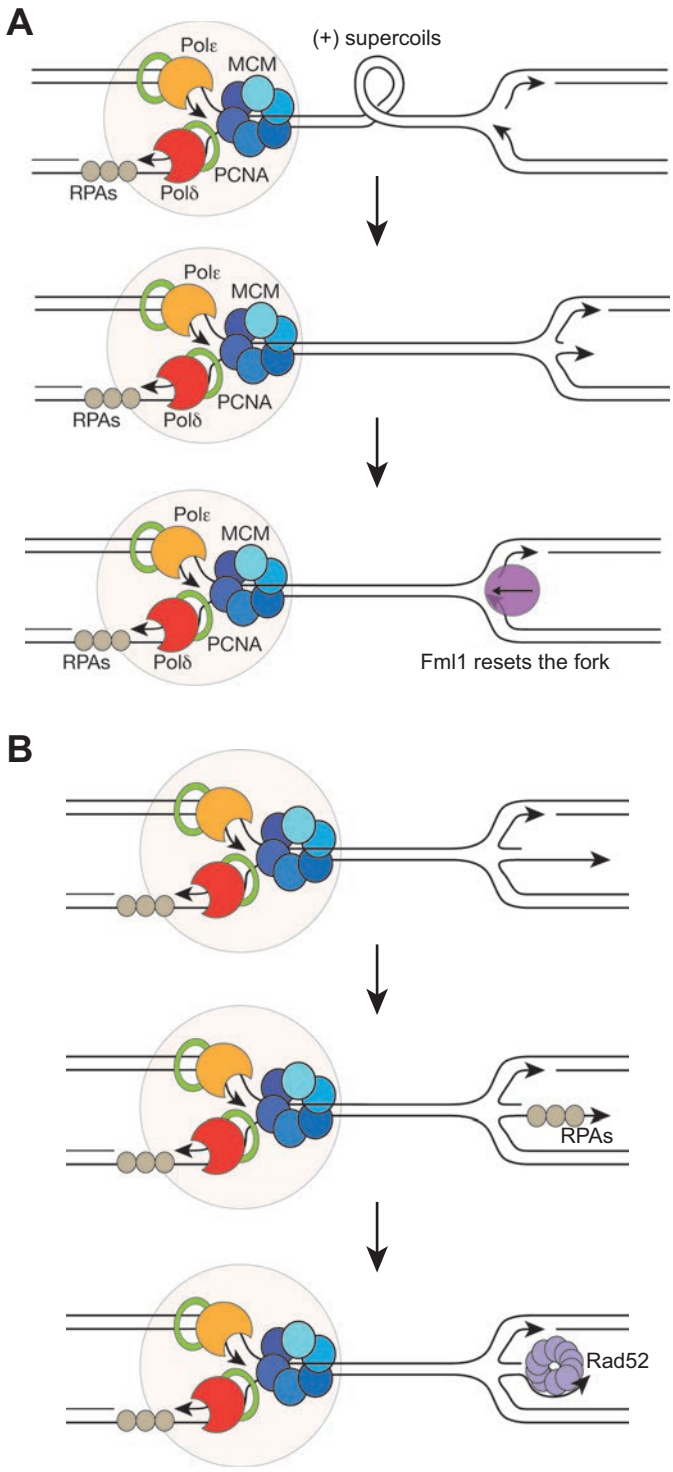


Figure 7.10 | Hypothetical model for Fml1's involvement in fork merging. Model depicting fork merging between an oncoming fork and an arrested fork. (A) As the oncoming fork progresses, positive supercoiling builds in front of the fork, which can reverse a collapsed fork. Fml1 may reset the reversed fork to promote merging with the oncoming fork. (B) In the absence of Fml1, RPA and subsequently, Rad52 can be loaded at the reversed fork. Rad52 can then promote SSA between homologous sequences during fork merging as depicted in Figure 3.10.

to deletion-type formation during fork termination as previously depicted in Figure 3.10. In this model, fork termination could become problematic if the fork is not reset and/or if Rad52 does not promote strand annealing between the two converging forks to complete fork termination. In this case, if the oncoming fork is not stopped, it may continue to approach the stalled fork and drive the regression of the stalled fork further behind the site where it arrested such that the oncoming fork re-replicates some of the already replicated DNA and the two forks do not properly fuse. This would generate a local aberrant replication structure that would then need to be resolved, presumably through the aid of endonucleases and exonucleases. To prevent these instances of over-replication, there must be factors that promote the orderly fusion between a converging fork and a stalled fork. In their absence, situations that lead to pathological fork merging events such as these could potentially explain the longer Rad52-*lacO*-LacI co-localizations that are seen in *RTS1-AO fml1Δ* mutants compared to wild-type. Interestingly, deletion of *fml1* leads to an increase in the average number of time points that cells exhibit a Rad52-YFP focus, irrespective of its co-localization, in both *RTS1* orientations compared to wild-type (both $P = < 0.001$) (Figure S7.2). This could suggest that Fml1 may have a global role in promoting fork termination and suppressing Rad52-dependent deletions. This is reminiscent of a recent finding that the RecG DNA translocase may similarly prevent over-replication when replication forks collide during fork convergence in *E. coli* (Rudolph et al. 2013).

7.3.2 Fork convergence at *RTS1* in *pfh1* mutants

In the last part of this chapter, I wanted to explore whether fork merging in the absence of the Pfh1 sweepase could be problematic, particularly when the turnover of the Rad51 protein that is loaded at the stalled fork is impaired by the loss of Rad54. However, I found that strains with deletion of *rad54* in combination with either *pfh1-m21* or *pfh1-mt** alleles did not exhibit any elevated level of sensitivity compared to a *rad54Δ* single mutant when challenged with various genotoxins. Furthermore, I found that the hyperrecombinant phenotype of the *pfh1* mutants is partially suppressed by *rad54* deletion. The latter result is similar to how deletion of *rad51* suppresses the hyperrecombinant phenotype of *RTS1-AO pfh1-mt** mutants (Steinacher et al. 2012). The results in this chapter suggest that in the absence of Rad54, Rad51 may not be loaded at blocked replication forks to the same extent as wild-type. Thus, deletion of *rad54* may have had the opposite effect of what I had predicted. Instead of deleting *rad54*, a better strategy may be to use the $rad54^{K300A}$ allele. This is because the low frequency of *RTS1*-induced deletion-types in a $rad54^{K300A}$ mutant, which is a similar level to a *rad55Δ* mutant, suggests that Rad51 loading may not be impaired in a $rad54^{K300A}$ mutant. If this is the case, then to investigate the potential pathological consequences of fork convergence at a restarted fork in a *pfh1* mutant, strains with both $rad54^{K300A}$ and *pfh1* mutant alleles should be studied. Our laboratory is currently pursuing this option.

Chapter 8

Importance of the Cds1 Checkpoint Kinase in Processing the Fork at *RTS1*

8.1 Introduction

DNA replication checkpoint kinases, such as Rad53 in *S. cerevisiae* and Cds1 in *S. pombe*, play a key role in the maintenance of replication fork stability, particularly by preventing replisomes from dissociating from stalled replication forks (Lopes et al. 2001; Tercero and Diffley 2001; Cobb et al. 2003; Meister et al. 2005; Trenz et al. 2006; Ragland et al. 2013). Cds1 also has a role in regulating various substrates through its forkhead-associated (FHA) domain. This includes Mus81, a subunit of the Mus81-Eme1 structure-specific endonuclease that is able to cleave model replication forks and recombination intermediates, such as D-loops and HJs *in vitro* (Boddy et al. 2000; Osman and Whitby 2007). Following replication perturbation, Cds1 negatively regulates Mus81's nuclease activity by phosphorylating it to reduce its binding to chromatin (Boddy et al. 2000; Kai et al. 2005; Froget et al. 2008). Thus, Mus81's role in fork cleavage *in vivo* may represent an alternative pathway for RDR. In this chapter, I investigate how the loss of Cds1 influences RDR at replication forks blocked at *RTS1* to examine whether Cds1 constrains recombination from occurring earlier in the cell cycle following fork blockage by regulating fork integrity and actively preventing Mus81 from cleaving the fork.

8.2 Results

8.2.1 Cds1 has a role in suppressing recombination at *RTS1*

To determine the role of Cds1 in spontaneous and *RTS1*-induced recombination, I assessed the effect of *cds1Δ* on the frequency of direct

repeat recombination. Deletion of *cds1* lead to a ~ 2.5-fold increase in the frequency of both spontaneous conversion- and deletion-types compared to wild-type (both P = < 0.001) (Figure 8.1A). In contrast, *cds1Δ* mutants had an even greater effect on the frequency of deletion-types (~ 7.2-fold increase compared to wild-type) than the frequency of conversion-types (~ 2.3-fold increase compared to wild-type) when replication forks are blocked at *RTS1* (both P = < 0.001) (Figure 8.1B). To see whether the hyperrecombination in *cds1Δ* mutants was related to the loss of Cds1's negative regulation of Mus81, I tested recombinant formation in *cds1Δmus81Δ* mutants. I found that deleting *mus81* in *cds1Δ* mutants suppresses most of the hyperrecombination that occurs spontaneously and at forks blocked at *RTS1* (all P = < 0.004) (Figure 8.1). Similarly, deleting *rad51* in *cds1Δ* mutants also suppresses the hyperrecombination at forks blocked at *RTS1* (both P = < 0.001) while additionally eliminating all conversion-type formation (Figure 8.1B). The *cds1Δmus81Δrad51Δ* triple mutant is epistatic to *cds1Δrad51Δ* in recombinant formation (Figure 8.1). Interestingly, deleting *cds1* in a *rad51Δ* single mutant or a *mus81Δrad51Δ* double mutant increases the frequency of deletion-types in both spontaneous and *RTS1*-induced recombination (all P = < 0.001). Taken together, these data suggest that Cds1 has a role in suppressing Mus81-dependent recombination at spontaneous lesions and at blocked replication forks, presumably through its function in preventing Mus81's association to chromatin to preclude it from aberrantly cleaving DNA. Additionally, these data suggest that Cds1 also has a function in suppressing Mus81- and Rad51-independent deletions at spontaneous lesions and at

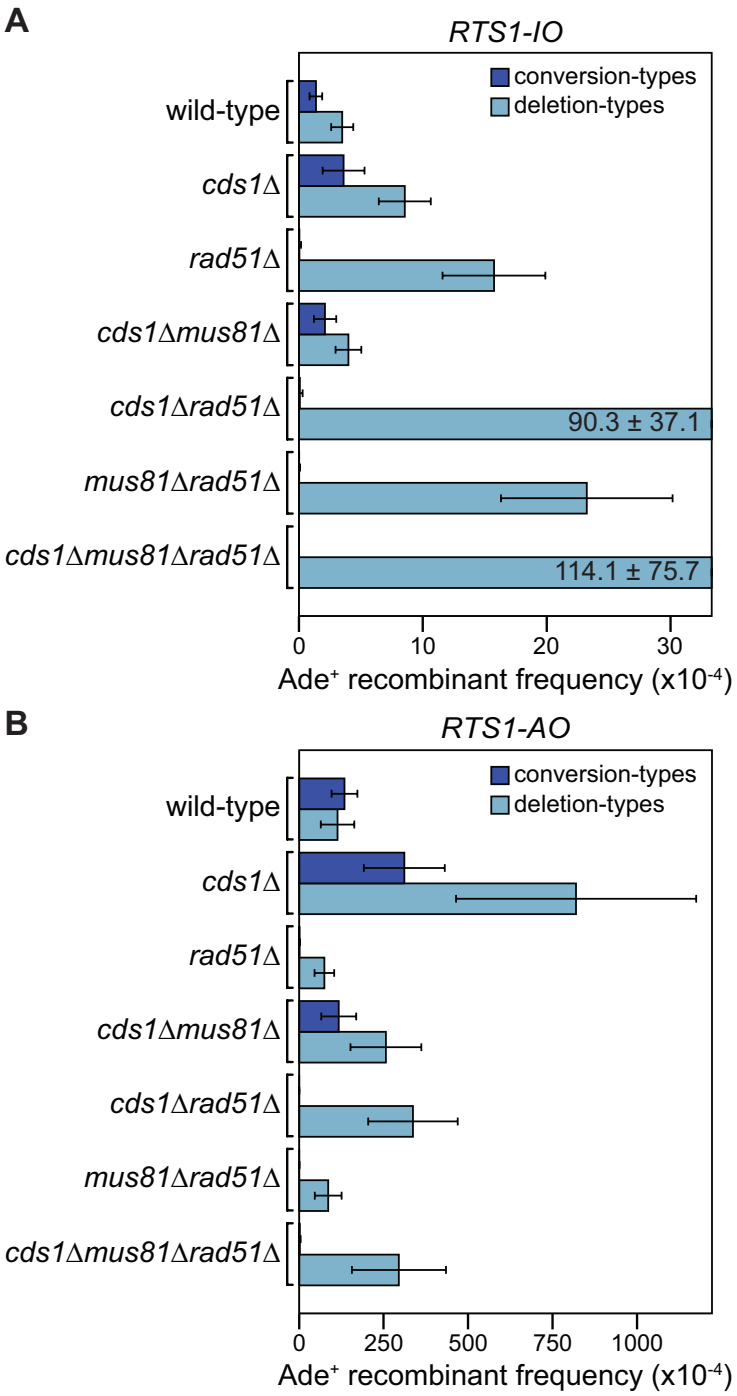


Figure 8.1 | Cds1 has a role in suppressing Mus81-dependent recombination at *RTS1*. Bar chart showing the frequency of conversion- and deletion-type Ade$^+$ recombinants in wild-type, *cds1Δ, rad51Δ*, *cds1Δmus81Δ*, *cds1Δrad51Δ*, *mus81Δrad51Δ*, and *cds1Δmus81Δrad51Δ* strains with either *RTS1-IO* (A) or *RTS1-AO* (B). Error bars represent ± one standard deviation. In order of presentation, the strains are MCW4712, MCW2220, MCW1691, MCW2906, MCW3374, MCW3376, MCW3377, MCW4713, MCW2222, MCW1692, MCW2910, MCW3379, MCW3380, and MCW3381. The recombination assay values presented in this chart and the remaining charts in this chapter are also listed in Tables S1 and S2 with statistical analysis in the appendix.

blocked replication forks. This may be related to Cds1's role in regulating the disassembly of replisomes to prevent pathological DNA structures, which may be inappropriately processed and/or cause problems during fork merging.

8.2.2 Mus81-dependent replication fork block-induced recombination is prevented by Cds1

To see whether Mus81 may promote unscheduled DNA breaks at blocked replication forks when its interaction with Cds1 is disrupted, I examined the effect of *mus81*^{T239A} on direct repeat recombination. *Mus81*^{T239A} mutants harbor a mutation in the Mus81 FHA-binding motif that eliminates its Cds1-binding and Cds1-dependent phosphorylation such that Mus81 remains associated with the chromatin following replication perturbation (Boddy et al. 2000; Kai et al. 2005; Froget et al. 2008). Intriguingly, the *mus81*^{T239A} mutant exhibits a small increase in the frequency of conversion- and deletion-types at replication forks blocked at *RTS1* compared to wild-type (both $P = < 0.01$) (Figure 8.2). However, the conversion- and deletion-type frequency is not as elevated as a *cds1Δ* mutant (both $P = < 0.001$), nor does it account for the amount of Mus81-dependent recombination found in a *cds1Δ* mutant. This suggests that in the presence of Cds1, Mus81 is largely occluded from accessing the fork, presumably due to how Cds1 may protect the fork and regulate replisome dissociation, rather than by phosphorylation of T239.

8.2.3 Cds1 limits deletions independently of Fml1 at *RTS1-AO*

In Chapter 7, I showed that Fml1 plays a role in suppressing Rad52-

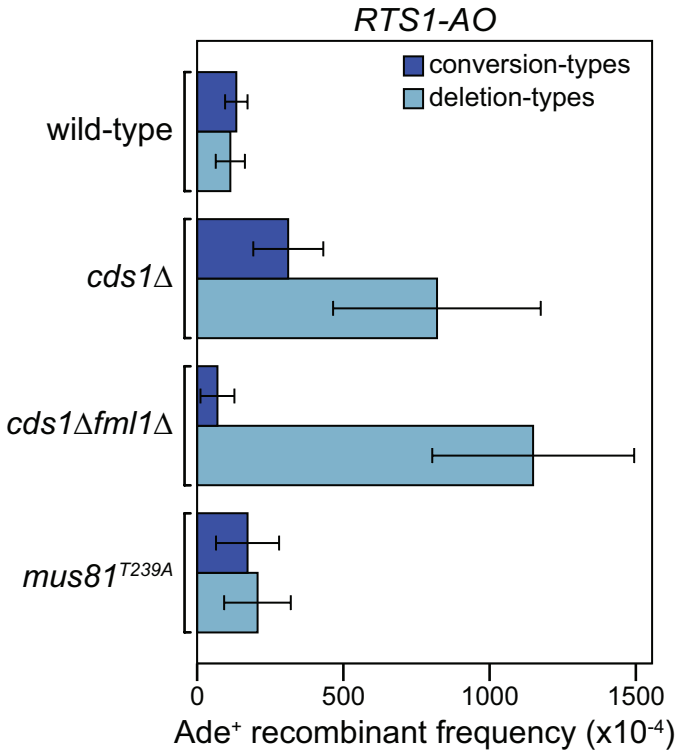


Figure 8.2 | Cds1 prevents Mus81-dependent replication fork block-induced recombination and limits deletions independently of Fml1. Bar chart showing the frequency of conversion- and deletion-type Ade$^+$ recombinants in wild-type, *cds1Δ, cds1Δfml1Δ*, and *mus81*^{T239A} strains with either *RTS1-IO* (A) or *RTS1-AO* (B). Error bars represent ± one standard deviation. In order of presentation, the strains are MCW4713, MCW2222, MCW6443, and MCW3329.

dependent deletions. To determine whether this activity is part of a Cds1-dependent pathway, I determined recombinant frequency in a *cds1Δfml1Δ RTS1-AO* strain. I found that while the frequency of conversion-types decreased, the frequency of deletion-types increased relative to either *fml1Δ* or *cds1Δ* single mutants (both P = < 0.011) (Figure 8.2). This suggests that Fml1 has a role that is independent of Cds1 in limiting the formation of deletions.

8.2.4 Rad52-YFP foci persists longer at *RTS1-AO* in *cds1Δ* and *mus81Δ* mutants

Having established that Cds1 has a role in limiting direct repeat recombination at *RTS1-AO*, I also examined Rad52-YFP kinetics in *cds1Δ* and *mus81Δ* single and double mutants (Figure S8.1 – S8.3). Surprisingly, I determined that Rad52-YFP foci, on average, persist longer at *RTS1-AO* in *cds1Δ* mutants compared to wild-type (P = < 0.001) (Figure 8.3). Furthermore, the increased length of Rad52-*lacO*-LacI co-localization in a *cds1Δ* mutant is not suppressed by deleting *mus81* (Figure 8.3). This suggests that Cds1 has a role in clearing Rad52 in a manner that does not depend on Mus81. However, I also found that *mus81Δ* single mutants also exhibit an increase in the length of Rad52-*lacO*-LacI co-localization (Figure 8.3). This suggests that Mus81 also has a role in promoting the displacement of Rad52 from the *RTS1* RFB. How Cds1 and Mus81 do this is unclear and will require further investigation to determine.

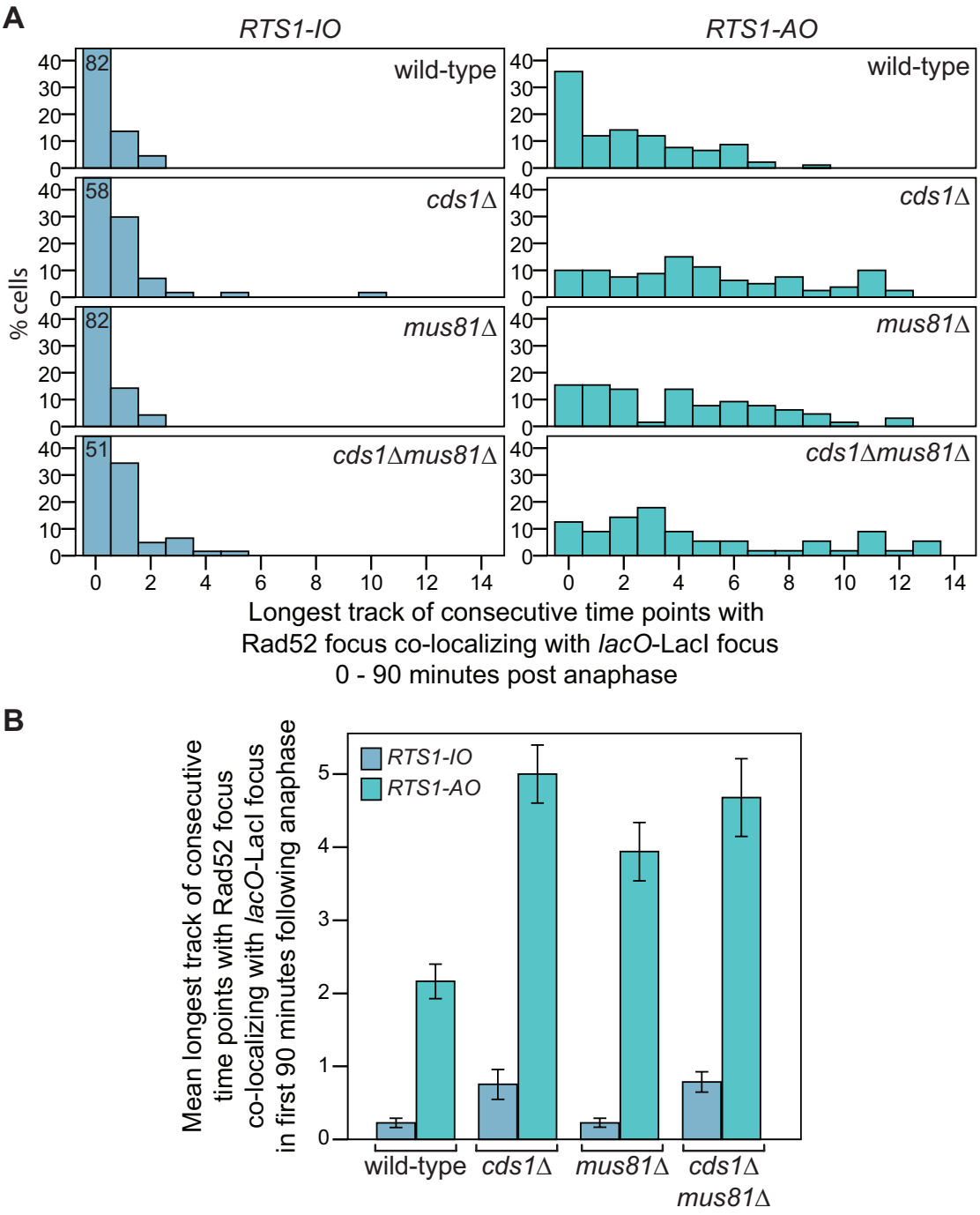


Figure 8.3 | Rad52-YFP foci persist longer at *RTS1-AO* in *cds1Δ* and *mus81Δ* mutants. (A) Histogram showing the percentage of cells with a given number of uninterrupted time points in which a Rad52-YFP focus co-localizes with a *lacO*-LacI focus within the first 90 minutes following anaphase. (B) Bar chart of the mean number of uninterrupted time points cells display a Rad52-YFP focus that co-localizes with a *lacO*-LacI focus during the first 90 minutes following anaphase. Error bars represent ± one standard error of the mean. The *RTS1-IO* strains are MON110 (wild-type), MON190 (*cds1Δ*), MON307 (*mus81Δ*), and MON198 (*cds1Δmus81Δ*). The *RTS1-AO* strains are MON148 (wild-type), MON196 (*cds1Δ*), MON309 (*mus81Δ*), and MON202 (*cds1Δmus81Δ*).

8.2.5 Timing of Rad52-YFP focus formation at *RTS1-AO* is not significantly changed in the absence of Cds1 or Mus81

In the absence of Cds1, the replication fork may not be protected following its blockage at *RTS1*, which may allow recombinases to access it immediately following a deregulated collapse of the replisome. To see whether Rad52 may be recruited to forks earlier, I assessed the timing at which Rad52 foci formed at *RTS1-AO* in *cds1Δ* and *mus81Δ* single and double mutants (Figure 8.4). However, I found that there is no significant change in the mean time for when Rad52 foci appear at *RTS1-AO* in *cds1Δ* or *mus81Δ* single mutants compared to wild-type (Figure 8.4B). In contrast, the *cds1Δmus81Δ* double mutant appears to have earlier Rad52 recruitment to *RTS1* than wild-type ($P = 0.003$). However, this result is likely affected by chance co-localization events that occur as a result of the significant increase in overall Rad52 foci in the first 90 minutes post anaphase in *cds1Δmus81Δ* double mutants compared to either of its single mutants (both $P = < 0.001$) (Figure S8.4). Excluding this result, these data indicate that the loss of Cds1 or Mus81 does not significantly change the timing of Rad52 recruitment to forks blocked at *RTS1*. This supports the idea that RDR is initiated within a few minutes of fork blockage in either the presence or absence of the Cds1 checkpoint kinase.

8.2.6 Detecting breaks at *RTS1-AO* in a *cds1Δ* mutant

To determine whether blocked replication forks might be more susceptible to being cleaved by Mus81 in the absence of Cds1, I attempted to detect one-sided DSBs at the *RTS1* RFB in *cds1Δ* strains. I prepared genomic DNA from

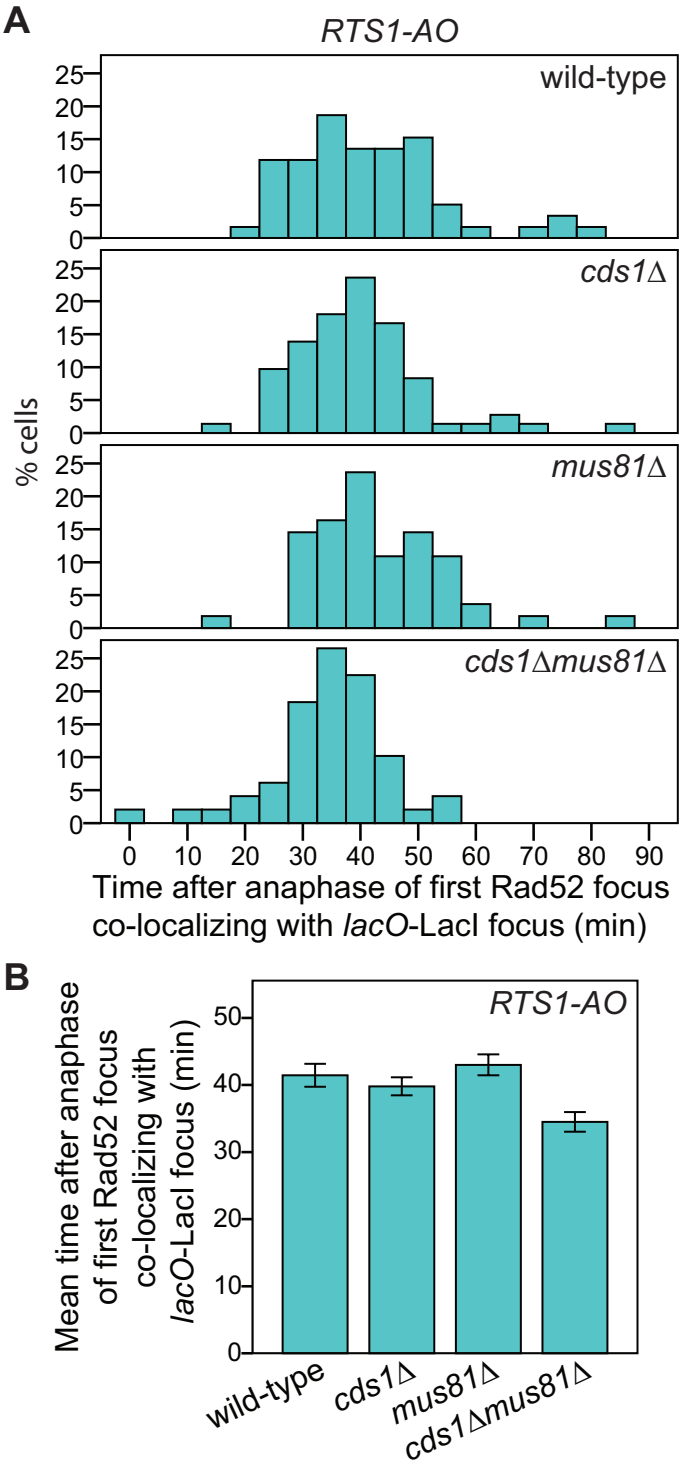


Figure 8.4 | Rad52 recruitment to forks blocked at *RTS1-AO* is not significantly changed in the absence of *cds1* or *mus81*. (A) Histogram showing the percentage of cells at a given time after anaphase in which the first Rad52-YFP focus co-localizes with a *lacO*-LacI focus. (B) Bar chart of the mean time after anaphase of when the first Rad52-YFP focus co-localizes with a *lacO*-LacI focus. Error bars represent ± one standard error of the mean. The *RTS1-IO* strains are MON110 (wild-type), MON190 (*cds1Δ*), MON307 (*mus81Δ*), and MON198 (*cds1Δmus81Δ*). The *RTS1-AO* strains are MON148 (wild-type), MON196 (*cds1Δ*), MON309 (*mus81*Δ), and MON202 (*cds1Δmus81Δ*).

wild-type and *cds1Δ RTS1-AO* strains that I digested with PstI, separated on a 1-D gel, and analyzed by Southern blotting using radiolabelled probes A and B (Figure 8.5). Probes A and B are specific to regions that flank *RTS1* (Figure 8.5A). Both probes detect the full length PstI fragment (~ 9.2 kb) from wild-type and *cds1Δ* DNA (Figure 8.5B). However, there is no clear detection of a one-sided or two-sided DSB. In the case of a one-sided DSB that is mapped at *RTS1*, there should be a band at ~ 7.6 kb that would be detected by probe B (Ahn et al. 2005). If there was a two-sided DSB, then a ~ 2 kb band would be detected by probe A. Although these data fail to detect DSBs in *cds1Δ* strains, this does not rule out the idea that there is increased breakage of replication forks in the absence of Cds1. This is because these intermediates may be short lived and quickly processed by resection proteins. Furthermore, the fork may be blocked at different points, which may lead to different breakage sites. Thus, further investigation is needed to establish that DSBs may be formed at or near *RTS1* in the replicated arms of the blocked replication fork in the absence of Cds1.

8.2.7 Mus81 resolves toxic intermediates in cells treated with hydroxyurea in the absence of Cds1

Lastly, having seen that there is a significant increase in the amount of spontaneous Rad52 foci in *cds1Δmus81Δ* mutants compared to either of its single mutants, I also investigated whether Mus81 could become required in resolving toxic intermediates that accumulate in a *cds1Δ* mutant. I tested the sensitivity of *cds1Δ*, *mus81Δ*, and *cds1Δmus81Δ* mutants to a range of

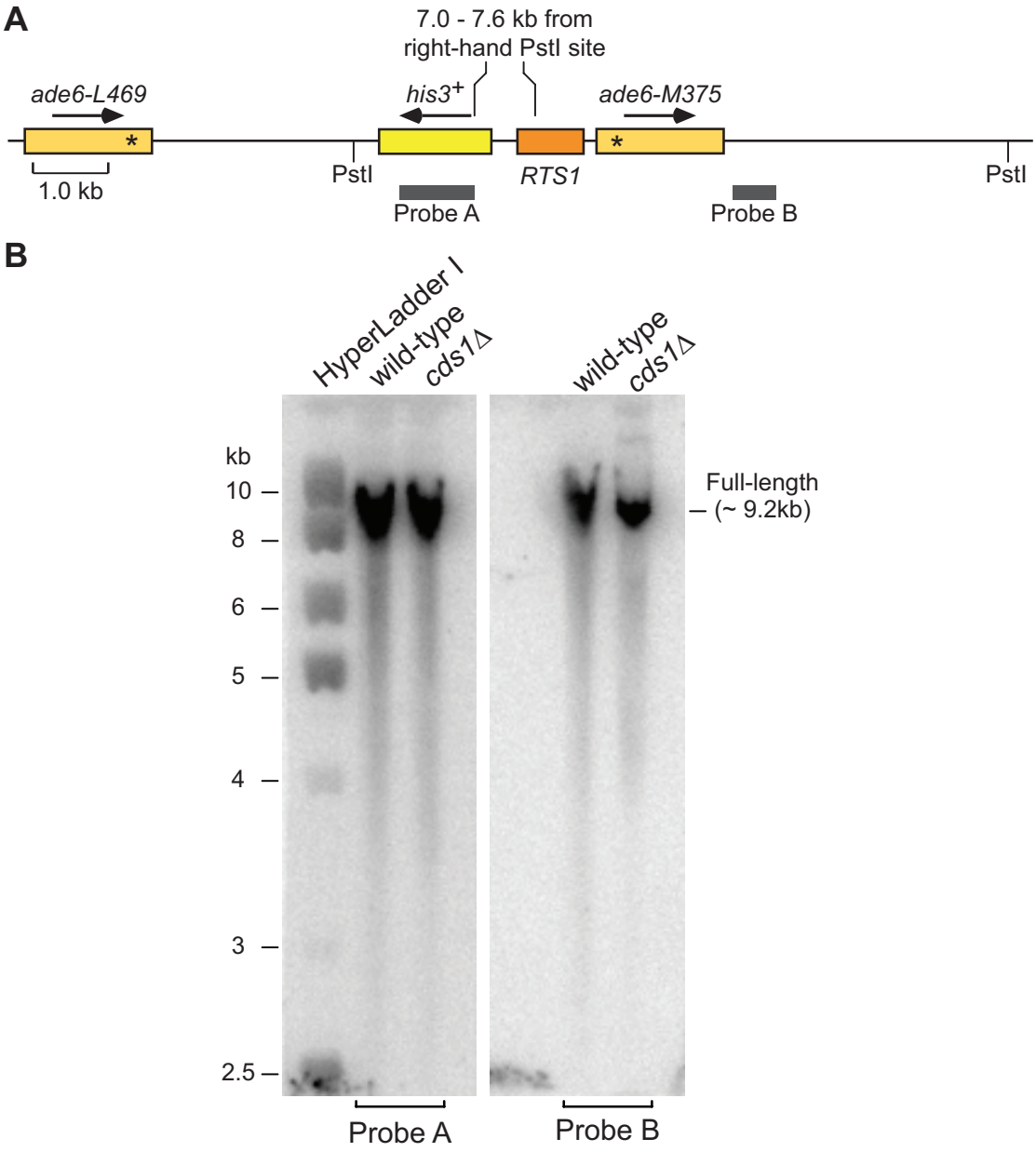


Figure 8.5 | Breaks at *RTS1* are not detectable in a *cds1Δ* mutant. (A) Schematic of the recombination substrate showing the position of PstI sites and DNA probes. The region between 7 and 7.6 kb from the right-hand PstI site, in which the DSB maps, is also marked. (B) Analysis of genomic DNA, prepared in agarose plugs and restricted with PstI, on a 1-D gel using radiolabelled probe A or B as indicated. The *RTS1-AO* strains are MCW4713 (wild-type) and MCW2222 (*cds1Δ*).

genotoxins (Figure 8.6). I found that the sensitivity of the *cds1Δmus81Δ* mutant is epistatic to the sensitivity of the *mus81Δ* mutant in repairing CPT-, MMS-, and UV-induced lesions. This is likely due to there already being a requirement for Mus81 in repairing these lesions, particularly in the case of MMS-induced lesions where *mus81Δ* single mutants are clearly hypersensitive compared to wild-type. However, I also found that the *cds1Δmus81Δ* double mutant is more sensitive than either of its single mutants when challenged with HU. This suggests that in the absence of Cds1, there is a requirement of Mus81 in promoting an alternative pathway to dealing with chronic exposure to HU. In the presence of Cds1, however, the cell may rely on Mus81-independent pathways for overcoming HU-induced lesions.

8.3 Discussion

In this chapter, I have demonstrated that the loss of Cds1 leads to an increase in recombinant frequency at both spontaneous lesions and blocked replication forks. This hyperrecombination is partly dependent on Mus81. I also showed, however, that the mutant form of Mus81, which does not get phosphorylated by Cds1 in response to replication perturbation, induces a relatively minor increase in recombinant formation compared to the high levels of hyperrecombination in a *cds1Δ* mutant. These findings are similar to another study that showed that in the absence of Cds1, Mus81 induces DNA breaks in cells treated with HU, but that HU-induced DNA breaks are not found in *mus81*^{T239A} mutants in the presence of Cds1 (Froget et al. 2008). Taken

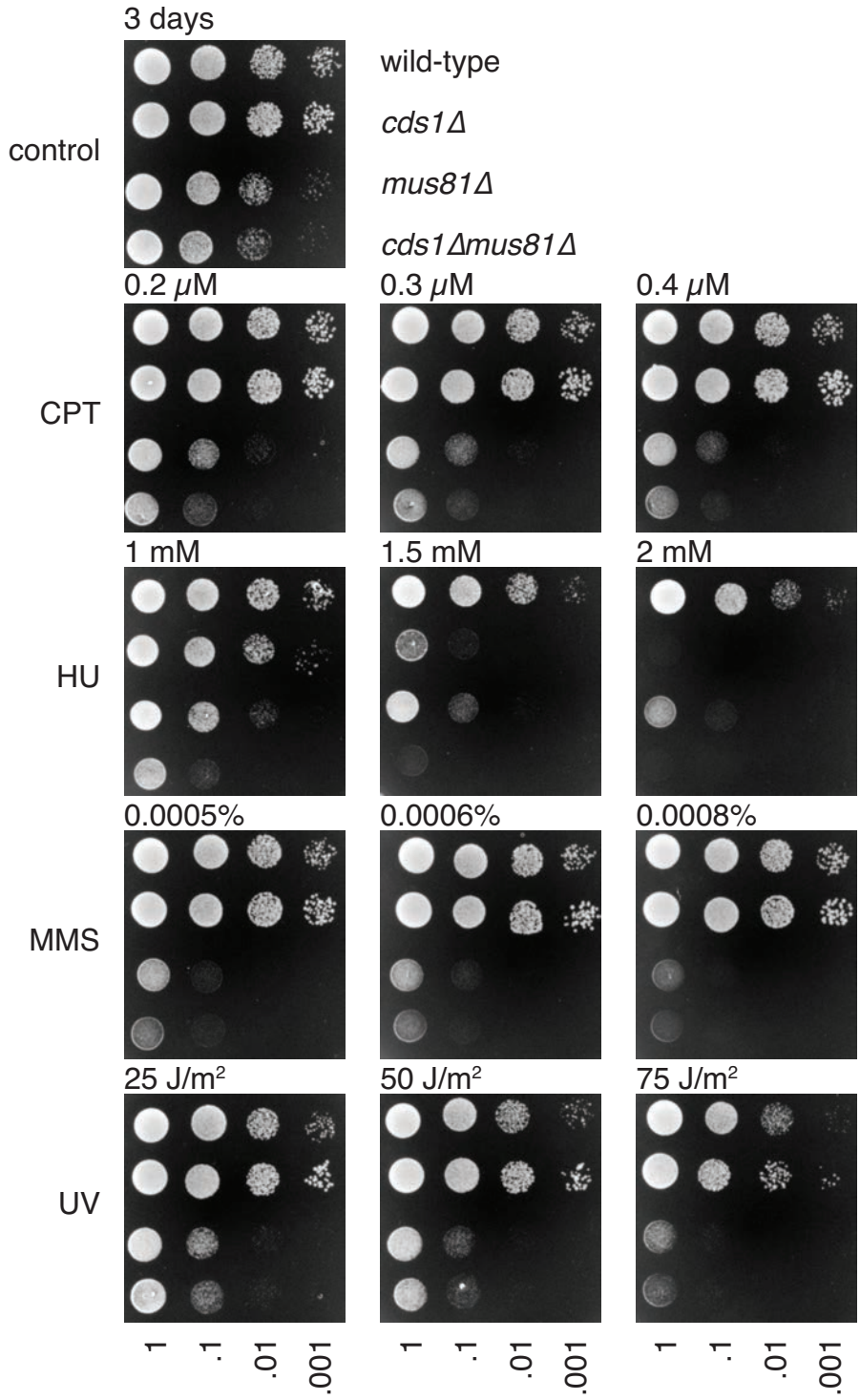


Figure 8.6 | Mus81 resolves toxic intermediates in cells treated with HU in the absence of Cds1. Spot assays comparing the growth and sensitivity of wild-type (MCW1221), *cds1Δ* (MON301), *mus81Δ* (MCW1779), and *cds1Δmus81Δ* (MCW2907) to different genotoxins. Strains were grown on complete media for 3 days at 30°C before being photographed.

together, this suggests that Cds1 may have a two-tier system for inhibiting unscheduled DNA breaks resulting from Mus81 activity at stalled/blocked replication forks. In addition to phosphorylating Mus81 to reduce its binding to chromatin, Cds1 is also able to stabilize an arrested replication fork and protect it in a manner that prevents Mus81 from physically accessing the fork and cleaving it. In contrast, in the absence of Cds1, the replisome dissociates at stalled replication forks and the resulting unprotected fork can become susceptible to Mus81 cleavage. The exact nature of the fork structure that is cleaved by Mus81, however, remains unknown.

Our laboratory has previously observed that the frequency of *RTS1*-induced direct repeat recombination is not significantly affected by *mus81Δ* single mutants compared to wild-type (unpublished data). This suggests that Mus81 may not normally have a role in the repair of replication forks blocked at *RTS1*, and instead may function as a second restart pathway behind Fml1-driven RDR. Although Mus81 is thought to be able to promote RDR, it may be an undesirable pathway because cleavage of the fork could lead to one arm of the replicated fork structure being detached such that an oncoming replication fork could not simply converge with it if the detached arm did not re-engage with the DNA. Because an event like this would lead to over-replication, a safer alternative may be to restart the fork without breaking it. Thus, factors, such as Cds1, may help coordinate the restart such that Fml1 is preferably initially recruited to the blocked replication fork to catalyze fork reversal for Rad51-dependent RDR. Consistent with the idea that Fml1 and Mus81 may

promote alternative RDR pathways, *fml1Δmus81Δ* double mutants exhibit a marked reduction in viability and enhanced genotoxin sensitivity to CPT-, HU-, MMS-, and UV-induced lesions compared with either single mutant (Sun et al. 2008).

Lastly, deleting *cds1* has pleotropic effects. Besides Mus81, another substrate that Cds1 targets by phosphorylation is Dna2 (Hu et al. 2012). Phosphorylated Dna2 is thought to cleave regressed leading or lagging strands that are the precursors of reversed forks as a means to prevent them from occurring (Hu et al. 2012). Our laboratory also explored whether the hyperrecombination in a *cds1Δ* mutant could be due to a failure to phosphorylate Dna2. However, we found that neither the phospho-dead nor phospho-mimetic Dna2 mutant had an effect on *RTS1*-induced recombination (unpublished data). This suggests that the hyperrecombination in *cds1Δ* cannot be due to the loss of Dna2's function in preventing fork reversal. From the data presented in this chapter, it is clear that Cds1 has a critical role in preventing the formation of gross chromosomal rearrangements and deletions following replication fork blockage. In addition to preventing Mus81 cleavage, however, it is currently unclear what other roles Cds1 may be playing in aiding the transition of the stalled fork to one that goes on to be remodeled by recombination, and furthermore, how the restarted fork may merge with an oncoming fork.

Chapter 9

Concluding Remarks

In an effort to learn more about replication fork block-induced recombination, I have exploited a site-specific RFB in *S. pombe* to investigate the consequences of perturbing a single replication fork. Through a live-cell imaging approach, I have demonstrated that recombinases are recruited to the *RTS1* RFB within a few minutes of fork blockage in a majority of cells. Although I did not formally establish myself that the recombinases function in a restart role at *RTS1*, work from our laboratory and others support this model (Ahn et al. 2005; Lambert et al. 2005; Sun et al. 2008; Lorenz et al. 2009; Lambert et al. 2010; Iraqui et al. 2012; Mizuno et al. 2013). In this dissertation, I have also presented data that is consistent with a restart role for recombinases at forks blocked at *RTS1*. First, in a wild-type background, every cell does not exhibit a co-localizing Rad52-*lacO*-LacI focus, which would be expected if recombinases were instead loaded during fork merging. Second, when fork merging is delayed by deleting *ori-1253*, there is a significant increase in recombination activity as determined by *RTS1*-induced direct repeat recombination and in the percentage of cells displaying a co-localizing Rad52 focus compared to wild-type. Additionally, in a *rad51Δ* mutant, which is believed to be defective in RDR, there is not a significant change in the percentage of cells exhibiting a co-localizing Rad52 focus compared to wild-type despite there being a likely increase in fork termination at the site. Further experiments, such as 2D gel and/or DNA combing analysis, which would provide physical evidence for replication restart, are needed to confirm our model.

Another system that has been extensively used to explore RDR in eukaryotes is BIR in *S. cerevisiae*. Although both the *RTS1* system in fission yeast and the BIR system in budding yeast are being used to gain insights into RDR, there are a few major differences between their experimental setups. This includes the distinction that BIR has thus far been limited to studying the repair of a one-ended DSB that is introduced into a mitotically arrested cell, which triggers the initiation of long stretches of newly synthesized DNA (Anand et al. 2013; Malkova and Ira 2013). In contrast, I have shown that the repair of forks blocked at *RTS1* commences in S-phase, which indicates that the *RTS1* system more directly addresses the problem of repairing a stalled replication fork in the context of an actively replicating chromosome. Moreover, BIR presupposes how a broken replication fork is restarted whereas RDR at the *RTS1* RFB is believed to occur without breakage of the blocked fork (Ahn et al. 2005; Mizuno et al. 2009; Lambert et al. 2010).

Despite the disparities between the *RTS1* and BIR systems, there appear to be a similar requirement of HR factors for fork restart. In BIR, there are two replication restart pathways in *S. cerevisiae*. Both of them are Rad52-dependent but one is Rad51-independent (Lundblad and Blackburn 1993; McEachern and Blackburn 1996; Teng and Zakian 1999; Teng et al. 2000; Signon et al. 2001). In the Rad51-dependent BIR pathway, Rad52, Rad51, Rad55-Rad57, and Rad54 are required in *S. cerevisiae* (Le et al. 1999; Teng and Zakian 1999). In addition to these factors, the Shu complex, Psy3-Csm2-Shu1-Shu2, has also been reported as being more important for Rad51-

dependent BIR than in the HR repair of DSBs (Lydeard et al. 2010; Anand et al. 2013). My experiments suggest that there is also a Rad51-dependent RDR pathway at *RTS1*, but it is unclear whether there is a Rad51-independent pathway as well. In a *rad51Δ* mutant, I showed that Rad52 still robustly forms a focus at forks blocked at *RTS1* and that direct repeat recombinants can still form, albeit there are no conversion-types and only deletion-types. I suggested that these deletion-types in a *rad51Δ* mutant may be byproducts of Rad52-dependent SSA events between converging forks as depicted in Figure 3.10 that do not in effect lead to productive replication restart. Thus, it remains uncertain whether there is a Rad52-dependent, Rad51-independent pathway that leads to efficient replication restart at the *RTS1* barrier. If the ability to promote *RTS1*-induced direct repeat conversion-types is representative of Rad51-dependent RDR at *RTS1*, then similarly, I demonstrated that Rad52, Rad51, Rad55-Rad57, and Rad54 are required for RDR in *S. pombe* as loss of any of these proteins leads to the elimination of gene conversion formation at *RTS1-AO*. Likewise, I also showed that the fission yeast equivalent to the Shu complex, Rdl1-Rlp1-Sws1, is analogously more important for replication fork block-induced conversion-type formation than spontaneous conversion-type formation.

There are also insights into BIR that can be used to shape our thinking of RDR at *RTS1*. One of these observations is that the initiation of DNA synthesis from BIR is a very slow process, approximately two to four hours slower than at DSBs (Malkova et al. 2005). This study also reported that the

rate of DNA synthesis in BIR is comparable to S-phase replication. I have demonstrated that Rad52 is recruited to forks blocked at *RTS1* within a few minutes of fork blockage, but it is unclear how long it takes after Rad52 recruitment for replication to be restarted at *RTS1* and whether the rate of DNA synthesis at the restarted fork is kinetically comparable to forks that emanate from an origin of replication. Intriguingly, there is no significant change in the growth or viability of wild-type cells with *RTS1-AO* compared to *RTS1-IO* (Ahn et al. 2005), suggesting that cells are able to overcome the *RTS1* RFB in a timely manner. This could either be due to productive fork restart at *RTS1* and/or additional DNA synthesis catalyzed by the opposing replication fork. In comparison, however, the subset of *ori-1253Δ* cells that exhibit prolonged Rad52-*lacO*-LacI co-localization (over 2 hours) could be a result of the slow initiation of DNA synthesis during fork restart and/or the long distance the fork needs to travel to complete replication. Intriguingly, centromeres have been found to inhibit BIR (Morrow et al. 1997). If centromeres also pose barriers to forks restarted by RDR, then the *ori-1253Δ* cells that display this prolonged Rad52 co-localization may also reflect the restarted fork having difficulty replicating in the centromere if the restarted fork has actually needed to travel that far. In a related observation, it is also interesting to note that the average length of Rad52-*lacO*-LacI co-localization does not significantly change between wild-type and *rad51Δ* cells. This may suggest that most wild-type cells overcome the *RTS1* RFB by having the opposing oncoming fork catalyze additional DNA synthesis and/or that most restarted forks do not travel far from the site of stalling.

The replication machinery loaded at the restarted fork is also likely to be different than the prototypical replisome assembled at an origin of replication. Studies in *S. cerevisiae* have demonstrated that BIR is dependent on the nonessential DNA polymerase Polδ subunit Pol32 (Lydeard et al. 2007). It is currently unknown, however, which DNA polymerases are required for RDR in *S. pombe*. Replication forks from BIR are also susceptible to template switching from multiple rounds of dissociation and re-invasion events within the first 10 kb of initial DNA synthesis at which it is then thought to transition into a "mature" and processive fork (Smith et al. 2007). Similar to BIR, our laboratory also found that forks restarted at *RTS1* are prone to template switching at least as far as 10 kb downstream of the RFB. Based on the dynamics of Rad52 co-localization in my live cell imaging experiments, this propensity for template switching may be a consequence of the Rad52 protein remaining associated with the restarted fork. Building on this work, our laboratory is continuing to explore the stability of the restarted fork to assess whether restarted forks may be prone to template switching further than what has been shown in BIR and/or collapsing at pausing sites that do not normally induce fork collapse.

Lastly, restarted forks may also differ from forks that originate from an origin of replication in their mode of DNA synthesis. A pair of recent papers has shown that the nascent strands from BIR are synthesized by a conservative mechanism as opposed to a semi-conservative mechanism (Donnianni and Symington 2013; Saini et al. 2013). Conservative DNA synthesis is proposed

to occur through a bubble migration model in which the leading strand progressively polymerizes DNA from the parental strand in a migrating D-loop. The lagging strand then uses the displaced leading strand as its template instead of the parental strand. This contrasts with the semi-conservative mode at forks from origins of replication in which both the leading and lagging strands prime DNA synthesis from the parental duplex. Intriguingly, as a comparison to the aforementioned *in vivo* BIR study, *in vitro* studies with reconstituted bacteriophage T4 and *E. coli* RDR proteins support a model for these proteins establishing a replisome that progresses semi-conservatively (Kreuzer 2000; Xu and Marians 2003). In the case of fork restart at *RTS1*, it is unknown whether the restarted fork progresses through a conservative or semi-conservative mechanism. If the restarted fork proceeds through a conservative mechanism like BIR, then there must be some regulatory factor that would facilitate how a conservative fork would terminate with an oncoming fork that is proceeding in a semi-conservative manner. Otherwise, this would lead to over-replication because the lagging strand from the restarted fork, which is not using the parental strand as its template, would not properly merge with the leading strand from the opposing fork, which is using the parental strand as its template.

The restart of a collapsed fork by HR is believed to be a mechanism that is conserved from phages to yeast and to humans. Although the risk of failing to complete DNA replication is such that RDR may be initiated as a default response to fork collapse, its use can be a double-edge sword. In addition to

potentially restarting at the wrong, non-contiguous sequence and generating a non-allelic recombination event during the initial strand invasion step, RDR also produces a replication fork that progresses along the chromosome with mutagenic potential. Both of these consequences can ultimately lead to genomic changes that drive the development of diseases such as cancer, which further underscores the importance of continuing these investigations.

Appendix

Table S1 | Effect of different mutants on *RTS1-IO* direct repeat recombination. All means are presented with ± one standard deviation in parenthesis. P-values are derived from independent-sample t-tests comparing the mean values of the respective mutant to the corresponding mean value found in the wild-type.

Genotype	Number of Colonies Analyzed	$Ade^+ His^+$ recombinant frequency (x 10^{-4})		$Ade^+ His^-$ recombinant frequency (x 10^{-4})	
		Mean	P-value	Mean	P-value
wild-type	77	1.36 (±0.51)	-	3.48 (±0.89)	-
cds1Δ	17	3.60 (±1.69)	<0.001	8.55 (±2.10)	<0.001
cds1Δmus81Δ	16	2.10 (±0.90)	0.005	3.99 (±1.04)	0.047
cds1Δmus81Δ rad51Δ	13	0.00 (±0.00)	<0.001	114.07 (±75.72)	<0.001
cds1Δrad51Δ	18	0.07 (±0.22)	<0.001	90.29 (±37.14)	<0.001
fml1Δ	16	0.53 (±0.29)	<0.001	3.41 (±1.28)	0.781
fml1Δrad51Δ	19	0.02 (±0.05)	<0.001	11.78 (±3.58)	<0.001
fml1Δrad52Δ	18	0.40 (±0.34)	<0.001	2.99 (±1.13)	0.048
fml1Δrad54Δ	18	0.03 (±0.05)	<0.001	4.75 (±1.21)	<0.001
fml1Δrad55Δ	17	0.06 (±0.07)	<0.001	13.08 (±3.25)	<0.001
mus81Δrad51Δ	17	0.02 (±0.06)	<0.001	23.24 (±6.93)	<0.001
ori-1253Δ	15	2.33 (±1.86)	0.060	4.80 (±1.58)	0.007
rad51Δ	45	0.03 (±0.12)	<0.001	15.74 (±4.15)	<0.001
rad51Δrad55Δ	15	0.09 (±0.19)	<0.001	27.18 (±12.19)	<0.001
rad51Δrdl1Δ	20	0.04 (±0.07)	<0.001	16.49 (±5.18)	<0.001

rad51Δswi5Δ	19	0.13 (±0.29)	<0.001	31.57 (±7.96)	<0.001
rad54^{+}	18	1.41 (±0.46)	0.691	4.90 (±0.91)	<0.001
rad54^{K300A}	17	0.04 (±0.07)	<0.001	13.85 (±4.13)	<0.001
rad54Δ	19	0.00 (±0.01)	<0.001	5.49 (±1.86)	<0.001
rad54Δrad51Δ	26	0.05 (±0.11)	<0.001	28.44 (±11.36)	<0.001
rad54Δrad52Δ	18	0.00 (±0.00)	<0.001	0.76 (±0.47)	<0.001
rad54Δpfh1^{+}	19	0.04 (±0.06)	<0.001	7.71 (±2.88)	<0.001
rad54Δpfh1-m21	19	0.10 (±0.15)	<0.001	13.12 (±3.15)	<0.001
*rad54Δpfh1-mt**	19	0.16 (±0.16)	<0.001	9.66 (±5.26)	<0.001
rad55Δ	43	0.10 (±0.15)	<0.001	13.34 (±4.58)	<0.001
rad55Δrdl1Δ	17	0.07 (±0.18)	<0.001	20.51 (±7.11)	<0.001
rad55Δswi5Δ	38	0.02 (±0.11)	<0.001	32.94 (±14.78)	<0.001
rad57Δ	19	0.13 (±0.15)	<0.001	12.84 (±4.59)	<0.001
rdl1Δ	27	0.66 (±0.33)	<0.001	6.05 (±1.28)	<0.001
rlp1Δ	20	0.80 (±0.28)	<0.001	5.21 (±1.81)	<0.001
sfr1Δ	25	1.00 (±0.48)	0.002	5.86 (±2.24)	<0.001
swi5Δ	34	1.15 (±0.56)	0.048	6.31 (±1.72)	<0.001
sws1Δ	18	0.97 (±0.41)	0.003	2.96 (±1.06)	0.03

Table S2 | Effect of different mutants on *RTS1-AO* direct repeat recombination. All means are presented with ± one standard deviation in parenthesis. P-values are derived from independent-sample t-tests comparing the mean values of the respective mutant to the corresponding mean value found in the wild-type.

Genotype	Number of Colonies Analyzed	$Ade^+ His^+$ recombinant frequency (x 10^{-4})		$Ade^+ His^-$ recombinant frequency (x 10^{-4})	
		Mean	P-value	Mean	P-value
wild-type	77	134.03 (±38.50)	-	113.41 (±49.72)	-
*cds1*Δ	20	311.36 (±120.00)	<0.001	819.78 (±355.35)	<0.001
*cds1*Δ*fml1*Δ	19	69.45 (±58.08)	<0.001	1149.02 (±345.14)	<0.001
*cds1*Δ*mus81*Δ	21	116.95 (±51.67)	0.099	256.89 (±105.02)	<0.001
*cds1*Δ*rad51*Δ	19	0.00 (±0.00)	<0.001	336.60 (±132.51)	<0.001
*cds1*Δ*mus81*Δ *rad51*Δ	17	1.72 (±2.36)	<0.001	295.17 (±139.31)	<0.001
*fml1*Δ	22	17.25 (±8.87)	<0.001	108.31 (±53.51)	0.678
*fml1*Δ*rad51*Δ	16	0.00 (±0.00)	<0.001	136.51 (±51.37)	0.096
*fml1*Δ*rad52*Δ	19	0.21 (±0.30)	<0.001	22.50 (±12.5)	<0.001
*fml1*Δ*rad54*Δ	16	6.35 (±6.38)	<0.001	397.50 (±177.83)	<0.001
*fml1*Δ*rad55*Δ	16	0.96 (±1.40)	<0.001	78.97 (±39.36)	0.011
mus81^{T239A}	23	172.07 (±107.86)	0.010	206.37 (±114.03)	<0.001
*mus81*Δ*rad51*Δ	37	0.43 (±0.53)	<0.001	86.23 (±39.73)	0.004
*ori-1253*Δ	16	339.88 (±83.61)	<0.001	221.02 (±57.21)	<0.001
*rad51*Δ	48	1.12 (±1.24)	<0.001	74.69 (±29.12)	<0.001

*rad51*Δ*rad55*Δ	19	2.07 (±1.57)	<0.001	81.43 (±26.61)	<0.001
*rad51*Δ*rdl1*Δ	15	2.14 (±1.91)	<0.001	163.4 (±79.65)	0.032
*rad51*Δ*swi5*Δ	17	2.96 (±2.84)	<0.001	114.49 (±43.54)	0.934
rad54^{+}	19	87.13 (±36.44)	<0.001	86.97 (±45.38)	0.038
rad54^{K300A}	18	0.57 (±0.63)	<0.001	32.28 (±11.22)	<0.001
*rad54*Δ	14	7.20 (±6.03)	<0.001	256.60 (±87.93)	<0.001
*rad54*Δ*pfh1*$^{+}$	24	1.67 (±4.31)	<0.001	162.43 (±88.95)	0.016
*rad54*Δ*pfh1-m21*	20	3.59 (±4.68)	<0.001	558.43 (±182.41)	<0.001
*rad54*Δ*pfh1-mt**	27	0.19 (±1.01)	<0.001	479.86 (±142.55)	<0.001
*rad54*Δ*rad51*Δ	25	2.95 (±4.34)	<0.001	287.65 (±172.89)	<0.001
*rad54*Δ*rad52*Δ	18	0.00 (±0.00)	<0.001	3.73 (±2.39)	<0.001
*rad55*Δ	42	0.92 (±0.76)	<0.001	32.33 (±20.93)	<0.001
*rad55*Δ*rdl1*Δ	18	1.33 (±1.55)	<0.001	42.61 (±18.81)	<0.001
*rad55*Δ*swi5*Δ	30	0.63 (±0.65)	<0.001	52.17 (±15.72)	<0.001
*rad57*Δ	20	0.67 (±0.66)	<0.001	44.14 (±15.01)	<0.001
*rdl1*Δ	19	8.05 (±3.36)	<0.001	35.85 (±9.59)	<0.001
*rlp1*Δ	23	9.18 (±5.15)	<0.001	32.87 (±13.02)	<0.001
*sfr1*Δ	19	96.65 (±26.56)	<0.001	116.00 (±26.18)	0.755
*swi5*Δ	34	74.14 (±21.72)	<0.001	79.17 (±37.14)	<0.001
*sws1*Δ	21	30.45 (±8.74)	<0.001	26.37 (±10.08)	<0.001

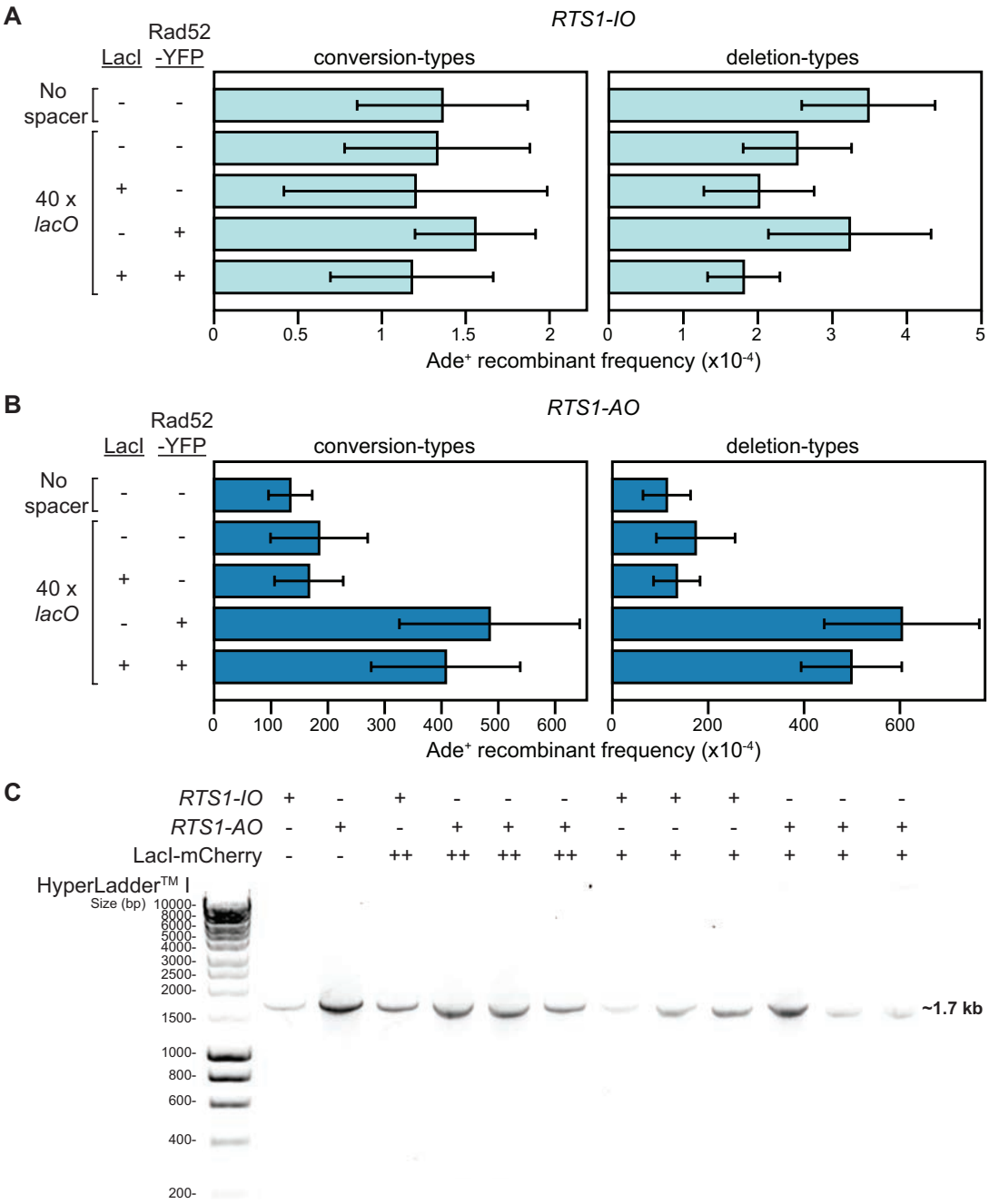


Figure S3.1 | Effect of 40 x *lacO*-LacI and Rad52-YFP on direct repeat recombination and *lacO* stability. Bar charts showing the frequency of *ade*$^+$ recombinants in *RTS1-IO* (A) and *RTS1-AO* (B) strains with and without 40 x *lacO*, LacI, and/or Rad52-YFP as indicated. Recombination assays were done on complete media. Error bars represent ± one standard deviation. In order of presentation, the strains are MCW4712, FO1791, MON31, MCW2726, MON10, MCW4713, FO1792, MON37, MCW2728, and MON1. (C) Colony PCRs with primers (oMW1493, oMW1494) amplifying the 40 x *lacO* array. *RTS1-IO* and *RTS1-AO* strains with LacI-mCherry expression driven by P_{nmt81} (+), P_{nmt41} (++), or not integrated in the strain (-). A 1.7 kb fragment was amplified, corresponding to the 40 x *lacO* repeat. From left to right, strains used were MCW2726, MCW2728, MCW5686, MON1, MON2, MON3, MON4, MON5, MON6, MON7, MON8, and MON9.

Table S3.1 | Effect of 40 x *lacO*-LacI and Rad52-YFP on direct repeat recombination. Direct repeat recombination data presented in the same order as Figure S3.1A and B. All means are presented with ± one standard deviation in parenthesis. P-values are derived from independent-sample t-tests comparing the mean values of the respective mutant to the corresponding mean value found in the control strain.

Genotype	Number of Colonies Analyzed	$Ade^+ His^+$ recombinant frequency (x 10^{-4})		$Ade^+ His^-$ recombinant frequency (x 10^{-4})	
		Mean	P-value	Mean	P-value
RTS1-IO					
No spacer, - LacI, - Rad52-YFP	77	1.36 (±0.51)	-	3.48 (±0.89)	-
40 x *lacO,* - LacI, - Rad52-YFP	9	1.33 (±0.55)	0.863	2.53 (±0.73)	0.003
40 x *lacO,* + LacI, - Rad52-YFP	8	1.20 (±0.79)	0.426	2.02 (±0.74)	<0.001
40 x *lacO,* - LacI, + Rad52-YFP	8	1.56 (±0.36)	0.291	3.23 (±1.09)	0.462
40 x *lacO,* + LacI, + Rad52-YFP	9	1.18 (±0.49)	0.310	1.81 (±0.49)	<0.001
RTS1-AO					
No Spacer, - LacI, - Rad52-YFP	77	134.03 (±38.50)	-	113.41 (±49.72)	-
40 x *lacO,* - LacI, - Rad52-YFP	8	184.57 (±85.53)	0.140	173.82 (±82.19)	0.078
40 x *lacO,* + LacI, - Rad52-YFP	7	166.67 (±60.44)	0.044	134.38 (±48.59)	0.288
40 x *lacO,* - LacI, + Rad52-YFP	7	484.53 (±158.56)	0.001	604.06 (±161.88)	<0.001
40 x *lacO,* + LacI, + Rad52-YFP	8	407.38 (±131.20)	0.001	498.84 (±105.07)	<0.001

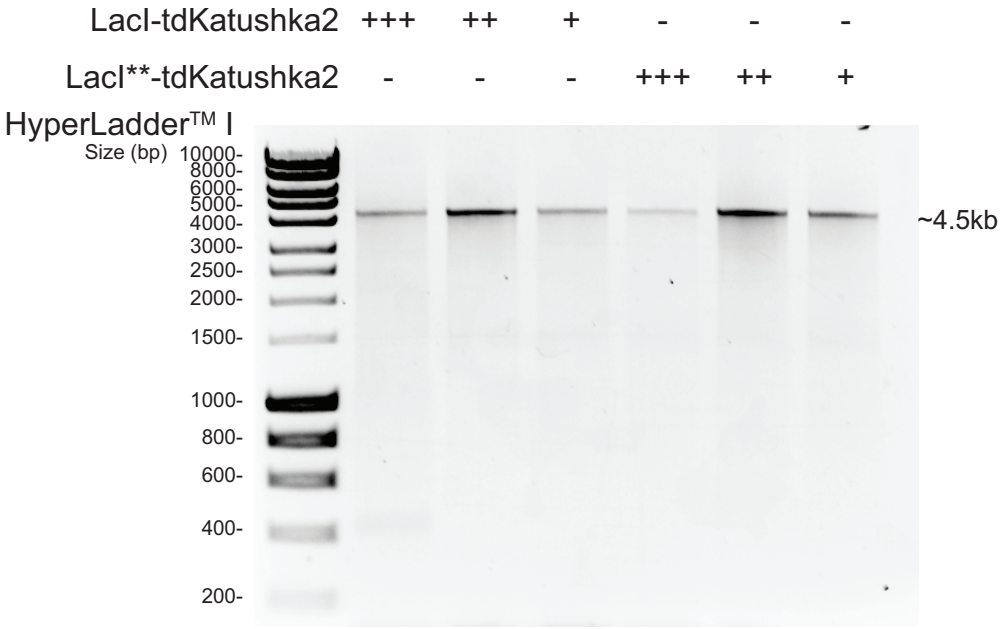


Figure S3.2 | The integrated 115 x *lacO* repeat array is stable in a most cells under various levels of LacI expression. Colony PCR (oMW1493, oMW1494) amplifying 115 x *lacO* repeat array. *RTS1-IO* strains with LacI-tdKatushka2 (MON97) or LacI**-tdKatushka2 (MON102) expression driven by P_{nmt41} under unrepressed (0 μM, +++), partially repressed (0.1 μM, ++), and fully repressed (4 μM, +) conditions as indicated. A 4.5 kb fragment was amplified, corresponding to the 115 x *lacO* repeat array.

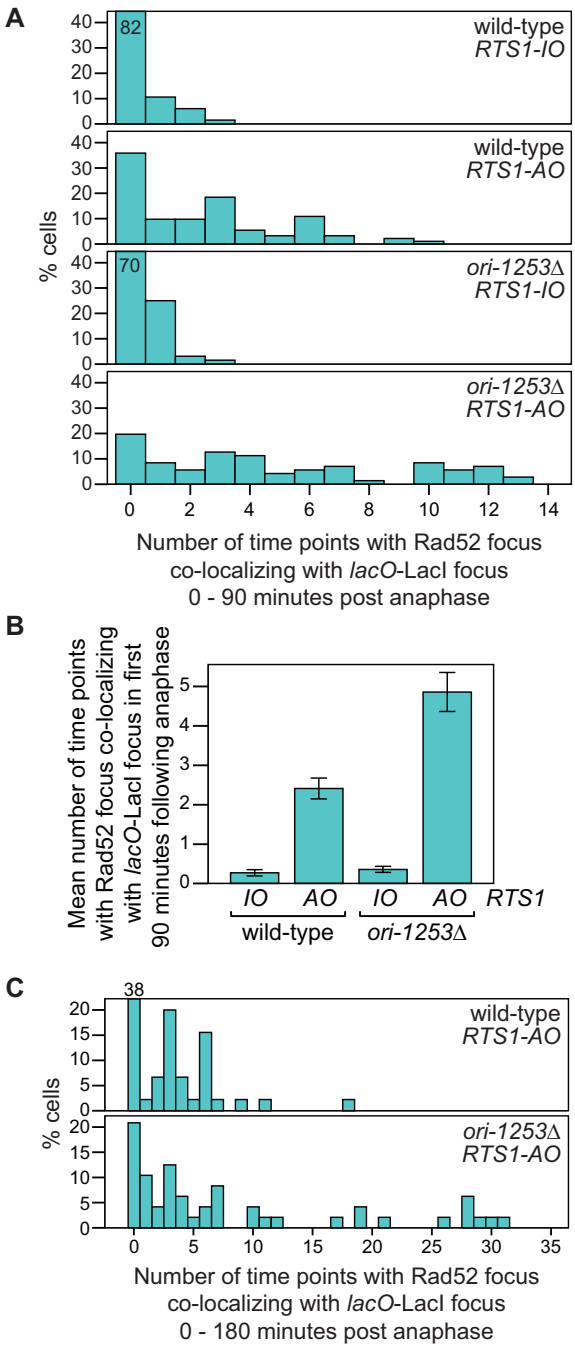


Figure S5.1 | *ori-1253Δ* cells display more time points with a Rad52-YFP focus at the *RTS1* RFB. (A) Histogram showing the percentage of cells with a given number of time points in which a Rad52-YFP focus co-localizes with a *lacO*-LacI focus within the first 90 minutes following anaphase. (B) Bar chart of the mean number of time points cells exhibit a Rad52-YFP focus that co-localizes with a *lacO*-LacI focus during the first 90 minutes following anaphase. Error bars represent ± one standard error of the mean. (C) Histogram showing the percentage of cells with a given number of time points in which a Rad52-YFP focus co-localizes with a *lacO*-LacI focus within the first 180 minutes following anaphase. The *RTS1-IO* strains are MON110 (wild-type) and MON297 (*ori-1253Δ*). The *RTS1-AO* strains are MON148 (wild-type) and MON259 (*ori-1253Δ*).

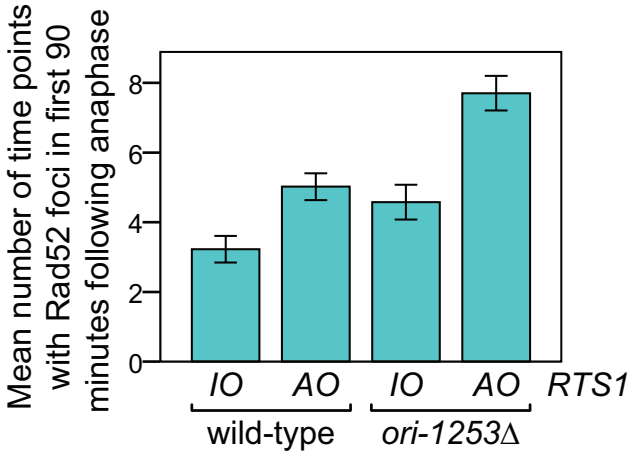


Figure S5.2 | *ori-1253Δ* cells display more Rad52-YFP foci. Bar chart of the mean number of time points cells exhibit a Rad52-YFP focus during the first 90 minutes following anaphase. Error bars represent ± one standard error of the mean. The *RTS1-IO* strains are MON110 (wild-type) and MON297 (*ori-1253Δ*). The *RTS1-AO* strains are MON148 (wild-type) and MON259 (*ori-1253Δ*).

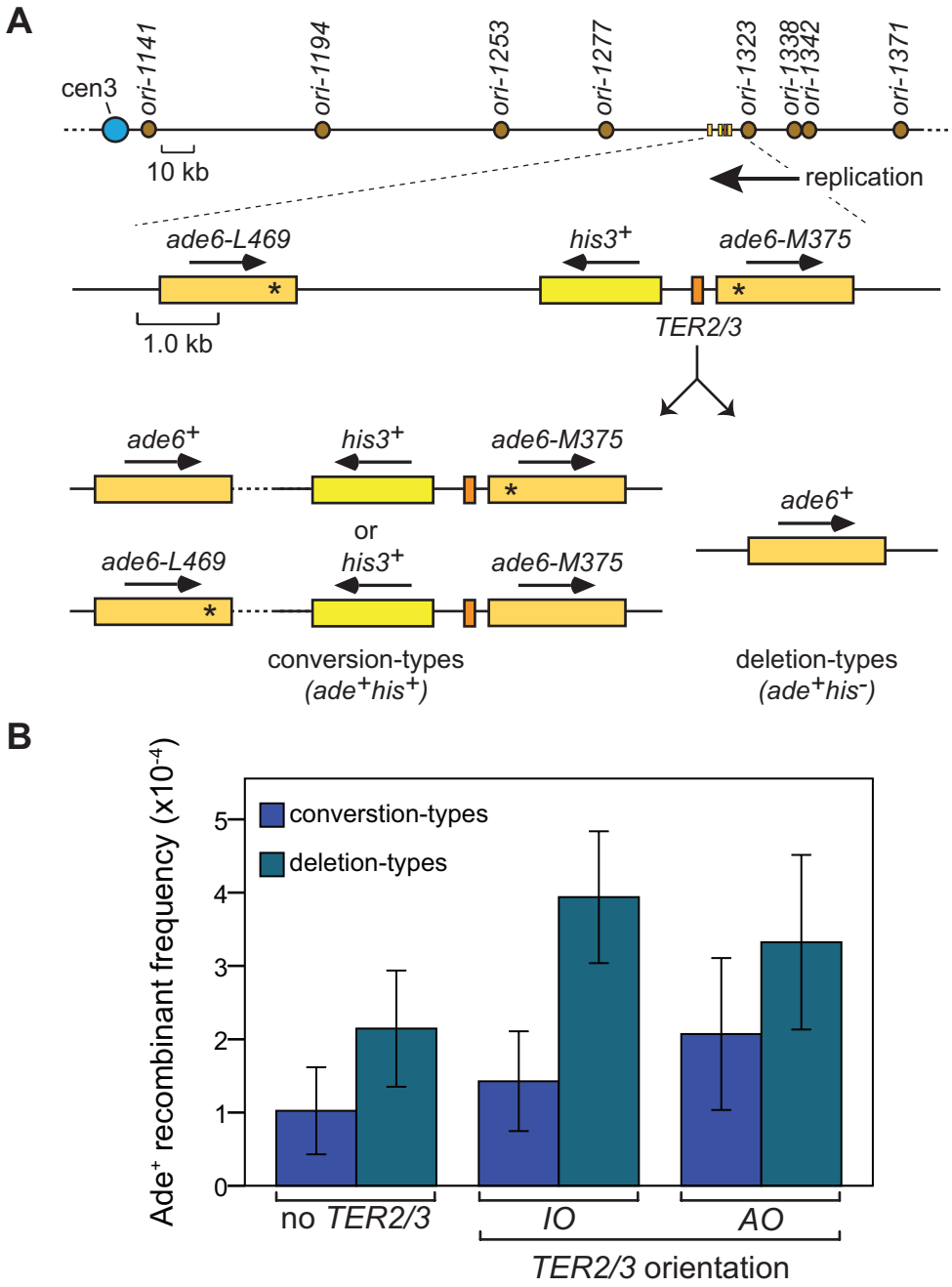


Figure S5.3 | The *TER2/3* pausing element does not strongly induce direct repeat recombination. (A) Schematic showing the position of the *ade6*$^{-}$ intrachromosomal recombination substrate along with an intervening *his3*$^{+}$ gene and *TER2/3* pausing element in relation to nearby replication origins on chromosome III. (B) Bar chart showing the frequency of conversion- and deletion-type Ade^{+} recombinants in strains with and without the *TER2/3* element, which can be inserted in either a non-blocking (inactive) or blocking (active) orientation, indicated by '*IO*' and '*AO*' respectively. Error bars represent ± one standard deviation. In order of presentation, the strains are FO645, MCW7045, and MCW7046.

Table S5.1 | The *TER2/3* pausing element does not strongly induce direct repeat recombination. Direct repeat recombination data presented in the same order as Figure S5.3B. All means are presented with ± one standard deviation in parenthesis. P-values are derived from independent-sample t-tests comparing the mean values of the respective mutant to the corresponding mean value found in the control strain.

Genotype	Number of Colonies Analyzed	$Ade^+ His^+$ recombinant frequency (x 10^{-4})		$Ade^+ His^-$ recombinant frequency (x 10^{-4})	
		Mean	P-value	Mean	P-value
no TER2/3	17	1.02 (±0.59)	-	2.14 (±0.79)	-
TER2/3-IO	17	1.43 (±0.68)	0.075	3.94 (±0.90)	<0.001
TER2/3-AO	19	2.07 (±1.04)	0.001	3.32 (±1.19)	0.002

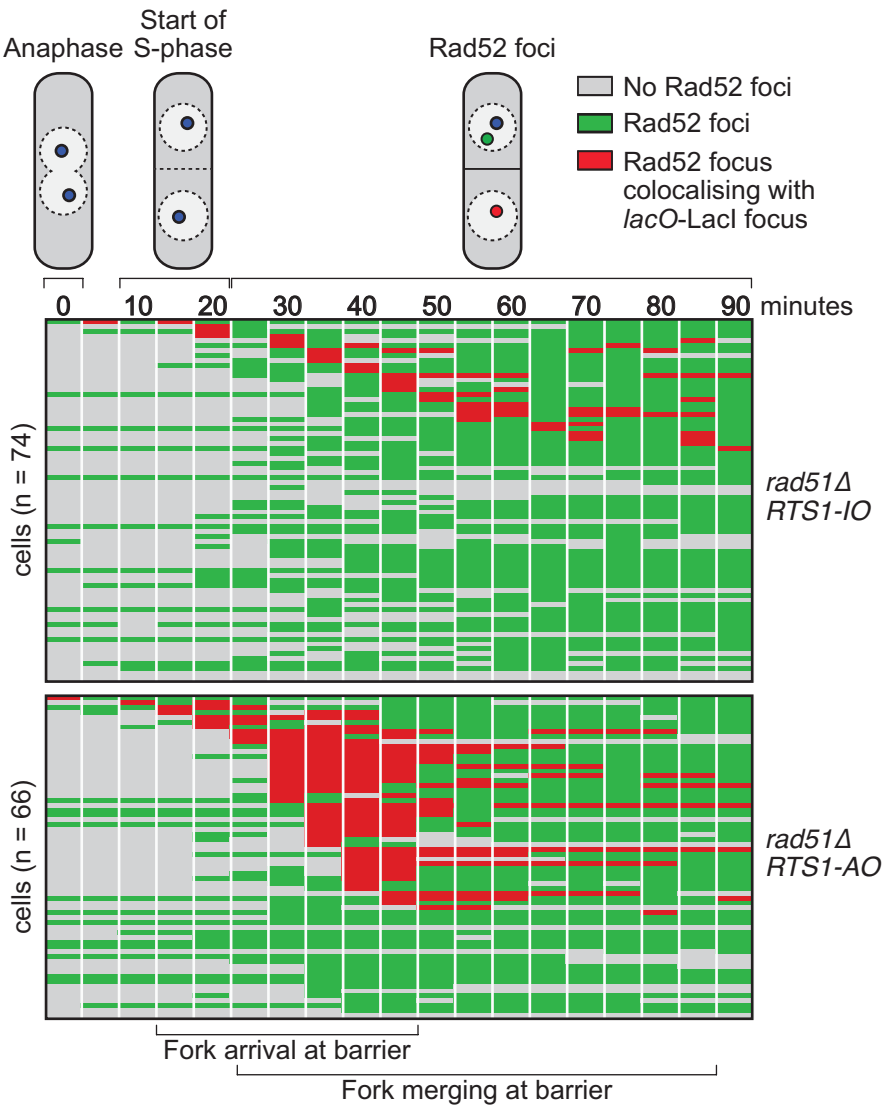


Figure S6.1 | Recruitment of Rad52-YFP to *RTS1-AO* is not significantly affected by the loss of Rad51. Analysis of time-lapse movies of *rad51Δ* cells with either *RTS1-IO* (MON163) or *RTS1-AO* (MON167).

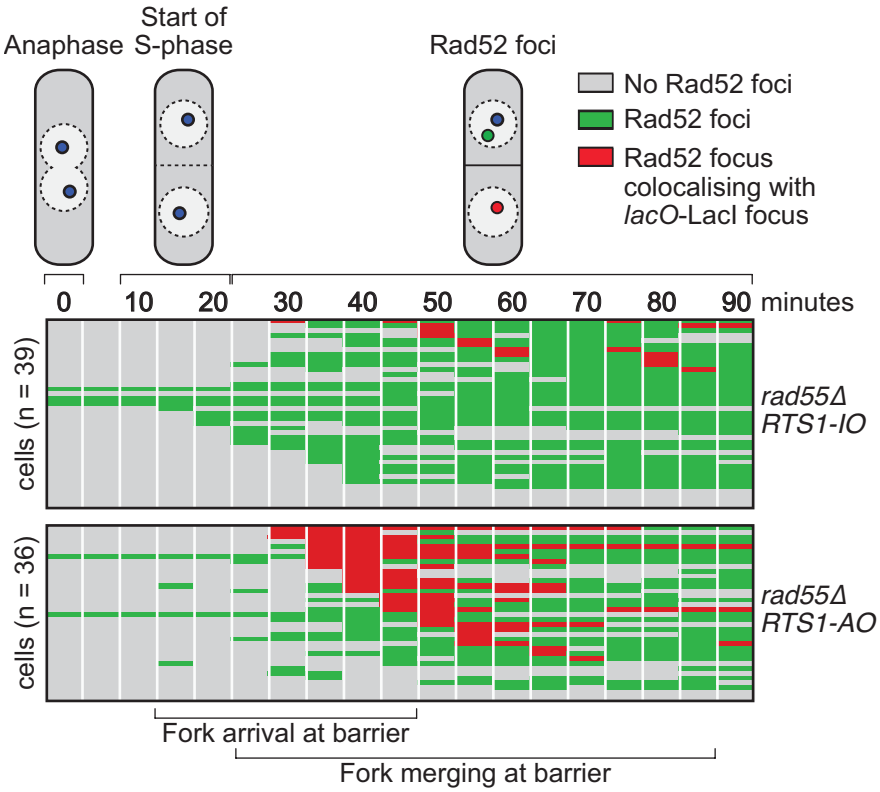


Figure S6.2 | Recruitment of Rad52-YFP to *RTS1-AO* is not significantly affected by the loss of Rad55. Analysis of time-lapse movies of *rad55Δ* cells with either *RTS1-IO* (MCW6955) or *RTS1-AO* (MCW6958).

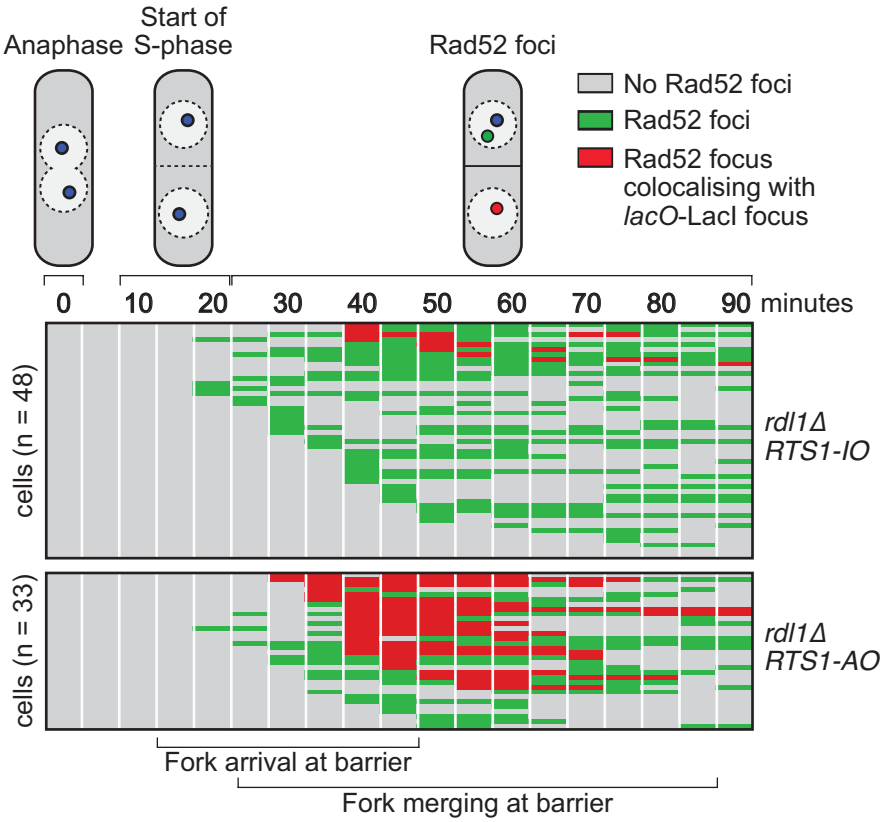


Figure S6.3 | Recruitment of Rad52-YFP to *RTS1-AO* is not significantly affected by the loss of Rdl1. Analysis of time-lapse movies of *rdl1Δ* cells with either *RTS1-IO* (MCW6985) or *RTS1-AO* (MCW6988).

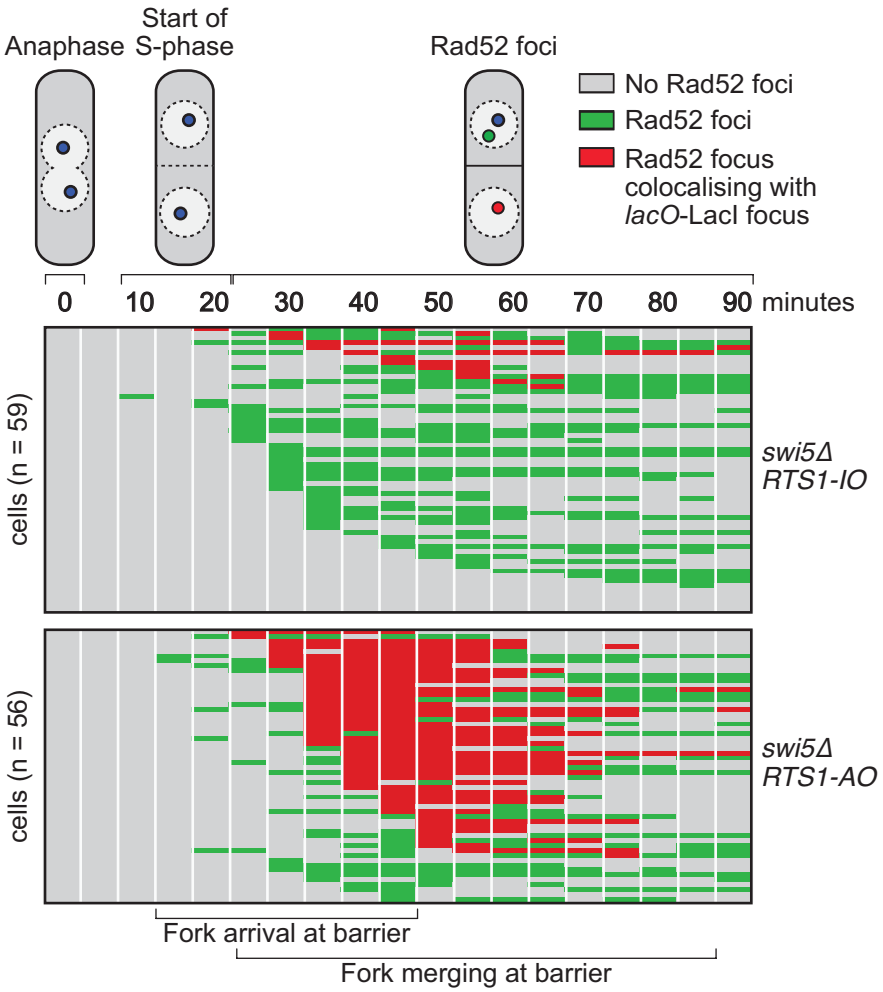


Figure S6.4 | Recruitment of Rad52-YFP to *RTS1-AO* is not significantly affected by the loss of Swi5. Analysis of time-lapse movies of *swi5Δ* cells with either *RTS1-IO* (MCW6961) or *RTS1-AO* (MCW6964).

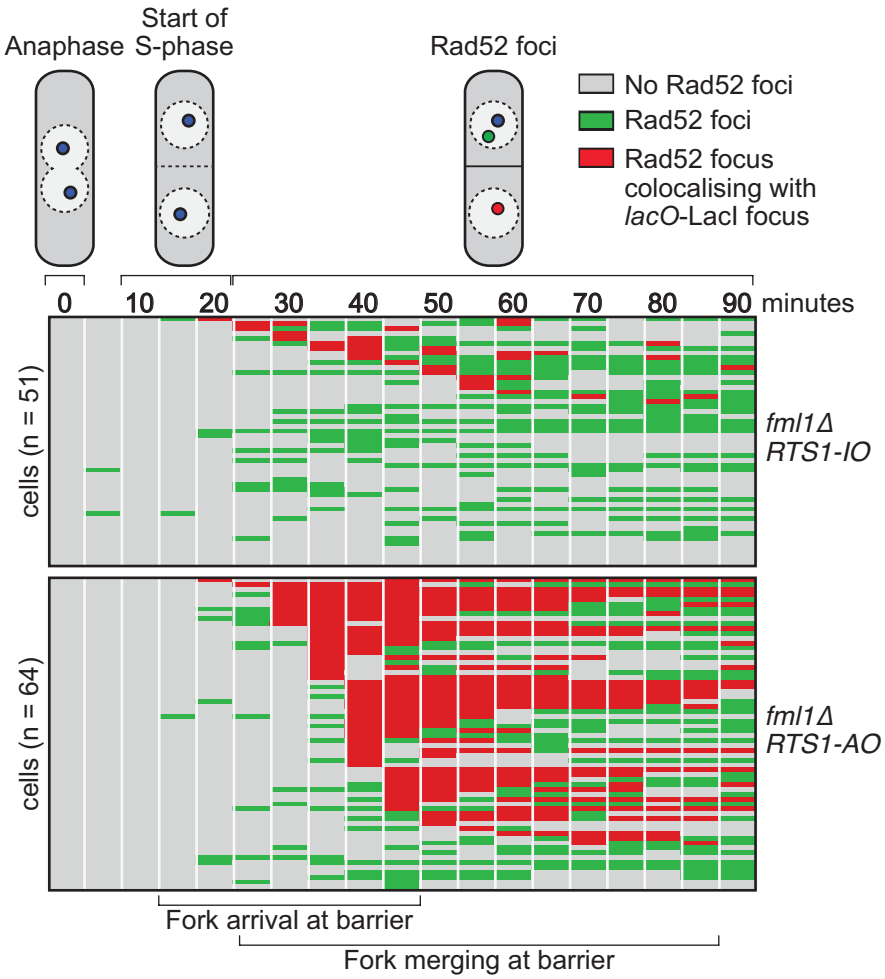


Figure S7.1 | Rad52 persists at blocked forks longer in the absence of Fml1. Analysis of time-lapse movies of *fml1Δ* cells with either *RTS1-IO* (MON172) or *RTS1-AO* (MON177).

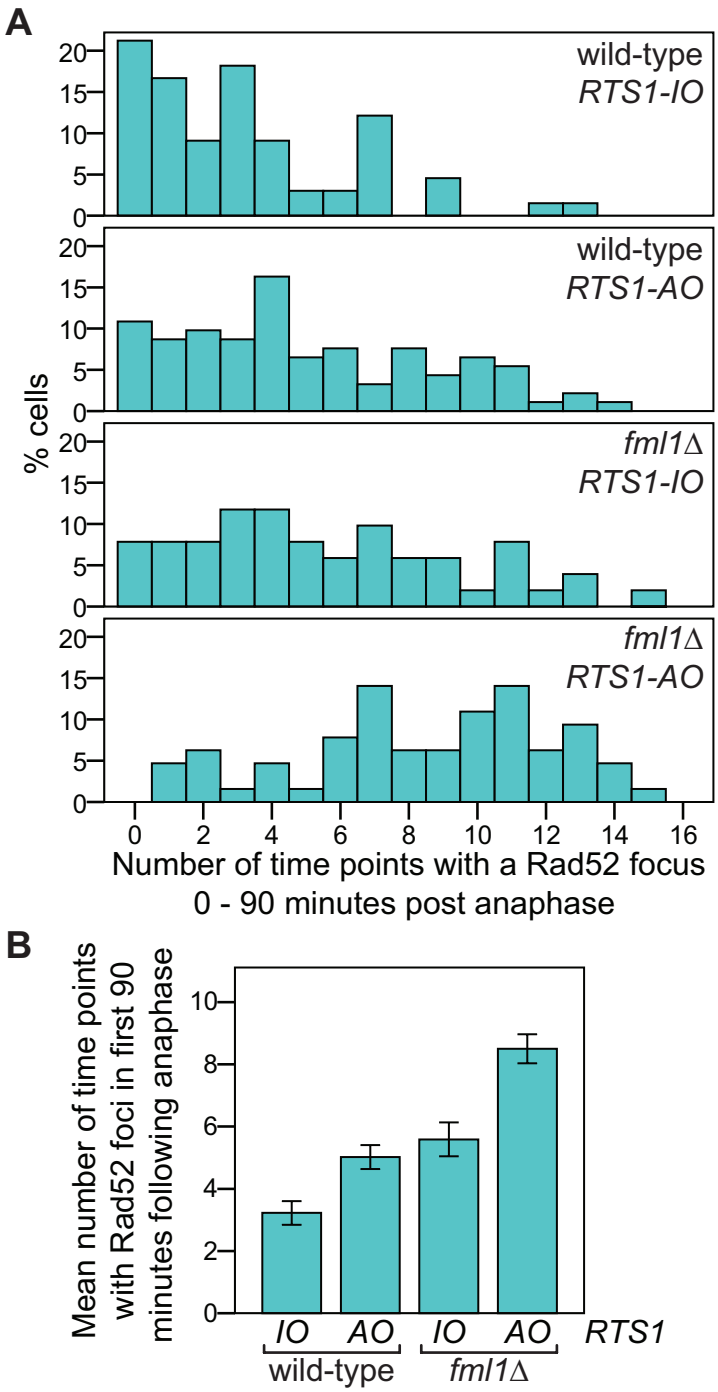


Figure S7.2 | Rad52 foci increase in the absence of *fml1*. (A) Histogram showing the percentage of cells with a given number of time points in which a Rad52-YFP focus is detected within the first 90 minutes following anaphase. (B) Bar chart of the mean number of time points cells display a Rad52-YFP focus in the first 90 minutes following anaphase. Error bars represent ± one standard error of the mean. The *RTS1-IO* strains are MON110 (wild-type) and MON172 (*fml1Δ*). The *RTS1-AO* strains are MON148 (wild-type) and MON177 (*fml1Δ*).

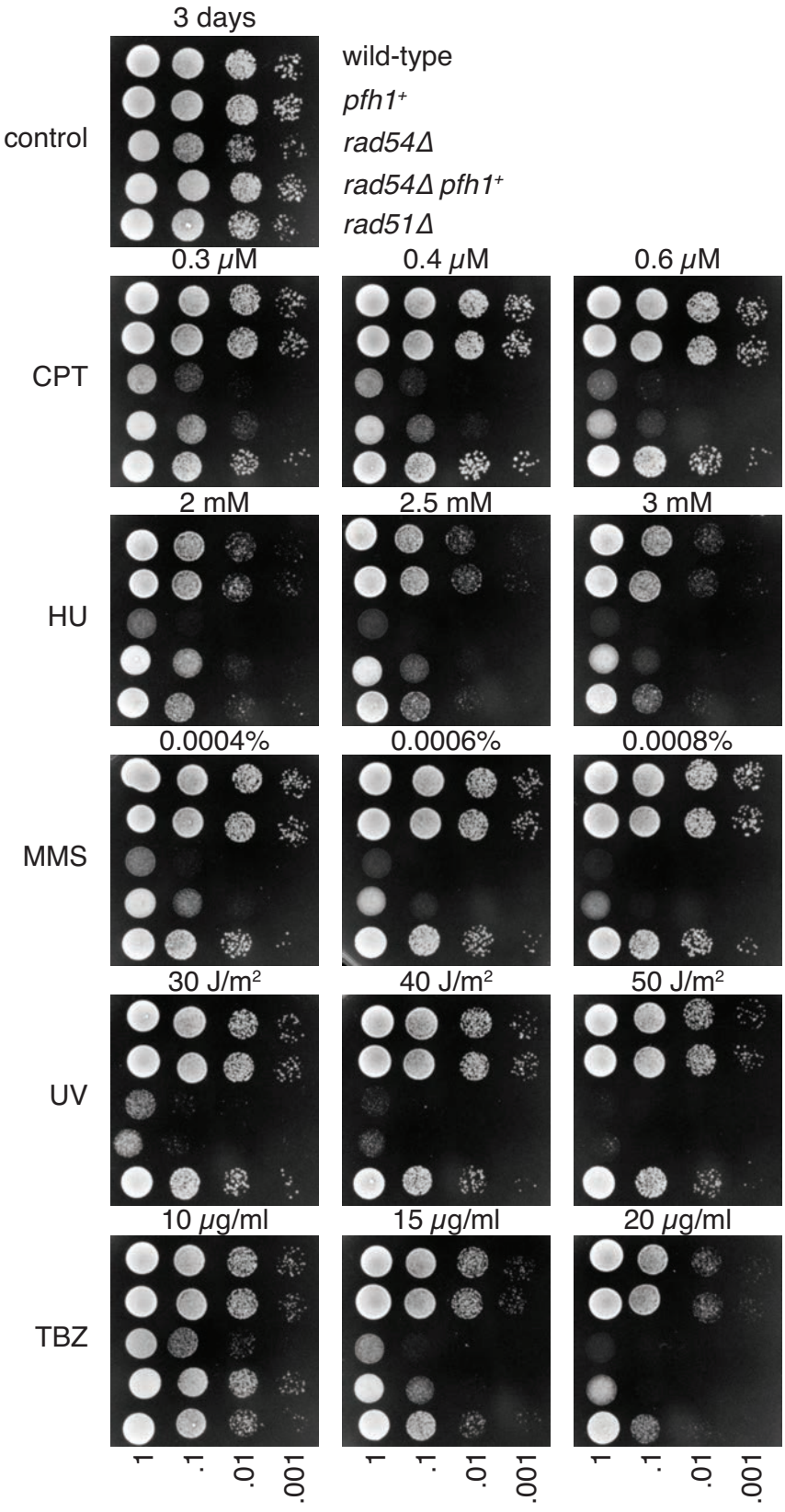


Figure S7.3 | **Pfh1$^+$ cells do not exhibit more genotoxin sensitivity**. Spot assays comparing the sensitivity of wild-type (MCW1221), *pfh1$^+$* (MCW5447), *rad54Δ* (MCW1230), *rad54Δpfh1$^+$* (MCW6542) and *rad51Δ* (MCW1088) to different genotoxins. Strains were grown on complete media for 3 days at 30°C before being photographed.

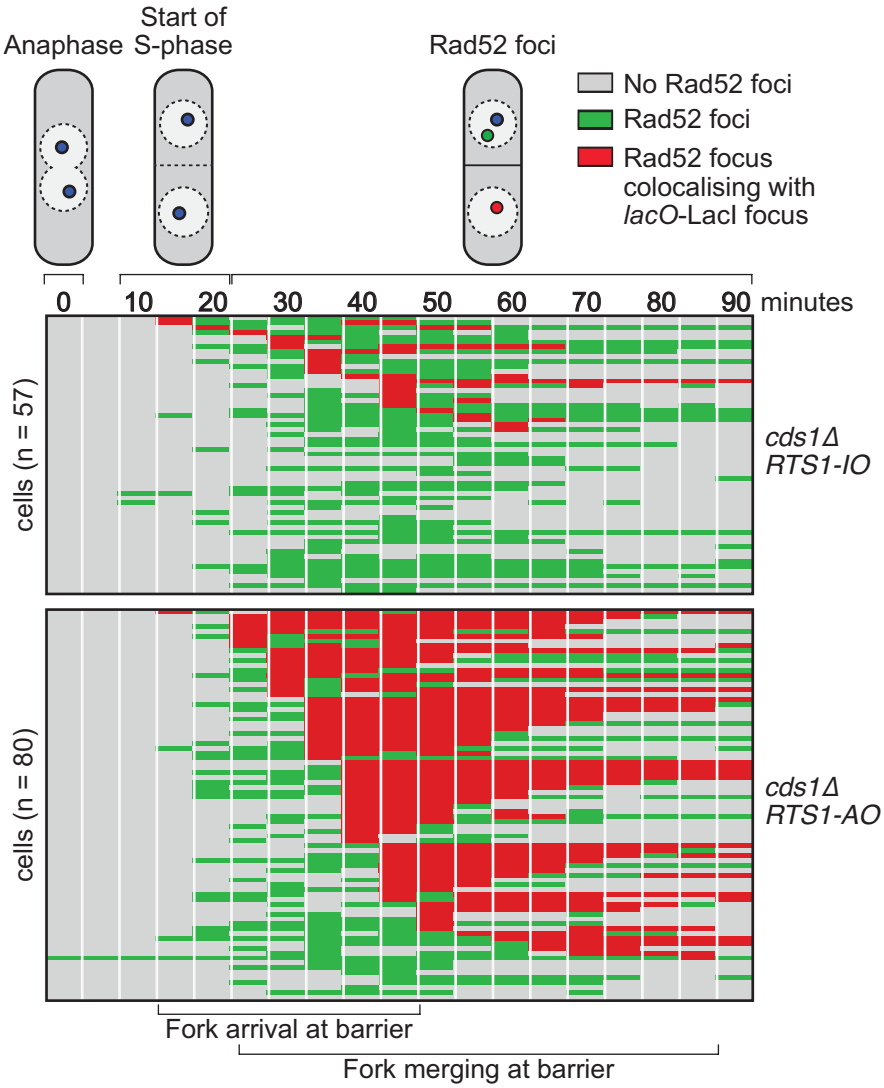


Figure S8.1 | Rad52 persists at blocked forks longer in the absence of Cds1. Analysis of time-lapse movies of *cds1Δ* cells with either *RTS1-IO* (MON190) or *RTS1-AO* (MON196).

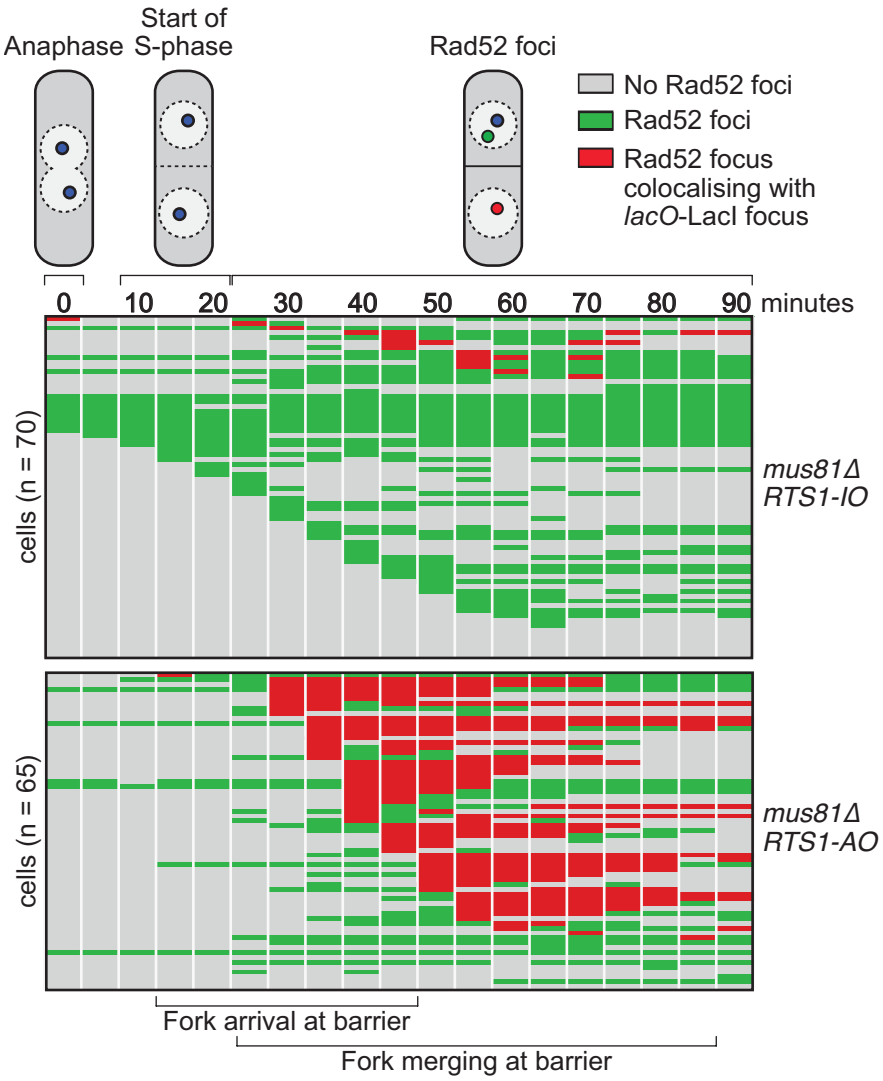


Figure S8.2 | Rad52 persists at blocked forks longer in the absence of Mus81. Analysis of time-lapse movies of *mus81Δ* cells with either *RTS1-IO* (MON307) or *RTS1-AO* (MON309).

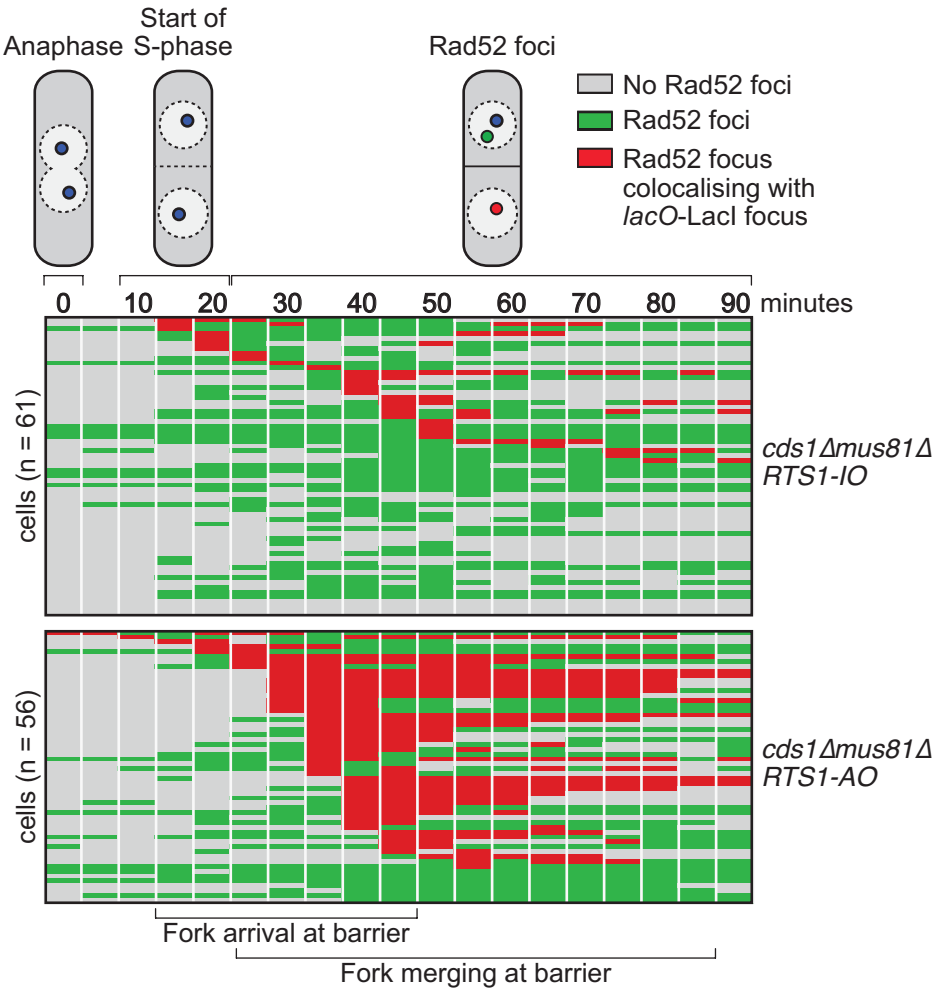


Figure S8.3 | Rad52 persists at blocked forks longer in *cds1Δmus81Δ* mutants. Analysis of time-lapse movies of *cds1Δmus81Δ* cells with either *RTS1-IO* (MON198) or *RTS1-AO* (MON202).

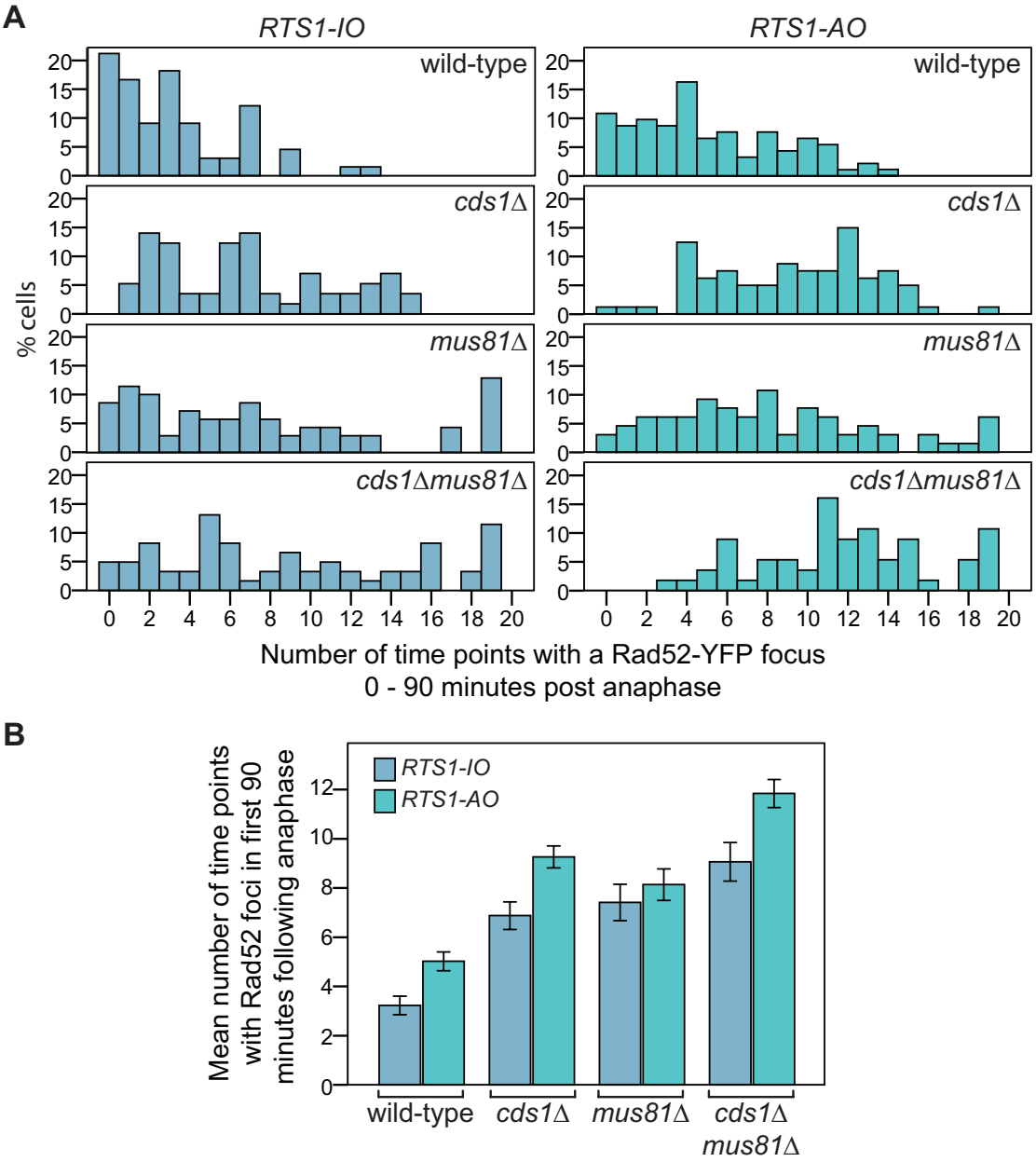


Figure S8.4 | Rad52 foci increase in the absence of *cds1* and *mus81*. (A) Histogram showing the percentage of cells with a given number of time points in which a Rad52-YFP focus is detected within the first 90 minutes following anaphase. (B) Bar chart of the mean number of time points cells display a Rad52-YFP focus in the first 90 minutes following anaphase. Error bars represent ± one standard error of the mean. The *RTS1-IO* strains are MON110 (wild-type), MON190 (*cds1Δ*), MON307 (*mus81Δ*), and MON198 (*cds1Δmus81Δ*). The *RTS1-AO* strains are MON148 (wild-type), MON196 (*cds1Δ*), MON309 (*mus81Δ*), and MON202 (*cds1Δmus81Δ*).

Bibliography

Agarwal S, van Cappellen WA, Guenole A, Eppink B, Linsen SE, Meijering E, Houtsmuller A, Kanaar R, Essers J. 2011. ATP-dependent and independent functions of Rad54 in genome maintenance. *J Cell Biol* **192**: 735-750.

Ahmad F, Stewart E. 2005. The N-terminal region of the Schizosaccharomyces pombe RecQ helicase, Rqh1p, physically interacts with Topoisomerase III and is required for Rqh1p function. *Mol Genet Genomics* **273**: 102-114.

Ahn JS, Osman F, Whitby MC. 2005. Replication fork blockage by RTS1 at an ectopic site promotes recombination in fission yeast. *Embo J* **24**: 2011-2023.

Akamatsu Y, Dziadkowiec D, Ikeguchi M, Shinagawa H, Iwasaki H. 2003. Two different Swi5-containing protein complexes are involved in mating-type switching and recombination repair in fission yeast. *Proc Natl Acad Sci U S A* **100**: 15770-15775.

Akamatsu Y, Tsutsui Y, Morishita T, Siddique MS, Kurokawa Y, Ikeguchi M, Yamao F, Arcangioli B, Iwasaki H. 2007. Fission yeast Swi5/Sfr1 and Rhp55/Rhp57 differentially regulate Rhp51-dependent recombination outcomes. *Embo J* **26**: 1352-1362.

Alexeev A, Mazin A, Kowalczykowski SC. 2003. Rad54 protein possesses chromatin-remodeling activity stimulated by the Rad51-ssDNA nucleoprotein filament. *Nat Struct Biol* **10**: 182-186.

Allers T, Lichten M. 2001. Differential timing and control of noncrossover and crossover recombination during meiosis. *Cell* **106**: 47-57.

Anand RP, Lovett ST, Haber JE. 2013. Break-induced DNA replication. *Cold Spring Harb Perspect Biol* **5**: a010397.

Andersen SL, Bergstralh DT, Kohl KP, LaRocque JR, Moore CB, Sekelsky J. 2009. Drosophila MUS312 and the vertebrate ortholog BTBD12 interact with DNA structure-specific endonucleases in DNA repair and recombination. *Mol Cell* **35**: 128-135.

Andreassen PR, D'Andrea AD, Taniguchi T. 2004. ATR couples FANCD2 monoubiquitination to the DNA-damage response. *Genes Dev* **18**: 1958-1963.

Antony E, Tomko EJ, Xiao Q, Krejci L, Lohman TM, Ellenberger T. 2009. Srs2 disassembles Rad51 filaments by a protein-protein interaction triggering ATP turnover and dissociation of Rad51 from DNA. *Mol Cell* **35**: 105-115.

Arcangioli B. 1998. A site- and strand-specific DNA break confers asymmetric switching potential in fission yeast. *Embo J* **17**: 4503-4510.

Arcangioli B, de Lahondes R. 2000. Fission yeast switches mating type by a replication-recombination coupled process. *Embo J* **19**: 1389-1396.

Aylon Y, Liefshitz B, Kupiec M. 2004. The CDK regulates repair of double-strand breaks by homologous recombination during the cell cycle. *Embo J* **23**: 4868-4875.

Azvolinsky A, Dunaway S, Torres JZ, Bessler JB, Zakian VA. 2006. The S. cerevisiae Rrm3p DNA helicase moves with the replication fork and affects replication of all yeast chromosomes. *Genes Dev* **20**: 3104-3116.

Bachrati CZ, Borts RH, Hickson ID. 2006. Mobile D-loops are a preferred substrate for the Bloom's syndrome helicase. *Nucleic Acids Res* **34**: 2269-2279.

Ball LG, Zhang K, Cobb JA, Boone C, Xiao W. 2009. The yeast Shu complex couples error-free post-replication repair to homologous recombination. *Mol Microbiol* **73**: 89-102.

Bashkirov VI, King JS, Bashkirova EV, Schmuckli-Maurer J, Heyer WD. 2000. DNA repair protein Rad55 is a terminal substrate of the DNA damage checkpoints. *Mol Cell Biol* **20**: 4393-4404.

Basi G, Schmid E, Maundrell K. 1993. TATA box mutations in the Schizosaccharomyces pombe nmt1 promoter affect transcription efficiency but not the transcription start point or thiamine repressibility. *Gene* **123**: 131-136.

Bastin-Shanower SA, Fricke WM, Mullen JR, Brill SJ. 2003. The mechanism of Mus81-Mms4 cleavage site selection distinguishes it from the homologous endonuclease Rad1-Rad10. *Mol Cell Biol* **23**: 3487-3496.

Baumann P, Benson FE, West SC. 1996. Human Rad51 protein promotes ATP-dependent homologous pairing and strand transfer reactions in vitro. *Cell* **87**: 757-766.

Bennett RJ, Noirot-Gros MF, Wang JC. 2000. Interaction between yeast Sgs1 helicase and DNA topoisomerase III. *Journal of Biological Chemistry* **275**: 26898-26905.

Bennett RJ, West SC. 1995. RuvC protein resolves Holliday junctions via cleavage of the continuous (noncrossover) strands. *Proc Natl Acad Sci U S A* **92**: 5635-5639.

Berdichevsky A, Izhar L, Livneh Z. 2002. Error-free recombinational repair predominates over mutagenic translesion replication in E. coli. *Mol Cell* **10**: 917-924.

Bernstein KA, Gangloff S, Rothstein R. 2010. The RecQ DNA helicases in DNA repair. *Annu Rev Genet* **44**: 393-417.

Bernstein KA, Reid RJ, Sunjevaric I, Demuth K, Burgess RC, Rothstein R. 2011. The Shu complex, which contains Rad51 paralogues, promotes DNA repair through inhibition of the Srs2 anti-recombinase. *Mol Biol Cell* **22**: 1599-1607.

Bertrand P, Tishkoff DX, Filosi N, Dasgupta R, Kolodner RD. 1998. Physical interaction between components of DNA mismatch repair and nucleotide excision repair. *Proc Natl Acad Sci U S A* **95**: 14278-14283.

Beuzer P, Quivy JP, Almouzni G. 2014. Establishment of a replication fork barrier following induction of DNA binding in mammalian cells. *Cell Cycle* **13**.

Bidnenko V, Ehrlich SD, Michel B. 2002. Replication fork collapse at replication terminator sequences. *Embo J* **21**: 3898-3907.

Bieche I, Lidereau R. 1995. Genetic alterations in breast cancer. *Genes Chromosomes Cancer* **14**: 227-251.

Bienko M, Green CM, Crosetto N, Rudolf F, Zapart G, Coull B, Kannouche P, Wider G, Peter M, Lehmann AR et al. 2005. Ubiquitin-binding domains in Y-family polymerases regulate translesion synthesis. *Science* **310**: 1821-1824.

Binz SK, Sheehan AM, Wold MS. 2004. Replication protein A phosphorylation and the cellular response to DNA damage. *DNA Repair (Amst)* **3**: 1015-1024.

Boddy MN, Gaillard PH, McDonald WH, Shanahan P, Yates JR, 3rd, Russell P. 2001. Mus81-Eme1 are essential components of a Holliday junction resolvase. *Cell* **107**: 537-548.

Boddy MN, Lopez-Girona A, Shanahan P, Interthal H, Heyer WD, Russell P. 2000. Damage tolerance protein Mus81 associates with the FHA1 domain of checkpoint kinase Cds1. *Mol Cell Biol* **20**: 8758-8766.

Bosco G, Haber JE. 1998. Chromosome break-induced DNA replication leads to nonreciprocal translocations and telomere capture. *Genetics* **150**: 1037-1047.

Brewer BJ, Fangman WL. 1988. A replication fork barrier at the 3' end of yeast ribosomal RNA genes. *Cell* **55**: 637-643.

Buades A, Coll B, Morel JM. 2005. A review of image denoising algorithms, with a new one. *Multiscale Model Sim* **4**: 490-530.

Bugreev DV, Hanaoka F, Mazin AV. 2007. Rad54 dissociates homologous recombination intermediates by branch migration. *Nat Struct Mol Biol* **14**: 746-753.

Bugreev DV, Mazina OM, Mazin AV. 2006. Rad54 protein promotes branch migration of Holliday junctions. *Nature* **442**: 590-593.

Bugreev DV, Rossi MJ, Mazin AV. 2011. Cooperation of RAD51 and RAD54 in regression of a model replication fork. *Nucleic Acids Res* **39**: 2153-2164.

Burma S, Chen BP, Murphy M, Kurimasa A, Chen DJ. 2001. ATM phosphorylates histone H2AX in response to DNA double-strand breaks. *J Biol Chem* **276**: 42462-42467.

Bzymek M, Thayer NH, Oh SD, Kleckner N, Hunter N. 2010. Double Holliday junctions are intermediates of DNA break repair. *Nature* **464**: 937-941.

Calzada A, Hodgson B, Kanemaki M, Bueno A, Labib K. 2005. Molecular anatomy and regulation of a stable replisome at a paused eukaryotic DNA replication fork. *Genes Dev* **19**: 1905-1919.

Carr AM, Lambert S. 2013. Replication stress-induced genome instability: the dark side of replication maintenance by homologous recombination. *J Mol Biol* **425**: 4733-4744.

Carter SD, Vigasova D, Chen J, Chovanec M, Astrom SU. 2009. Nej1 recruits the Srs2 helicase to DNA double-strand breaks and supports repair by a single-strand annealing-like mechanism. *Proc Natl Acad Sci U S A* **106**: 12037-12042.

Cavero S, Limbo O, Russell P. 2010. Critical functions of Rpa3/Ssb3 in S-phase DNA damage responses in fission yeast. *PLoS Genet* **6**: e1001138.

Cejka P, Cannavo E, Polaczek P, Masuda-Sasa T, Pokharel S, Campbell JL, Kowalczykowski SC. 2010. DNA end resection by Dna2-Sgs1-RPA and its stimulation by Top3-Rmi1 and Mre11-Rad50-Xrs2. *Nature* **467**: 112-116.

Chagin VO, Stear JH, Cardoso MC. 2010. Organization of DNA replication. *Cold Spring Harb Perspect Biol* **2**: a000737.

Chan KL, North PS, Hickson ID. 2007. BLM is required for faithful chromosome segregation and its localization defines a class of ultrafine anaphase bridges. *Embo J* **26**: 3397-3409.

Chedin F, Dervyn E, Dervyn R, Ehrlich SD, Noirot P. 1994. Frequency of deletion formation decreases exponentially with distance between short direct repeats. *Mol Microbiol* **12**: 561-569.

Chen JM, Cooper DN, Ferec C, Kehrer-Sawatzki H, Patrinos GP. 2010. Genomic rearrangements in inherited disease and cancer. *Semin Cancer Biol* **20**: 222-233.

Chen L, Nievera CJ, Lee AY, Wu X. 2008a. Cell cycle-dependent complex formation of BRCA1.CtIP.MRN is important for DNA double-strand break repair. *J Biol Chem* **283**: 7713-7720.

Chen Z, Yang H, Pavletich NP. 2008b. Mechanism of homologous recombination from the RecA-ssDNA/dsDNA structures. *Nature* **453**: 489-484.

Chi P, Kwon Y, Seong C, Epshtein A, Lam I, Sung P, Klein HL. 2006. Yeast recombination factor Rdh54 functionally interacts with the Rad51 recombinase and catalyzes Rad51 removal from DNA. *J Biol Chem* **281**: 26268-26279.

Chiolo I, Saponaro M, Baryshnikova A, Kim JH, Seo YS, Liberi G. 2007. The human F-Box DNA helicase FBH1 faces Saccharomyces cerevisiae Srs2 and postreplication repair pathway roles. *Mol Cell Biol* **27**: 7439-7450.

Ciccia A, Ling C, Coulthard R, Yan Z, Xue Y, Meetei AR, Laghmani el H, Joenje H, McDonald N, de Winter JP et al. 2007. Identification of FAAP24, a Fanconi anemia core complex protein that interacts with FANCM. *Mol Cell* **25**: 331-343.

Clever B, Interthal H, SchmuckliMaurer J, King J, Sigrist M, Heyer WD. 1997. Recombinational repair in yeast: Functional interactions between Rad51 and Rad54 proteins. *Embo Journal* **16**: 2535-2544.

Clever B, Schmuckli-Maurer J, Sigrist M, Glassner BJ, Heyer WD. 1999. Specific negative effects resulting from elevated levels of the recombinational repair protein Rad54p in Saccharomyces cerevisiae. *Yeast* **15**: 721-740.

Cobb JA, Bjergbaek L, Shimada K, Frei C, Gasser SM. 2003. DNA polymerase stabilization at stalled replication forks requires Mec1 and the RecQ helicase Sgs1. *Embo J* **22**: 4325-4336.

Codlin S, Dalgaard JZ. 2003. Complex mechanism of site-specific DNA replication termination in fission yeast. *Embo J* **22**: 3431-3440.

Cohn MA, Kowal P, Yang K, Haas W, Huang TT, Gygi SP, D'Andrea AD. 2007. A UAF1-containing multisubunit protein complex regulates the Fanconi anemia pathway. *Mol Cell* **28**: 786-797.

Constantinou A, Tarsounas M, Karow JK, Brosh RM, Bohr VA, Hickson ID, West SC. 2000. Werner's syndrome protein (WRN) migrates Holliday junctions and co-localizes with RPA upon replication arrest. *EMBO Rep* **1**: 80-84.

Cortes-Ledesma F, Aguilera A. 2006. Double-strand breaks arising by replication through a nick are repaired by cohesin-dependent sister-chromatid exchange. *EMBO Rep* **7**: 919-926.

Coulon S, Gaillard PHL, Chahwan C, McDonald WH, Yates JR, Russell P. 2004. Slx1-Slx4 are subunits of a structure-specific endonuclease that maintains ribosomal DNA in fission yeast. *Mol Biol Cell* **15**: 71-80.

Courcelle J, Donaldson JR, Chow KH, Courcelle CT. 2003. DNA damage-induced replication fork regression and processing in Escherichia coli. *Science* **299**: 1064-1067.

Cox MM. 2001. Recombinational DNA repair of damaged replication forks in Escherichia coli: questions. *Annu Rev Genet* **35**: 53-82.

Crasta K, Ganem NJ, Dagher R, Lantermann AB, Ivanova EV, Pan Y, Nezi L, Protopopov A, Chowdhury D, Pellman D. 2012. DNA breaks and chromosome pulverization from errors in mitosis. *Nature* **482**: 53-58.

Crowley DJ, Courcelle J. 2002. Answering the Call: Coping with DNA Damage at the Most Inopportune Time. *J Biomed Biotechnol* **2**: 66-74.

D'Amours D, Jackson SP. 2002. The Mre11 complex: at the crossroads of dna repair and checkpoint signalling. *Nat Rev Mol Cell Biol* **3**: 317-327.

Dalgaard JZ, Klar AJ. 1999. Orientation of DNA replication establishes mating-type switching pattern in S. pombe. *Nature* **400**: 181-184.

-. 2000. swi1 and swi3 perform imprinting, pausing, and termination of DNA replication in S. pombe. *Cell* **102**: 745-751.

-. 2001. A DNA replication-arrest site RTS1 regulates imprinting by determining the direction of replication at mat1 in S. pombe. *Genes Dev* **15**: 2060-2068.

Davis AP, Symington LS. 2001. The yeast recombinational repair protein Rad59 interacts with Rad52 and stimulates single-strand annealing. *Genetics* **159**: 515-525.

-. 2004. RAD51-dependent break-induced replication in yeast. *Mol Cell Biol* **24**: 2344-2351.

Deem A, Keszthelyi A, Blackgrove T, Vayl A, Coffey B, Mathur R, Chabes A, Malkova A. 2011. Break-Induced Replication Is Highly Inaccurate. *Plos Biol* **9**.

Delviks KA, Pathak VK. 1999. Effect of distance between homologous sequences and 3' homology on the frequency of retroviral reverse transcriptase template switching. *J Virol* **73**: 7923-7932.

DiNardo S, Voelkel K, Sternglanz R. 1984. DNA topoisomerase II mutant of Saccharomyces cerevisiae: topoisomerase II is required for segregation of daughter molecules at the termination of DNA replication. *Proc Natl Acad Sci U S A* **81**: 2616-2620.

Doe CL, Ahn JS, Dixon J, Whitby MC. 2002. Mus81-Eme1 and Rqh1 involvement in processing stalled and collapsed replication forks. *J Biol Chem* **277**: 32753-32759.

Doe CL, Osman F, Dixon J, Whitby MC. 2004. DNA repair by a Rad22-Mus81-dependent pathway that is independent of Rhp51. *Nucleic Acids Res* **32**: 5570-5581.

Donnianni RA, Symington LS. 2013. Break-induced replication occurs by conservative DNA synthesis. *Proc Natl Acad Sci U S A* **110**: 13475-13480.

Downs JA, Lowndes NF, Jackson SP. 2000. A role for Saccharomyces cerevisiae histone H2A in DNA repair. *Nature* **408**: 1001-1004.

Dubarry M, Loiodice I, Chen CL, Thermes C, Taddei A. 2011. Tight protein-DNA interactions favor gene silencing. *Genes Dev* **25**: 1365-1370.

Dupaigne P, Le Breton C, Fabre F, Gangloff S, Le Cam E, Veaute X. 2008. The Srs2 helicase activity is stimulated by Rad51 filaments on dsDNA: Implications for crossover incidence during mitotic recombination. *Mol Cell* **29**: 243-254.

Egel R. 2005. Fission yeast mating-type switching: programmed damage and repair. *DNA Repair (Amst)* **4**: 525-536.

Egel R, Beach DH, Klar AJ. 1984. Genes required for initiation and resolution steps of mating-type switching in fission yeast. *Proc Natl Acad Sci U S A* **81**: 3481-3485.

Eggler AL, Inman RB, Cox MM. 2002. The Rad51-dependent pairing of long DNA substrates is stabilized by replication protein A. *J Biol Chem* **277**: 39280-39288.

El-Shemerly M, Hess D, Pyakurel AK, Moselhy S, Ferrari S. 2008. ATR-dependent pathways control hEXO1 stability in response to stalled forks. *Nucleic Acids Res* **36**: 511-519.

Ellermeier C, Schmidt H, Smith GR. 2004. Swi5 acts in meiotic DNA joint molecule formation in Schizosaccharomyces pombe. *Genetics* **168**: 1891-1898.

Ellis NA, Groden J, Ye TZ, Straughen J, Lennon DJ, Ciocci S, Proytcheva M, German J. 1995. The Blooms-Syndrome Gene-Product Is Homologous to Recq Helicases. *Cell* **83**: 655-666.

Esta A, Ma E, Dupaigne P, Maloisel L, Guerois R, Le Cam E, Veaute X, Coic E. 2013. Rad52 sumoylation prevents the toxicity of unproductive Rad51 filaments independently of the anti-recombinase Srs2. *PLoS Genet* **9**: e1003833.

Eydmann T, Sommariva E, Inagawa T, Mian S, Klar AJ, Dalgaard JZ. 2008. Rtf1-mediated eukaryotic site-specific replication termination. *Genetics* **180**: 27-39.

Falcon CM, Matthews KS. 1999. Glycine insertion in the hinge region of lactose repressor protein alters DNA binding. *J Biol Chem* **274**: 30849-30857.

Fekairi S, Scaglione S, Chahwan C, Taylor ER, Tissier A, Coulon S, Dong MQ, Ruse C, Yates JR, Russell P et al. 2009. Human SLX4 Is a Holliday Junction Resolvase Subunit that Binds Multiple DNA Repair/Recombination Endonucleases. *Cell* **138**: 78-89.

Feng W, Collingwood D, Boeck ME, Fox LA, Alvino GM, Fangman WL, Raghuraman MK, Brewer BJ. 2006. Genomic mapping of single-stranded DNA in hydroxyurea-challenged yeasts identifies origins of replication. *Nat Cell Biol* **8**: 148-155.

Feng Z, Scott SP, Bussen W, Sharma GG, Guo G, Pandita TK, Powell SN. 2011. Rad52 inactivation is synthetically lethal with BRCA2 deficiency. *Proc Natl Acad Sci U S A* **108**: 686-691.

Fishmanlobell J, Haber JE. 1992. Removal of Nonhomologous DNA Ends in Double-Strand Break Recombination - the Role of the Yeast Ultraviolet Repair Gene Rad1. *Science* **258**: 480-484.

Forget AL, Kowalczykowski SC. 2012. Single-molecule imaging of DNA pairing by RecA reveals a three-dimensional homology search. *Nature* **482**: 423-427.

Forment JV, Blasius M, Guerini I, Jackson SP. 2011. Structure-specific DNA endonuclease Mus81/Eme1 generates DNA damage caused by Chk1 inactivation. *PLoS One* **6**: e23517.

Formosa T, Alberts BM. 1986. DNA synthesis dependent on genetic recombination: characterization of a reaction catalyzed by purified bacteriophage T4 proteins. *Cell* **47**: 793-806.

Forsburg SL. 1993. Comparison of Schizosaccharomyces pombe expression systems. *Nucleic Acids Res* **21**: 2955-2956.

Fortin GS, Symington LS. 2002. Mutations in yeast Rad51 that partially bypass the requirement for Rad55 and Rad57 in DNA repair by increasing the stability of Rad51-DNA complexes. *Embo Journal* **21**: 3160-3170.

Fricke WM, Brill SJ. 2003. Slx1-Slx4 is a second structure-specific endonuclease functionally redundant with Sgs1-Top3. *Genes Dev* **17**: 1768-1778.

Froget B, Blaisonneau J, Lambert S, Baldacci G. 2008. Cleavage of stalled forks by fission yeast Mus81/Eme1 in absence of DNA replication checkpoint. *Mol Biol Cell* **19**: 445-456.

Furnari B, Blasina A, Boddy MN, McGowan CH, Russell P. 1999. Cdc25 inhibited in vivo and in vitro by checkpoint kinases Cds1 and Chk1. *Mol Biol Cell* **10**: 833-845.

Furuse M, Nagase Y, Tsubouchi H, Murakami-Murofushi K, Shibata T, Ohta K. 1998. Distinct roles of two separable in vitro activities of yeast Mre11 in mitotic and meiotic recombination. *Embo J* **17**: 6412-6425.

Garcia V, Phelps SE, Gray S, Neale MJ. 2011. Bidirectional resection of DNA double-strand breaks by Mre11 and Exo1. *Nature* **479**: 241-244.

Garcia-Higuera I, Taniguchi T, Ganesan S, Meyn MS, Timmers C, Hejna J, Grompe M, D'Andrea AD. 2001. Interaction of the Fanconi anemia proteins and BRCA1 in a common pathway. *Mol Cell* **7**: 249-262.

Gari K, Decaillet C, Delannoy M, Wu L, Constantinou A. 2008a. Remodeling of DNA replication structures by the branch point translocase FANCM. *Proc Natl Acad Sci U S A* **105**: 16107-16112.

Gari K, Decaillet C, Stasiak AZ, Stasiak A, Constantinou A. 2008b. The Fanconi anemia protein FANCM can promote branch migration of Holliday junctions and replication forks. *Mol Cell* **29**: 141-148.

Gasior SL, Olivares H, Ear U, Hari DM, Weichselbaum R, Bishop DK. 2001. Assembly of RecA-like recombinases: distinct roles for mediator proteins in mitosis and meiosis. *Proc Natl Acad Sci U S A* **98**: 8411-8418.

Gerber JK, Gogel E, Berger C, Wallisch M, Muller F, Grummt I, Grummt F. 1997. Termination of mammalian rDNA replication: polar arrest of replication fork movement by transcription termination factor TTF-I. *Cell* **90**: 559-567.

Gilbertson LA, Stahl FW. 1996. A test of the double-strand break repair model for meiotic recombination in Saccharomyces cerevisiae. *Genetics* **144**: 27-41.

Godin S, Wier A, Kabbinavar F, Bratton-Palmer DS, Ghodke H, Van Houten B, VanDemark AP, Bernstein KA. 2013. The Shu complex interacts with Rad51 through the Rad51 paralogues Rad55-Rad57 to mediate error-free recombination. *Nucleic Acids Res* **41**: 4525-4534.

Gotta SL, Miller OL, Jr., French SL. 1991. rRNA transcription rate in Escherichia coli. *J Bacteriol* **173**: 6647-6649.

Gray MD, Shen JC, KamathLoeb AS, Blank A, Sopher BL, Martin GM, Oshima J, Loeb LA. 1997. The Werner syndrome protein is a DNA helicase. *Nat Genet* **17**: 100-103.

Greenfeder SA, Newlon CS. 1992. Replication forks pause at yeast centromeres. *Mol Cell Biol* **12**: 4056-4066.

Grimme JM, Honda M, Wright R, Okuno Y, Rothenberg E, Mazin AV, Ha T, Spies M. 2010. Human Rad52 binds and wraps single-stranded DNA and mediates annealing via two hRad52-ssDNA complexes. *Nucleic Acids Res* **38**: 2917-2930.

Gupta MK, Guy CP, Yeeles JT, Atkinson J, Bell H, Lloyd RG, Marians KJ, McGlynn P. 2013. Protein-DNA complexes are the primary sources of replication fork pausing in Escherichia coli. *Proc Natl Acad Sci U S A* **110**: 7252-7257.

Haber JE. 1998. Mating-type gene switching in Saccharomyces cerevisiae. *Annu Rev Genet* **32**: 561-599.

-. 1999. DNA recombination: the replication connection. *Trends Biochem Sci* **24**: 271-275.

Halazonetis TD, Gorgoulis VG, Bartek J. 2008. An oncogene-induced DNA damage model for cancer development. *Science* **319**: 1352-1355.

Hamann U, Herbold C, Costa S, Solomayer EF, Kaufmann M, Bastert G, Ulmer HU, Frenzel H, Komitowski D. 1996. Allelic imbalance on chromosome 13q: evidence for the involvement of BRCA2 and RB1 in sporadic breast cancer. *Cancer Res* **56**: 1988-1990.

Hanada K, Budzowska M, Davies SL, van Drunen E, Onizawa H, Beverloo HB, Maas A, Essers J, Hickson ID, Kanaar R. 2007. The structure-specific endonuclease Mus81 contributes to replication restart by generating double-strand DNA breaks. *Nat Struct Mol Biol* **14**: 1096-1104.

Haracska L, Kondratick CM, Unk I, Prakash S, Prakash L. 2001. Interaction with PCNA is essential for yeast DNA polymerase eta function. *Mol Cell* **8**: 407-415.

Harper JV, Anderson JA, O'Neill P. 2010. Radiation induced DNA DSBs: Contribution from stalled replication forks? *DNA Repair (Amst)* **9**: 907-913.

Hartsuiker E, Neale MJ, Carr AM. 2009. Distinct requirements for the Rad32(Mre11) nuclease and Ctp1(CtIP) in the removal of covalently bound topoisomerase I and II from DNA. *Mol Cell* **33**: 117-123.

Haruta N, Kurokawa Y, Murayama Y, Akamatsu Y, Unzai S, Tsutsui Y, Iwasaki H. 2006. The Swi5-Sfr1 complex stimulates Rhp51/Rad51- and Dmc1-mediated DNA strand exchange in vitro. *Nat Struct Mol Biol* **13**: 823-830.

Hashimoto Y, Puddu F, Costanzo V. 2012. RAD51- and MRE11-dependent reassembly of uncoupled CMG helicase complex at collapsed replication forks. *Nat Struct Mol Biol* **19**: 17-24.

Hashimoto Y, Ray Chaudhuri A, Lopes M, Costanzo V. 2010. Rad51 protects nascent DNA from Mre11-dependent degradation and promotes continuous DNA synthesis. *Nat Struct Mol Biol* **17**: 1305-1311.

Hawkins M, Malla S, Blythe MJ, Nieduszynski CA, Allers T. 2013. Accelerated growth in the absence of DNA replication origins. *Nature* **503**: 544-547.

Hayano M, Kanoh Y, Matsumoto S, Renard-Guillet C, Shirahige K, Masai H. 2012. Rif1 is a global regulator of timing of replication origin firing in fission yeast. *Genes Dev* **26**: 137-150.

Hayase A, Takagi M, Miyazaki T, Oshiumi H, Shinohara M, Shinohara A. 2004. A protein complex containing Mei5 and Sae3 promotes the assembly of the meiosis-specific RecA homolog Dmc1. *Cell* **119**: 927-940.

Hayashi M, Katou Y, Itoh T, Tazumi A, Yamada Y, Takahashi T, Nakagawa T, Shirahige K, Masukata H. 2007. Genome-wide localization of pre-RC sites and identification of replication origins in fission yeast. *Embo J* **26**: 1327-1339.

Hays SL, Firmenich AA, Berg P. 1995. Complex-Formation in Yeast Double-Strand Break Repair - Participation of Rad51, Rad52, Rad55, and Rad57 Proteins. *Proc Natl Acad Sci U S A* **92**: 6925-6929.

Hays SL, Firmenich AA, Massey P, Banerjee R, Berg P. 1998. Studies of the interaction between Rad52 protein and the yeast single-stranded DNA binding protein RPA. *Mol Cell Biol* **18**: 4400-4406.

Heichinger C, Penkett CJ, Bahler J, Nurse P. 2006. Genome-wide characterization of fission yeast DNA replication origins. *Embo J* **25**: 5171-5179.

Herzberg K, Bashkirov VI, Rolfsmeier M, Haghnazari E, McDonald WH, Anderson S, Bashkirova EV, Yates JR, 3rd, Heyer WD. 2006. Phosphorylation of Rad55 on serines 2, 8, and 14 is required for efficient homologous recombination in the recovery of stalled replication forks. *Mol Cell Biol* **26**: 8396-8409.

Heyer WD, Ehmsen KT, Liu J. 2010. Regulation of homologous recombination in eukaryotes. *Annu Rev Genet* **44**: 113-139.

Heyer WD, Li X, Rolfsmeier M, Zhang XP. 2006. Rad54: the Swiss Army knife of homologous recombination? *Nucleic Acids Res* **34**: 4115-4125.

Hiasa H, DiGate RJ, Marians KJ. 1994. Decatenating activity of Escherichia coli DNA gyrase and topoisomerases I and III during oriC and pBR322 DNA replication in vitro. *J Biol Chem* **269**: 2093-2099.

Hiasa H, Marians KJ. 1994. Tus prevents overreplication of oriC plasmid DNA. *J Biol Chem* **269**: 26959-26968.

Higgins NP, Kato K, Strauss B. 1976. A model for replication repair in mammalian cells. *J Mol Biol* **101**: 417-425.

Hill TM, Marians KJ. 1990. Escherichia coli Tus protein acts to arrest the progression of DNA replication forks in vitro. *Proc Natl Acad Sci U S A* **87**: 2481-2485.

Hinz JM. 2010. Role of homologous recombination in DNA interstrand crosslink repair. *Environ Mol Mutagen* **51**: 582-603.

Hirose S, Hiraga S, Okazaki T. 1983. Initiation site of deoxyribonucleotide polymerization at the replication origin of the Escherichia coli chromosome. *Mol Gen Genet* **189**: 422-431.

Hoege C, Pfander B, Moldovan GL, Pyrowolakis G, Jentsch S. 2002. RAD6-dependent DNA repair is linked to modification of PCNA by ubiquitin and SUMO. *Nature* **419**: 135-141.

Hoffelder DR, Luo L, Burke NA, Watkins SC, Gollin SM, Saunders WS. 2004. Resolution of anaphase bridges in cancer cells. *Chromosoma* **112**: 389-397.

Hofmann RM, Pickart CM. 1999. Noncanonical MMS2-encoded ubiquitin-conjugating enzyme functions in assembly of novel polyubiquitin chains for DNA repair. *Cell* **96**: 645-653.

Holmes AM, Kaykov A, Arcangioli B. 2005. Molecular and cellular dissection of mating-type switching steps in Schizosaccharomyces pombe. *Mol Cell Biol* **25**: 303-311.

Hope JC, Cruzata LD, Duvshani A, Mitsumoto J, Maftahi M, Freyer GA. 2007. Mus81-Eme1-dependent and -independent crossovers form in mitotic cells during double-strand break repair in Schizosaccharomyces pombe. *Mol Cell Biol* **27**: 3828-3838.

Horiuchi T, Fujimura Y. 1995. Recombinational rescue of the stalled DNA replication fork: a model based on analysis of an Escherichia coli strain with a chromosome region difficult to replicate. *J Bacteriol* **177**: 783-791.

Howlett NG, Taniguchi T, Olson S, Cox B, Waisfisz Q, De Die-Smulders C, Persky N, Grompe M, Joenje H, Pals G et al. 2002. Biallelic inactivation of BRCA2 in Fanconi anemia. *Science* **297**: 606-609.

Hu J, Sun L, Shen F, Chen Y, Hua Y, Liu Y, Zhang M, Hu Y, Wang Q, Xu W et al. 2012. The intra-S phase checkpoint targets Dna2 to prevent stalled replication forks from reversing. *Cell* **149**: 1221-1232.

Huang J, Liu S, Bellani MA, Thazhathveetil AK, Ling C, de Winter JP, Wang Y, Wang W, Seidman MM. 2013. The DNA translocase FANCM/MHF promotes replication traverse of DNA interstrand crosslinks. *Mol Cell* **52**: 434-446.

Huang TT, Nijman SM, Mirchandani KD, Galardy PJ, Cohn MA, Haas W, Gygi SP, Ploegh HL, Bernards R, D'Andrea AD. 2006. Regulation of monoubiquitinated PCNA by DUB autocleavage. *Nat Cell Biol* **8**: 339-347.

Huertas P, Cortes-Ledesma F, Sartori AA, Aguilera A, Jackson SP. 2008. CDK targets Sae2 to control DNA-end resection and homologous recombination. *Nature* **455**: 689-692.

Huertas P, Jackson SP. 2009. Human CtIP mediates cell cycle control of DNA end resection and double strand break repair. *J Biol Chem* **284**: 9558-9565.

Hyppa RW, Smith GR. 2009. Using Schizosaccharomyces pombe meiosis to analyze DNA recombination intermediates. *Methods Mol Biol* **557**: 235-252.

Inagawa T, Yamada-Inagawa T, Eydmann T, Mian IS, Wang TS, Dalgaard JZ. 2009. Schizosaccharomyces pombe Rtf2 mediates site-specific replication termination by inhibiting replication restart. *Proc Natl Acad Sci U S A* **106**: 7927-7932.

Ip SCY, Rass U, Blanco MG, Flynn HR, Skehel JM, West SC. 2008. Identification of Holliday junction resolvases from humans and yeast. *Nature* **456**: 357-U339.

Ira G, Malkova A, Liberi G, Foiani M, Haber JE. 2003. Srs2 and Sgs1-Top3 suppress crossovers during double-strand break repair in yeast. *Cell* **115**: 401-411.

Ira G, Pellicioli A, Balijja A, Wang X, Fiorani S, Carotenuto W, Liberi G, Bressan D, Wan L, Hollingsworth NM et al. 2004. DNA end resection, homologous recombination and DNA damage checkpoint activation require CDK1. *Nature* **431**: 1011-1017.

Iraqui I, Chekkal Y, Jmari N, Pietrobon V, Freon K, Costes A, Lambert SA. 2012. Recovery of arrested replication forks by homologous recombination is error-prone. *PLoS Genet* **8**: e1002976.

Ivessa AS, Lenzmeier BA, Bessler JB, Goudsouzian LK, Schnakenberg SL, Zakian VA. 2003. The Saccharomyces cerevisiae helicase Rrm3p facilitates replication past nonhistone protein-DNA complexes. *Mol Cell* **12**: 1525-1536.

Ivessa AS, Zhou JQ, Schulz VP, Monson EK, Zakian VA. 2002. Saccharomyces Rrm3p, a 5' to 3' DNA helicase that promotes replication fork progression through telomeric and subtelomeric DNA. *Genes Dev* **16**: 1383-1396.

Iwasaki H, Takahagi M, Shiba T, Nakata A, Shinagawa H. 1991. Escherichia-Coli Ruvc Protein Is an Endonuclease That Resolves the Holliday Structure. *Embo Journal* **10**: 4381-4389.

Jacome A, Fernandez-Capetillo O. 2011. Lac operator repeats generate a traceable fragile site in mammalian cells. *EMBO Rep* **12**: 1032-1038.

Jain S, Sugawara N, Lydeard J, Vaze M, Tanguy Le Gac N, Haber JE. 2009. A recombination execution checkpoint regulates the choice of homologous recombination pathway during DNA double-strand break repair. *Genes Dev* **23**: 291-303.

Janion C. 2008. Inducible SOS response system of DNA repair and mutagenesis in Escherichia coli. *Int J Biol Sci* **4**: 338-344.

Janke R, Herzberg K, Rolfsmeier M, Mar J, Bashkirov VI, Haghnazari E, Cantin G, Yates JR, 3rd, Heyer WD. 2010. A truncated DNA-damage-

signaling response is activated after DSB formation in the G1 phase of Saccharomyces cerevisiae. *Nucleic Acids Res* **38**: 2302-2313.

Jensen RB, Carreira A, Kowalczykowski SC. 2010. Purified human BRCA2 stimulates RAD51-mediated recombination. *Nature* **467**: 678-683.

Jia S, Yamada T, Grewal SI. 2004. Heterochromatin regulates cell type-specific long-range chromatin interactions essential for directed recombination. *Cell* **119**: 469-480.

Johnson RD, Symington LS. 1995. Functional Differences and Interactions among the Putative Reca Homologs Rad51, Rad55, and Rad57. *Mol Cell Biol* **15**: 4843-4850.

Kagawa W, Kurumizaka H, Ishitani R, Fukai S, Nureki O, Shibata T, Yokoyama S. 2002. Crystal structure of the homologous-pairing domain from the human Rad52 recombinase in the undecameric form. *Mol Cell* **10**: 359-371.

Kai M, Boddy MN, Russell P, Wang TS. 2005. Replication checkpoint kinase Cds1 regulates Mus81 to preserve genome integrity during replication stress. *Genes Dev* **19**: 919-932.

Kang HY, Choi E, Bae SH, Lee KH, Gim BS, Kim HD, Park C, MacNeill SA, Seo YS. 2000. Genetic analyses of Schizosaccharomyces pombe dna2(+) reveal that dna2 plays an essential role in Okazaki fragment metabolism. *Genetics* **155**: 1055-1067.

Kans JA, Mortimer RK. 1991. Nucleotide-Sequence of the Rad57 Gene of Saccharomyces-Cerevisiae. *Gene* **105**: 139-140.

Kappeler M, Kranz E, Woolcock K, Georgiev O, Schaffner W. 2008. Drosophila bloom helicase maintains genome integrity by inhibiting recombination between divergent DNA sequences. *Nucleic Acids Res* **36**: 6907-6917.

Karow JK, Constantinou A, Li JL, West SC, Hickson ID. 2000. The Bloom's syndrome gene product promotes branch migration of Holliday junctions. *Proc Natl Acad Sci U S A* **97**: 6504-6508.

Kennedy RD, D'Andrea AD. 2005. The Fanconi Anemia/BRCA pathway: new faces in the crowd. *Genes Dev* **19**: 2925-2940.

Khasanov FK, Salakhova AF, Chepurnaja OV, Korolev VG, Bashkirov VI. 2004. Identification and characterization of the rlp1+, the novel Rad51 paralog in the fission yeast Schizosaccharomyces pombe. *DNA Repair (Amst)* **3**: 1363-1374.

Khasanov FK, Savchenko GV, Bashkirova EV, Korolev VG, Heyer WD, Bashkirov VI. 1999. A new recombinational DNA repair gene from Schizosaccharomyces pombe with homology to Escherichia coli RecA. *Genetics* **152**: 1557-1572.

Khatri GS, MacAllister T, Sista PR, Bastia D. 1989. The replication terminator protein of E. coli is a DNA sequence-specific contra-helicase. *Cell* **59**: 667-674.

Kim SM, Huberman JA. 2001. Regulation of replication timing in fission yeast. *Embo J* **20**: 6115-6126.

Kim WJ, Lee S, Park MS, Jang YK, Kim JB, Park SD. 2000. Rad22 protein, a rad52 homologue in Schizosaccharomyces pombe, binds to DNA double-strand breaks. *J Biol Chem* **275**: 35607-35611.

Kitamura E, Blow JJ, Tanaka TU. 2006. Live-cell imaging reveals replication of individual replicons in eukaryotic replication factories. *Cell* **125**: 1297-1308.

Kitao S, Shimamoto A, Goto M, Miller RW, Smithson WA, Lindor NM, Furuichi Y. 1999. Mutations in RECQL4 cause a subset of cases of Rothmund-Thomson syndrome. *Nat Genet* **22**: 82-84.

Klapstein K, Chou T, Bruinsma R. 2004. Physics of RecA-mediated homologous recognition. *Biophys J* **87**: 1466-1477.

Klar AJ. 1990. The developmental fate of fission yeast cells is determined by the pattern of inheritance of parental and grandparental DNA strands. *Embo J* **9**: 1407-1415.

Kogoma T. 1997. Stable DNA replication: Interplay between DNA replication, homologous recombination, and transcription. *Microbiol Mol Biol R* **61**: 212-&.

Kommajosyula N, Rhind N. 2006. Cdc2 tyrosine phosphorylation is not required for the S-phase DNA damage checkpoint in fission yeast. *Cell Cycle* **5**: 2495-2500.

Krejci L, Altmannova V, Spirek M, Zhao X. 2012. Homologous recombination and its regulation. *Nucleic Acids Res* **40**: 5795-5818.

Krejci L, Van Komen S, Li Y, Villemain J, Reddy MS, Klein H, Ellenberger T, Sung P. 2003. DNA helicase Srs2 disrupts the Rad51 presynaptic filament. *Nature* **423**: 305-309.

Kreuzer KN. 2000. Recombination-dependent DNA replication in phage T4. *Trends Biochem Sci* **25**: 165-173.

Kreuzer KN, Brister JR. 2010. Initiation of bacteriophage T4 DNA replication and replication fork dynamics: a review in the Virology Journal series on bacteriophage T4 and its relatives. *Virol J* **7**: 358.

Krings G, Bastia D. 2004. swi1- and swi3-dependent and independent replication fork arrest at the ribosomal DNA of Schizosaccharomyces pombe. *Proc Natl Acad Sci U S A* **101**: 14085-14090.

Krogh BO, Llorente B, Lam A, Symington LS. 2005. Mutations in Mre11 phosphoesterase motif I that impair Saccharomyces cerevisiae Mre11-Rad50-Xrs2 complex stability in addition to nuclease activity. *Genetics* **171**: 1561-1570.

Kurokawa Y, Murayama Y, Haruta-Takahashi N, Urabe I, Iwasaki H. 2008. Reconstitution of DNA strand exchange mediated by Rhp51 recombinase and two mediators. *Plos Biol* **6**: e88.

Kuwabara N, Murayama Y, Hashimoto H, Kokabu Y, Ikeguchi M, Sato M, Mayanagi K, Tsutsui Y, Iwasaki H, Shimizu T. 2012. Mechanistic insights into the activation of Rad51-mediated strand exchange from the structure of a recombination activator, the Swi5-Sfr1 complex. *Structure* **20**: 440-449.

Labib K, Hodgson B. 2007. Replication fork barriers: pausing for a break or stalling for time? *EMBO Rep* **8**: 346-353.

Lambert S, Carr AM. 2005. Checkpoint responses to replication fork barriers. *Biochimie* **87**: 591-602.

-. 2013. Impediments to replication fork movement: stabilisation, reactivation and genome instability. *Chromosoma* **122**: 33-45.

Lambert S, Froget B, Carr AM. 2007. Arrested replication fork processing: interplay between checkpoints and recombination. *DNA Repair (Amst)* **6**: 1042-1061.

Lambert S, Mizuno K, Blaisonneau J, Martineau S, Chanet R, Freon K, Murray JM, Carr AM, Baldacci G. 2010. Homologous recombination restarts blocked replication forks at the expense of genome rearrangements by template exchange. *Mol Cell* **39**: 346-359.

Lambert S, Watson A, Sheedy DM, Martin B, Carr AM. 2005. Gross chromosomal rearrangements and elevated recombination at an inducible site-specific replication fork barrier. *Cell* **121**: 689-702.

Langerak P, Mejia-Ramirez E, Limbo O, Russell P. 2011. Release of Ku and MRN from DNA ends by Mre11 nuclease activity and Ctp1 is required for homologous recombination repair of double-strand breaks. *PLoS Genet* **7**: e1002271.

Langston LD, O'Donnell M. 2006. DNA replication: keep moving and don't mind the gap. *Mol Cell* **23**: 155-160.

Lao JP, Oh SD, Shinohara M, Shinohara A, Hunter N. 2008. Rad52 promotes postinvasion steps of meiotic double-strand-break repair. *Mol Cell* **29**: 517-524.

Larsen NB, Sass E, Suski C, Mankouri HW, Hickson ID. 2014. The Escherichia coli Tus-Ter replication fork barrier causes site-specific DNA replication perturbation in yeast. *Nat Commun* **5**: 3574.

Lau IF, Filipe SR, Soballe B, Okstad OA, Barre FX, Sherratt DJ. 2003. Spatial and temporal organization of replicating Escherichia coli chromosomes. *Mol Microbiol* **49**: 731-743.

Laursen LV, Ampatzidou E, Andersen AH, Murray JM. 2003. Role for the fission yeast RecQ helicase in DNA repair in G2. *Mol Cell Biol* **23**: 3692-3705.

Le S, Moore JK, Haber JE, Greider CW. 1999. RAD50 and RAD51 define two pathways that collaborate to maintain telomeres in the absence of telomerase. *Genetics* **152**: 143-152.

Li X, Heyer WD. 2009. RAD54 controls access to the invading 3'-OH end after RAD51-mediated DNA strand invasion in homologous recombination in Saccharomyces cerevisiae. *Nucleic Acids Res* **37**: 638-646.

Lim DS, Hasty P. 1996. A mutation in mouse rad51 results in an early embryonic lethal that is suppressed by a mutation in p53. *Mol Cell Biol* **16**: 7133-7143.

Limbo O, Chahwan C, Yamada Y, de Bruin RA, Wittenberg C, Russell P. 2007. Ctp1 is a cell-cycle-regulated protein that functions with Mre11 complex to control double-strand break repair by homologous recombination. *Mol Cell* **28**: 134-146.

Lin FL, Sperle K, Sternberg N. 1984. Model for Homologous Recombination during Transfer of DNA into Mouse L-Cells - Role for DNA Ends in the Recombination Process. *Mol Cell Biol* **4**: 1020-1034.

Lisby M, Barlow JH, Burgess RC, Rothstein R. 2004. Choreography of the DNA damage response: Spatiotemporal relationships among checkpoint and repair proteins. *Cell* **118**: 699-713.

Lisby M, Mortensen UH, Rothstein R. 2003. Colocalization of multiple DNA double-strand breaks at a single Rad52 repair centre. *Nat Cell Biol* **5**: 572-577.

Lisby M, Rothstein R, Mortensen UH. 2001. Rad52 forms DNA repair and recombination centers during S phase. *Proc Natl Acad Sci U S A* **98**: 8276-8282.

Liu J, Ehmsen KT, Heyer WD, Morrical SW. 2011a. Presynaptic filament dynamics in homologous recombination and DNA repair. *Crit Rev Biochem Mol Biol* **46**: 240-270.

Liu J, Marians KJ. 1999. PriA-directed assembly of a primosome on D loop DNA. *J Biol Chem* **274**: 25033-25041.

Liu J, Morrical SW. 2010. Assembly and dynamics of the bacteriophage T4 homologous recombination machinery. *Virol J* **7**: 357.

Liu J, Renault L, Veaute X, Fabre F, Stahlberg H, Heyer WD. 2011b. Rad51 paralogues Rad55-Rad57 balance the antirecombinase Srs2 in Rad51 filament formation. *Nature* **479**: 245-248.

Liu JI, Xu LW, Sandler SJ, Marians KJ. 1999a. Replication fork assembly at recombination intermediates is required for bacterial growth. *Proc Natl Acad Sci U S A* **96**: 3552-3555.

Liu VF, Bhaumik D, Wang TSF. 1999b. Mutator phenotype induced by aberrant replication. *Mol Cell Biol* **19**: 1126-1135.

Lobachev K, Vitriol E, Stemple J, Resnick MA, Bloom K. 2004. Chromosome fragmentation after induction of a double-strand break is an active process prevented by the RMX repair complex. *Curr Biol* **14**: 2107-2112.

London TB, Barber LJ, Mosedale G, Kelly GP, Balasubramanian S, Hickson ID, Boulton SJ, Hiom K. 2008. FANCJ is a structure-specific DNA helicase associated with the maintenance of genomic G/C tracts. *J Biol Chem* **283**: 36132-36139.

Lopes M, Cotta-Ramusino C, Pellicioli A, Liberi G, Plevani P, Muzi-Falconi M, Newlon CS, Foiani M. 2001. The DNA replication checkpoint response stabilizes stalled replication forks. *Nature* **412**: 557-561.

Lopes M, Foiani M, Sogo JM. 2006. Multiple mechanisms control chromosome integrity after replication fork uncoupling and restart at irreparable UV lesions. *Mol Cell* **21**: 15-27.

Lorenz A, Osman F, Folkyte V, Sofueva S, Whitby MC. 2009. Fbh1 Limits Rad51-Dependent Recombination at Blocked Replication Forks. *Mol Cell Biol* **29**: 4742-4756.

Lorenz A, Osman F, Sun W, Nandi S, Steinacher R, Whitby MC. 2012. The fission yeast FANCM ortholog directs non-crossover recombination during meiosis. *Science* **336**: 1585-1588.

Lovett ST. 1994. Sequence of the Rad55 Gene of Saccharomyces-Cerevisiae - Similarity of Rad55 to Prokaryotic Reca and Other Reca-Like Proteins. *Gene* **142**: 103-106.

Lovett ST, Gluckman TJ, Simon PJ, Sutera VA, Jr., Drapkin PT. 1994. Recombination between repeats in Escherichia coli by a recA-independent, proximity-sensitive mechanism. *Mol Gen Genet* **245**: 294-300.

Lovett ST, Mortimer RK. 1987. Characterization of null mutants of the RAD55 gene of Saccharomyces cerevisiae: effects of temperature, osmotic strength and mating type. *Genetics* **116**: 547-553.

Lundblad V, Blackburn EH. 1993. An alternative pathway for yeast telomere maintenance rescues est1- senescence. *Cell* **73**: 347-360.

Lydeard JR, Jain S, Yamaguchi M, Haber JE. 2007. Break-induced replication and telomerase-independent telomere maintenance require Pol32. *Nature* **448**: 820-U810.

Lydeard JR, Lipkin-Moore Z, Sheu YJ, Stillman B, Burgers PM, Haber JE. 2010. Break-induced replication requires all essential DNA replication factors except those specific for pre-RC assembly. *Genes Dev* **24**: 1133-1144.

Maftahi M, Han CS, Langston LD, Hope JC, Zigouras N, Freyer GA. 1999. The top3(+) gene is essential in Schizosaccharomyces pombe and the lethality associated with its loss is caused by Rad12 helicase activity. *Nucleic Acids Res* **27**: 4715-4724.

Maiorano D, Lutzmann M, Mechali M. 2006. MCM proteins and DNA replication. *Curr Opin Cell Biol* **18**: 130-136.

Majka J, Burgers PM. 2004. The PCNA-RFC families of DNA clamps and clamp loaders. *Prog Nucleic Acid Res Mol Biol* **78**: 227-260.

Maki K, Inoue T, Onaka A, Hashizume H, Somete N, Kobayashi Y, Murakami S, Shigaki C, Takahashi TS, Masukata H et al. 2011. Abundance of prereplicative complexes (Pre-RCs) facilitates recombinational repair under replication stress in fission yeast. *J Biol Chem* **286**: 41701-41710.

Malkova A, Ira G. 2013. Break-induced replication: functions and molecular mechanism. *Curr Opin Genet Dev* **23**: 271-279.

Malkova A, Ivanov EL, Haber JE. 1996. Double-strand break repair in the absence of RAD51 in yeast: A possible role for break-induced DNA replication. *Proc Natl Acad Sci U S A* **93**: 7131-7136.

Malkova A, Naylor ML, Yamaguchi M, Ira G, Haber JE. 2005. RAD51-dependent break-induced replication differs in kinetics and checkpoint responses from RAD51-mediated gene conversion. *Mol Cell Biol* **25**: 933-944.

Mankouri HW, Hickson ID. 2007. The RecQ helicase-topoisomerase III-Rmi1 complex: a DNA structure-specific 'dissolvasome'? *Trends Biochem Sci* **32**: 538-546.

Manosas M, Perumal SK, Croquette V, Benkovic SJ. 2012. Direct observation of stalled fork restart via fork regression in the T4 replication system. *Science* **338**: 1217-1220.

Martin V, Chahwan C, Gao H, Blais V, Wohlschlegel J, Yates JR, 3rd, McGowan CH, Russell P. 2006. Sws1 is a conserved regulator of homologous recombination in eukaryotic cells. *Embo J* **25**: 2564-2574.

Masai H, Asai T, Kubota Y, Arai K, Kogoma T. 1994. Escherichia coli PriA protein is essential for inducible and constitutive stable DNA replication. *Embo J* **13**: 5338-5345.

Matos J, Blanco MG, Maslen S, Skehel JM, West SC. 2011. Regulatory control of the resolution of DNA recombination intermediates during meiosis and mitosis. *Cell* **147**: 158-172.

Matsuo Y, Asakawa K, Toda T, Katayama S. 2006. A rapid method for protein extraction from fission yeast. *Biosci Biotechnol Biochem* **70**: 1992-1994.

Mazin AV, Alexeev AA, Kowalczykowski SC. 2003. A novel function of Rad54 protein. Stabilization of the Rad51 nucleoprotein filament. *J Biol Chem* **278**: 14029-14036.

Mazin AV, Bornarth CJ, Solinger JA, Heyer WD, Kowalczykowski SC. 2000. Rad54 protein is targeted to pairing loci by the Rad51 nucleoprotein filament. *Mol Cell* **6**: 583-592.

Mazin AV, Mazina OM, Bugreev DV, Rossi MJ. 2010. Rad54, the motor of homologous recombination. *DNA Repair (Amst)* **9**: 286-302.

Mcanulty MM, Lippard SJ. 1995. The Hmg-Domain Protein Ixr1 Blocks Repair of Cisplatin-DNA Adducts by Yeast Excision-Repair Proteins Rad2, Rad4, and Rad14, but Not Rad1 or Rad10. *J Cell Biochem*: 280-280.

McEachern MJ, Blackburn EH. 1996. Cap-prevented recombination between terminal telomeric repeat arrays (telomere CPR) maintains telomeres in Kluyveromyces lactis lacking telomerase. *Genes Dev* **10**: 1822-1834.

McGlynn P. 2004. Links between DNA replication and recombination in prokaryotes. *Curr Opin Genet Dev* **14**: 107-112.

McGlynn P, Al-Deib AA, Liu J, Marians KJ, Lloyd RG. 1997. The DNA replication protein PriA and the recombination protein RecG bind D-loops. *J Mol Biol* **270**: 212-221.

McGlynn P, Lloyd RG. 2002a. Genome stability and the processing of damaged replication forks by RecG. *Trends Genet* **18**: 413-419.

-. 2002b. Recombinational repair and restart of damaged replication forks. *Nat Rev Mol Cell Biol* **3**: 859-870.

McGlynn P, Savery NJ, Dillingham MS. 2012. The conflict between DNA replication and transcription. *Mol Microbiol* **85**: 12-20.

McHugh PJ, Ward TA, Chovanec M. 2012. A prototypical Fanconi anemia pathway in lower eukaryotes? *Cell Cycle* **11**.

McIlwraith MJ, Van Dyck E, Masson JY, Stasiak AZ, Stasiak A, West SC. 2000. Reconstitution of the strand invasion step of double-strand break repair using human Rad51 Rad52 and RPA proteins. *J Mol Biol* **304**: 151-164.

McIlwraith MJ, West SC. 2008. DNA repair synthesis facilitates RAD52-mediated second-end capture during DSB repair. *Mol Cell* **29**: 510-516.

McKee AH, Kleckner N. 1997. Mutations in Saccharomyces cerevisiae that block meiotic prophase chromosome metabolism and confer cell cycle arrest at pachytene identify two new meiosis-specific genes SAE1 and SAE3. *Genetics* **146**: 817-834.

Meister P, Poidevin M, Francesconi S, Tratner I, Zarzov P, Baldacci G. 2003. Nuclear factories for signalling and repairing DNA double strand breaks in living fission yeast. *Nucleic Acids Res* **31**: 5064-5073.

Meister P, Taddei A, Ponti A, Baldacci G, Gasser SM. 2007. Replication foci dynamics: replication patterns are modulated by S-phase checkpoint kinases in fission yeast. *Embo J* **26**: 1315-1326.

Meister P, Taddei A, Vernis L, Poidevin M, Gasser SM, Baldacci G. 2005. Temporal separation of replication and recombination requires the intra-S checkpoint. *J Cell Biol* **168**: 537-544.

Merrikh H, Machon C, Grainger WH, Grossman AD, Soultanas P. 2011. Co-directional replication-transcription conflicts lead to replication restart. *Nature* **470**: 554-557.

Michel B, Flores MJ, Viguera E, Grompone G, Seigneur M, Bidnenko V. 2001. Rescue of arrested replication forks by homologous recombination. *Proc Natl Acad Sci U S A* **98**: 8181-8188.

Mimitou EP, Symington LS. 2008. Sae2, Exo1 and Sgs1 collaborate in DNA double-strand break processing. *Nature* **455**: 770-774.

Mirchandani KD, D'Andrea AD. 2006. The Fanconi anemia/BRCA pathway: a coordinator of cross-link repair. *Exp Cell Res* **312**: 2647-2653.

Miyabe I, Kunkel TA, Carr AM. 2011. The major roles of DNA polymerases epsilon and delta at the eukaryotic replication fork are evolutionarily conserved. *PLoS Genet* **7**: e1002407.

Miyata H, Miyata M. 1981. Mode of Conjugation in Homothallic Cells of Schizosaccharomyces-Pombe. *J Gen Appl Microbiol* **27**: 365-371.

Mizuno K, Lambert S, Baldacci G, Murray JM, Carr AM. 2009. Nearby inverted repeats fuse to generate acentric and dicentric palindromic chromosomes by a replication template exchange mechanism. *Genes Dev* **23**: 2876-2886.

Mizuno K, Miyabe I, Schalbetter SA, Carr AM, Murray JM. 2013. Recombination-restarted replication makes inverted chromosome fusions at inverted repeats. *Nature* **493**: 246-249.

Morin I, Ngo HP, Greenall A, Zubko MK, Morrice N, Lydall D. 2008. Checkpoint-dependent phosphorylation of Exo1 modulates the DNA damage response. *Embo J* **27**: 2400-2410.

Morishita T, Furukawa F, Sakaguchi C, Toda T, Carr AM, Iwasaki H, Shinagawa H. 2005. Role of the Schizosaccharomyces pombe F-Box DNA helicase in processing recombination intermediates. *Mol Cell Biol* **25**: 8074-8083.

Morrow DM, Connelly C, Hieter P. 1997. "Break copy" duplication: a model for chromosome fragment formation in Saccharomyces cerevisiae. *Genetics* **147**: 371-382.

Mortensen UH, Bendixen C, Sunjevaric I, Rothstein R. 1996. DNA strand annealing is promoted by the yeast Rad52 protein. *Proc Natl Acad Sci U S A* **93**: 10729-10734.

Mosig G. 1987. The Essential Role of Recombination in Phage-T4 Growth. *Annu Rev Genet* **21**: 347-371.

Munoz IM, Hain K, Declais AC, Gardiner M, Toh GW, Sanchez-Pulido L, Heuckmann JM, Toth R, Macartney T, Eppink B et al. 2009. Coordination of structure-specific nucleases by human SLX4/BTBD12 is required for DNA repair. *Mol Cell* **35**: 116-127.

Nakanishi K, Cavallo F, Perrouault L, Giovannangeli C, Moynahan ME, Barchi M, Brunet E, Jasin M. 2011. Homology-directed Fanconi anemia pathway cross-link repair is dependent on DNA replication. *Nat Struct Mol Biol* **18**: 500-503.

Nakanishi K, Yang YG, Pierce AJ, Taniguchi T, Digweed M, D'Andrea AD, Wang ZQ, Jasin M. 2005. Human Fanconi anemia monoubiquitination pathway promotes homologous DNA repair. *Proc Natl Acad Sci U S A* **102**: 1110-1115.

Namsaraev E, Berg P. 1997. Characterization of strand exchange activity of yeast Rad51 protein. *Mol Cell Biol* **17**: 5359-5368.

Nandi S, Whitby MC. 2012. The ATPase activity of Fml1 is essential for its roles in homologous recombination and DNA repair. *Nucleic Acids Res*.

Narod SA, Foulkes WD. 2004. BRCA1 and BRCA2: 1994 and beyond. *Nat Rev Cancer* **4**: 665-676.

Nassif N, Penney J, Pal S, Engels WR, Gloor GB. 1994. Efficient copying of nonhomologous sequences from ectopic sites via P-element-induced gap repair. *Mol Cell Biol* **14**: 1613-1625.

Neale MJ, Keeney S. 2006. Clarifying the mechanics of DNA strand exchange in meiotic recombination. *Nature* **442**: 153-158.

Nicolette ML, Lee K, Guo Z, Rani M, Chow JM, Lee SE, Paull TT. 2010. Mre11-Rad50-Xrs2 and Sae2 promote 5' strand resection of DNA double-strand breaks. *Nat Struct Mol Biol* **17**: 1478-1485.

Nishinaka T, Shinohara A, Ito Y, Yokoyama S, Shibata T. 1998. Base pair switching by interconversion of sugar puckers in DNA extended by proteins of RecA-family: a model for homology search in homologous genetic recombination. *Proc Natl Acad Sci U S A* **95**: 11071-11076.

Niu H, Chung WH, Zhu Z, Kwon Y, Zhao W, Chi P, Prakash R, Seong C, Liu D, Lu L et al. 2010. Mechanism of the ATP-dependent DNA end-resection machinery from Saccharomyces cerevisiae. *Nature* **467**: 108-111.

Noguchi E, Noguchi C, McDonald WH, Yates JR, 3rd, Russell P. 2004. Swi1 and Swi3 are components of a replication fork protection complex in fission yeast. *Mol Cell Biol* **24**: 8342-8355.

Oestergaard VH, Langevin F, Kuiken HJ, Pace P, Niedzwiedz W, Simpson LJ, Ohzeki M, Takata M, Sale JE, Patel KJ. 2007. Deubiquitination of FANCD2 is required for DNA crosslink repair. *Mol Cell* **28**: 798-809.

Ogawa T, Yu X, Shinohara A, Egelman EH. 1993. Similarity of the yeast RAD51 filament to the bacterial RecA filament. *Science* **259**: 1896-1899.

Okazaki K, Okazaki N, Kume K, Jinno S, Tanaka K, Okayama H. 1990. High-frequency transformation method and library transducing vectors for cloning mammalian cDNAs by trans-complementation of Schizosaccharomyces pombe. *Nucleic Acids Res* **18**: 6485-6489.

Osman F, Dixon J, Barr AR, Whitby MC. 2005. The F-Box DNA helicase Fbh1 prevents Rhp51-dependent recombination without mediator proteins. *Mol Cell Biol* **25**: 8084-8096.

Osman F, Dixon J, Doe CL, Whitby MC. 2003. Generating crossovers by resolution of nicked Holliday junctions: a role for Mus81-Eme1 in meiosis. *Mol Cell* **12**: 761-774.

Osman F, Fortunato EA, Subramani S. 1996. Double-strand break-induced mitotic intrachromosomal recombination in the fission yeast Schizosaccharomyces pombe. *Genetics* **142**: 341-357.

Osman F, Whitby MC. 2007. Exploring the roles of Mus81-Eme1/Mms4 at perturbed replication forks. *DNA Repair (Amst)* **6**: 1004-1017.

-. 2009. Monitoring homologous recombination following replication fork perturbation in the fission yeast Schizosaccharomyces pombe. *Methods Mol Biol* **521**: 535-552.

Paeschke K, Capra JA, Zakian VA. 2011. DNA Replication through G-Quadruplex Motifs Is Promoted by the Saccharomyces cerevisiae Pif1 DNA Helicase. *Cell* **145**: 678-691.

Palmer GH, Bankhead T, Lukehart SA. 2009. 'Nothing is permanent but change'- antigenic variation in persistent bacterial pathogens. *Cell Microbiol* **11**: 1697-1705.

Papouli E, Chen S, Davies AA, Huttner D, Krejci L, Sung P, Ulrich HD. 2005. Crosstalk between SUMO and ubiquitin on PCNA is mediated by recruitment of the helicase Srs2p. *Mol Cell* **19**: 123-133.

Park JS, Marr MT, Roberts JW. 2002. E. coli Transcription repair coupling factor (Mfd protein) rescues arrested complexes by promoting forward translocation. *Cell* **109**: 757-767.

Patel PK, Arcangioli B, Baker SP, Bensimon A, Rhind N. 2006. DNA replication origins fire stochastically in fission yeast. *Mol Biol Cell* **17**: 308-316.

Payne BT, van Knippenberg IC, Bell H, Filipe SR, Sherratt DJ, McGlynn P. 2006. Replication fork blockage by transcription factor-DNA complexes in Escherichia coli. *Nucleic Acids Res* **34**: 5194-5202.

Petermann E, Orta ML, Issaeva N, Schultz N, Helleday T. 2010. Hydroxyurea-stalled replication forks become progressively inactivated and require two different RAD51-mediated pathways for restart and repair. *Mol Cell* **37**: 492-502.

Petrini JH. 2000. The Mre11 complex and ATM: collaborating to navigate S phase. *Curr Opin Cell Biol* **12**: 293-296.

Petukhova G, Stratton S, Sung P. 1998. Catalysis of homologous DNA pairing by yeast Rad51 and Rad54 proteins. *Nature* **393**: 91-94.

Petukhova G, Stratton SA, Sung P. 1999a. Single strand DNA binding and annealing activities in the yeast recombination factor Rad59. *Journal of Biological Chemistry* **274**: 33839-33842.

Petukhova G, Van Komen S, Vergano S, Klein H, Sung P. 1999b. Yeast Rad54 promotes Rad51-dependent homologous DNA pairing via ATP hydrolysis-driven change in DNA double helix conformation. *J Biol Chem* **274**: 29453-29462.

Pfander B, Moldovan GL, Sacher M, Hoege C, Jentsch S. 2005. SUMO-modified PCNA recruits Srs2 to prevent recombination during S phase. *Nature* **436**: 428-433.

Pinter SF, Aubert SD, Zakian VA. 2008. The Schizosaccharomyces pombe Pfh1p DNA helicase is essential for the maintenance of nuclear and mitochondrial DNA. *Mol Cell Biol* **28**: 6594-6608.

Plate I, Albertsen L, Lisby M, Hallwyl SCL, Feng Q, Seong C, Rothstein R, Sung P, Mortensen UH. 2008. Rad52 multimerization is important for its nuclear localization in Saccharomyces cerevisiae. *DNA Repair (Amst)* **7**: 57-66.

Pomerantz RT, O'Donnell M. 2010. What happens when replication and transcription complexes collide? *Cell Cycle* **9**: 2537-2543.

Possoz C, Filipe SR, Grainge I, Sherratt DJ. 2006. Tracking of controlled Escherichia coli replication fork stalling and restart at repressor-bound DNA in vivo. *Embo J* **25**: 2596-2604.

Postow L, Ullsperger C, Keller RW, Bustamante C, Vologodskii AV, Cozzarelli NR. 2001. Positive torsional strain causes the formation of a four-way junction at replication forks. *J Biol Chem* **276**: 2790-2796.

Prakash R, Satory D, Dray E, Papusha A, Scheller J, Kramer W, Krejci L, Klein H, Haber JE, Sung P et al. 2009. Yeast Mph1 helicase dissociates Rad51-made D-loops: implications for crossover control in mitotic recombination. *Genes Dev* **23**: 67-79.

Prakash S, Johnson RE, Prakash L. 2005. Eukaryotic translesion synthesis DNA polymerases: specificity of structure and function. *Annu Rev Biochem* **74**: 317-353.

Qiu Y, Antony E, Doganay S, Koh HR, Lohman TM, Myong S. 2013. Srs2 prevents Rad51 filament formation by repetitive motion on DNA. *Nat Commun* **4**: 2281.

Ragland RL, Patel S, Rivard RS, Smith K, Peters AA, Bielinsky AK, Brown EJ. 2013. RNF4 and PLK1 are required for replication fork collapse in ATR-deficient cells. *Genes Dev* **27**: 2259-2273.

Ragunathan K, Liu C, Ha T. 2012. RecA filament sliding on DNA facilitates homology search. *Elife* **1**: e00067.

Ralf C, Hickson ID, Wu L. 2006. The Bloom's syndrome helicase can promote the regression of a model replication fork. *Journal of Biological Chemistry* **281**: 22839-22846.

Rass U, Compton SA, Matos J, Singleton MR, Ip SC, Blanco MG, Griffith JD, West SC. 2010. Mechanism of Holliday junction resolution by the human GEN1 protein. *Genes Dev* **24**: 1559-1569.

Regairaz M, Zhang YW, Fu H, Agama KK, Tata N, Agrawal S, Aladjem MI, Pommier Y. 2011. Mus81-mediated DNA cleavage resolves replication forks stalled by topoisomerase I-DNA complexes. *J Cell Biol* **195**: 739-749.

Resnick MA. 1976. The repair of double-strand breaks in DNA; a model involving recombination. *J Theor Biol* **59**: 97-106.

Reuven NB, Tomer G, Livneh Z. 1998. The mutagenesis proteins UmuD' and UmuC prevent lethal frameshifts while increasing base substitution mutations. *Mol Cell* **2**: 191-199.

Rijkers T, Van Den Ouweland J, Morolli B, Rolink AG, Baarends WM, Van Sloun PP, Lohman PH, Pastink A. 1998. Targeted inactivation of

mouse RAD52 reduces homologous recombination but not resistance to ionizing radiation. *Mol Cell Biol* **18**: 6423-6429.

Robert T, Dervins D, Fabre F, Gangloff S. 2006. Mrc1 and Srs2 are major actors in the regulation of spontaneous crossover. *Embo Journal* **25**: 2837-2846.

Rocha EP. 2003. An appraisal of the potential for illegitimate recombination in bacterial genomes and its consequences: from duplications to genome reduction. *Genome Res* **13**: 1123-1132.

Rong L, Klein HL. 1993. Purification and characterization of the SRS2 DNA helicase of the yeast Saccharomyces cerevisiae. *J Biol Chem* **268**: 1252-1259.

Roseaulin L, Yamada Y, Tsutsui Y, Russell P, Iwasaki H, Arcangioli B. 2008. Mus81 is essential for sister chromatid recombination at broken replication forks. *Embo Journal* **27**: 1378-1387.

Rothstein R, Michel B, Gangloff S. 2000. Replication fork pausing and recombination or "gimme a break". *Genes Dev* **14**: 1-10.

Rouzeau S, Cordelieres FP, Buhagiar-Labarchede G, Hurbain I, Onclercq-Delic R, Gemble S, Magnaghi-Jaulin L, Jaulin C, Amor-Gueret M. 2012. Bloom's syndrome and PICH helicases cooperate with topoisomerase IIalpha in centromere disjunction before anaphase. *PLoS One* **7**: e33905.

Rudolph CJ, Upton AL, Stockum A, Nieduszynski CA, Lloyd RG. 2013. Avoiding chromosome pathology when replication forks collide. *Nature* **500**: 608-611.

Rupp WD, Howard-Flanders P. 1968. Discontinuities in the DNA synthesized in an excision-defective strain of Escherichia coli following ultraviolet irradiation. *J Mol Biol* **31**: 291-304.

Sabatinos SA, Forsburg SL. 2010. Molecular genetics of Schizosaccharomyces pombe. *Methods Enzymol* **470**: 759-795.

Sabouri N, McDonald KR, Webb CJ, Cristea IM, Zakian VA. 2012. DNA replication through hard-to-replicate sites, including both highly transcribed RNA Pol II and Pol III genes, requires the S. pombe Pfh1 helicase. *Genes Dev* **26**: 581-593.

Sabourin M, Zakian VA. 2008. ATM-like kinases and regulation of telomerase: lessons from yeast and mammals. *Trends Cell Biol* **18**: 337-346.

Sacher M, Pfander B, Hoege C, Jentsch S. 2006. Control of Rad52 recombination activity by double-strand break-induced SUMO modification. *Nat Cell Biol* **8**: 1284-1290.

Saini N, Ramakrishnan S, Elango R, Ayyar S, Zhang Y, Deem A, Ira G, Haber JE, Lobachev KS, Malkova A. 2013. Migrating bubble during break-induced replication drives conservative DNA synthesis. *Nature* **502**: 389-392.

Saintigny Y, Delacote F, Vares G, Petitot F, Lambert S, Averbeck D, Lopez BS. 2001. Characterization of homologous recombination induced by replication inhibition in mammalian cells. *Embo J* **20**: 3861-3870.

Saito TT, Youds JL, Boulton SJ, Colaiacovo MP. 2009. Caenorhabditis elegans HIM-18/SLX-4 interacts with SLX-1 and XPF-1 and maintains

genomic integrity in the germline by processing recombination intermediates. *PLoS Genet* **5**: e1000735.

Salakhova AF, Savchenko GV, Khasanov FK, Chepurnaia OV, Korolev VG, Bashkirov VI. 2005. The dds20+ gene controls a novel Rad51Sp-dependent pathway of recombinational repair in Schizosaccharomyces pombe. *Genetika* **41**: 736-745.

Sambrook J, Russell DW. 2001. *Molecular cloning : a laboratory manual*. Cold Spring Harbor Laboratory Press, Cold Spring Harbor, N.Y.

San Filippo J, Sung P, Klein H. 2008. Mechanism of eukaryotic homologous recombination. *Annu Rev Biochem* **77**: 229-257.

Sanchez-Gorostiaga A, Lopez-Estrano C, Krimer DB, Schvartzman JB, Hernandez P. 2004. Transcription termination factor reb1p causes two replication fork barriers at its cognate sites in fission yeast ribosomal DNA in vivo. *Mol Cell Biol* **24**: 398-406.

Sandler SJ, Marians KJ. 2000. Role of PriA in replication fork reactivation in Escherichia coli. *J Bacteriol* **182**: 9-13.

Santocanale C, Diffley JF. 1998. A Mec1- and Rad53-dependent checkpoint controls late-firing origins of DNA replication. *Nature* **395**: 615-618.

Sarkies P, Murat P, Phillips LG, Patel KJ, Balasubramanian S, Sale JE. 2012. FANCJ coordinates two pathways that maintain epigenetic stability at G-quadruplex DNA. *Nucleic Acids Res* **40**: 1485-1498.

Sartori AA, Lukas C, Coates J, Mistrik M, Fu S, Bartek J, Baer R, Lukas J, Jackson SP. 2007. Human CtIP promotes DNA end resection. *Nature* **450**: 509-514.

Sasaki MS. 1975. Is Fanconi's anaemia defective in a process essential to the repair of DNA cross links? *Nature* **257**: 501-503.

Sasaki MS, Tonomura A. 1973. A high susceptibility of Fanconi's anemia to chromosome breakage by DNA cross-linking agents. *Cancer Res* **33**: 1829-1836.

Schlacher K, Christ N, Siaud N, Egashira A, Wu H, Jasin M. 2011. Double-strand break repair-independent role for BRCA2 in blocking stalled replication fork degradation by MRE11. *Cell* **145**: 529-542.

Schlacher K, Wu H, Jasin M. 2012. A Distinct Replication Fork Protection Pathway Connects Fanconi Anemia Tumor Suppressors to RAD51-BRCA1/2. *Cancer Cell* **22**: 106-116.

Schmidt H, Kapitza-Fecke P, Stephen ER, Gutz H. 1989. Some of the swi genes of Schizosaccharomyces pombe also have a function in the repair of radiation damage. *Curr Genet* **16**: 89-94.

Schmidt KH, Derry KL, Kolodner RD. 2002. Saccharomyces cerevisiae RRM3, a 5' to 3' DNA helicase, physically interacts with proliferating cell nuclear antigen. *J Biol Chem* **277**: 45331-45337.

Segurado M, de Luis A, Antequera F. 2003. Genome-wide distribution of DNA replication origins at A+T-rich islands in Schizosaccharomyces pombe. *EMBO Rep* **4**: 1048-1053.

Seigneur M, Bidnenko V, Ehrlich SD, Michel B. 1998. RuvAB acts at arrested replication forks. *Cell* **95**: 419-430.

Seigneur M, Ehrlich SD, Michel B. 2000. RuvABC-dependent double-strand breaks in dnaBts mutants require recA. *Mol Microbiol* **38**: 565-574.

Shah PP, Zheng X, Epshtein A, Carey JN, Bishop DK, Klein HL. 2010. Swi2/Snf2-related translocases prevent accumulation of toxic Rad51 complexes during mitotic growth. *Mol Cell* **39**: 862-872.

Shah R, Cosstick R, West SC. 1997. The RuvC protein dimer resolves Holliday junctions by a dual incision mechanism that involves base-specific contacts. *Embo Journal* **16**: 1464-1472.

Sharan SK, Morimatsu M, Albrecht U, Lim DS, Regel E, Dinh C, Sands A, Eichele G, Hasty P, Bradley A. 1997. Embryonic lethality and radiation hypersensitivity mediated by Rad51 in mice lacking Brca2. *Nature* **386**: 804-810.

Sharma S, Sommers JA, Choudhary S, Faulkner JK, Cui S, Andreoli L, Muzzolini L, Vindigni A, Brosh RM, Jr. 2005. Biochemical analysis of the DNA unwinding and strand annealing activities catalyzed by human RECQ1. *J Biol Chem* **280**: 28072-28084.

Shcherbo D, Murphy CS, Ermakova GV, Solovieva EA, Chepurnykh TV, Shcheglov AS, Verkhusha VV, Pletnev VZ, Hazelwood KL, Roche PM et al. 2009. Far-red fluorescent tags for protein imaging in living tissues. *Biochem J* **418**: 567-574.

Shim EY, Chung WH, Nicolette ML, Zhang Y, Davis M, Zhu Z, Paull TT, Ira G, Lee SE. 2010. Saccharomyces cerevisiae Mre11/Rad50/Xrs2 and Ku proteins regulate association of Exo1 and Dna2 with DNA breaks. *Embo J* **29**: 3370-3380.

Shinohara A, Ogawa H, Ogawa T. 1992. Rad51 protein involved in repair and recombination in S. cerevisiae is a RecA-like protein. *Cell* **69**: 457-470.

Shirahige K, Hori Y, Shiraishi K, Yamashita M, Takahashi K, Obuse C, Tsurimoto T, Yoshikawa H. 1998. Regulation of DNA-replication origins during cell-cycle progression. *Nature* **395**: 618-621.

Signon L, Malkova A, Naylor ML, Klein H, Haber JE. 2001. Genetic requirements for RAD51- and RAD54-independent break-induced replication repair of a chromosomal double-strand break. *Mol Cell Biol* **21**: 2048-2056.

Simandlova J, Zagelbaum J, Payne MJ, Chu WK, Shevelev I, Hanada K, Chatterjee S, Reid DA, Liu Y, Janscak P et al. 2013. FBH1 helicase disrupts RAD51 filaments in vitro and modulates homologous recombination in mammalian cells. *J Biol Chem* **288**: 34168-34180.

Siow CC, Nieduszynska SR, Muller CA, Nieduszynski CA. 2012. OriDB, the DNA replication origin database updated and extended. *Nucleic Acids Res* **40**: D682-686.

Smith CE, Llorente B, Symington LS. 2007. Template switching during break-induced replication. *Nature* **447**: 102-105.

Smith GR, Boddy MN, Shanahan P, Russell P. 2003. Fission yeast Mus81.Eme1 Holliday junction resolvase is required for meiotic crossing over but not for gene conversion. *Genetics* **165**: 2289-2293.

Sofueva S, Osman F, Lorenz A, Steinacher R, Castagnetti S, Ledesma J, Whitby MC. 2011. Ultrafine anaphase bridges, broken DNA and illegitimate recombination induced by a replication fork barrier. *Nucleic Acids Res* **39**: 6568-6584.

Sogo JM, Lopes M, Foiani M. 2002. Fork reversal and ssDNA accumulation at stalled replication forks owing to checkpoint defects. *Science* **297**: 599-602.

Solinger JA, Kiianitsa K, Heyer WD. 2002. Rad54, a Swi2/Snf2-like recombinational repair protein, disassembles Rad51:dsDNA filaments. *Mol Cell* **10**: 1175-1188.

Stankiewicz P, Lupski JR. 2002. Genome architecture, rearrangements and genomic disorders. *Trends Genet* **18**: 74-82.

Steinacher R, Osman F, Dalgaard JZ, Lorenz A, Whitby MC. 2012. The DNA helicase Pfh1 promotes fork merging at replication termination sites to ensure genome stability. *Genes Dev* **26**: 594-602.

Stewart JA, Campbell JL, Bambara RA. 2009. Significance of the dissociation of Dna2 by flap endonuclease 1 to Okazaki fragment processing in Saccharomyces cerevisiae. *J Biol Chem* **284**: 8283-8291.

Stewart JA, Miller AS, Campbell JL, Bambara RA. 2008. Dynamic removal of replication protein A by Dna2 facilitates primer cleavage during Okazaki fragment processing in Saccharomyces cerevisiae. *J Biol Chem* **283**: 31356-31365.

Sugawara N, Paques F, Colaiacovo M, Haber JE. 1997. Role of Saccharomyces cerevisiae Msh2 and Msh3 repair proteins in double-strand break-induced recombination. *Proc Natl Acad Sci U S A* **94**: 9214-9219.

Sugiyama T, Kowalczykowski SC. 2002. Rad52 protein associates with replication protein a (RPA)-single-stranded DNA to accelerate Rad51-mediated displacement of RPA and presynaptic complex formation. *Journal of Biological Chemistry* **277**: 31663-31672.

Sugiyama T, New JH, Kowalczykowski SC. 1998. DNA annealing by Rad52 Protein is stimulated by specific interaction with the complex of replication protein A and single-stranded DNA. *Proc Natl Acad Sci U S A* **95**: 6049-6054.

Sun W, Nandi S, Osman F, Ahn JS, Jakovleska J, Lorenz A, Whitby MC. 2008. The FANCM Ortholog Fml1 Promotes Recombination at Stalled Replication Forks and Limits Crossing Over during DNA Double-Strand Break Repair. *Mol Cell* **32**: 118-128.

Sung P. 1994. Catalysis of ATP-dependent homologous DNA pairing and strand exchange by yeast RAD51 protein. *Science* **265**: 1241-1243.

-. 1997a. Communication - Function of yeast Rad52 protein as a mediator between replication protein A and the Rad51 recombinase. *Journal of Biological Chemistry* **272**: 28194-28197.

-. 1997b. Yeast Rad55 and Rad57 proteins form a heterodimer that functions with replication protein A to promote DNA strand exchange by Rad51 recombinase. *Genes Dev* **11**: 1111-1121.

Sung P, Krejci L, Van Komen S, Sehorn MG. 2003. Rad51 recombinase and recombination mediators. *J Biol Chem* **278**: 42729-42732.

Svendsen JM, Smogorzewska A, Sowa ME, O'Connell BC, Gygi SP, Elledge SJ, Harper JW. 2009. Mammalian BTBD12/SLX4 assembles a Holliday junction resolvase and is required for DNA repair. *Cell* **138**: 63-77.

Symington LS. 2002. Role of RAD52 epistasis group genes in homologous recombination and double-strand break repair. *Microbiol Mol Biol R* **66**: 630-+.

Szankasi P, Smith GR. 1992. A DNA exonuclease induced during meiosis of Schizosaccharomyces pombe. *J Biol Chem* **267**: 3014-3023.

Szostak JW, Orrweaver TL, Rothstein RJ, Stahl FW. 1983. The Double-Strand-Break Repair Model for Recombination. *Cell* **33**: 25-35.

Takahashi K, Imano R, Kibe T, Seimiya H, Muramatsu Y, Kawabata N, Tanaka G, Matsumoto Y, Hiromoto T, Koizumi Y et al. 2011. Fission yeast Pot1 and RecQ helicase are required for efficient chromosome segregation. *Mol Cell Biol* **31**: 495-506.

Takaki K, Cosma CL, Troll MA, Ramakrishnan L. 2012. An in vivo platform for rapid high-throughput antitubercular drug discovery. *Cell Rep* **2**: 175-184.

Tan TL, Kanaar R, Wyman C. 2003. Rad54, a Jack of all trades in homologous recombination. *DNA Repair (Amst)* **2**: 787-794.

Tang MJ, Shen X, Frank EG, O'Donnell M, Woodgate R, Goodman MF. 1999. UmuD ' C-2 is an error-prone DNA polymerase, Escherichia coli pol V. *Proc Natl Acad Sci U S A* **96**: 8919-8924.

Taniguchi T, Garcia-Higuera I, Andreassen PR, Gregory RC, Grompe M, D'Andrea AD. 2002a. S-phase-specific interaction of the Fanconi anemia protein, FANCD2, with BRCA1 and RAD51. *Blood* **100**: 2414-2420.

Taniguchi T, Garcia-Higuera I, Xu B, Andreassen PR, Gregory RC, Kim ST, Lane WS, Kastan MB, D'Andrea AD. 2002b. Convergence of the fanconi anemia and ataxia telangiectasia signaling pathways. *Cell* **109**: 459-472.

Tarsounas M, West SC. 2005. Recombination at mammalian telomeres: an alternative mechanism for telomere protection and elongation. *Cell Cycle* **4**: 672-674.

Teng SC, Chang J, McCowan B, Zakian VA. 2000. Telomerase-independent lengthening of yeast telomeres occurs by an abrupt Rad50p-dependent, Rif-inhibited recombinational process. *Mol Cell* **6**: 947-952.

Teng SC, Zakian VA. 1999. Telomere-telomere recombination is an efficient bypass pathway for telomere maintenance in Saccharomyces cerevisiae. *Mol Cell Biol* **19**: 8083-8093.

Tercero JA, Diffley JF. 2001. Regulation of DNA replication fork progression through damaged DNA by the Mec1/Rad53 checkpoint. *Nature* **412**: 553-557.

Thoma NH, Czyzewski BK, Alexeev AA, Mazin AV, Kowalczykowski SC, Pavletich NP. 2005. Structure of the SWI2/SNF2 chromatin-remodeling domain of eukaryotic Rad54. *Nat Struct Mol Biol* **12**: 350-356.

Thon G, Klar AJ. 1993. Directionality of fission yeast mating-type interconversion is controlled by the location of the donor loci. *Genetics* **134**: 1045-1054.

Thorslund T, McIlwraith MJ, Compton SA, Lekomtsev S, Petronczki M, Griffith JD, West SC. 2010. The breast cancer tumor suppressor BRCA2

promotes the specific targeting of RAD51 to single-stranded DNA. *Nat Struct Mol Biol* **17**: 1263-1265.

Thorslund T, West SC. 2007. BRCA2: a universal recombinase regulator. *Oncogene* **26**: 7720-7730.

Tittel-Elmer M, Alabert C, Pasero P, Cobb JA. 2009. The MRX complex stabilizes the replisome independently of the S phase checkpoint during replication stress. *Embo J* **28**: 1142-1156.

Tomita K, Cooper JP. 2008. Fission yeast Ccq1 is telomerase recruiter and local checkpoint controller. *Genes Dev* **22**: 3461-3474.

Torres JZ, Bessler JB, Zakian VA. 2004. Local chromatin structure at the ribosomal DNA causes replication fork pausing and genome instability in the absence of the S. cerevisiae DNA helicase Rrm3p. *Genes Dev* **18**: 498-503.

Trenz K, Smith E, Smith S, Costanzo V. 2006. ATM and ATR promote Mre11 dependent restart of collapsed replication forks and prevent accumulation of DNA breaks. *Embo J* **25**: 1764-1774.

Trickey M, Grimaldi M, Yamano H. 2008. The anaphase-promoting complex/cyclosome controls repair and recombination by ubiquitylating Rhp54 in fission yeast. *Mol Cell Biol* **28**: 3905-3916.

Trujillo KM, Roh DH, Chen L, Van Komen S, Tomkinson A, Sung P. 2003. Yeast xrs2 binds DNA and helps target rad50 and mre11 to DNA ends. *J Biol Chem* **278**: 48957-48964.

Trujillo KM, Sung P. 2001. DNA structure-specific nuclease activities in the Saccharomyces cerevisiae Rad50*Mre11 complex. *J Biol Chem* **276**: 35458-35464.

Tsukamoto K, Ito N, Yoshimoto M, Iwase T, Tada T, Kasumi F, Nakamura Y, Emi M. 1996. Two distinct commonly deleted regions on chromosome 13q suggest involvement of BRCA2 and retinoblastoma genes in sporadic breast carcinomas. *Cancer* **78**: 1929-1934.

Tsutsui Y, Morishita T, Iwasaki H, Toh H, Shinagawa H. 2000. A recombination repair gene of Schizosaccharomyces pombe, rhp57, is a functional homolog of the Saccharomyces cerevisiae RAD57 gene and is phylogenetically related to the human XRCC3 gene. *Genetics* **154**: 1451-1461.

Tsuzuki T, Fujii Y, Sakumi K, Tominaga Y, Nakao K, Sekiguchi M, Matsushiro A, Yoshimura Y, Morita T. 1996. Targeted disruption of the Rad51 gene leads to lethality in embryonic mice. *Proc Natl Acad Sci U S A* **93**: 6236-6240.

Ueno M, Nakazaki T, Akamatsu Y, Watanabe K, Tomita K, Lindsay HD, Shinagawa H, Iwasaki H. 2003. Molecular characterization of the Schizosaccharomyces pombe nbs1+ gene involved in DNA repair and telomere maintenance. *Mol Cell Biol* **23**: 6553-6563.

Vainio O, Imhof BA. 1995. The Immunology and Developmental Biology of the Chicken. *Immunol Today* **16**: 365-370.

van Gent DC, Hoeijmakers JH, Kanaar R. 2001. Chromosomal stability and the DNA double-stranded break connection. *Nat Rev Genet* **2**: 196-206.

van Gool AJ, Hajibagheri NM, Stasiak A, West SC. 1999. Assembly of the Escherichia coli RuvABC resolvasome directs the orientation of holliday junction resolution. *Genes Dev* **13**: 1861-1870.

Van Komen S, Petukhova G, Sigurdsson S, Stratton S, Sung P. 2000. Superhelicity-driven homologous DNA pairing by yeast recombination factors Rad51 and Rad54. *Mol Cell* **6**: 563-572.

Veaute X, Jeusset J, Soustelle C, Kowalczykowski SC, Le Cam E, Fabre F. 2003. The Srs2 helicase prevents recombination by disrupting Rad51 nucleoprotein filaments. *Nature* **423**: 309-312.

Vengrova S, Dalgaard JZ. 2006. The wild-type Schizosaccharomyces pombe mat1 imprint consists of two ribonucleotides. *EMBO Rep* **7**: 59-65.

Voineagu I, Narayanan V, Lobachev KS, Mirkin SM. 2008. Replication stalling at unstable inverted repeats: Interplay between DNA hairpins and fork stabilizing proteins. *Proc Natl Acad Sci U S A* **105**: 9936-9941.

Waga S, Stillman B. 1998. The DNA replication fork in eukaryotic cells. *Annu Rev Biochem* **67**: 721-751.

Wang W. 2007. Emergence of a DNA-damage response network consisting of Fanconi anaemia and BRCA proteins. *Nat Rev Genet* **8**: 735-748.

Watts FZ. 2006. Sumoylation of PCNA: Wrestling with recombination at stalled replication forks. *DNA Repair (Amst)* **5**: 399-403.

Whitby MC. 2005. Making crossovers during meiosis. *Biochem Soc Trans* **33**: 1451-1455.

Williams RS, Dodson GE, Limbo O, Yamada Y, Williams JS, Guenther G, Classen S, Glover JN, Iwasaki H, Russell P et al. 2009. Nbs1 flexibly tethers Ctp1 and Mre11-Rad50 to coordinate DNA double-strand break processing and repair. *Cell* **139**: 87-99.

Williams RS, Williams JS, Tainer JA. 2007. Mre11-Rad50-Nbs1 is a keystone complex connecting DNA repair machinery, double-strand break signaling, and the chromatin template. *Biochem Cell Biol* **85**: 509-520.

Wilson MA, Kwon Y, Xu Y, Chung WH, Chi P, Niu H, Mayle R, Chen X, Malkova A, Sung P et al. 2013. Pif1 helicase and Poldelta promote recombination-coupled DNA synthesis via bubble migration. *Nature* **502**: 393-396.

Wolner B, van Komen S, Sung P, Peterson CL. 2003. Recruitment of the recombinational repair machinery to a DNA double-strand break in yeast. *Mol Cell* **12**: 221-232.

Wu D, Topper LM, Wilson TE. 2008a. Recruitment and dissociation of nonhomologous end joining proteins at a DNA double-strand break in Saccharomyces cerevisiae. *Genetics* **178**: 1237-1249.

Wu L, Davies SL, North PS, Goulaouic H, Riou JF, Turley H, Gatter KC, Hickson ID. 2000. The Bloom's syndrome gene product interacts with topoisomerase III. *Journal of Biological Chemistry* **275**: 9636-9644.

Wu L, Hickson ID. 2003. The Bloom's syndrome helicase suppresses crossing over during homologous recombination. *Nature* **426**: 870-874.

Wu Y, Kantake N, Sugiyama T, Kowalczykowski SC. 2008b. Rad51 protein controls Rad52-mediated DNA annealing. *J Biol Chem* **283**: 14883-14892.

Wu Y, Shin-ya K, Brosh RM, Jr. 2008c. FANCJ helicase defective in Fanconia anemia and breast cancer unwinds G-quadruplex DNA to defend genomic stability. *Mol Cell Biol* **28**: 4116-4128.

Xu L, Marians KJ. 2003. PriA mediates DNA replication pathway choice at recombination intermediates. *Mol Cell* **11**: 817-826.

Xu X, Ball L, Chen W, Tian X, Lambrecht A, Hanna M, Xiao W. 2013. The yeast Shu complex utilizes homologous recombination machinery for error-free lesion bypass via physical interaction with a Rad51 paralogue. *PLoS One* **8**: e81371.

Yamada-Inagawa T, Klar AJ, Dalgaard JZ. 2007. Schizosaccharomyces pombe switches mating type by the synthesis-dependent strand-annealing mechanism. *Genetics* **177**: 255-265.

Yang W, Woodgate R. 2007. What a difference a decade makes: insights into translesion DNA synthesis. *Proc Natl Acad Sci U S A* **104**: 15591-15598.

Yeeles JT, Marians KJ. 2011. The Escherichia coli replisome is inherently DNA damage tolerant. *Science* **334**: 235-238.

Yu CE, Oshima J, Fu YH, Wijsman EM, Hisama F, Alisch R, Matthews S, Nakura J, Miki T, Ouais S et al. 1996. Positional cloning of the Werner's syndrome gene. *Science* **272**: 258-262.

Yu VP, Koehler M, Steinlein C, Schmid M, Hanakahi LA, van Gool AJ, West SC, Venkitaraman AR. 2000. Gross chromosomal rearrangements and genetic exchange between nonhomologous chromosomes following BRCA2 inactivation. *Genes Dev* **14**: 1400-1406.

Yuzhakov A, Turner J, O'Donnell M. 1996. Replisome assembly reveals the basis for asymmetric function in leading and lagging strand replication. *Cell* **86**: 877-886.

Zhang Y, Shim EY, Davis M, Lee SE. 2009. Regulation of repair choice: Cdk1 suppresses recruitment of end joining factors at DNA breaks. *DNA Repair (Amst)* **8**: 1235-1241.

Zheng XF, Prakash R, Saro D, Longerich S, Niu H, Sung P. 2011. Processing of DNA structures via DNA unwinding and branch migration by the S. cerevisiae Mph1 protein. *DNA Repair (Amst)* **10**: 1034-1043.

Zhu Z, Chung WH, Shim EY, Lee SE, Ira G. 2008. Sgs1 helicase and two nucleases Dna2 and Exo1 resect DNA double-strand break ends. *Cell* **134**: 981-994.

Zou L, Elledge SJ. 2003. Sensing DNA damage through ATRIP recognition of RPA-ssDNA complexes. *Science* **300**: 1542-1548.